

Mechanistic study of the high-temperature Fischer-Tropsch synthesis using transient kinetics

Citation for published version (APA):

Govender, N. S. (2010). *Mechanistic study of the high-temperature Fischer-Tropsch synthesis using transient kinetics*. [Phd Thesis 1 (Research TU/e / Graduation TU/e), Chemical Engineering and Chemistry]. Technische Universiteit Eindhoven. <https://doi.org/10.6100/IR689931>

DOI:

[10.6100/IR689931](https://doi.org/10.6100/IR689931)

Document status and date:

Published: 01/01/2010

Document Version:

Publisher's PDF, also known as Version of Record (includes final page, issue and volume numbers)

Please check the document version of this publication:

- A submitted manuscript is the version of the article upon submission and before peer-review. There can be important differences between the submitted version and the official published version of record. People interested in the research are advised to contact the author for the final version of the publication, or visit the DOI to the publisher's website.
- The final author version and the galley proof are versions of the publication after peer review.
- The final published version features the final layout of the paper including the volume, issue and page numbers.

[Link to publication](#)

General rights

Copyright and moral rights for the publications made accessible in the public portal are retained by the authors and/or other copyright owners and it is a condition of accessing publications that users recognise and abide by the legal requirements associated with these rights.

- Users may download and print one copy of any publication from the public portal for the purpose of private study or research.
- You may not further distribute the material or use it for any profit-making activity or commercial gain
- You may freely distribute the URL identifying the publication in the public portal.

If the publication is distributed under the terms of Article 25fa of the Dutch Copyright Act, indicated by the "Taverne" license above, please follow below link for the End User Agreement:

www.tue.nl/taverne

Take down policy

If you believe that this document breaches copyright please contact us at:

openaccess@tue.nl

providing details and we will investigate your claim.

Mechanistic study of the High- Temperature Fischer-Tropsch Synthesis using transient kinetics

PROEFSCHRIFT

ter verkrijging van de graad van doctor aan de
Technische Universiteit Eindhoven, op gezag van de
Rector Magnificus, prof.dr.ir. C.J. van Duijn, voor een
commissie aangewezen door het College voor
Promoties in het openbaar te verdedigen
op maandag 15 November 2010 om 16.00 uur

door

Nilenindran Sundra Govender

geboren te Durban, Zuid-Afrika

Dit proefschrift is goedgekeurd door de promotor:

prof.dr.ir. J.C. Schouten

Copromotor:

dr. M.H.J.M. de Croon

A catalogue record is available from the Library Eindhoven University of Technology

ISBN: 978-90-386-2340-5

Copyright © 2010 by Nilenindran Sundra Govender

Printed by Ridderprint BV, Ridderkerk, The Netherlands

Cover page design by Gideon Botes and Nilenindran Sundra Govender

Image Credit: T.A. Rector and B.A. Wolpa, NOAO, AURA, and NSF.

Dedicated to my wife, Ashriti and daughter, Suhina.

CONTENTS

Summary

Samenvatting

1. Introduction.....	1
2. Experimental methodology and model development.....	23
3. Reactivity of surface carbonaceous intermediates on an iron based Fischer-Tropsch catalyst.....	45
4. Mechanistic pathway for methane formation over an iron based catalyst.....	75
5. Effects of co-fed ethylene during the high temperature Fischer-Tropsch synthesis....	95
6. Mechanistic pathway for C ₂₊ hydrocarbon formation over an iron based catalyst....	115
7. A comparative study of CO and CO ₂ hydrogenation on Fe catalysts.....	141
8. Conclusions and Outlook.....	163

Nomenclature

Appendix A: The gPROMs modeling language

Appendix B: Fischer-Tropsch product distribution models schemes as published
in the open literature

Appendix C: Model equations for the ¹³CO-labelling of C₂₊ hydrocarbons for
models B and C (see Chapter 6)

Appendix D: Relationship between the reaction mechanism and isotopic decay
plots from SSITKA data

Acknowledgements

List of publications

About the author

Summary

Mechanistic study of the High- Temperature Fischer-Tropsch Synthesis using transient kinetics

The Fischer-Tropsch synthesis (FTS) is a heterogeneously catalysed process whereby synthesis gas (a mixture of carbon monoxide and hydrogen) is converted to liquid fuels (gasoline and diesel) and chemicals. There are two modes of operation for the Fischer-Tropsch synthesis, each with its specific selectivity targets. The high temperature (300–350 °C) Fischer-Tropsch process (HTFT) aims at the production of gasoline and linear low molecular mass olefins, whereas the low temperature (200–240 °C) Fischer-Tropsch process (LTFT) is used for the production of diesel and high molecular mass linear waxes. The HTFT process comprises a complex network of elementary reaction steps. Apart from the usual linear FT products (olefins and paraffins), these steps include the formation of CO₂, carbon, branched products, aromatics and oxygenates (alcohols, acids, aldehydes and ketones). To date, the product distribution of the HTFT process has not been fully described by the mechanisms in the literature. This thesis employs isotopic techniques to elucidate the mechanism of the HTFT process.

The Steady-State Isotopic Transient Kinetic Analysis (SSITKA) technique was mainly used in this thesis. This method keeps the catalyst under steady-state conditions and introduces an isotopic transient by abruptly replacing one reactant with its isotope (e.g. H₂/¹²CO/Ar → H₂/¹³CO/He) with minimum disturbance to the system. The inert gas is also switched to determine the gas hold-up in the reactor. Apart from isothermal and isobaric reactor conditions, the surface composition of the catalyst does not change during SSITKA, making this technique ideal for reaction mechanistic studies. The methodology included the solution of ordinary differential equations (or ODE's) which were mole balances written for the labeled atom (in this

thesis, mainly ^{13}C from ^{13}CO SSITKA experiments) and for a plug flow reactor at isobaric and isothermal conditions.

Two reaction mechanisms for the methanation reaction were proposed, using the SSITKA technique over an Fe-based catalyst at HTFT conditions (330 °C, 1.2 bar, and $\text{H}_2/\text{CO} = 15$). Both mechanisms have two active pools of carbon (C_α and C_β) on the catalyst surface with both leading towards the formation of methane and higher hydrocarbons. The C_β pool was 25 to 50 times less active than the C_α pool for methanation and occupied 92% of the total CH_x coverage (0.25 ML). The C-C coupling reaction was shown to involve both the C_α and C_β pools. Another important conclusion from this study was that the concentration of molecularly adsorbed CO on the Fe-based catalyst is extremely low, with an estimated surface coverage of 9×10^{-4} ML.

Deuterium tracing experiments in combination with hydrogenation experiments (both isothermal and temperature programmed) provided information on the nature and reactivity of the surface intermediates on an Fe-based catalyst at HTFT conditions. This was performed on both fresh and carbided catalysts. On both catalysts, carbon deposition occurred to the same extent but water formation and methane formation were faster on the carbided catalyst. More reaction intermediates for C_2 hydrocarbon formation were detected at the start of the Fischer-Tropsch reaction on the freshly reduced catalyst. However, the CH_3 intermediate for methane formation and the CCH_3 intermediate for C_2 hydrocarbon formation were found to be the most stable surface intermediates on both catalysts. Surface carbon ($^{13}\text{C}_s$), deposited via the Boudouard reaction using ^{13}CO , was active and was detected in the C_{2+} hydrocarbon products as the result of a coupling reaction with $^{12}\text{C}_s$ rather than with $^{13}\text{C}_s$. Six distinct carbon pools ($\text{C}_{\alpha 1}$, $\text{C}_{\alpha 2}$, $\text{C}_{\beta 1}$, $\text{C}_{\gamma 1}$, $\text{C}_{\gamma 2}$ and $\text{C}_{\delta 1}$) were identified during isothermal and temperature programmed surface reactions of which graphitic carbon ($\text{C}_{\delta 1}$) had the highest coverage on the end of the run sample.

The effect of co-fed ethene on the Fischer-Tropsch synthesis was also investigated. The main aim was to identify reaction pathways for readsorbed olefins. Steady state results (at 330°C, 1.2 bar, $\text{H}_2/\text{CO} = 15$ and $7580 \text{ ml.g}_{\text{cat}}^{-1}.\text{hr}^{-1}$) showed

that the hydrogenation of ethene to ethane is the main reaction pathway but chain growth does occur to a lesser extent. Repeating these co-fed ethene experiments at the same reaction conditions but with ^{13}C O in the feed showed that in terms of chain growth, propene formation was favoured instead of propane. This suggests that the olefins share the same surface intermediate. This result allowed for the development of different mechanistic pathways for olefin and paraffin formation, which were later used for the development of the FT mechanisms.

The mechanism of the methanation reaction pathway was extended to account for the formation of C_{2+} hydrocarbons at the same reaction conditions. Three different mechanistic models were tested whilst considering two cases; in the first case, the initiation and chain growth rates coefficients are equal ($k_{\text{ini}} = k_{\text{p}}$) and in the second case, these rate coefficients differ ($k_{\text{ini}} \neq k_{\text{p}}$). Only one model, in which there are two surface intermediates for the C_n hydrocarbons ($n \geq 2$) with direct olefin readsorption towards the surface intermediate for paraffin formation, gave the best fit.

The hydrogenation of CO_2 was investigated and compared to CO hydrogenation (normal Fischer-Tropsch synthesis) over an iron based catalyst at high temperature (330 °C). In comparison to CO hydrogenation, the catalyst activity, deactivation and olefinicity were the same during CO_2 hydrogenation at similar reactor operating conditions, especially the H_2/CO ratio. However, the transients obtained during ^{13}C O and $^{13}\text{CO}_2$ SSITKA experiments differ in both cases. During CO_2 hydrogenation, the reactant and product (CO_2 and CO) became kinetically indistinguishable. From some of the data, a two pool model was proposed based on the shape of the ^{13}C decay in $^{13}\text{CO}_2$. A formate mechanism, in which CHO_s and COOH_s are the surface intermediates during the water-gas-shift reaction, is the most plausible for the water-gas-shift mechanism.

The hypothesis in this thesis was that C_s is active and should play a role in the mechanism of the HTFT process. This was shown to be true (see Chapter 3) with the ^{13}C O deposition (Boudouard reaction) experiment in which the $^{13}\text{C}_s$ was active for Fischer-Tropsch. Moreover, in the deuterium tracing experiment, CCH_s was identified as an active species for C_2 formation. This intermediate most probably

forms from the reaction of C_s and CH_s . The latter intermediate is most likely the monomer in the HTFT process.

Samenvatting

De Fischer-Tropsch synthese (FTS) is een heterogeen-gekatalyseerd proces waarin synthesegas, een mengsel van koolmonoxide en waterstof, wordt omgezet in vloeibare brandstoffen (benzine en diesel) en chemicaliën. Er zijn twee manieren waarop de Fischer-Tropsch synthese kan worden uitgevoerd, waarbij elk een specifieke selectiviteit tot doel heeft. Het hoge temperatuur Fischer-Tropsch proces (HTFT, $T = 300 - 350 \text{ }^\circ\text{C}$) richt zich op de productie van benzine en lineaire olefines met lage moleculaire massa, terwijl het lage temperatuur proces (LTFT, $T = 200 - 240 \text{ }^\circ\text{C}$) wordt gebruikt voor de productie van diesel en lineaire wassen met een hoge moleculaire massa. Het HTFT-proces bestaat uit een complex netwerk van elementaire reactiestappen. Naast de vorming van de gebruikelijke FTS producten, zoals olefines en parafines, worden in deze reactiestappen ook CO_2 , koolstof, vertakte producten, aromaten en zuurstofhoudende producten, zoals alcoholen, zuren, aldehydes en ketonen gevormd. Momenteel kan de productverdeling van het HTFT-proces nog niet volledig worden beschreven met de in de literatuur voorhanden zijnde mechanismes. Dit proefschrift maakt gebruik van isotooptechnieken om het mechanisme van het HTFT-proces op te helderen.

In dit proefschrift is vooral gebruik gemaakt van de Steady-State Isotopic Transient Kinetic Analysis (SSITKA) techniek. In deze methode wordt de katalysator onder stationaire condities gehouden en wordt een isotooptransiënt geïntroduceerd door het abrupt vervangen van één van de reactanten door zijn isotoop (bijv. $\text{H}_2/^{12}\text{CO}/\text{Ar} \rightarrow \text{H}_2/^{13}\text{CO}/\text{He}$) met daarbij een minimale verstoring van het systeem. Daarbij wordt ook een inert gas in- respectievelijk uitgeschakeld ten einde de ruimtetijd van het gas in de reactor te bepalen. Onder isotherme en isobare reactorcondities verandert de oppervlaksamenstelling van de katalysator niet tijdens het SSITKA-experiment. Dit maakt deze techniek dan ook ideaal voor mechanistische studies van reacties. De werkwijze behelst het oplossen van gewone differentiaalvergelijkingen (of ODEs), die de molbalansen zijn voor de gelabelde atomen (in dit proefschrift vooral ^{13}C uit ^{13}CO SSITKA-experimenten) voor het geval van een propstroomreactor bij isobare en isotherme condities.

Op basis van de resultaten verkregen met de SSITKA-techniek voor een ijzerkatalysator bij HTFT-condities (330 °C, 1.2 bar en $H_2/CO = 15$) zijn twee reactiemechanismen voorgesteld. Beide mechanismes hebben twee actieve koolstofpoelen (C_α en C_β) op het katalysatoroppervlak. Beide leiden tot de vorming van methaan en hogere koolwaterstoffen. De C_β -poel was 25 tot 50 keer minder actief dan de C_α -poel voor methaanvorming. Hij bevat 92% van de totale CH_x -bezetting (0.25 ML). Er is aangetoond dat zowel de C_α - als de C_β -poel betrokken zijn bij de C-C koppelingsreactie. Een andere belangrijke conclusie van dit onderzoek is dat de concentratie van moleculair-geadsorbeerd CO op de ijzerkatalysator extreem laag is, met een geschatte oppervlaktebezetting van $9 \cdot 10^{-4}$ ML.

Tracing-experimenten met deuterium in combinatie met zowel isotherme als temperatuur-geprogrammeerde hydrogeneringsexperimenten verschaften informatie over de aard en reactiviteit van de oppervlakintermediaren op een ijzerkatalysator bij HTFT-condities. Deze experimenten zijn uitgevoerd zowel met verse als met gecarbidiseerde katalysator. Op beide katalysatoren komt koolstofdepositie in gelijke mate voor, maar watervorming en methaanvorming verlopen sneller bij de gecarbidiseerde katalysator. Meerdere reactie-intermediaren voor de vorming van C_2 - koolwaterstoffen werden gedetecteerd bij het begin van de Fischer-Tropsch reactie over de vers-gereduceerde katalysator. Het CH_5 -intermediair voor de methaanvorming en het CCH_5 -intermediair voor de C_2 -koolwaterstofvorming blijken echter de stabielste intermediaren op beide katalysatoren. Oppervlakkoolstof ($^{13}C_s$), gedeponeerd door middel van de Boudouard reactie met ^{13}CO , is actief en wordt gedetecteerd in de C_{2+} -koolwaterstofproducten als het resultaat van een koppelingsreactie met $^{12}C_s$ in plaats van met $^{13}C_s$. Zes duidelijk onderscheidbare koolstofpoelen ($C_{\alpha 1}$, $C_{\alpha 2}$, $C_{\beta 1}$, $C_{\gamma 1}$, $C_{\gamma 2}$ en $C_{\delta 1}$) zijn geïdentificeerd gedurende isotherme en temperatuur-geprogrammeerde oppervlakreacties. Grafische koolstof ($C_{\delta 1}$) heeft de hoogste bezetting op de gebruikte katalysator.

Ook het effect van het bijvoeden van etheen op het Fischer-Tropsch proces is onderzocht. Het belangrijkste doel was het identificeren van reactiepaden voor gereadsorbeerde olefines. Resultaten van stationaire experimenten (bij 330°C, 1.2 bar, $H_2/CO = 15$ en $7580 \text{ ml } g_{\text{cat}}^{-1} \cdot \text{hr}^{-1}$) laten zien dat de hydrogenering van etheen tot

ethaan het belangrijkste reactiepad is, maar dat ketengroei in mindere mate ook optreedt. Herhaling van deze experimenten met etheenbijvoeding onder dezelfde reactiecondities, maar met ^{13}C O in de voeding, laat zien dat in termen van ketengroei meer propeenvorming optreedt dan propaanvorming. Dit suggereert eenzelfde oppervlakintermediair voor de olefines. Het resultaat bood de mogelijkheid verschillende mechanistische paden te ontwikkelen voor de vorming van olefines en paraffines, die vervolgens konden worden gebruikt voor de ontwikkeling van mechanismes voor Fischer-Tropsch synthese.

Het mechanisme voor de methaanvorming is uitgebreid om rekening te kunnen houden met de vorming van C_{2+} -koolwaterstoffen bij dezelfde reactiecondities. Drie verschillende mechanistische modellen zijn getest. Daarbij zijn twee gevallen beschouwd. In het eerste geval zijn de reactiesnelheidscoëfficiënten voor initiatie en ketengroei gelijk gesteld ($k_{\text{ini}} = k_{\text{p}}$), in het tweede geval zijn ze verschillend genomen ($k_{\text{ini}} \neq k_{\text{p}}$). Slechts één model gaf een goede fit aan de data. In dit model zijn er twee oppervlakintermediaren voor C_n -koolwaterstoffen ($n \geq 2$) en treedt er een directe olefine-readsorptie op, die leidt tot het oppervlakintermediair voor paraffinevorming.

De hydrogenering van CO_2 is onderzocht en er is een vergelijking gemaakt met CO -hydrogenering, d.w.z. normale Fischer-Tropsch synthese, over een ijzerkatalysator bij hoge temperatuur (330 °C). In vergelijking met CO -hydrogenering zijn de katalysatoractiviteit, de deactivering en de selectiviteit naar olefines hetzelfde voor CO_2 -hydrogenering bij gelijke bedrijfscondities van de reactor en speciaal bij gelijke H_2/CO verhouding. De transiënte data, verkregen via ^{13}C O- en $^{13}\text{CO}_2$ -SSITKA experimenten, zijn echter verschillend in beide gevallen. Tijdens CO_2 -hydrogenering worden reactant en product (CO_2 en CO) kinetisch ononderscheidbaar. Op grond van een beperkt aantal data is een model voorgesteld met twee intermediaren. Dit model is gebaseerd op de vorm van het ^{13}C -verval in CO_2 . Een formaat-mechanisme met CHO_s en COOH_s als oppervlakintermediaren bij de watergasshift is het meest waarschijnlijke mechanisme voor deze reactie.

De hypothese in dit proefschrift was dat C_s actief is een rol speelt in het mechanisme van het HTFT-proces. In Hoofdstuk 3 is aangetoond dat dit correct is

door middel van een ^{13}CO -disproportioneringsexperiment (Boudouard reactie), waarin het $^{13}\text{C}_s$ -species actief is in de Fischer-Tropsch synthese. Bovendien is met een tracing-experiment met deuterium CCH_s geïdentificeerd als een actief species voor C_2 -vorming. Dit intermediair wordt hoogstwaarschijnlijk gevormd via de reactie van C_s en CH_s . Het CH_s -intermediair komt het meest in aanmerking voor het monomeer in het HTFT-proces.

1

Introduction

1.1. The Fischer-Tropsch process

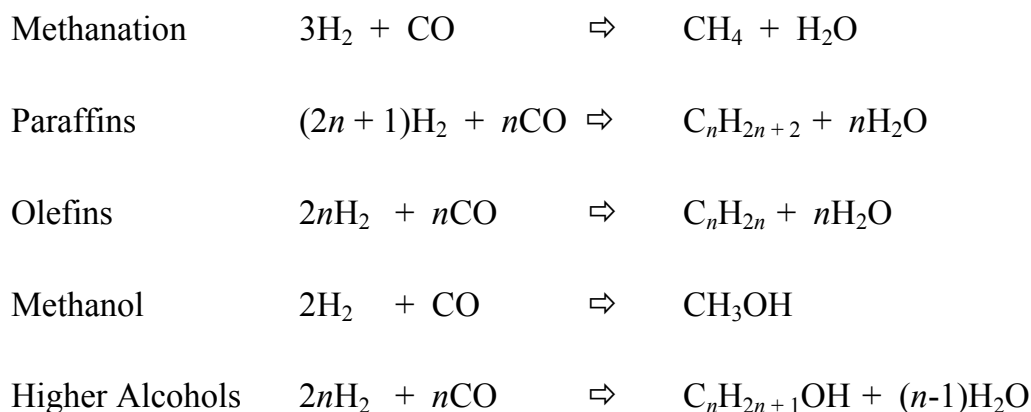
Fischer-Tropsch synthesis is a heterogeneously catalysed process whereby synthesis gas (a mixture of carbon monoxide and hydrogen) is converted to a range of alkenes, alkanes and oxygenated compounds. Synthesis gas can be produced from carbon-based materials such as coal, biomass, refinery bottoms and natural gas. Hence, the Fischer-Tropsch synthesis can be considered as an alternate to crude oil for the production of liquid fuels (gasoline and diesel) and chemicals [1].

There are a number of metals, which have sufficient activity in the Fischer-Tropsch synthesis for industrial application, such as iron, cobalt, nickel and ruthenium [2,3]. Nickel is, however, too hydrogenating, resulting in high CH₄ yields whereas ruthenium is rare and too expensive for use in large scales. Therefore, only iron and cobalt-based catalysts are being used in commercial Fischer-Tropsch plants.

There are currently two modes of operation for the Fischer-Tropsch synthesis, each with its specific selectivity targets. The high temperature (300–350°C) Fischer-Tropsch process (HTFT) aims at the production of gasoline and linear low molecular mass olefins whereas the low temperature

(200–240°C) Fischer-Tropsch process (LTFT) is used for the production of diesel and high molecular mass linear waxes [4].

The Fischer-Tropsch reaction yields a wide spectrum of hydrocarbons and oxygenated compounds [5]. These reactions producing water as a co-product can stoichiometrically be written as:



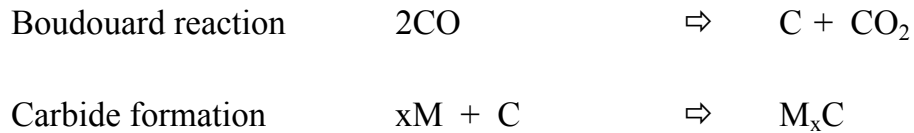
The formation of methane is a limiting case in the Fischer-Tropsch synthesis, in which the formation of the C-C bond does not occur. Olefins and paraffins are the major products of the Fischer-Tropsch synthesis. The formation of oxygenated compounds, such as alcohols, is observed to some extent during the Fischer-Tropsch synthesis [5].

Water can react further in the water gas shift reaction yielding carbon dioxide.



Other reactions that may occur under the conditions of the Fischer-Tropsch synthesis are:





The Fischer-Tropsch synthesis is currently commercially applied at five different locations in the world, i.e. Sasolburg, Secunda, and Mossel Bay (all in South Africa), Bintulu (Malaysia) and Ras Laffan (Qatar). Brief details of these plants are presented in Figure 1.1. Both Sasol and Shell are continuing to invest in new FT plants. Sasol is planning to start-up its new Gas-to-Liquids (GTL) plant in Nigeria in December 2010 (with capacity of 34 000 bpd) whilst Shell has announced their start-up of a 70 000 bpd plant in Qatar in 2010 with the expansion to 140 000 bpd later on. There has also been interest in FT technology from countries with huge coal reserves such as India, China and the US, all wanting their economies to become less dependent on oil imports. The renewed interest in the Fischer-Tropsch process is also related to the recent high crude oil prices as shown in Figure 1.2.

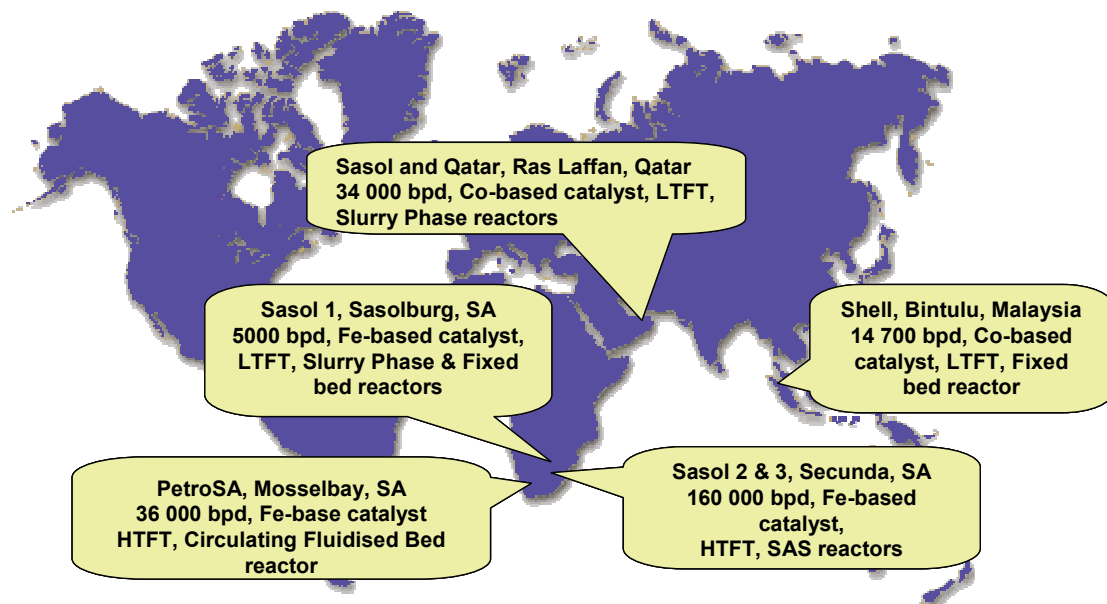


Figure 1.1: Current operating commercial Fischer-Tropsch plants worldwide. Sources: <http://www.petrosa.co.za/>, www.shell.com, www.sasol.com.

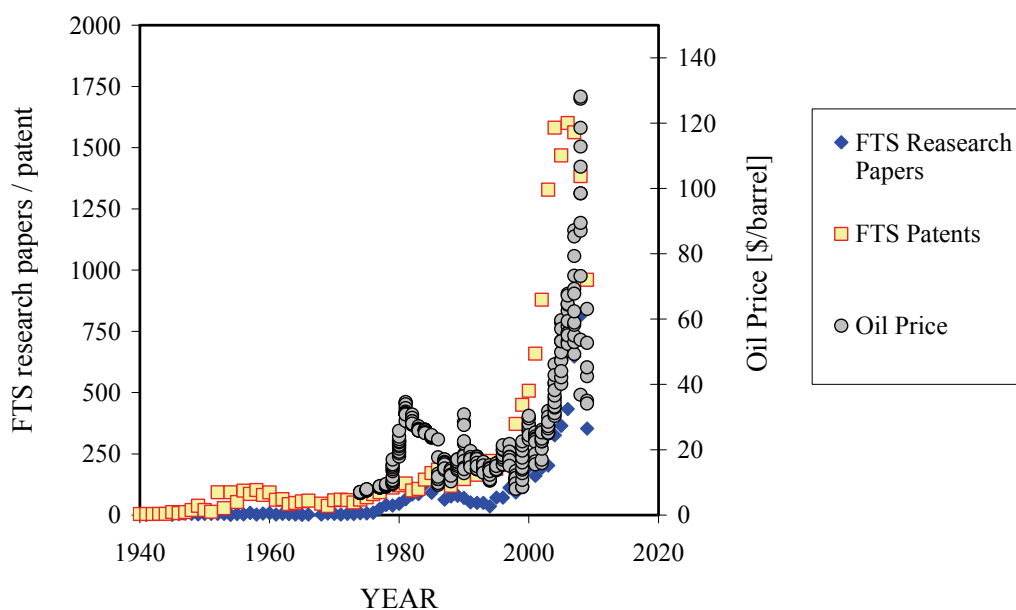


Figure 1.2: Relationship between the number of Fischer-Tropsch publications and the crude oil price. Source: www.oil-price.net for the oil price data and Scopus search for the keyword “Tropsch” for the data on publications.

Although the FT technology has been around since the 1920’s and has been successfully commercialized, there is still a challenge to improve its selectivity. To accomplish this, a fundamental understanding of the reaction mechanism is required which allow for better design of catalysts. The mechanism is still a subject of great debate in the literature.

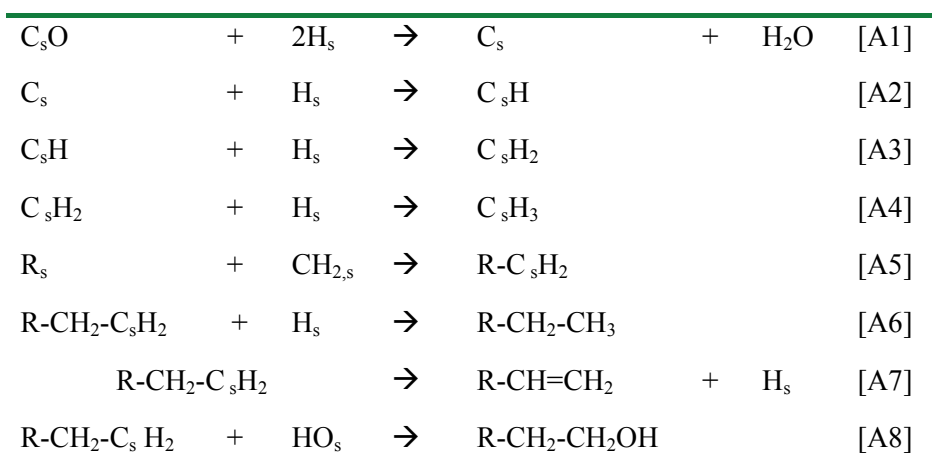
1.2. Fischer-Tropsch mechanisms

The High Temperature Fischer-Tropsch (HTFT) process comprises a complex network of elementary reaction steps. These steps need to include the formation of CO_2 , carbon and oxygenates (alcohols, acids, aldehydes and ketones) at these conditions. To date, mechanisms in literature do not fully

explain the product distribution of the HTFT process. With advanced in-situ techniques available, many of the older mechanisms have been modified. The following sections provide a brief description of the main mechanisms reported. Review articles [6-8] (and references therein) provide more details on these mechanisms.

The carbide mechanism

The carbide mechanism, also referred to as the alkyl mechanism, was initially developed by Fischer and Tropsch [9]. The reaction steps, A1-A8, are the main pathways for this mechanism. The initiation steps (A1-A4) begins with the successive hydrogenation of surface carbon, C_s . The C_sH_3 surface species is regarded as the chain initiator whilst the C_sH_2 species is the monomer. Chain growth is by successive incorporation of the monomer (example A5). This mechanism explains the formation of n-paraffins by H-addition (A6) and α -olefins by β -H-abstraction (A7) but not the formation of branched hydrocarbons and oxygenates [10].



Schulz et al. [11] proposed a reaction pathway analogous to the carbide mechanism (see Figure 1.3), for the formation of branched hydrocarbons. This involves the reaction of an alkylidene surface species and methyl surface species. The branched alkyl species undergo similar reactions to those proposed for n-alkyl surface species. Johnston and Joyner [12] proposed the involvement of surface hydroxyl groups in the formation of oxygenates. The coupling of a surface hydroxyl group with an alkyl group may lead to the formation of alcohols (A8). However, more experimental evidence is required to verify this reaction pathway.

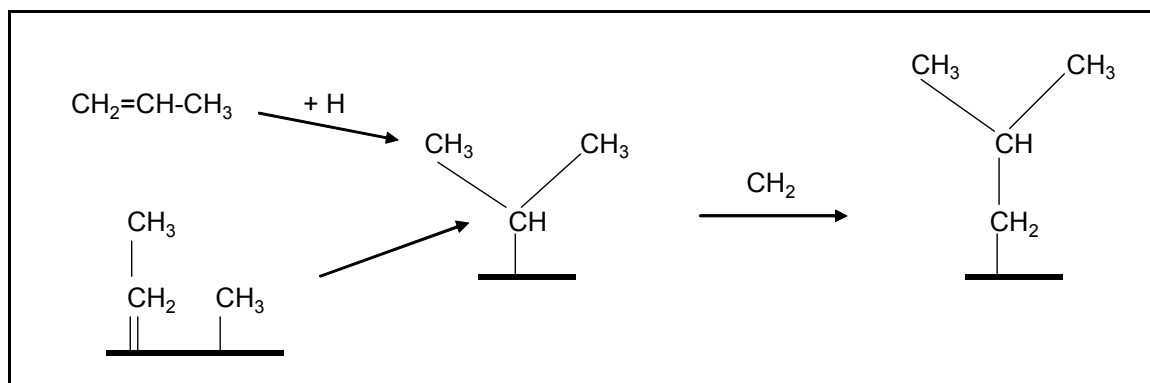
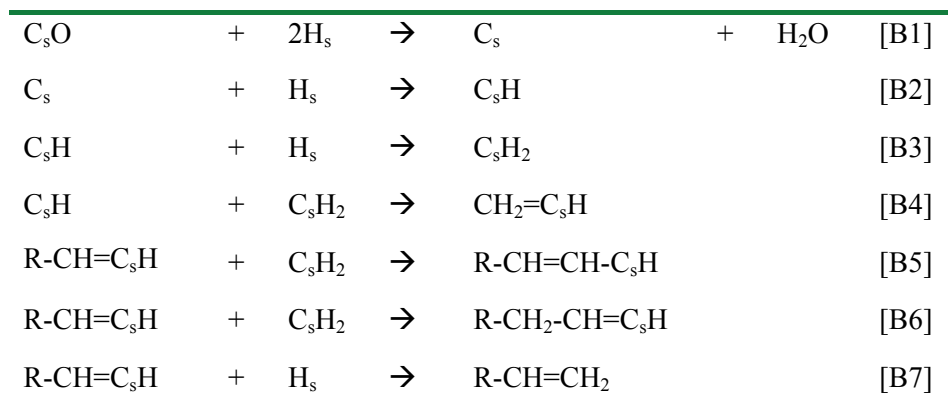


Figure 1.3. Proposed reaction pathways for the formation of branched hydrocarbons in the FTS, according to Schulz et al. [1990].

The Alkenyl mechanism

Maitlis and his co-workers [13-18] proposed the alkenyl mechanism to predict the formation of olefins in the FTS. The initiation steps (B1-B3) are identical to the carbide mechanism. The formation of the first C-C bond occurs through the coupling of methylidyne and methylene to form a vinyl surface species (see step B4). This surface species, $\text{CH}_2=\text{CH}_s$, is considered the chain initiator in this mechanism. Chain propagation occurs through the

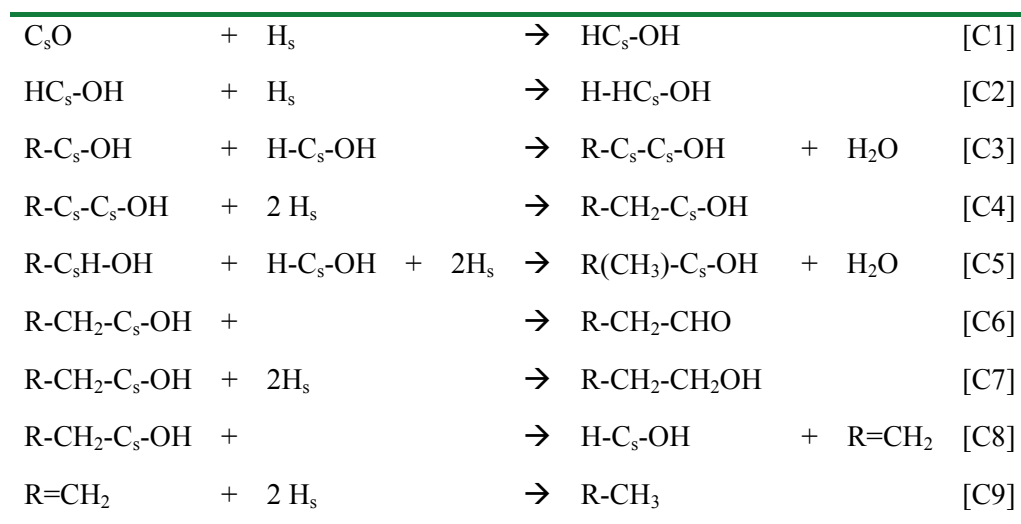
addition of a methylene species to a surface alkenyl species yielding a surface allyl species, which is followed by isomerisation yielding alkenyl species (steps B5 and B6). Product desorption involves H-addition to an alkenyl species resulting in α -olefins.



Ndlovu *et al.* [19] tested the isomerisation reported by Maitlis and his co-workers using organometallic compounds. They reported no observed isomerisation and went on to refute the alkenyl mechanism. However, this was later retracted [20] stating that their results were based on poorly characterised model compounds. Claeys and Van Steen [10] state that the alkenyl mechanism fails to explain the formation of n-paraffins and oxygenates. However, if the formation of the olefin is feasible, then it is conceivable that the corresponding paraffin can also form, either by hydrogenation of the olefin intermediate or via readsorption of the olefin and subsequent hydrogenation.

The Enol mechanism

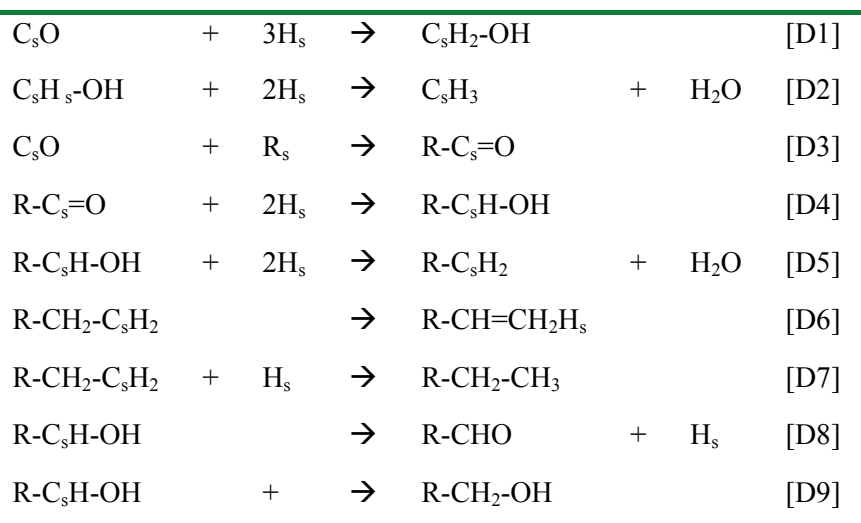
Storch [21] proposed the enolic theory in which the reaction pathways (C1-C8) involve oxygen containing surface species (enol). This mechanism accounts for the formation of oxygenates (alcohols, aldehydes, acids and esters), olefins and paraffins. In this mechanism, an associatively adsorbed linear CO molecule is partially hydrogenated (see step C1). Chain growth occurs through a condensation reaction between enol species, resulting in the elimination of water. Branched hydrocarbons involve the reaction of a R-CH_s-OH surface species (C5). Aldehydes and alcohols may result from desorption and dehydrogenation of the alcohol-like groups at the surface (steps C6 and C7). Acids may result from Cannizzaro reactions of the so formed aldehyde-like groups, or by reactions of carbon monoxide with water or alcohols. Esters can be produced by subsequent reactions. The decomposition of the adsorbed alcohol-like intermediates results in the formation of olefins and paraffins (steps C8 and C9).



The pitfall of this mechanism is that the formation of n-paraffins is only by secondary hydrogenation of primarily formed olefins. Therefore the primary formation of n-paraffins requires an alternative reaction pathway.

The CO-insertion mechanism

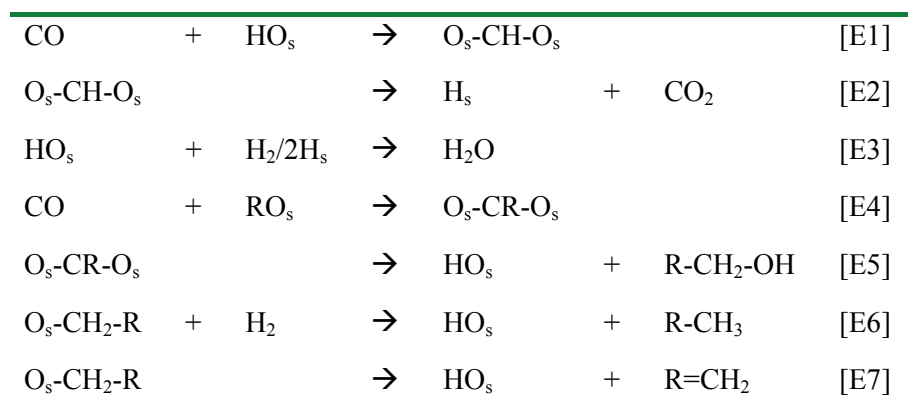
The CO-insertion mechanism, in which chemisorbed CO is the monomer, was originally proposed by Sternberg and Wender [22] and later fully formulated by Pichler and Schultz [23]. The chain initiator is thought to be the surface methyl species, C_sH_3 . Chain growth occurs by CO-insertion in a metal-alkyl bond (D3) leading to a surface acyl species. In one of the termination reaction pathways, these oxygen containing species react with surface hydrogen to give alcohols (D4). The reaction steps leading to the formation of n-paraffins and α -olefins are identical to the carbide mechanism (D6 and D7). The CO-insertion mechanism can also explain the formation of aldehydes and ketones.



Henrici-Olivé and Olivé [24] have confirmed most of these reaction steps and intermediates with homogeneous catalytic systems containing soluble transition metal complexes making the CO-insertion mechanism the main reaction pathway for the formation of oxygenates.

Other FT Mechanisms

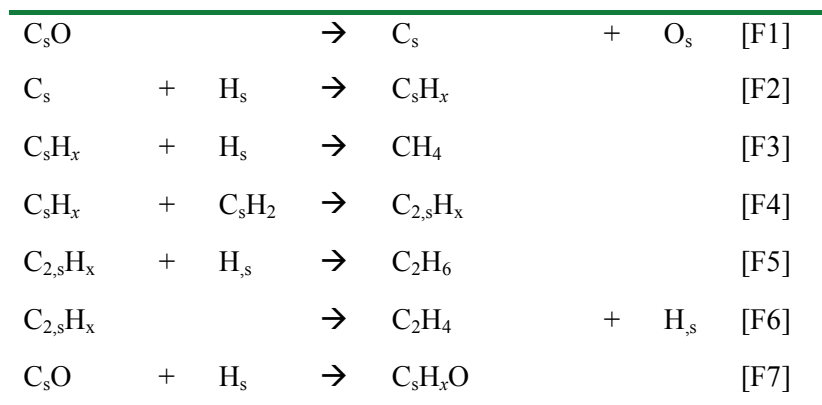
Frennet *et al.* [25,26] proposed a reaction scheme (E1-E7) for the CO-H₂ reaction based on the **formate** surface radical species. The formulation of the mechanism was based on chemical transient kinetics (CTK) and pulsed field desorption mass spectroscopy (PFDMS). The initiation step is the CO-insertion within a surface hydroxyl to form the formate species (E1). The progressive hydrogenation of that precursor may lead to methanol and to CH₄ formation. The hydrogenated carbon atom here bonds to an oxygen and not to the metal surface and may react with one CO molecule to form the first carbon---carbon bond. This insertion is of the same type as the one corresponding to the initiation step on the OH radical. The only difference is that here the H atom of that OH is replaced by a CH_x. Hence, the initiation step and the chain lengthening are of the same nature. In this scheme, the selectivity of hydrocarbons/oxygenates involves only one precursor. The oxygen atoms on the surface are also consumed to form water and carbon dioxide (see steps E2 and E3). The steps leading to the C₂₊ hydrocarbons, alcohols and alkenes, shown in steps E5 to E7, involve the formate radical and generate surface hydroxyls species as well.

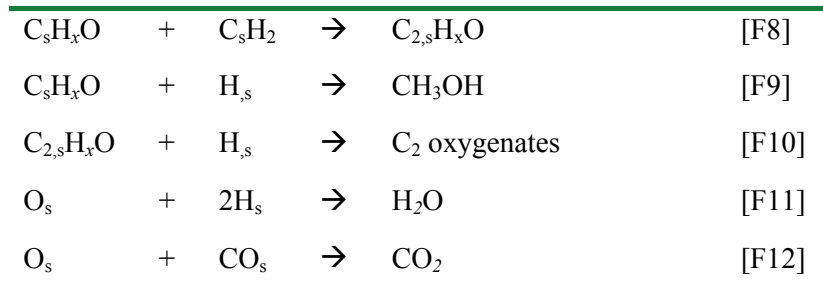


The formation of the hydroxyl surface species is not fully explained by Frennet. The most plausible reaction route, based on literature [27-30], is the reaction between adsorbed oxygen and adsorbed hydrogen (or H₂):

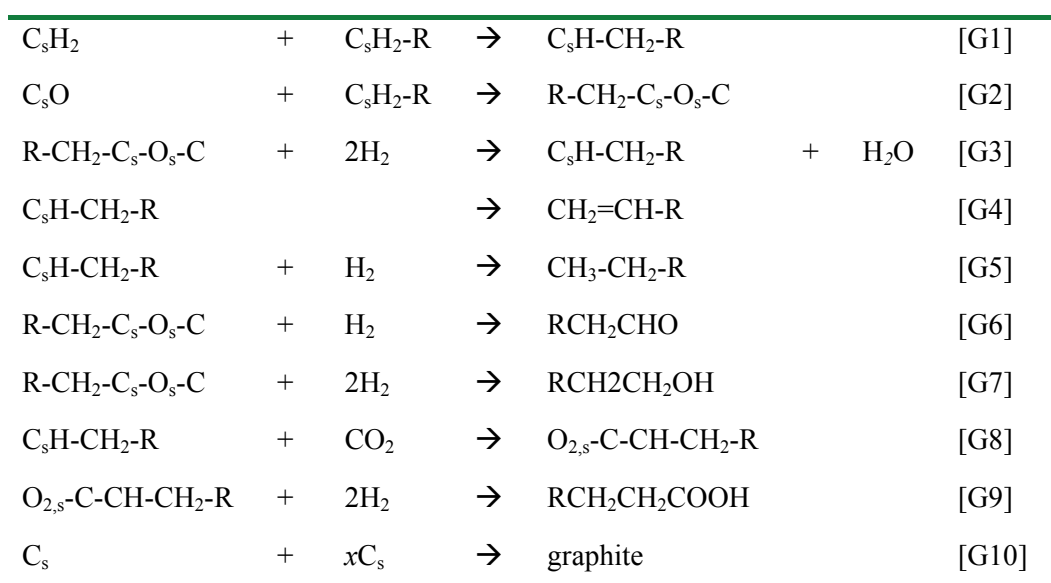


A mechanism for the synthesis of C₂₊ **oxygenates** on Rh catalysts was proposed by Chuang *et al.* [31]. In their original work [32,33], the reaction pathway (F1-F12) was developed using probe molecules (ethane, ethanol and acetaldehyde) under synthesis conditions (300°C; 10bar, H₂/CO = 1). The catalysts were chosen to show different activities to the hydrogenation, hydrogenolysis, dehydrogenation, decarbonylation, CH_x- and CO-insertion reactions rather than just CO dissociation. In this reaction pathway, the hydrogenation of CH_x/C₂H_x species to hydrocarbons (steps F3-F6) and the insertion of CO to produce C₂₊ oxygenates (steps F7-F10) are the chain termination reactions. Surface oxygen species are removed by hydrogenation and CO-insertion as well to produce water and carbon dioxide respectively (see F11 and F12).





Other researchers have proposed FT mechanisms based on combinations of the aforementioned mechanisms. For example, Dry [34] proposes that both CH_2 and CO insert at the carbon-metal bond to form two classes of surface intermediates as shown in reactions steps G1 and G2. Desorption or subsequent hydrogenation of these intermediates results in the formation of alkenes, alkanes, aldehydes and alcohols which are primary products (steps G4-G7). Dry observed a good correlation between the acid selectivity and the partial pressures of CO_2 and hence proposed the CO_2 insertion step (G8) and subsequent hydrogenation (step G9) to form acids. Bulk carbon or graphite is formed by the agglomeration of the surface C atoms as shown in step G10.



1.3. Challenges in elucidating the Fischer-Tropsch mechanism

The most challenging aspect of proving a specific Fischer-Tropsch mechanism is identifying the proposed surface intermediates at realistic Fischer-Tropsch conditions. The research group lead by Professor Burton Davis [35-39] have done extensive work on the use of isotopic tracers (mostly ^{14}C -labelled reactants) to elucidate the mechanism of the Fischer-Tropsch synthesis on iron-based catalysts. The work demonstrates the power of proper isotopic experiments but since it was done at low temperatures, only certain conclusions might be relevant to this thesis. Furthermore, one of the mechanistic uncertainties for the results based on ^{14}C -labelled experiments is that it was not possible to determine whether the ^{14}C -labelled species are added in the initiation or termination step. For this reason, the Steady-State Isotopic Transient Kinetic Analysis (SSITKA) technique has been chosen. This technique has been successfully utilized within this research group [40] to develop a mechanistic pathway for cobalt Fischer-Tropsch catalysts.

1.4. STEADY STATE isotopic transient kinetic analysis (SSITKA): Background

A steady state kinetic model can be applied if a time-invariant reaction rate is observed for fixed process conditions or if the process conditions are changed on a time scale much larger than the relaxation time of the catalytic reaction [41]. In contrast, a transient kinetic model (also called dynamic kinetic model) is needed if the process conditions are changed on a time scale similar to or smaller than the relaxation time of the reaction.

The rates of the elementary steps of CO hydrogenation are in the milliseconds range and require relaxation techniques with similar response times to measure their rate constants. Two popular techniques make use of step inputs and pulse inputs, viz., SSITKA and temporal analysis of products (TAP). Present TAP apparatuses have response times of 10 ms to 10 s [42] whilst SSITKA apparatuses have response times from 1 to 100 s [43].

The SSITKA technique was developed by Happel, Biloen and Bennett [44-46] for in-situ kinetic information about reaction mechanisms and reaction intermediates on the catalyst surface. An extensive review of the SSITKA methodology is given by Shannon and Goodwin [43]. In a nutshell, this technique keeps the catalyst under steady-state conditions and introduces an isotopic transient by abruptly replacing one reactant with its isotope. For example, a feed of $\text{H}_2/^{12}\text{CO}/\text{Ar}$ is switched to $\text{H}_2/^{13}\text{CO}/\text{He}$ with minimum disturbance to the system. The inert gas is also switched to determine the gas hold-up in the reactor. Apart from isothermal and isobaric reactor conditions, the surface composition of the catalyst does not change during SSITKA, making this technique ideal for reaction mechanistic studies.

The SSITKA technique has already been applied to numerous catalyzed reactions. These include the ammonia synthesis [47-50], CO oxidation [51,52], ethylene hydroformylation [53,54], methanation [55-58], methanol synthesis [59,60], methanol reforming [61], NO_x reduction [62-65], propene epoxidation [66] and most relevant to this study, the Fischer-Tropsch synthesis [58,67-91]. The relevant background literature is discussed in the various chapters of this thesis and hence not repeated here.

1.5. Hypothesis and key questions

In this study, SSITKA will be used to determine the mechanism of a Fe-based catalyst under HTFT conditions. The following key questions have been identified for this thesis:

1. Which is the principal monomer in the mechanism of the HTFT synthesis?
2. Which is the most abundant surface species during the HTFT synthesis?
3. Can the formation of olefins, paraffins, oxygenates and CO₂ be incorporated into a single FT mechanism?
4. How important is surface carbide, C_s, in the mechanism and kinetics of the HTFT synthesis?
5. How important is H₂O and CO₂ in the formation and/or consumption of C_s?
6. How important is the readsorption of 1-olefins or alcohols in the overall mechanism of the HTFT synthesis?
7. Is CO₂ formed by the reaction between CO and H₂O or can CO₂ be directly formed to a significant extent by the Boudouard reaction ($2\text{CO} \rightarrow \text{CO}_2 + \text{C}_s$)?

The hypothesis is that surface carbide, C_s, is formed and consumed at HTFT conditions and is converted to CH₂ by a series of consecutive irreversible hydrogenation steps. SSITKA can be used to show that this C_s plays an important role in the mechanism of the HTFT process on an Fe-based catalyst.

1.6. Aims and approach

Current mechanisms in literature fail to describe the product distribution of Fischer-Tropsch at higher temperatures. A combination of two or more mechanism can explain the product distribution but these mechanisms lack proper experimental evidence. Kinetic equations proposed have either been developed empirically or based on a mechanism, using a postulated rate determining step. Hence these expressions do not illustrate a uniform picture. Furthermore, the expressions for Fe-based catalysts have been developed at lower temperatures and thus have limitations at higher temperatures. Elementary reactions which are usually ignored at lower temperatures due to negligible rate coefficients must be considered at HTFT conditions. Moreover, it is expected that the rate determining step, usually assumed to be the formation of the monomer, would be different at these conditions.

The SSITKA technique can provide extensive insight into the surface reactions leading to detailed mechanistic and kinetic information. This technique has already been successful in providing a mechanistic pathway for a cobalt-based catalyst [40]. The current study is an extension of this work to higher temperatures over an Fe-based catalyst with the main aim being the development of the mechanistic pathway. Such a study on Fe-based catalysts at HTFT conditions is the first to our knowledge.

1.7. Thesis Outline

In Chapter 2, detailed experimental methodology is reported. The mechanistic models developed in gPROMS and its validation is also included in this chapter. In chapter 3, the carbonaceous intermediates on a fresh and carbided Fe catalyst are identified using isotopic transient methods,

specifically H₂-D₂ exchange reactions. A mechanistic pathway for methane formation under HTFT conditions is proposed in Chapter 4. The effect of co-fed ethene with ¹³CO SSITKA is discussed in Chapter 5. The methanation model is extended to account for the higher hydrocarbons (C₂-C₃'s) and presented in Chapter 6. Finally, a comparison between CO and CO₂ hydrogenation with ¹³CO and ¹³CO₂ SSITKA results is discussed in Chapter 7 and the conclusions and recommendations for future work are presented in Chapter 8.

References

- (1) M.E. Dry, *Appl. Catal. A* **189** (1999) 185-190.
- (2) H. Schulz, *Appl. Catal. A* **186** (1999) 3-12.
- (3) M.E. Dry, *ACS Div. Fuel Chem., Preprints* **48** (2003) 211.
- (4) M.E. Dry, *Catal. Today* **71** (2002) 227-241.
- (5) I. Wender, *Fuel proc. tech.* **48** (1996) 189-297.
- (6) C.K. Rofer-DePoorter, *Chem. Rev.* **81** (1981) 447-474.
- (7) B.H. Davis, *Fuel proc. tech.* **71** (2001) 157-166.
- (8) P.M. Maitlis, *J. Organo. Chem.* **689** (2004) 4366-4374.
- (9) F. Fischer and H. Tropsch, *Brennstoff-Chem.* **7** (1926) 97-104.
- (10) M. Claeys and E. Van Steen, *Stud.. Surf. Sci. Catal.* **152**, Elsevier, (2004) 601-680.
- (11) H. Schulz, E. Erich, H. Gorre and E. Steen, *Catal. Lett.* **7** (1990) 157-167.
- (12) O. Johnston and R. Joyner, *Stud.. Surf. Sci. Catal.* **75** Elsevier, (1993) 165.
- (13) P.M. Maitlis, H.C. Long, R. Quayoum, M.L. Turner and Z.Q. Wang, *J. Chem. Soc., Chem. Commun.* **1** (1996).

- (14) P.M. Maitlis and M.L. Turner, *Catal. Today* **65** (2001) 91-97.
- (15) P.M. Maitlis, R. Quyoum, H.C. Long and M.L. Turner, *Appl. Catal.* **A186** (1999) 363-374.
- (16) M.L. Turner, P.K. Byers, H.C. Long and P.M. Maitlis, *J. Am. Chem. Soc.* **115** (1993) 4417-4418.
- (17) J.M. Martinez, H. Adams, N.A. Bailey and P.M. Maitlis, *J. Chem. Soc., Chem. Commun.* (1989) 286-287.
- (18) H.C. Long, M.L. Turner, P. Fornasiero, J. Kašpar, M. Graziani and P.M. Maitlis, *J. Catal.* **167** (1997) 172-179.
- (19) S.B. Ndlovu, N.S. Phala, M. Hearshaw-Timme, P. Beagly, J.R. Moss, M. Claeys and E. Van Steen, *Catal. Today* **71** (2002) 343-349.
- (20) S.B. Ndlovu, N.S. Phala, M. Hearshaw-Timme, P. Beagly, J.R. Moss, M. Claeys and E. Van Steen, *Catal. Today* **78** (2003) 581.
- (21) H.H. Storch, N. Golumbic and R.B. Anderson, *The Fischer-Tropsch and Related Syntheses* (1951).
- (22) A.W. Sternberg and I. Wender, *Proc. Intern. Conf. on Coordin. Chem.* (1959) 53.
- (23) H. Pichler, H. Schulz and D. Kühne, *Brennstoff-Chem.* **49** (1968) 36.
- (24) G. Henrici-Olivé and S. Olivé, *J. Mol. Catal.* **24** (1984) 7-13.
- (25) A. Frennet, B. De, J.M. Bastin and N. Kruse, *J. Phys. Chem. B* **109** (2005) 2350-2359.
- (26) A. Frennet and C. Hubert, *J. Mol. Catal. A: Chem.* **163** (2000) 163-188.
- (27) D.K. Matsumoto and C.N. Satterfield, *Energy & Fuels* **3** (1989) 249-254.
- (28) M. Araki and V. Ponec, *J. Catal.* **44** (1976) 439-448.
- (29) R.W. Joyner, *J. Catal.* **50** (1977) 176-180.
- (30) J.G. McCarty and H. Wise, *J. Catal.* **57** (1979) 406-416.
- (31) S.S.C. Chuang, J. Stevens and R. Khatri, *Top. Catal.* **32** (2005) 225-232.
- (32) S.C. Chuang, Y.H. Tian, J.G. Goodwin and I. Wender, *J. Catal.* **96** (1985) 396-407.
- (33) S.C. Chuang, J.G. Goodwin and I. Wender, *J. Catal.* **92** (1985) 416-421.
- (34) M.E. Dry, *Catal. Today* **6** (1990) 183-206.

- (35) A. Sarkar, R. Keogh, S. Bao and B. Davis, *Catal. Lett.* **120** (2008) 25-33.
- (36) B. Shi, G. Jacobs, D. Sparks and B.H. Davis, *Fuel* **84** (2005) 1093-1098.
- (37) L.M. Tau, H.A. Dabbagh, J. Halasz and B.H. Davis, *J. Mol. Catal.* **71** (1992) 37-55.
- (38) L.M. Tau, H.A. Dabbagh and B.H. Davis, *Energy & Fuels* **5** (1991) 174-179.
- (39) B.H. Davis, *Catal. Today* **141** (2009) 25-33.
- (40) H.A.J. Van Dijk, *A mechanistic study using transient isotopic tracing*, Ph.D thesis, 2001, Technische Universiteit Eindhoven, Eindhoven, the Netherlands. <http://alexandria.tue.nl/extra2/200111083.pdf>
- (41) R.H. Nibbelke, *Steady State, Transient and Non-Linear Kinetics in Automotive Exhaust Gas Catalysis*, Ph.D thesis, 1998, Technische Universiteit Eindhoven, Eindhoven, the Netherlands.
- (42) J. Perez-Ramirez and E.V. Kondratenko, *Catal. Today* **121** (2007) 160-169.
- (43) S.L. Shannon and J. Goodwin, *Chem. Rev.* **95** (1995) 677-695.
- (44) J. Happel, *Chem. Eng. Sci.* **33** (1978) 1567.
- (45) P. Biloen, *J. Mol. Catal.* **21** (1983) 17-24.
- (46) C.O. Bennett, in: *Understanding Heterogeneous Catalysis through the Transient Method*, eds. A.T. Bell and L.L. Hegedus, Catalysis under Transient Conditions, American Chemical Society, (1982) 1-32.
- (47) J.U. Nwalor and J.G. Goodwin, *Top. Catal.* **1** (1994) 285-293.
- (48) R.J. Davis and B.C. McClaine, *J. Catal.* **210** (2002) 387-396.
- (49) B.C. McClaine and R.J. Davis, *J. Catal.* **211** (2002) 379-386.
- (50) B.C. McClaine and R.J. Davis, *J. Catal.* **210** (2002) 387-396.
- (51) A. Sirijaruphan, J. Goodwin, R.W. Rice, D. Wei, K.R. Butcher, G.W. Roberts and J.J. Spivey, *Appl. Catal. A* **281** (2005) 1-9.
- (52) S.S. Pansare, J. Goodwin and A. Sirijaruphan, *J. Catal.* **234** (2005) 151-160.
- (53) M.W. Balakos and S.S.C. Chuang, *J. Catal.* **151** (1995) 266-278.
- (54) M.W. Balakos and S.S.C. Chuang, *J. Catal.* **151** (1995) 253-265.
- (55) Y. Soong and P. Biloen, *Langmuir* **1** (1985) 768-770.
- (56) Y. Soong, K. Krishna and P. Biloen, *J. Catal.* **97** (1986) 330-343.

- (57) I.G. Bajusz, D.J. Kwik and J.G. Goodwin Jr, *Catal. Lett.* **48** (1997) 151-157.
- (58) G.J. Haddad, B. Chen and J. Goodwin, *J. Catal.* **161** (1996) 274-281.
- (59) S.H. Ali and J. Goodwin, *J. Catal.* **170** (1997) 265-274.
- (60) S.H. Ali and J. Goodwin, *J. Catal.* **171** (1997) 339-344.
- (61) J. Papavasiliou, G. Avgouropoulos and T. Ioannides, *Appl. Catal. B: Environ.* **88** (2009) 490-496.
- (62) E.M. Sadovskaya, A.P. Suknev, L.G. Pinaeva, V.B. Goncharov, B.S. Bal'zhinimaev, C. Chupin, R. Pérez and C. Mirodatos, *J. Catal.* **225** (2004) 179-189.
- (63) R. Burch, A.A. Shestov and J.A. Sullivan, *J. Catal.* **182** (1999) 497-506.
- (64) R. Burch, A.A. Shestov and J.A. Sullivan, *J. Catal.* **186** (1999) 353-361.
- (65) R. Burch, A.A. Shestov and J.A. Sullivan, *J. Catal.* **188** (1999) 69-82.
- (66) T.A. Nijhuis, E. Sacaliuc-Parvulescu, N.S. Govender, J.C. Schouten and B.M. Weckhuysen, *J. Catal.* **265** (2009) 161-169.
- (67) E. Rytter, S. Eri, T.H. Skagseth, D. Schanke, E. Bergene, R. Myrstad and A. Lindvåg, *IECR* **46** (2007) 9032-9036.
- (68) J. Panpranot, J. Goodwin and A. Sayari, *J. Catal.* **211** (2002) 530-539.
- (69) M. Rothaemel, K.F. Hanssen, E.A. Blekkan, A. Holmen and D. Schanke, *Catal. Today* **40** (1998) 171-179.
- (70) K. Sudsakorn, J. Goodwin and A.A. Adeyiga, *J. Catal.* **213** (2003) 204-210.
- (71) N. Lohitharn and J. Goodwin, *J. Catal.* **260** (2008) 7-16.
- (72) M. Rothaemel, K.F. Hanssen, E.A. Blekkan, A. Holmen and D. Schanke, *Catal. Today* **38** (1997) 79-84.
- (73) F. Rohr, O.A. Lindvag, A. Holmen and E.A. Blekkan, *Catal. Today* **58** (2000) 247-254.
- (74) N. Lohitharn and J. Goodwin, *J. Catal.* **257** (2008) 142-151.
- (75) N.S. Govender, F.G. Botes, M.H.J.M. de Croon and J.C. Schouten, *J. Catal.* **260** (2008) 254-261.
- (76) T. Van de Vin, *A mechanistic study of the High Temperature Fischer-Tropsch process using SSITKA - C₂₊ formation*, Masters graduation report, 2007, Technische Universiteit Eindhoven, Eindhoven, the Netherlands.

- (77) F. Rohr, A. Holmen, K.K. Barbo, P. Warloe and E.A. Blekkan, *Stud. Surf. Sci. Catal.* **119** (1998) 107-112.
- (78) P.B. Radstake, J.P. Breejen, G.L. Bezemer, J.H. Bitter, K.P. Jong, V. Frøseth and A. Holmen, *Stud. Surf. Sci. Catal.* **167**, (2007) 85-90.
- (79) F. Rohr, A. Holmen and E.A. Blekkan, *ACS, Div. Petr. Chem., Preprints* **44** (1999) 73-75.
- (80) H.A.J. Van Dijk, J.H.B.J. Hoebink and J.C. Schouten, *Stud. Surf. Sci. Catal.* **130 A** (2000) 383-388.
- (81) H.A.V. Van Dijk, J.H.B.J. Hoebink and J.C. Schouten, *Chem. Eng. Sci.* **56** (2001) 1211-1219.
- (82) V. Frøseth, S. Storsæter, O. Borg, E.A. Blekkan, M. Rønning and A. Holmen, *Appl. Catal. A* **289** (2005) 10-15.
- (83) K.F. Hanssen, E.A. Blekkan, D. Schanke and A. Holmen, *Stud. Surf. Sci. Catal.* **109** (1997) 193-202.
- (84) C.A. Mims and L.E. McCandish, *J. Am. Chem. Soc.* **107** (1985) 696-697.
- (85) C.J. Bertole, C.A. Mims and G. Kiss, *J. Catal.* **223** (2004) 309-318.
- (86) C.J. Bertole, C.A. Mims and G. Kiss, *J. Catal.* **210** (2002) 84-96.
- (87) C.A. Mims and L.E. McCandish, *J. Phys. Chem.* **91** (1987) 929-937.
- (88) L.E. McCandish and C.A. Mims., Isotopic Transient studies of the Fischer-Tropsch reaction, *AIChE National meeting* (1985).
- (89) C.J. Bertole, C.A. Mims, G. Kiss and P. Joshi, *Stud. Surf. Sci. Catal.* **136** (2001) 369-374.
- (90) C.J. Bertole, C.A. Mims and G. Kiss, *J. Catal.* **221** (2004) 191-203.
- (91) C.A. Mims and C.J. Bertole, *Stud. Surf. Sci. Catal.* **136** (2001) 375-380.

2

Experimental methodology and model development

In this chapter, details about the experimental procedures for each of the main chapters are reported. The modelling software, gPROMS, used in this study is evaluated and shown to be a robust tool for the estimation of parameters in complex simulation models such as those for the description of Steady-State Isotopic Transient Kinetic Analysis (SSITKA) experiments during the Fischer-Tropsch (FT) synthesis reaction. A kinetic FT model is presented that is implemented in gPROMS and validated using the kinetic data from a previous study [1-3] for the formation of ethane during the Fischer-Tropsch synthesis. gPROMS model simulation results show that the predicted gas-phase and catalyst surface concentrations are similar as previously reported. Two kinetic rate parameters are also re-optimised using the parameter estimation tool box in gPROMS, and the results are comparable to the previous work.

2.1. The SSITKA Setup

A typical SSITKA system consists of two reactant streams, a 4-port switching valve, a reactor, a gas chromatograph (GC) and a mass spectrometer (MS) as shown in Figure 2.1

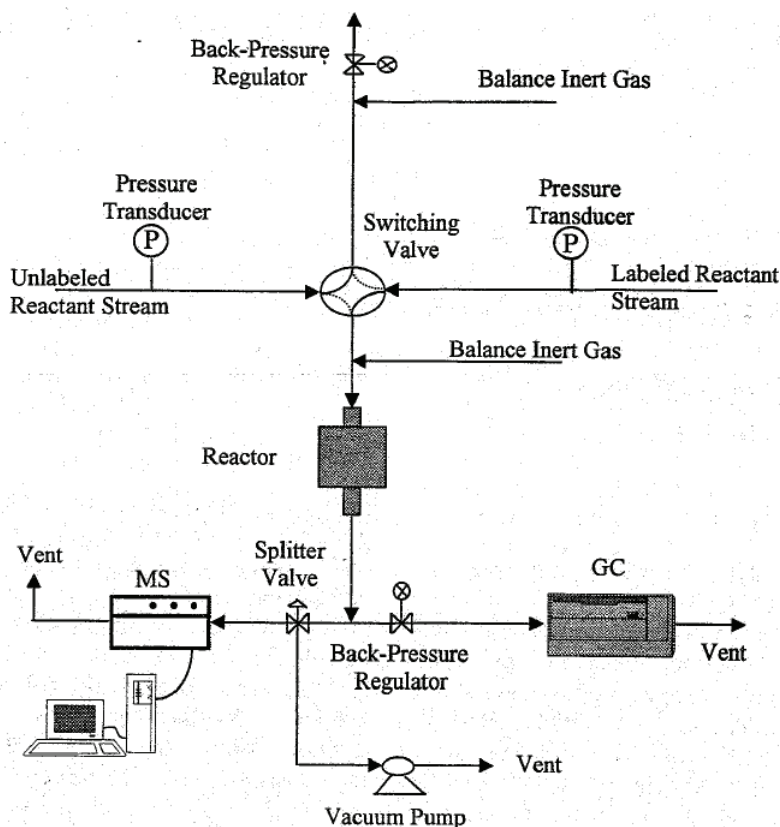


Figure 2.1: Schematic of a typical SSITKA setup [4]

For most reactions, this would be sufficient for proper analysis. However, for the Fischer-Tropsch reaction a MS alone is not sufficient for the isotopic analysis. Hence, in our system we also include an online GC-MS (see Figure 2.2) for isotopic analysis of the larger molecules which cannot be easily detected by the MS [5,6].

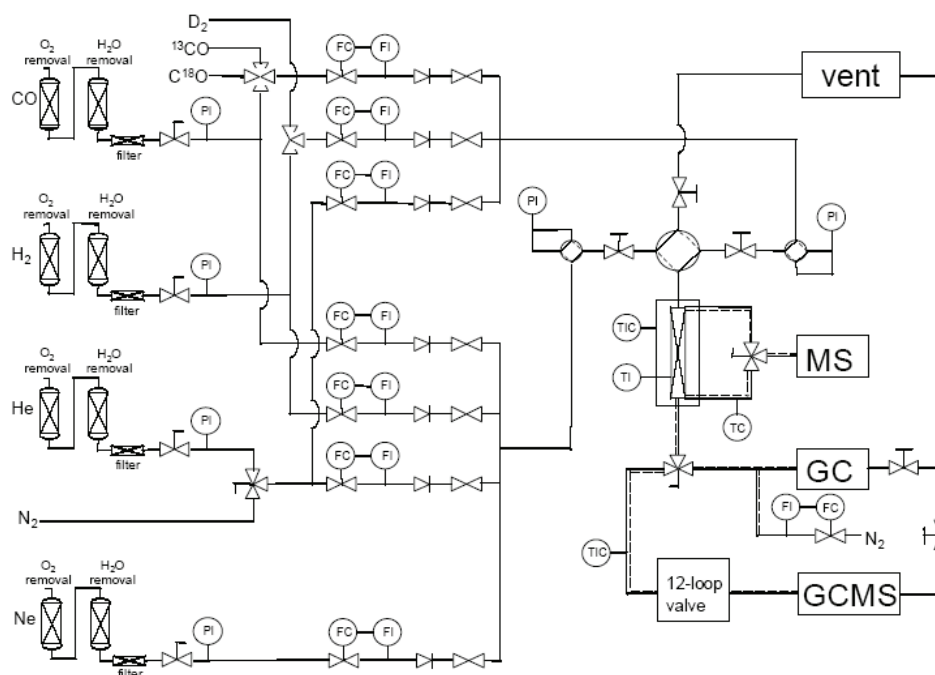


Figure 2.2: Schematic of the SSITKA setup used in this work.

2.2. The catalyst

The catalyst is prepared by co-precipitation of the metal nitrates as described by Espinoza *et al.* [7]. The catalyst used in this study was supplied by Sasol Technology Research and Development and contains only potassium as a promoter. The exact composition is not mentioned due to confidentiality. The surface area measured by N₂ physisorption is 27 m²·g_{cat}⁻¹, which is in the range specified by Espinoza *et al.* [7] for this type of Fe-based catalyst.

2.3. Catalyst loading, reduction and activation

Typically 0.5-1.0 gram of Fe/K catalyst (150-250 μm) is weighed and mixed with 1.0-2.5 gram of SiC (250-300 μm) to create the catalyst bed (~ 20 mm). The catalyst is reduced with a mixture of H_2 and Ar flow (both 40 ml min^{-1}) at 420 $^\circ\text{C}$ and 1.2 bar for 16 hours. After the reduction the reactor is cooled down to the synthesis temperature, 330 $^\circ\text{C}$, under an Ar flow. At 330 $^\circ\text{C}$ the Fischer-Tropsch synthesis is started by introducing H_2 and CO flows. These flows are varied to obtain different H_2/CO feed ratios and gas hourly space velocities (GHSV) in the experiments. The catalyst mass is varied to obtain a different GHSV.

2.4. Catalyst characterisation

2.4.1. In-situ temperature programmed hydrogenation

The Fischer-Tropsch reaction was abruptly stopped by switching between the synthesis gas feed and an inert. The reactor was cooled down as fast as possible to 30 $^\circ\text{C}$ whilst purging the system with inert. After sufficient purging to remove the chemisorbed species, the reactor temperature was ramped, typically at 5 $^\circ\text{C}\cdot\text{min}^{-1}$ to a maximum attainable temperature of 450 $^\circ\text{C}$ whilst feeding a mixture of 50% H_2 in Ar. The product gases, mainly CH_4 , H_2O and CO_2 and the reactants H_2 and CO were continuously monitored with the online mass spectrometer.

2.4.2. In-situ isothermal hydrogenation

The aforementioned procedure was followed to stop the Fischer-Tropsch reaction. However, here the reactor was kept at the synthesis temperature whilst purging with an inert to remove the chemisorbed species. Thereafter, a 50% mixture of H₂/Ar was fed into the reactor and the product gases, mainly CH₄, H₂O and CO₂ and the reactants H₂ and CO were continuously monitored with the online MS.

2.4.3. Ex-situ temperature programmed surface reactions

A Temperature Programmed Reactor system with on-line mass spectroscopy was used for the Temperature Programmed Hydrogenation (TPH) and Temperature Programmed Oxidation (TPO) experiments. Typically, 0.20 g of the spent Fe catalyst was loaded into a quartz tube reactor at room temperature. The temperature was increased to 100°C at 10 °C.min⁻¹ and held until any moisture in the system was removed and the correct vacuum condition was obtained. Thereafter, it was ramped to 270°C at 5 °C.min⁻¹ and held at 270°C for 60 min. The final stage was ramping to 800°C at 2 °C.min⁻¹ and holding for 60 min. The reactor was then allowed to cool to room temperature. The feed gases (total flow of 40 ml.min⁻¹) were 50 vol.% H₂/He and 10 vol.% O₂/He for the TPH and TPO experiments, respectively.

2.5. Surface characterisation using isotopic methods

2.5.1. Transients at the start of the Fischer-Tropsch reaction

In these experiments, the reactor was cooled to the synthesis temperature in flowing Ar after the catalyst reduction. The synthesis was started by a fast switch from Ar to a H₂/CO or D₂/CO mixture which resulted in transients of the reactants and products. This was performed with minimal disturbances in the reactor pressure. The reactant and product transients were captured with the online MS and online GCMS.

2.5.2. CO disproportionation

The carbon is deposited on a freshly reduced catalyst by the disproportionation of ¹³C¹⁸O at 330°C and 1.2 bar :



The catalyst surface, covered with ¹³C_{ads} and ¹³CO₂, is then exposed to a mixture of H₂/CO initiating the Fischer-Tropsch synthesis. The incorporation of ¹³C in the products is measured with the online MS and GCMS.

2.5.3. SSITKA experiments

For a SSITKA experiment, an abrupt switch was made from a normal feed (for example H₂/¹²CO/Ar) to one with an isotopically labelled reactant, for example H₂/¹³CO/Ar/Ne in the case of ¹³CO SSITKA. In some experiments, Kr was used instead of Ne as the inert. This was mainly due to the lack of Ne at the time of these experiments and also the preference of Kr for deuterium experiments (to avoid overlapping of fragmentation patterns).

2.5.4. H₂/D₂ tracing or Deuterium flushing

H₂/D₂ exchange reactions were carried out similar to the aforementioned SSITKA experiments. An abrupt switch was made using a Valco 4-way switching valve, allowing one feed (H₂/CO/Ar) to bypass the reactor to the vent line and another feed (D₂/CO/Ar/Ne) to enter the reactor. The resulting transients were captured with the online MS for the smaller molecules and the online GCMS for the heavier products. The overlapping of the fragmentation patterns going from CH₄ to CD₄ using the online MS is well known in the literature. The correction for the contribution of H₂O to the methane signals has been discussed in previous work [3].

2.5.5. Co-fed ethylene experiments

The same procedure as above was followed for the reduction and pre-treatment. Once steady-state conditions (based on constant CO conversion) were reached, an abrupt switch was made from the normal feed (H₂/CO/Ar) to a mixture of (1 mol% C₂H₄ in H₂)/CO/Ar. The inlet partial pressures of H₂ and CO were kept constant by reducing the flow of Ar to compensate for the 1 mol% C₂H₄ added.

2.5.6. Co-fed ethylene experiments with ¹³CO SSITKA

In these experiments, an abrupt switch was made as follows: 1 mol% C₂H₄ in H₂/CO/Ar → 1 mol% C₂H₄ in H₂/¹³CO/Ar. The resulting transients were then monitored with the online MS and GCMS as described in sections 2.6.2 and 2.6.3.

2.6. Data analysis and treatment

2.6.1. Steady-state results

The steady state performance of the catalyst was monitored online by a Varian CP-3800 Gas Chromatograph consisting of one thermal conductivity detector (TCD) and two Flame Ionization detectors (FID). The unreacted feed and some hydrocarbon products (N₂, H₂, CO, CO₂, and CH₄) were analyzed by the TCD, whilst C₁ to C₅ hydrocarbons were analyzed by the FID.

2.6.2. Transients using the online Mass Spectrometer

A Balzers ThermoStarTM (GSD 301T) mass spectrometer was used to monitor the reactants (H₂ and CO), inerts (Ar and Ne), and small molecular weight products (for example CH₄ and CO₂). The m/e values used in our experiments were 2, 15, 17, 22, 28, 29, 40, 44, and 45 for H₂, ¹²CH₄, ¹³CH₄, Ne, ¹²CO, ¹³CO, Ar, ¹²CO₂, and ¹³CO₂. The transient responses are normalized between the initial MS intensity before the isotopic step change and the final MS intensity at the moment in time when the unlabeled atom in all surface and gas phase species is replaced by its labeled counterpart, as shown in equation 1 in the case of the inert Ne:

$$I_{Ne,N} = \frac{I_{Ne,t} - I_{Ne,min}}{I_{Ne,max} - I_{Ne,min}} \quad [2]$$

where $I_{Ne,N}$ is the normalized transient of Ne, $I_{Ne,t}$ is the MS intensity of Ne, $I_{Ne,max}$ is the maximum MS intensity of Ne, and $I_{Ne,min}$ is the minimum MS intensity of Ne.

2.6.3. Transients using the online GCMS

The transients of the smaller hydrocarbons (CH₄ and CO₂) and permanent gases (H₂, CO, Ne, Ar) were captured using the online MS as described in the aforementioned section. For the heavier hydrocarbons, an online GCMS (Shimadzu GCMS-QP 2010) was used. The non-, partially and fully labelled Fischer-Tropsch products are produced after the switch to the isotopically labelled reactant. The fragmentation pattern of each product is a linear combination of the fragmentation patterns of the corresponding isotopic product. This contribution can be calculated by minimizing the objective function,

$$S(x) = \sum_{i=1}^m \left(\sum_j^n (x_{ij} f_{ij}^{ref}) - f_i^{obs} \right)^2 \xrightarrow{x} \text{minimum} \quad [3]$$

in which $S(x)$ is the objective function, m is the number of m/e values of the fragmentation pattern of a given product, n is the number of isotopic combinations of a given product, x_{ij} is the fractional contribution of the j^{th} isotopic combination to the mixture at the i^{th} m/e value, f_{ij}^{ref} is the intensity of the fragmentation pattern of the j^{th} isotopic combination at the i^{th} m/e value and f_i^{obs} is the observed intensity of the fragmentation pattern of the mixture at the i^{th} m/e value. The fragmentation pattern for each isotopic product in the reaction mixture is required in order to apply this procedure. Van Dijk [3] provides detailed information on this calculation procedure for ¹³CO and D₂ - SSITKA experiments.

2.6.4. Reactor modeling

Happel [8] and Bennet et al. [9] showed that SSITKA experiments are optimal in plug flow reactors due to the fast isotopic step change. In a plug

flow regime, all changes relative to the inlet signal are ascribed to kinetics. The fixed-bed reactor used in this study is modeled as an isothermal and isobaric plug flow reactor. The total molar flow rate throughout the catalyst bed is assumed constant due to the low conversions.

Mass balances for only the labeled gaseous and surface species, represented by partial differential equations in time and space, are solved. The continuity equations for the labeled gaseous component $X^\#$ and the surface component $Y^\#$ are as follows:

$$\frac{\partial C_{X^\#}}{\partial t} + \frac{1}{\tau} \frac{\partial C_{X^\#}}{\partial x} = \frac{\rho}{\varepsilon_b} R_{W,X^\#} \quad [4]$$

$$\frac{\partial L_{Y^\#}}{\partial t} = R_{W,Y^\#} \quad [5]$$

The initial and boundary conditions for an isotopic step from gas-phase reactant Z to $Z^\#$ are as follows.

Initial conditions:

$$t = 0 \quad C_{X^\#} = L_{Y^\#} = 0 \quad \text{for any } x$$

Boundary conditions:

$$t > 0 \quad x = 0 \quad C_{Z^\#} = \text{input function, } f(t)$$

$$t > 0 \quad x = 0 \quad C_{X^\#} = 0 \quad \text{for } X^\# \neq Z^\# \quad [6]$$

where C_x [mol.m_g^{-3}] is the concentration of component X in the gas phase; L_Y [$\text{mol.kg}_{\text{cat}}^{-1}$] is the surface concentration of Y ; τ [s] is the residence time; t [s] is the time; ρ_b [$\text{kg}_{\text{cat}}/\text{m}_b^3$] is the density of the catalyst bed; ε_b [$\text{m}_g^3.\text{m}_b^{-3}$] is the catalyst bed porosity; $R_{W,X^\#}$ [$\text{mol.kg}_{\text{cat}}^{-1}.\text{s}^{-1}$] is the steady state production rate of X ; x is the dimensionless axial position in the catalyst bed.

The residence time τ can be calculated as:

$$\tau = \frac{\varepsilon_b V_R}{F_V} \quad [7]$$

where V_R [m_b^3] is the volume of the catalyst bed and F_V [$\text{m}_g^3 \cdot \text{s}^{-1}$] is the total volumetric flow rate at reaction temperature and pressure. The input function $f(t)$ is represented by the transient of the inert tracer. The optimal fit for the empirical input function used in this work is shown in Figure 2.3.

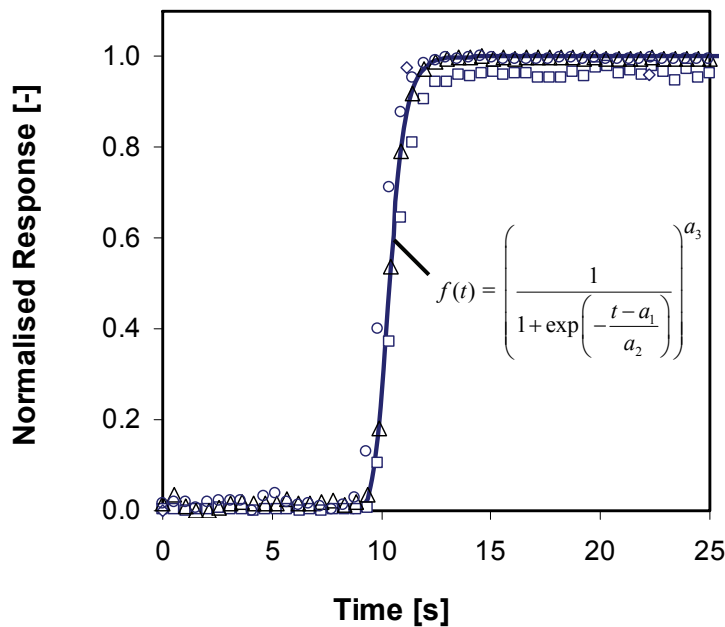


Figure 2.3: The optimal fit for the empirical function used in this study. The open markers (\circ , Δ , and \square) are Ne data collected during a SSITKA switch ($\text{H}_2/^{12}\text{CO}/\text{Ar} \rightarrow \text{H}_2/^{13}\text{CO}/\text{Ar}/\text{Ne}$) at $\text{H}_2/\text{CO} = 15$, 330°C , 1.2 bar , and $\text{GHSV} = 7412 \text{ ml.hr}^{-1} \cdot \text{g}_{\text{cat}}^{-1}$. The solid line is the optimal fit with $a_1 = 9.01$, $a_2 = 0.52$, and $a_3 = 10.81$.

2.6.5. Parameter estimation

The set of partial differential equations (equations 4 and 5) with its initial and boundary conditions (equation 6) is solved using the software package

gPROMS (general PROcess Modeling System). Parameter estimation in gPROMS {Process System Enterprise, 2005 2953 /id} uses a maximum likelihood objective function (equation 8) in which Φ is the objective function, N is the total number of measurements taken in all experiments, θ is the set of model parameters to be estimated, NE is the number of performed experiments, NV_i is the number of variables measured in experiment i , NM_{ij} is the number of measurements of variable j in experiment i , σ_{ijk}^2 is the variance of the k^{th} measurement of variable j in experiment i , \tilde{z}_{ijk} is the experimental value for the k^{th} measurement of variable j in experiment i , and z_{ijk} is the model prediction for the k^{th} measurement of variable j in experiment i .

$$\Phi = \frac{N}{2} \ln(2\pi) + \frac{1}{2} \min_{\theta} \left\{ \sum_{i=1}^{NE} \sum_{j=1}^{NV_i} \sum_{k=1}^{NM_{ij}} \left[\ln(\sigma_{ijk}^2) + \frac{(\tilde{z}_{ijk} - z_{ijk})^2}{\sigma_{ijk}^2} \right] \right\} \quad [8]$$

The principle of parameter estimation is based upon the minimization of the difference between the experimental values and the model predicted values (equation 9), in which ξ_i is the difference between experimental and predicted value for measurement i , \tilde{z}_i is the experimental value for measurement i , and $z_i(\theta)$ is the predicted value for measurement i .

$$\xi_i = \tilde{z}_i - z_i(\theta) \quad [9]$$

The maximum likelihood principle assumes ξ_i to be independent and normally distributed with zero mean and standard deviation σ_i . Several variance models that can describe the standard deviation for ξ_i are available in gPROMS. The constant variance model in which the measurement error has a constant standard deviation is used in our study.

2.7. Transient modelling of the Fischer-Tropsch synthesis using gPROMS

The mathematical description of SSITKA experiments involves a combination of partial differential equations (PDEs) expressing the transient responses and algebraic equations expressing the steady-state mole balances [3]. Nowadays the use of powerful computers and advanced modelling packages render easy and fast solutions to these type of equations. For example, our group has successfully utilized gPROMS (**g**eneral **P**rocess **M**odelling **S**ystem) for developing a model for the NO_x storage/reduction process in the presence of CO₂ [10].

The purpose of this part of the work is to demonstrate the capabilities of gPROMS for transient kinetic modelling, specifically for SSITKA experiments on the Fischer-Tropsch reaction. These types of models are not included in standard libraries provided by Process System Enterprise [11]. Here, we demonstrate the simulation and parameter estimation capabilities of gPROMS. The actual codes and details about the gPROMS language can be found in Appendix A. The results are compared to a previous study* [1-3]) in which the modelling was performed using FORTRAN.

* Fischer-Tropsch reaction using a cobalt-based catalyst.

2.7.1. Modeling description

2.7.1.1. Reactor configuration and reactor mechanism

A stainless steel tubular fixed bed reactor, shown in Figure 2.4, with an internal diameter of 7.0 mm and a bed length of 40.0 mm was used. The reactor contains a catalyst bed existing of Cobalt-based catalyst particles diluted with inert particles (SiC), placed between two sinter plates. Two sample chambers are present for online mass spectroscopy, one upstream and one downstream of the catalyst bed. The reaction mechanism chosen for this work, which was proposed by [3], is shown in Figure 2.5. The corresponding rate constants are reported in Table 2.1. In brief, this mechanistic model assumes two single-C species, denoted as $C_{\alpha,ads}$ and $C_{\beta,ads}$. The total fractional coverage of these surface species together with CO_{ads} was 90%. The experimental results indicated that the catalyst surface is heterogeneous towards the formation of methane and higher hydrocarbons.

The fixed-bed reactor used in this study is modelled as an isothermal and isobaric plug flow reactor. The total molar flow rate throughout the catalyst bed is assumed constant due to the low conversions (typically 5% for differential conditions).

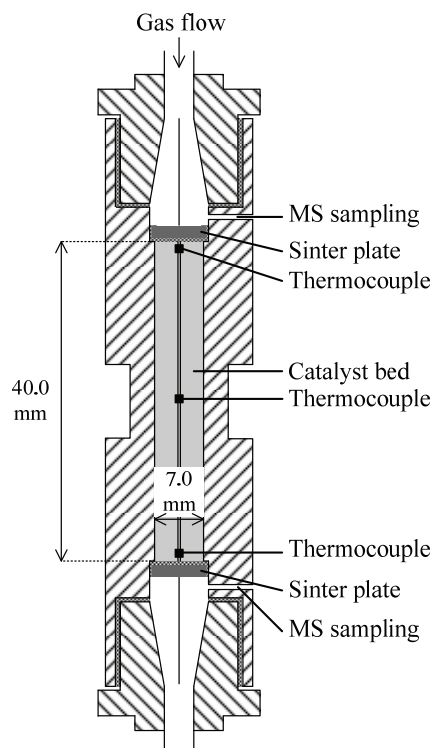


Figure 2.4: Schematic drawing of the reactor used for the SSITKA experiments in the previous work [3].

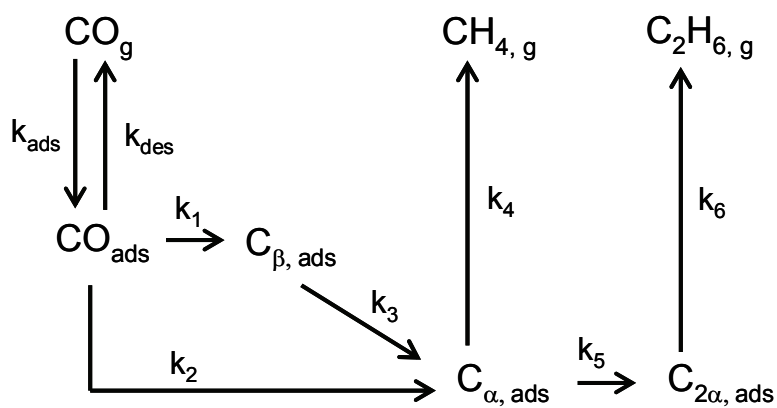


Figure 2.5: Mechanism for the formation of ethane during the Fischer-Tropsch synthesis as proposed in a previous study [3].

Table 2.1: Optimised kinetic rate parameters corresponding to the mechanism in **Figure 2.5** and calculated in a previous study [3]. Experimental conditions: 225°C, 1.2 bar, $W_{cat}.F^{-1} = 24.2 \text{ kg}_{cat}.s^{-1}.mole^{-1}$

k_{ads}	$m_g^3.kg_{cat}^{-1}.s^{-1}$	$5.9 \cdot 10^{-2}$
k_{des}	s^{-1}	9.0
k_1	s^{-1}	$7.2 \cdot 10^{-3}$
k_2	s^{-1}	$3.4 \cdot 10^{-3}$
k_3	s^{-1}	$3.3 \cdot 10^{-2}$
k_4	s^{-1}	$1.3 \cdot 10^{-1}$
k_5	$kg_{cat}.mole^{-1}.s^{-1}$	2.8
k_6	s^{-1}	$4.4 \cdot 10^{-1}$

Mole balances for the labelled gaseous and surface species, represented by partial differential equations in time and space, were solved (see equations 4 and 5)

2.7.2. Model validation

To validate our gPROMS model, the rate constants estimated in a previous study [3], presented in Table 2.1, corresponding to the mechanism in Figure 2.5, were fixed and the PROCESS was simulated. Steady-state and transient gas phase and surface concentrations were obtained as a function of time and reactor length. The transients for Ne, CO and CH₄ at the reactor outlet are presented in Figure 2.6a, and for clarity the transients for Ne and C₂H₆ are presented in Figure 2.6b. The fast exponential decay of the Ne transient with a time constant of 0.5 s and the delayed response of ¹³CO is correctly described as previously discussed by Van Dijk *et al.* [1]. The latter is caused by the reversible interaction of CO with the catalyst surface and is known as the chromatographic effect [12]. Furthermore, the earlier breakthrough of ¹³CH₄ compared to ¹³CO at the outlet of the reactor is also correctly described here.

This phenomenon is typical of a plug-flow reactor model and indicates the absence of any significant interaction of methane with the catalyst [3]. The predicted steady-state gas phase and surface concentrations, shown in Table 2.2, are similar to the previous work. Based on the aforementioned results, we conclude that the previous models describing the SSITKA experiments have been successfully reproduced in gPROMS.

Table 2.2: Calculated gas-phase and surface concentrations for the mechanism in Figure 2.5 obtained using the gPROMS model in this study. Values in brackets are from a previous work [3].

Gas phase concentration [mole.m _g ⁻³]		Surface concentrations [mole.kg _{cat} ⁻¹]	
CH ₄	2.51 10 ⁻¹ (2.53 10 ⁻¹)	CO	3.7 10 ⁻² (3.7 10 ⁻²)
C ₂ H ₆	1.47 10 ⁻² (1.53 10 ⁻²)	C _α	3.8 10 ⁻³ (3.8 10 ⁻³)
		C _β	2.7 10 ⁻³ (2.7 10 ⁻³)
		C _{2α}	4.5 10 ⁻⁵ (4.5 10 ⁻⁵)

2.7.3. Parameter quantification

To quantify the rate constants listed in Table 2.1 using gPROMS, the same set of experiments were chosen as used in the previous study [3]. The same modelling approach was also followed. The rate constants for the methanation reaction which were estimated in a separate model discrimination study [3] were fixed. The remaining two rates constants (k_5 and k_6) were then estimated. This approach helps to reduce the number of parameters to estimate. In gPROMS, the weighted residual is compared to the chi-squared value to determine the goodness of the fit. In our case, the obtained weighted residual (623) was lower than the chi-squared value (675), thus indicating a good fit. In comparison to the parameters in Table 2.1, the optimised parameters in this study, shown in Table 2.3, were within the 95% confidence

intervals. A 95% t-value is also calculated in gPROMS during parameter estimation. A 95% t-value for a parameter smaller than the reference t-value indicates that the data is not sufficient to estimate this parameter precisely implying more data points are required. In this study, the reference value was lower in both cases, thus indicating that sufficient data was used in our study. The simulated transients using the newly estimated rate constants are presented in Figure 2.7 with the experimental data points for comparison of the fit.

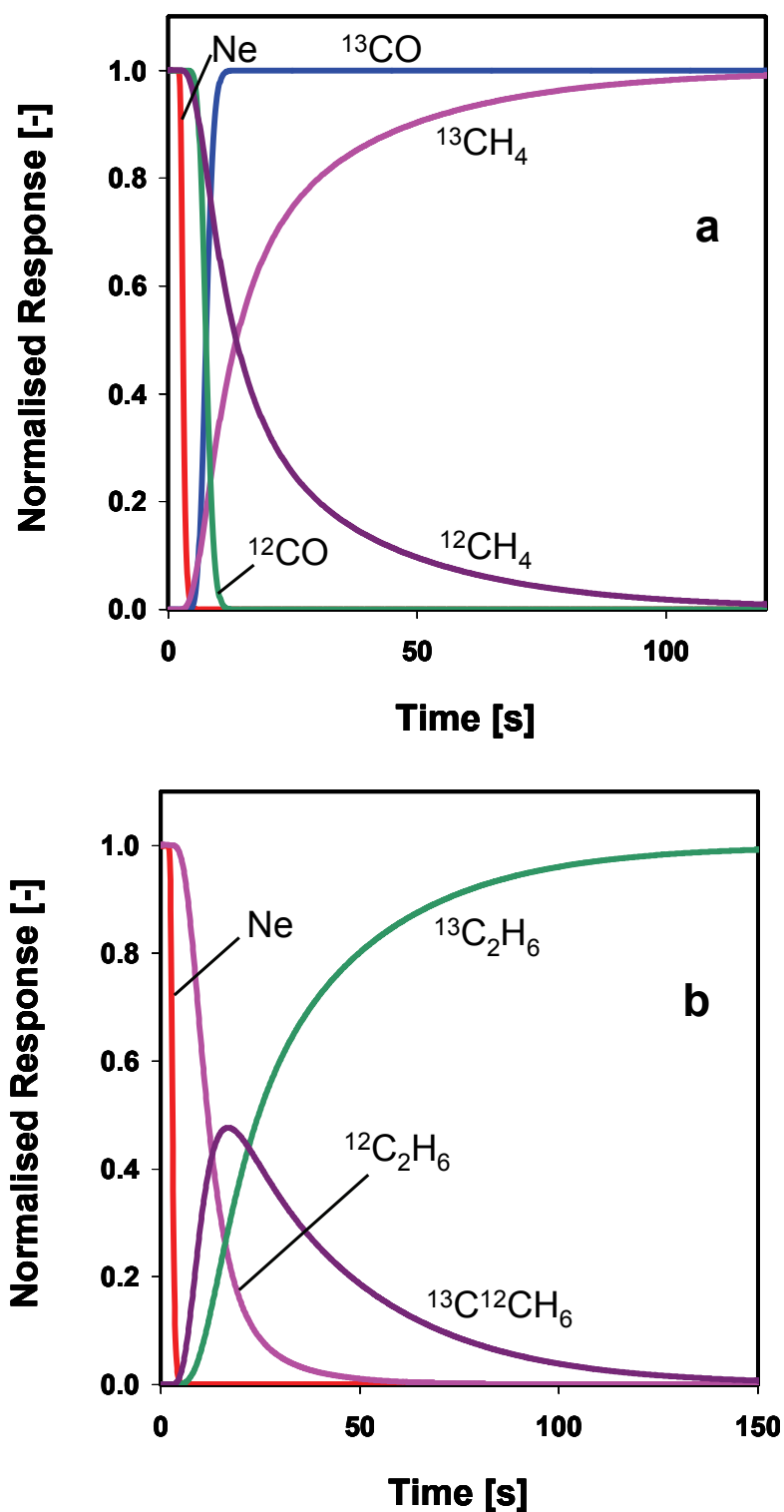


Figure 2.6: Model simulation for the formation of (a) methane, and (b) ethane under Fischer-Tropsch conditions for a SSITKA experiment ($^{13}\text{CO}/\text{H}_2/\text{Ar} \rightarrow ^{12}\text{CO}/\text{H}_2/\text{Ne}$ at 225°C , 1.2 bar, $W_{\text{cat}} \cdot F^{-1} = 24.2 \text{ kg}_{\text{cat}} \cdot \text{s}^{-1} \cdot \text{mole}^{-1}$ over a cobalt catalyst).

The aforementioned results show the robustness of gPROMS in modelling a complex reaction network such as in SSITKA experiments for the Fischer-Tropsch synthesis. The example presented here has already recently been extended successfully towards model discrimination using new data, parameter estimation solving more unknowns and lastly extending the model to account for the heavier hydrocarbons (see Chapters 4 and 6). In summary, gPROMS has proven to be an excellent tool for the modelling of transient experiments.

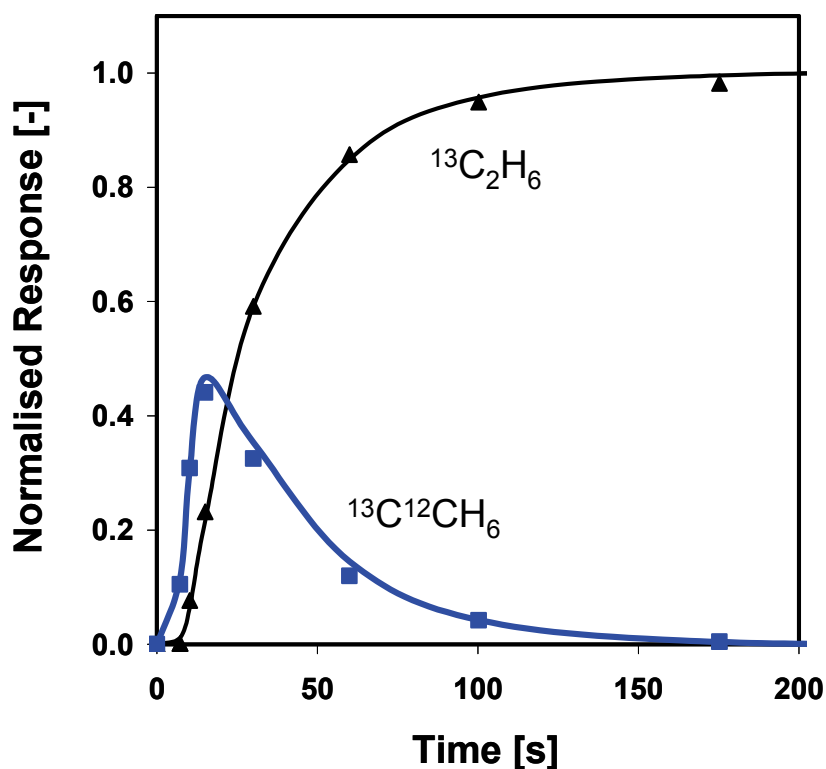


Figure 2.7.: Parameter estimation results for the formation of ethane under Fischer-Tropsch conditions for a SSITKA experiment ($^{13}\text{CO}/\text{H}_2/\text{Ar} \rightarrow ^{12}\text{CO}/\text{H}_2/\text{Ne}$ at 225°C , 1.2 bar, $W_{\text{cat}} \cdot F^{-1} = 24.2 \text{ kg}_{\text{cat}} \cdot \text{s}^{-1} \cdot \text{mole}^{-1}$ over a cobalt catalyst).

Table 2.3: The optimized kinetic rate constants, the 95% confidence intervals, and the 95% t-value calculated using parameter estimation in gPROMS.

Parameter	Optimal Estimate	95% Confidence Interval	95% t-value
k_5 [$\text{kg}_{\text{cat}}\cdot\text{mole}^{-1}\cdot\text{s}^{-1}$]	$2.3 \cdot 10^0$	$5.6 \cdot 10^{-1}$	$4.1 \cdot 10^0$
k_6 [s^{-1}]	$4.6 \cdot 10^{-1}$	$7.2 \cdot 10^{-2}$	$6.4 \cdot 10^0$

2.7.4. Summary

A gPROMS implementation of a SSITKA experiment for the formation of ethane during the Fischer-Tropsch synthesis was presented. This model was based on previous work and as such was validated using older data. The model in gPROMS predicted both steady-state and transient gas phase and surface concentrations both as a function of time and reactor length. Parameter estimation in gPROMS was also successfully completed and the results were in excellent agreement with the earlier work.

References

- (1) H.A.J. Van Dijk, J.H.B.J. Hoebink and J.C. Schouten, *Top. Catal.* **26** (2003) 163-171.
- (2) H.A.J. Van Dijk, J.H.B.J. Hoebink and J.C. Schouten, *Top. Catal.* **26** (2003) 111-119.
- (3) H.A.J. Van Dijk, *A mechanistic study using transient isotopic tracing*, Ph.D thesis, 2001, Technische Universiteit Eindhoven, Eindhoven, the Netherlands. <http://alexandria.tue.nl/extra2/200111083.pdf>
- (4) S. Hammache, J.G. Goodwin Jr, S.L. Shannon and S.Y. Kim, in: *In Situ Analysis of Reaction at the Site Level in Heterogeneous Catalysis*, eds. P. Somasundaran and A. Hubbard, Encyclopedia of Surface and Colloid Science, Marcel Dekker (2002) 2445-2454.

- (5) H.A.J. Van Dijk, J.H.B.J. Hoebink and J.C. Schouten, *Chem. Eng. Sci.* **56** (2001) 1211-1219.
- (6) H.A.J. Van Dijk, J.H.B.J. Hoebink and J.C. Schouten, *Stud. Surf. Sci. Catal.* **130 A** (2000) 383-388.
- (7) R.L. Espinoza, T.C. Bromfield, F.G. Botes, J.L. Visagie, K.H. Lawson and P. Gibson. *Hydrocarbon synthesis catalyst and process*, ed. Sasol Technology. US Patent, US 6844370, (2005).
- (8) J. Happel, *Isotopic Assessment of Heterogeneous Reactors*, Academic Press Inc., (1986).
- (9) C.O. Bennett, in: A.T. Bell, L.L. Hegedus (Editors), *Catalysis under Transient Conditions*. American Chemical Society, 1982, p. 1.
- (10) C.M.L. Scholz, K.M. Nauta, M.H.J.M. de Croon and J.C. Schouten, *Chem. Eng. Sci.* **63** (2008) 2843-2855.
- (11) Process System Enterprise. *gPROMS Advanced User Guide*. (2005).

3

Reactivity of surface carbonaceous intermediates on an iron-based Fischer-Tropsch catalyst

The reactivities of surface carbonaceous intermediates on both a freshly reduced and a carbided iron-based Fischer-Tropsch catalyst were characterised using isotopic transient kinetic analysis (ITKA), isothermal hydrogenation, and temperature programmed surface reactions. On both catalysts, carbon deposition occurred to the same extent but water formation and methane formation were faster on the carbided catalyst. More reaction intermediates for C₂ hydrocarbon formation were detected at the start of the Fischer-Tropsch reaction on the freshly reduced catalyst. However, the CH_s intermediate for methane formation and the CCH_s intermediate for C₂ hydrocarbon formation were found to be the most stable surface intermediates on both catalysts. Surface carbon (¹³C_s), deposited via the Boudouard reaction using ¹³CO, was active and was detected in the C₂₊ hydrocarbon products as the result of a coupling reaction with ¹²C_s rather than with ¹³C_s. Six distinct carbon pools (C_{α1}, C_{α2}, C_{β1}, C_{γ1}, C_{γ2} and C_{δ1}) were identified during isothermal and temperature programmed surface reactions. Graphitic carbon (C_{δ1}) has the highest coverage of all the surface carbonaceous species on the end of the run sample.

3.1. Introduction

The high temperature Fischer-Tropsch (HTFT) process [1,2] comprises a complex network of elementary reaction steps. Apart from the main HTFT products (olefins and paraffins), these steps need to account for the formation of CO₂, carbon and oxygenates (alcohols, acids, aldehydes and ketones) and aromatics. To date, the mechanisms in literature do not fully explain the product distribution of the HTFT process. In part, this is due to the complex products spectrum and the fact that the working iron-catalyst consists of a mixture of iron carbides, iron oxides, and α -iron [3,4]. Combining the knowledge of the rates of the elementary reaction steps with the reactivity of the surface intermediates and then correlating this to the formation of the various iron phases is paramount to understanding the overall mechanistic pathway. In this paper, we focus on the reactivity of the surface intermediates at HTFT conditions (330°C and 1.2 bar).

Knowledge about the surface species and reaction intermediates during the Fischer-Tropsch Synthesis (FTS) is essential in developing reaction pathways which can lead to a plausible mechanism. Many surface species have already been identified using techniques such as infra-red spectroscopy (IR), secondary ion mass spectroscopy (SIMS), and electron energy loss spectroscopy (EELS) which has been reviewed by Claeys and Van Steen [5]. Some of the relevant species are listed in Table 3.1, where the subscript *s* denotes adsorption of that atom onto the catalyst surface. Steady State Isotopic Transient Kinetic Analysis (SSITKA) [6-10] can also be used to identify possible reaction intermediates, their concentrations and possible reaction pathways.

Table 3.1: List of surface species identified on a Fischer Tropsch catalyst with techniques such as EELS, IR, etc. Adapted from Claeys and Van Steen [5].

Surface Species	Notation	Surface Species	Notation
Alkyl	$R-C_sH_2$	Formate	O_s-CH-O_s
Alkylidene	$R-C_sH$	Hydrogen	H_s
Alkylidyne	$R-C_s$	Hydroxyl	HO_s
Allyl	$R-CH=CH_2-C_sH_2$	Methylidyne	C_sH
Carbon Monoxide	C_sO	Methylene	C_sH_2
Carbon	C_s	Methyl	C_sH_3
Enol	HC_s-OH	Vinyl	$R-CH=C_sH$

$R = C_nH_{2n+1}$ with $n \geq 0$

Temperature programmed surface reaction (TPSR) methods with either hydrogen (TPH) or oxygen (TPO) are extremely powerful in characterising surface intermediates [11-13]. The challenge with the *ex-situ* TPSR methods for the FTS is passivating the catalyst. In the case of iron-based catalysts, phase changes can readily occur at ambient temperature [14] if the correct passivation method is not followed. *In-situ* TPSR measurements therefore provide more trustworthy data. Isothermal surface reaction (ISR) can also be applied to working catalysts at the reaction temperature to characterise the surface intermediates [12]. This technique is extremely useful for capturing those surface intermediates which cannot be detected with TPH.

The carbon deposited on the catalyst by CO disproportionation (or Boudouard reaction) prior to exposure to FTS conditions have been shown to have a high reactivity towards FT products [15,16]. These studies were performed on Ni, Co and Ru at low temperatures (<300°C) where it is difficult to distinguish between CO_{ads} and C_{ads} . At HTFT conditions, CO_{ads} will be lower [17] and there will be more C_{ads} deposited. However, less reactive surface carbon is also formed, making the analysis technique for active surface carbon very important. Mims and McCandlish [18,19] used

isotopic transient techniques to show that on an Fe/K catalyst (237°C, H₂/CO = 1, and 0.9 bar), the majority of the surface carbon is in the monomeric building block pool whilst only a small fraction is part of the pool of growing hydrocarbon chains. No measurable amount of CO_{ads} was detected. Stockwell *et al.* [20] also measured a very small amount of CO_{ads}, only 8 μmol CO_{ads}·g_{cat}⁻¹ equivalent to 0.1 monolayer of CO, on a 10 wt% Fe/Al₂O₃ catalyst (285°C, H₂/CO = 9, and 1 bar), using the same isotopic transient methods.

It is well known in the open literature that iron-based Fischer-Tropsch catalysts transform during the synthesis. This transformation reflects a change in the catalyst phases (α -Fe, iron oxides, and iron carbides). Datye *et al.* [3] used X-ray diffraction (XRD), transmission electron microscopy (TEM) and Mössbauer spectroscopy to correlate these phase changes to changes in the Fischer-Tropsch activity. The major challenge with *ex-situ* characterisation techniques is correlating the data to the Fischer-Tropsch activity and selectivity. Usually, numerous samples, at different times on stream, are required to formulate a plausible correlation to the FTS performance of the catalyst. The general trend in literature is therefore to use *in-situ* methods. Raupp and Delgass [21] used *in-situ* Mössbauer to link the FT activity to the extent of carbidation. Most recently, Du Plessis [22] used *in-situ* XRD in an attempt to correlate the phase changes to trends in the catalyst activity.

SSITKA studies using H₂/D₂ have been shown to be useful in characterising surface intermediates amid the kinetic isotopic effects. This is an *in-situ* technique at realistic reaction conditions and hence provides data which are more trustworthy than the traditional *ex-situ* methods. Marquez-Alvarez *et al.* [23] could detect all three surface intermediates of CH₄ following a H₂/D₂ exchange for a Ni-SiO₂ catalyst at 250°C, 1 bar, and H₂/CO = 2. The authors concluded that CH_{ads} was the most abundant intermediate and the rate determining step being the hydrogenation of CH_{ads}. Happel *et al.* [24-26] modelled their H₂/D₂ experiments for the methanation reaction on a

Ni-based catalyst at 210°C and came to a similar conclusion with C_{ads} also being as abundant as CH_{ads} .

The properties and the dynamic behaviour of each of the surface species need to be investigated in the working state of the catalyst to obtain fundamental mechanistic information. In this present work, the hydrogenation of carbon monoxide, on an iron-based catalyst at higher temperatures, is studied with the aim of understanding the reactivity of the surface carbonaceous species. Both *ex-situ* and *in-situ* temperature programmed surface reaction experiments and isotopic switching experiments were performed to elucidate the mechanistic pathway for the formation of methane and higher hydrocarbons. Experiments were performed on a freshly reduced catalyst, on a carbided catalyst, and on a spent catalyst.

3.2. Results and Discussion

3.2.1. Transients at the start of the Fischer-Tropsch synthesis

The introduction of synthesis gas into the reactor results in various transients. Schulz *et al.* [27,28] characterised transient kinetic regimes (or episodes) during the Fischer-Tropsch synthesis as a result of the changing phases (α -Fe, iron oxides, and iron carbides) of the iron catalyst. These transient regimes were linked to changes in both the catalyst activity and selectivity. In a similar approach, four distinct transient kinetic regimes are identified in Figure 3.1. In the first regime, H_2O formation is very fast and CO dissociation is observed. The latter was also observed by Schulz *et al.* [28] in their first episode. The breakthrough of H_2O first is due to the formation of Fe_3C (cementite) from metallic iron, according to the reaction:

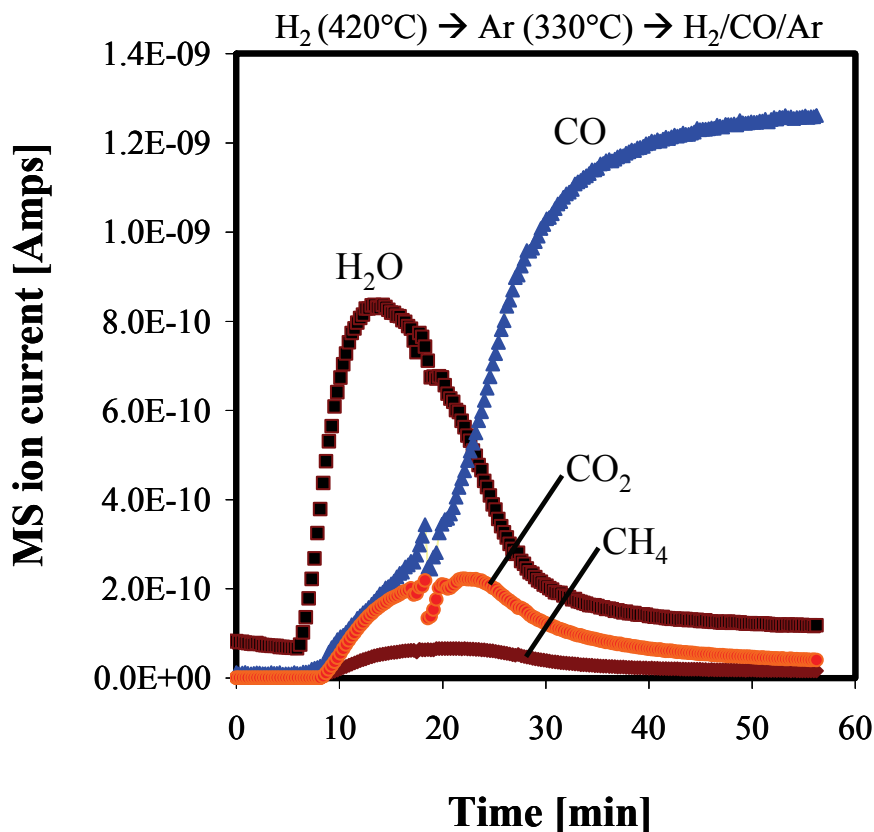


Figure 3.1: H₂O, CO₂, CO and CH₄ transients at the start of the Fischer Tropsch synthesis on a freshly reduced catalyst. Experimental conditions: reduction with 80 ml.min⁻¹ of 50 vol.% H₂/Ar at 420°C, the reactor is then cooled to 330°C under flowing Ar and the Fischer Tropsch reaction is started with 45 ml.min⁻¹ H₂, 3 ml.min⁻¹ CO and 15 ml.min⁻¹ Ar at 1.2 bar.

It is noteworthy to mention that these transients fit the in-situ XRD work by Du Plessis [22] in which a peak in activity (H₂O signal) is correlated with the formation of cementite (Fe₃C) before the steady state Hagg carbide (Fe₅C₂) is formed. In the second regime, CO₂, CO and CH₄ start to break through. Both the CO and CO₂ signals coincide suggesting that this CO is most probably a product from the fragmentation of CO₂. This conclusion is

based on the similar shapes of these transients. In typical ^{13}CO SSITKA experiments, one would expect the ^{13}CO signal to pass through the reactor. However, here the catalyst phase changes and various associated reactions either consume or produce CO.

In the third regime, the H_2O and CO_2 signals start to decline whilst CO increases sharply. The decreasing CO_2 signal together with the increasing CO signal is most probably due to the reverse water gas shift (RWGS) reaction. However, part of this CO could also be simply the reactant passing through the reactor. One would expect the H_2O signal to also increase with RWGS activity. The decreasing H_2O can be explained by a loss of metallic iron (active sites) as the iron catalyst starts to change into the different carbides [22].

In the fourth and final regime, pseudo steady state conditions are obtained. The time scales for these regimes are very different to those reported by Schulz *et al.* [28], especially with regards to reaching the steady state. Schulz *et al.* [28] worked at lower temperatures (250°C) and higher pressures (10 bar), both of which result in a longer residence time inside the reactor, compared to our reaction conditions. The high temperatures and lower pressures used in our study resulted in a faster first regime, 2-3 min for carbon deposition, compared to 10-15 min observed by Schulz *et al.* [28].

In Figure 3.2, the different regimes can also be identified. However, in this case the Fischer-Tropsch synthesis was started on a carbided catalyst as opposed to the freshly reduced catalyst in Figure 3.1. The carbided catalyst was exposed to synthesis gas for at least 20 hr. The first regime in which carbon deposition takes place is still 2-3 min for the carbided catalysts. However, now H_2O has already reached the maximum concentration. In the second regime, CO, CO_2 and CH_4 start to break through similarly as in Figure 3.1. In this case, the CO signal increases rapidly and could not be linked to the

CO₂ formation. The CH₄ formed also was much higher in this case than for the freshly reduced catalyst. This is most probably due to the reaction of surface carbon or hydrocarbon species which are still present on the catalyst surface. The maximum CH₄ concentration is also reached much faster in this case and steady-state conditions are obtained twice as fast as compared to a freshly reduced catalyst.

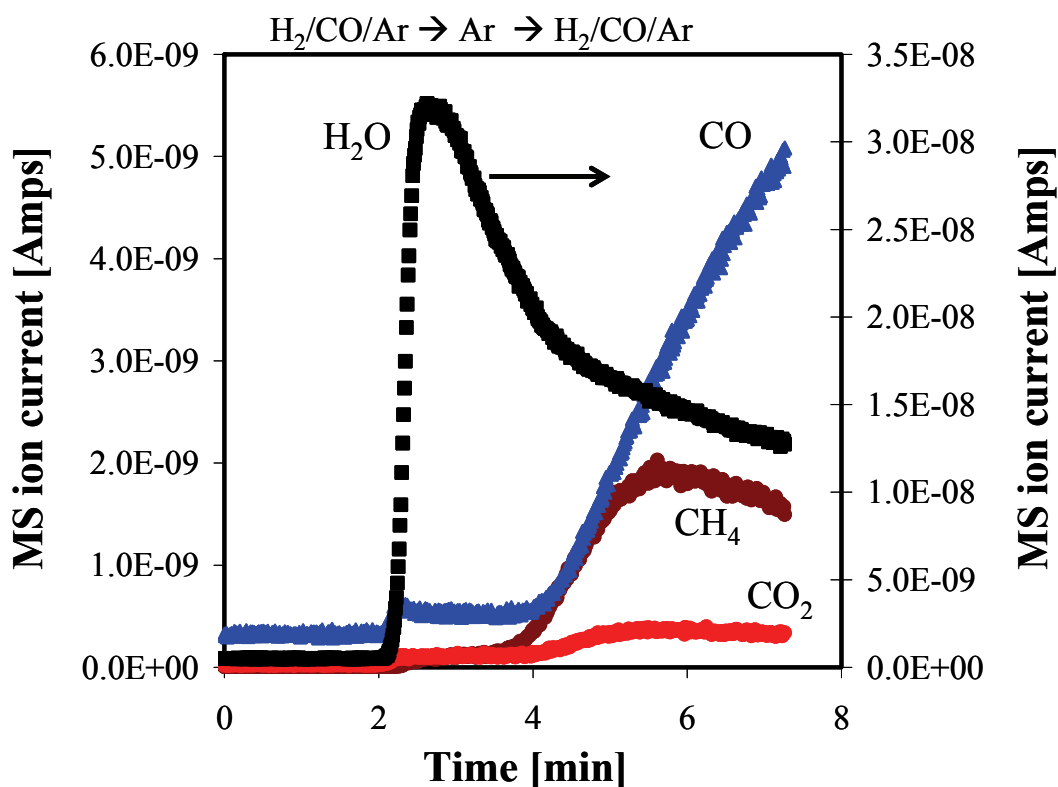


Figure 3.2: H₂O, CO₂, CO and CH₄ transients at the start of the Fischer Tropsch synthesis on a carbided catalyst. Experimental conditions: Fischer Tropsch reaction is stopped, the reactor is purged with Ar and the Fischer Tropsch reaction is restarted with 45 ml.min⁻¹ H₂, 3 ml.min⁻¹ CO, and 15 ml.min⁻¹ Ar at 330°C and 1.2 bar.

The Fischer-Tropsch synthesis was also started with D₂/CO on a freshly reduced catalyst. The resulting transients for ethane and ethene are shown in Figure 3.3 and 3.4, respectively. For ethane, two surface intermediates are observed, C₂H₅ and C₂H_{3,s}. It is noteworthy mentioning at this stage that

SSITKA experiments using D_2 are considered ITKA experiments due to the kinetic isotope effect [9] which disturbs the steady state behaviour of the catalyst. Therefore, these results are interpreted only qualitatively. In Figure 3.3, both surface intermediates break through at the same time indicating similar activities (ignoring kinetic isotope effects). The C_2H_s surface intermediate seems to occupy a larger surface area as its coverage is larger.

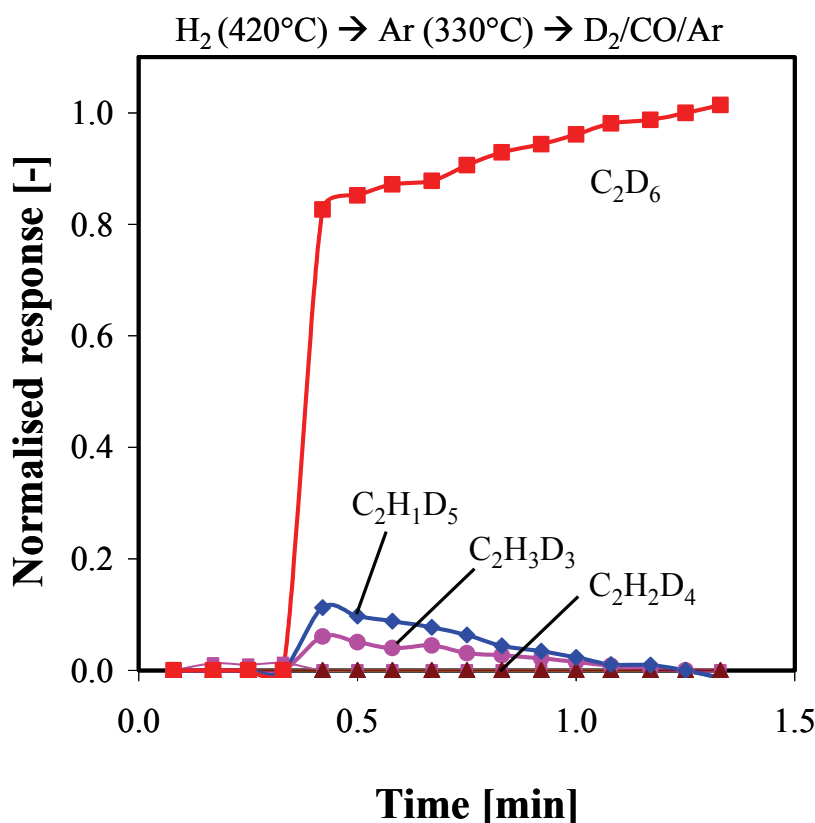


Figure 3.3: C_2H_6 transients at the start of the Fischer-Tropsch synthesis on a freshly reduced catalyst. Experimental conditions: reduction with 80 ml.min^{-1} of 50 vol.% H_2/Ar at 420°C , the reactor is then cooled to 330°C under flowing Ar and the Fischer-Tropsch reaction is started with 45 ml.min^{-1} D_2 , 3 ml.min^{-1} CO , and 15 ml.min^{-1} Ar at 1.2 bar.

In Figure 3.4, all three surface intermediates of ethene could be detected. The C_2H_s and $C_2H_{2,s}$ intermediates break through together with fully labelled ethene. The C_2H_s intermediate has a larger coverage and seems to be less

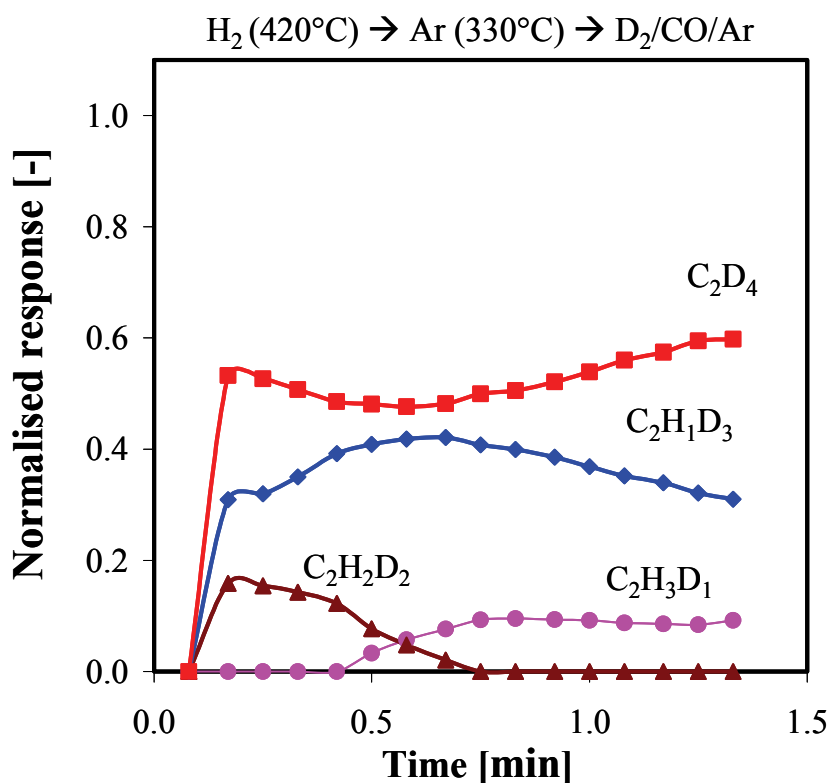


Figure 3.4: C_2H_4 transients at the start of the Fischer-Tropsch synthesis on a freshly reduced catalyst. Experimental conditions: reduction with $80 \text{ ml}\cdot\text{min}^{-1}$ of 50 vol.% H_2/Ar at 420°C , the reactor is then cooled to 330°C under flowing Ar and the Fischer-Tropsch reaction is started with $45 \text{ ml}\cdot\text{min}^{-1}$ D_2 , $3 \text{ ml}\cdot\text{min}^{-1}$ CO, and $15 \text{ ml}\cdot\text{min}^{-1}$ Ar at 1.2 bar.

reactive. Interestingly, the third intermediate, $C_2H_{3,s}$, which was detected together with C_2H_s in the case of ethane, only breaks through after *ca.* 30 seconds. This time lag coincides with a decrease in the $C_2H_{2,s}$ coverage.

Based on this observation, it seems that the $C_2H_{2,s}$ and $C_2H_{3,s}$ surface intermediates are interlinked carbon pools and that the C_2H_s surface intermediate is a larger and less reactive carbon pool. At this stage, we cannot provide a plausible mechanistic reason as to why no $C_2H_{2,s}$ surface intermediate was detected for ethane. One possible explanation could be that the $C_2H_{2,s}$ surface intermediate for ethane is extremely reactive with a very

small surface coverage, making it virtually undetectable with the technique used in this work. Mechanistically, this result also implies two different pathways towards ethene and ethane formation and most likely the C_2 's do not desorb from the same intermediate. The reason we observed fully labelled C_2H_4 and C_2H_6 on a freshly reduced catalyst is because H_2 was used during the reduction. It seems that although the reactor was purged with Ar, not all the chemisorbed H_2 was removed.

3.2.2. *CO disproportionation*

The carbon was deposited on a freshly reduced catalyst by ^{13}CO disproportionation (via the Boudouard reaction) at $330^\circ C$ and 1.2 bar for 3 min. The mass spectrometer intensities were traced over time when switching to inert and it was observed that the chemisorbed CO_2 elutes before 10 min. In these experiments, the chemisorbed ^{13}CO and $^{13}CO_2$ were first removed by purging the reactor with Ar for at least 15 min. Thereafter, the Fischer-Tropsch synthesis with $^{12}CO/H_2$ was started to determine if the deposited $^{13}C_s$ on the catalyst surface was reactive. The result, presented in Figure 3.5, shows the presence of $^{13}C_s$ in both the C_2 and C_3 hydrocarbons. In terms of C-C coupling, the combination of ^{13}C with ^{12}C was more significant than the combination of two $^{13}C_s$ species. The latter was observed (not shown here) but in small amounts (*ca.* 25% of the normalised intensity) and with a slight delay in the break through. This delay could be attributed to carbide formation in which the $^{13}C_s$ dissolves into the catalyst bulk but is still mobile and able to react. Alternatively, it could also be that certain $^{13}C_s$ species were deposited on less reactive sites. The main conclusion from this experiment is that $^{13}C_s$ deposited via CO disproportionation reacts into FT products. This also implies that the formation of unreactive C_s (or graphitic carbon), which is normally observed in the HTFT process, is a relatively slow reaction.

3.2.3. H_2/D_2 isotopic flushing

The results for the H_2/D_2 exchange reactions carried out on a carbided catalyst, which was online for *ca.* 20 hr, are presented in Figure 3.6 to 3.9 following a $H_2/CO/Ar/ \rightarrow D_2/CO/Ar/Ne$ switch. In Figure 3.6, the transients of Ne, H_2 , D_2 and HD are presented. The two main observations are: (1) an observable delay between the H_{ads} and Ne transient, and (2) the presence of the product HD. The former suggest that a measurable amount of H_{ads} is

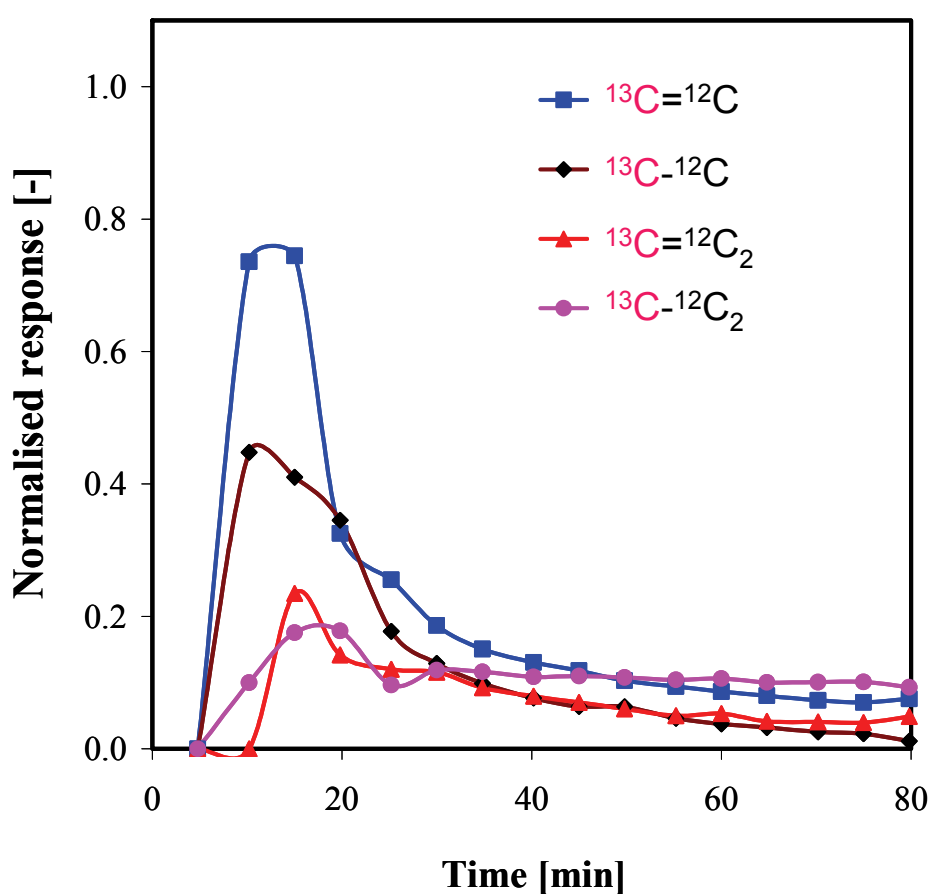


Figure 3.5 Normalised responses of ethane, ethane, propane and propene formed after ^{13}C CO disproportionation on a reduced Fe/K catalyst at 330°C, 1.2 bar and $H_2/CO = 9$.

present on the catalyst surface. The latter is indicative of the dissociative adsorption of H_2 . An exact value for H_{ads} is not reported since we can not accurately account for water and oxygenates which consume H_{ads} . In comparison to CO [29], the adsorption/desorption rate of H_2 is slower than CO. The break through of $^{13}CO/^{12}CO$ is immediate and overlaps with the Ne transient whilst the D_2/H_2 transients have a time lag. This behaviour is similar to the observation made by Van Dijk [10] for a cobalt based catalyst. In summary, this implies that H_2 adsorbs/desorbs slower than CO on an Fe-surface.

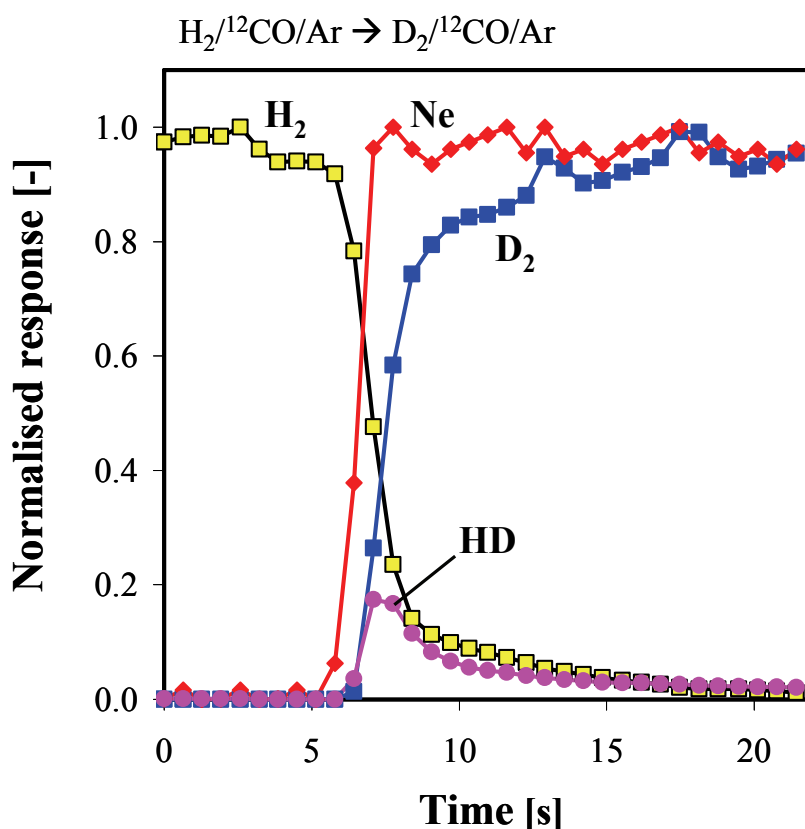


Figure 3.6: Evolution of H_2 , HD and D_2 species during an isotopic transient switch from H_2/CO to D_2/CO on the iron-based catalyst. (Reaction conditions, $330^\circ C$, 1.2 bar and $H_2/CO = 9$)

The normalised transients of $\text{CH}_x\text{D}_{4-x}$ ($x = 0-4$) are shown in Figure 3.7. All three methane intermediates were detectable (viz. CH_s , $\text{CH}_{2,s}$, and $\text{CH}_{3,s}$). The $\text{CH}_{3,s}$ surface intermediate breaks through slightly faster than the other two and also has a lower surface coverage. The CH_s surface intermediate has a longer tail than the other two surface intermediates, implying either a lower overall reactivity or its formation from the de-hydrogenation of the other two surface species.

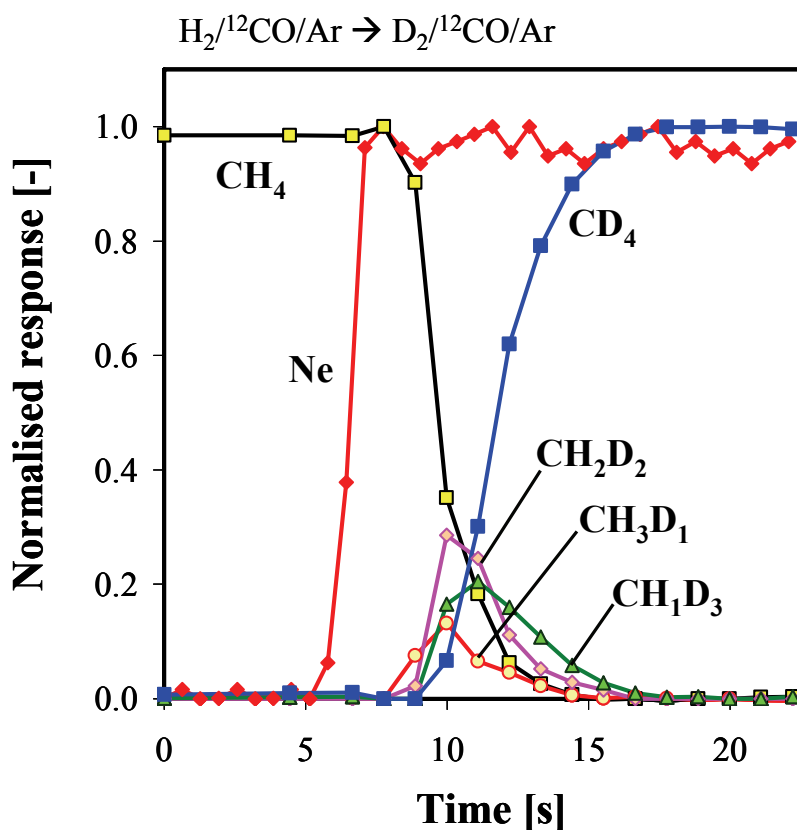


Figure 3.7: Responses of the isotopic variants of methane following the switch H_2/CO to D_2/CO for an iron-based catalyst at 330°C , 1.2 bar and $\text{H}_2/\text{CO} = 9$.

In Figure 3.8 and 3.9, the D-transients of ethane and ethene are presented, respectively. In comparison to the fresh catalyst (see Figures 3.3 and 3.4),

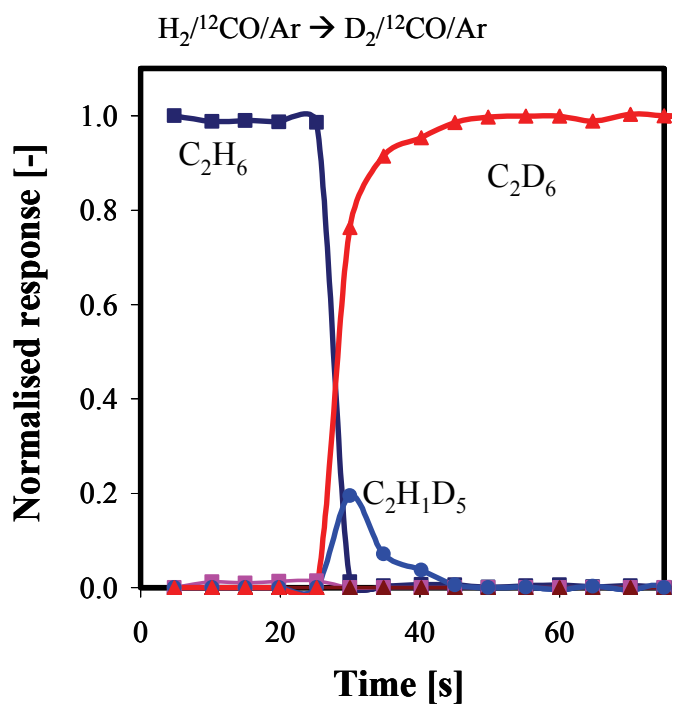


Figure 3.8: Responses of the isotopic variants of ethane following the switch H_2/CO to D_2/CO for an iron-based catalyst at 330°C, 1.2 bar and $H_2/CO = 9$.

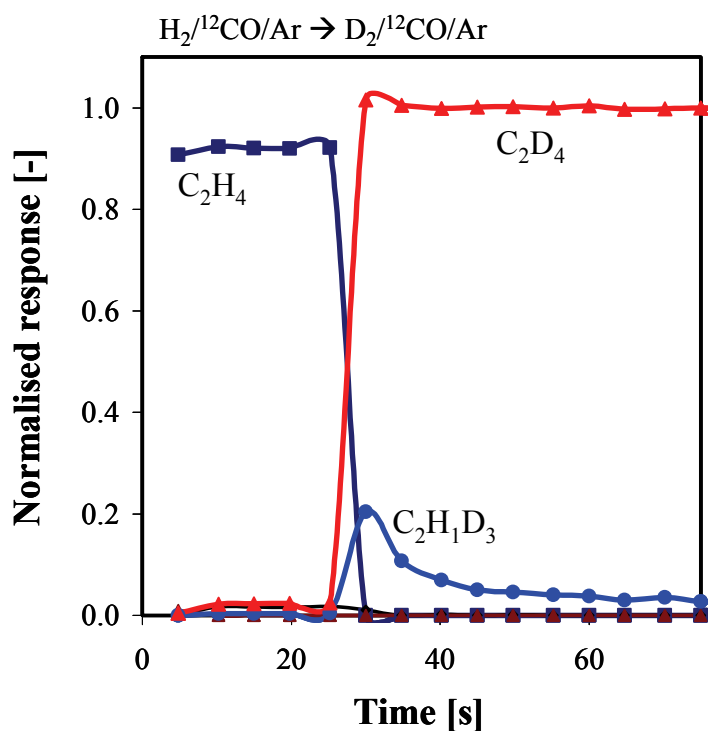


Figure 3.9: Responses of the isotopic variants of ethene following the switch H_2/CO to D_2/CO for an iron-based catalyst at 330°C, 1.2 bar and $H_2/CO = 9$.

only a single surface intermediate, C_2H_s , was detectable for both ethane and ethene on the carbided catalyst. The tailing of this surface intermediate is similar to that of the CH_s species detected for methane suggesting that the CH_s surface intermediate is the precursor for ethane and ethene formation. The formation of a C_2H_s species by CH_s diffusing onto C_s has been proposed by Liu and Hu [30] for a Ru-based catalyst. They also proposed that the C_2H_s species is the most stable and abundant intermediate as part of their ($C_s + C_s$ -R) mechanistic pathway to Fischer-Tropsch products. Our experimental result for the Fe-based catalyst supports their conclusion.

3.2.4. *In-situ isothermal hydrogenation*

The Fischer-Tropsch synthesis was abruptly stopped by switching to an inert feed. It can be expected that during this process, extremely reactive surface intermediates will continue to react whilst chemisorbed reactants will also be removed. The transients for this step change are shown in Figure 3.10a. For the 60 min duration, the only noticeable peak was $m/z = 44$ at *ca.* 10 min. This is most likely to be CO_2 , however as shown in Figure 10b, there was no associated peak for CO_2 at $m/z = 28$ (from the fragmentation to CO). So, this peak at $m/z = 44$ could be a higher hydrocarbon such as propane. These experiments were performed with the online MS, so further work using the online GCMS is required to correctly identify this peak.

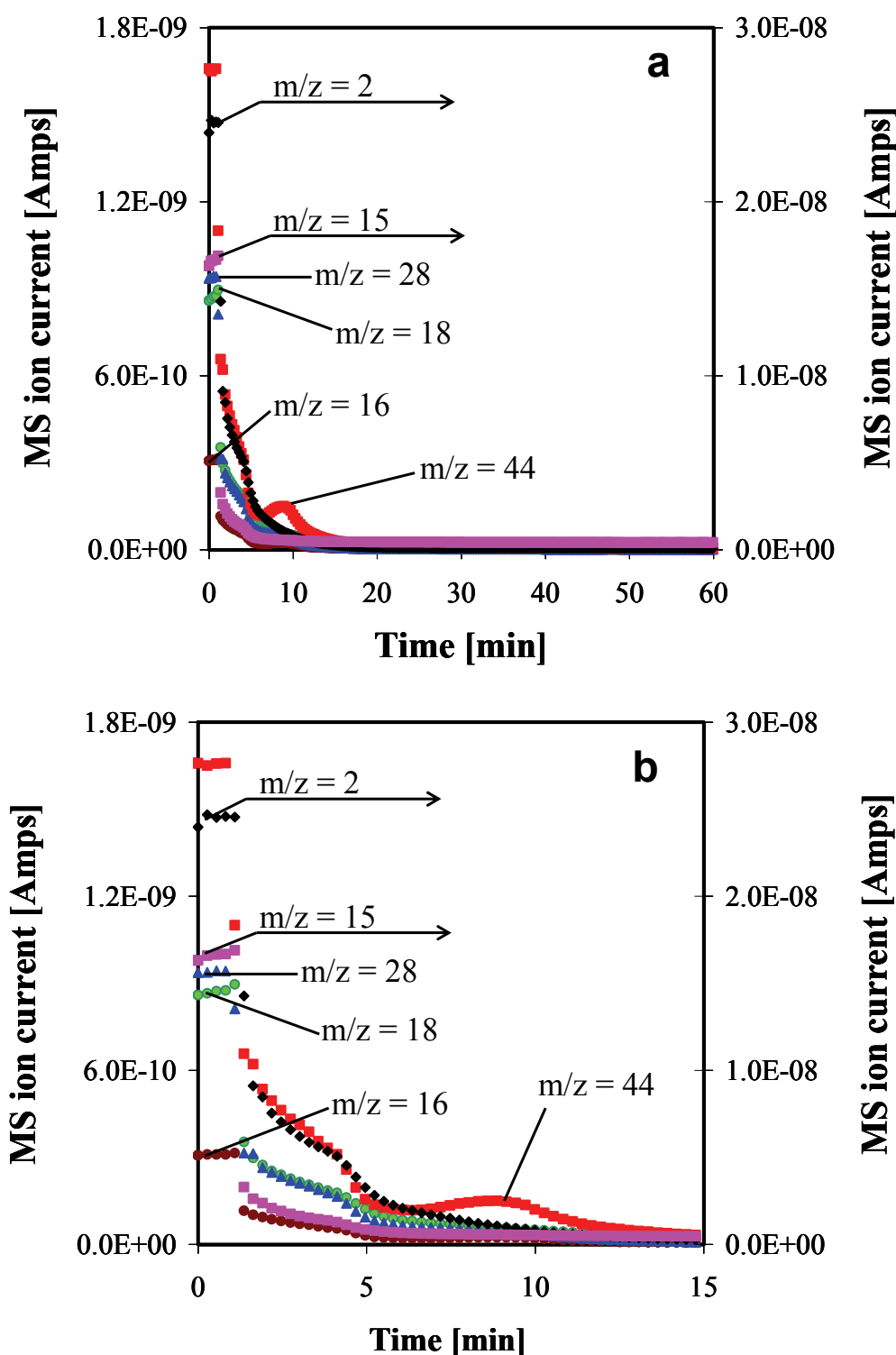


Figure 3.10: (a) Transients at the end of the FTS showing the first 60 min after switching from $H_2/CO = 9$ to an inert feed. Reaction temperature (330°C) and pressure (1.2 bar) were kept constant. (b) Transients at the end of the FTS showing the first 15 min after switching from $H_2/CO = 9$ to an inert feed. Reaction temperature (330°C) and pressure (1.2 bar) were kept constant.

The isothermal hydrogenation was started after purging the reactor to remove all the chemisorbed species. The profiles for CH₄ and H₂O are shown in Figure 3.11. Two distinct peaks are observed. Both peaks are associated with the formation of CH₄ and H₂O, implying two active sites for the Fischer-Tropsch reactions (see equations 2 and 3). The peaks are clearly deconvoluted which is not expected for an isothermal operation. This could be due to the faster reaction of the surface species compared to the sub-surface species. Alternatively, it could also be that unhydrogenated species requiring more H_{ads} additions take longer to react.

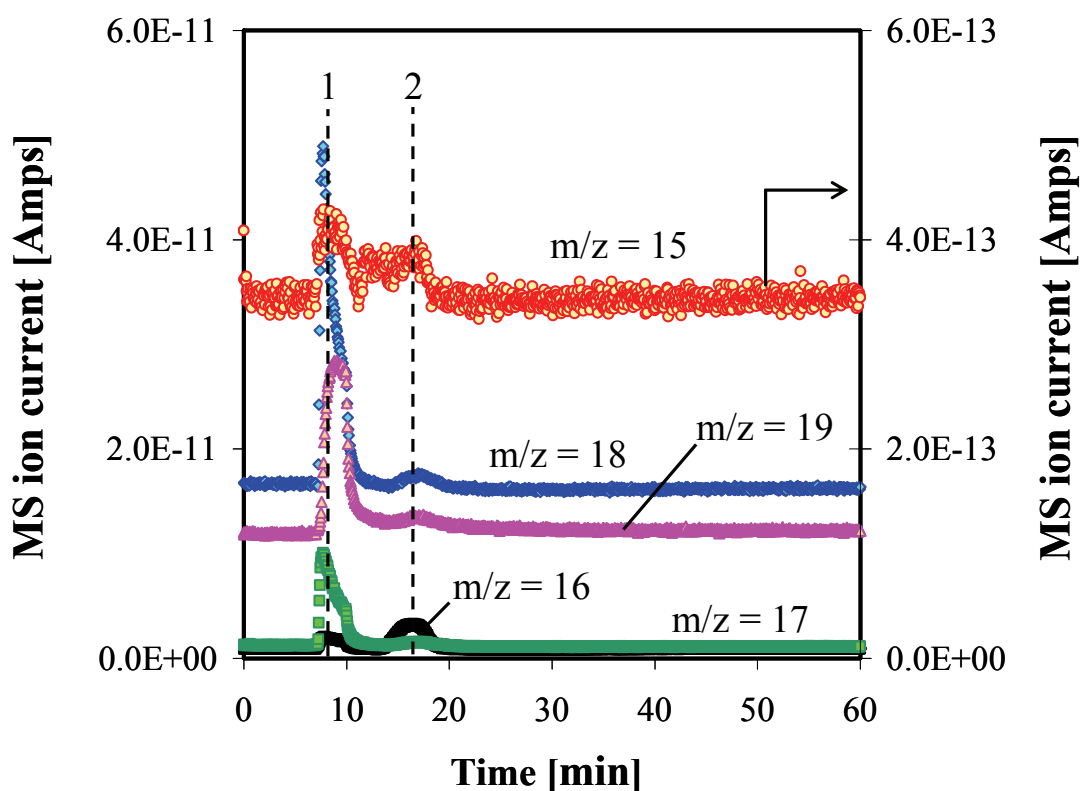


Figure 3.11: In-situ ISR results for a working Fe/K catalyst during the FTS at 330°C, 1.2 bar and H₂/CO = 9. Methane, water and oxygen (m/z = 16 -19) were monitored after a switch from H₂/CO = 9 to Ar (> 15 min) to D₂/Ar.

In Figure 3.12, the peaks for CO and CO₂ correspond to the same two active sites as in Figure 3.11. The formation of CO and CO₂ can either be from the reaction between surface oxygen and carbon or the hydrogenation of formate species and the subsequent WGS products as shown in equation [4]. This reaction corresponds more significantly with peak 2 in Figure 3.12. This also implies that sub-surface species become active when the surface species are cleaned (hydrogenated) away. Based on the peak areas, the first peak, which represents the more active site, has a lower coverage compared to the second peak, representing the less reactive peak.

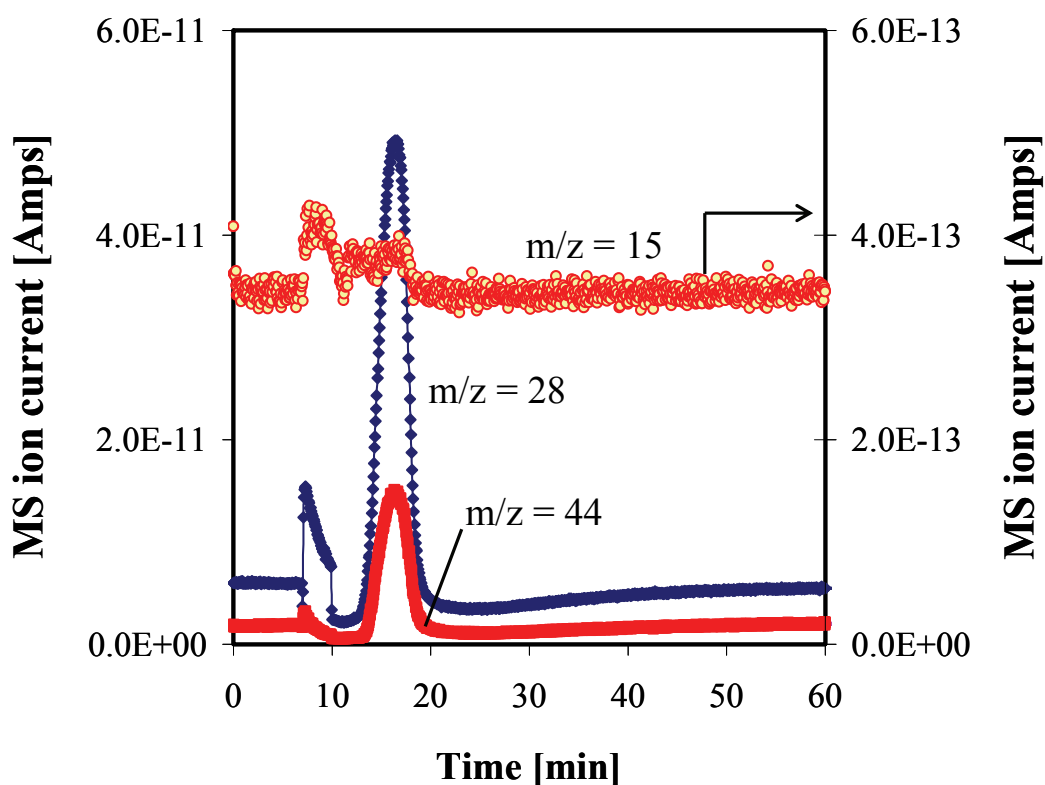


Figure 3.12: In-situ ISR results for a working Fe/K catalyst during the FTS at 330°C, 1.2 bar and H₂/CO = 9. Methane, carbon monoxide and carbon dioxide (m/z = 16, 28 and 44) were monitored after a switch from H₂/CO = 9 to Ar (> 15 min) to D₂/Ar.

3.2.5. *In-situ* temperature programmed hydrogenation

The *in-situ* TPH profiles for CH₄ and H₂O are shown in Figure 3.13. Initially, at low temperatures (below 150°C), there are high concentrations of H₂O, implying the presence of O_{ads} which can be hydrogenated easily. Two H₂O peaks were detected prior to the synthesis temperature (330°C), one at 205°C and the second at 310°C. The first CH₄ peak starts to break through at 350°C. The maximum temperature attainable in the *in-situ* reactor for TPH was 450°C which was not high enough to hydrogenate all of the CH₄ intermediates. However, holding the temperature at 450°C provided useful information. The CH₄ TPH profile can be deconvoluted into two peaks, one representing an intermediate (C_α) which can be hydrogenated at ~350°C, whilst the other (C_β) requires temperatures in excess of 450°C.

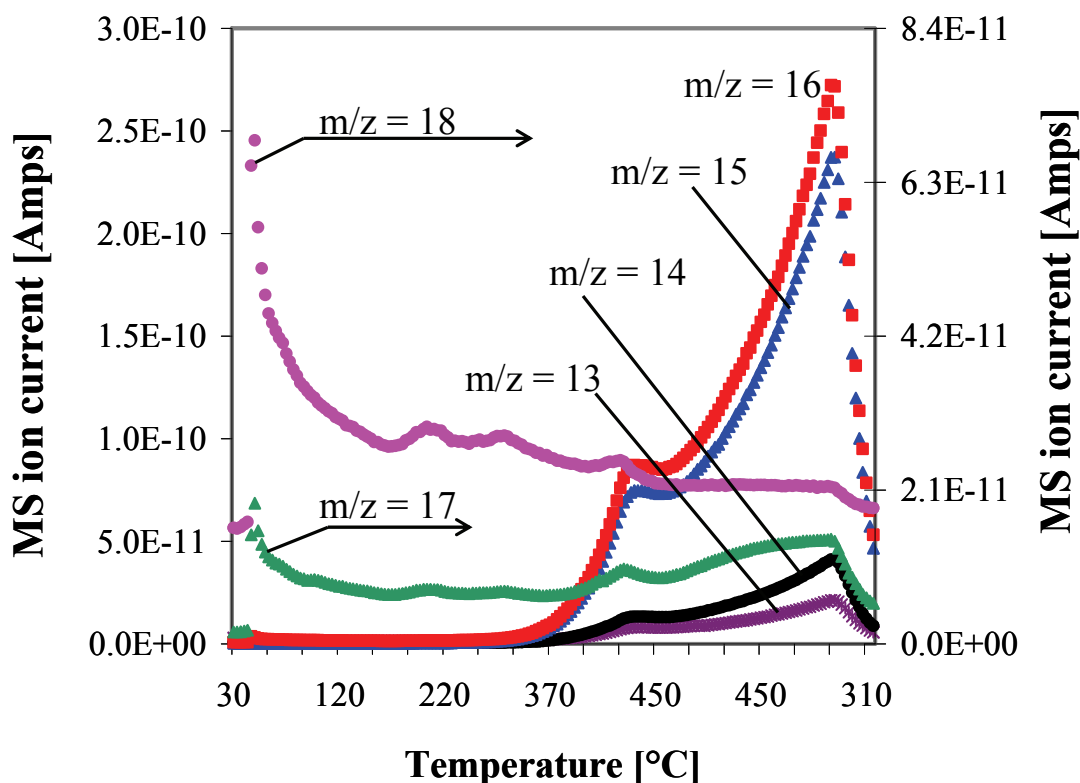


Figure 3.13: Methane and water produced during *in-situ* TPH for a Fe/K catalyst after FTS at 330°C, 1.2 bar and H₂/CO = 9. See Chapter 2 for TPH program.

There were also H₂O peaks at both temperatures corresponding to C_α and C_β, suggesting that these intermediates are active for Fischer-Tropsch synthesis. The profiles for m/z = 13 (¹³C) were only observed at temperatures in excess of 400°C implying that there exists some surface carbon which is inactive at reaction temperature but can be hydrogenated at higher temperatures. This carbon should not be confused with graphitic carbon (C_γ) which is also inactive at reaction temperature but cannot be hydrogenated. It usually requires a gasification type of reaction with either O₂ or CO. The higher molecular weight Fischer-Tropsch products (m/z = 30 to 56, representing C₂-C₄) were also captured during the *in-situ* TPH and are presented in Figure 3.14. In comparison to the CH₄ intermediate, which was not completed hydrogenated, the C₂-C₄ hydrocarbon intermediates were

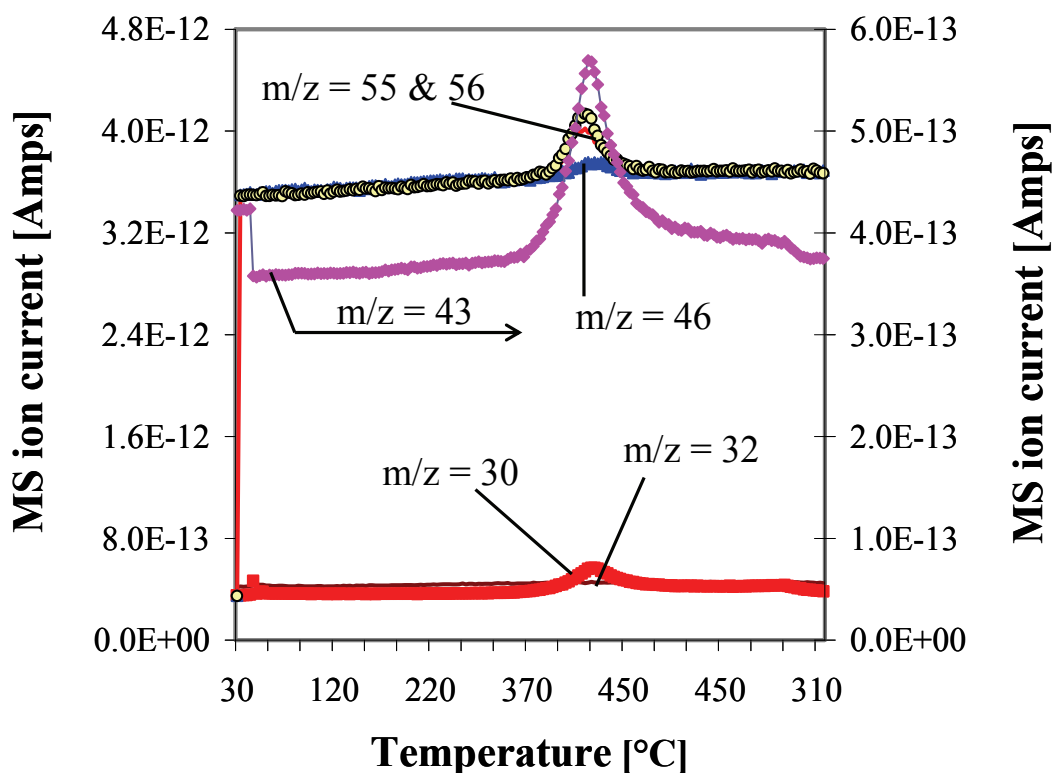


Figure 3.14: Fischer-Tropsch hydrocarbons produced during *in-situ* TPH for a Fe/K catalyst after FTS at 330°C, 1.2 bar and H₂/CO = 9. See Chapter 2 for TPH program.

completely hydrogenated at 450°C and were represented by only this single peak. This implies that the C₂₊ intermediates have a lower surface coverage than the CH₄ intermediates. Furthermore, C_s which diffuses into the catalyst bulk, is mostly hydrogenated to methane and does not contribute significantly to the C₂₊ hydrocarbons.

Finally, the TPH profile for CO₂ is presented in Figure 3.15. There are three distinct peaks for the unlabelled CO₂ (m/z = 44), observed at 75°C, 250°C, and 450°C. The peak at 250°C is broad, starting at 160°C and ending at 350°C whilst the one at 450°C is relatively small. On the other hand, there is a distinct peak at 450°C for labelled CO₂ (m/z 45 and 29). The labelled ¹³CO₂ is most probably formed from ¹³C_s which was deposited during the

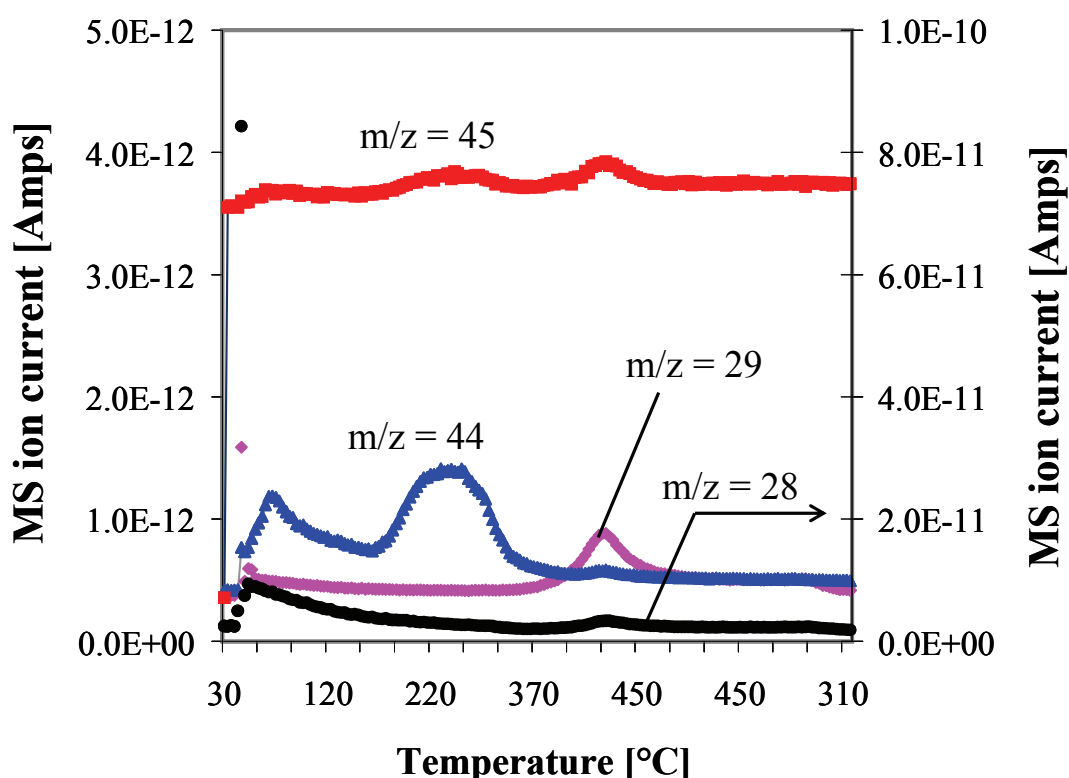


Figure 3.15: CO₂ produced during in-situ TPH for a Fe/K catalyst after FTS at 330°C, 1.2 bar and H₂/CO = 9. See Chapter 2 for TPH program.

^{13}CO dissociation experiments. This $^{13}\text{C}_s$ could have dissolved into the catalyst bulk and remained active but requires higher temperatures to be removed completely.

3.2.6. *Temperature programmed surface reactions*

The *ex-situ* TPH profile showing the evolution of CH_4 is presented in Figure 3.16. The temperatures in these experiments were as high as 800°C . In comparison to the *in-situ* TPH, the CH_4 intermediate could now be completely hydrogenated at 483°C . The second peak (at 483°C) is larger than the first at 360°C , implying that the less reactive surface intermediate has a greater surface coverage than the intermediate at 360°C . The TPO result, shown in Figure 3.17, indicates that the unreactive graphitic carbon covers most of the catalyst surface. Furthermore the species corresponding to the second peak at 450°C could also be oxygenated making mainly CO and not CO_2 .

Xu and Batholomew [31] used TPH and Mössbauer spectroscopy on an Fe-based catalyst to show the presence of four groups of carbonaceous species during the FTS (265°C , 10 atm, and $\text{H}_2/\text{CO} = 1$): (1) adsorbed atomic carbon (C_α), (2) polymerized hydrocarbon or adsorbed polymeric carbon or amorphous surface methylene chains (C_β), (3) bulk iron carbides ($\text{Fe}_{2.2}\text{C}$ and $\text{Fe}_{2.5}\text{C}$), and (4) graphitic carbon (C_δ). Their spectra could be fitted with Gaussian curves yielding seven peaks, α_1 , α_2 , β , γ_1 , γ_2 , δ_1 , and δ_2 . Based on the aforementioned study and the authors' previous work [13], we can assign similar nomenclature to our peaks for the combined *in-situ* and *ex-situ* TPH results. Carbidic carbon ($\text{C}_{\alpha 1}$ and $\text{C}_{\alpha 2}$) dominates initially during the FTS synthesis and can be removed at temperatures below and up to reaction conditions (typically below 330°C). There also seems to be the one type of

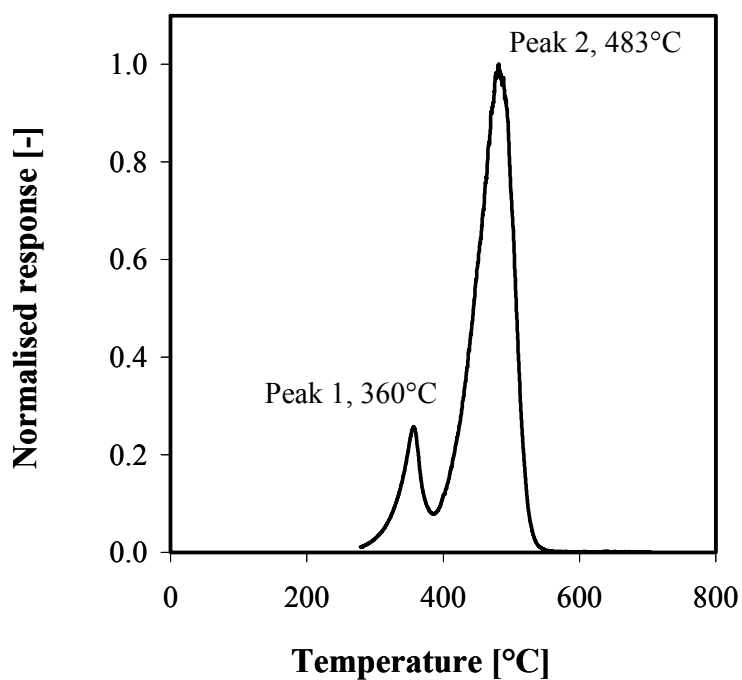


Figure 3.16: Methane produced from ex-situ TPH for a spent Fe/K catalyst after FTS at 330°C, 1.2 bar and $H_2/CO = 9$.

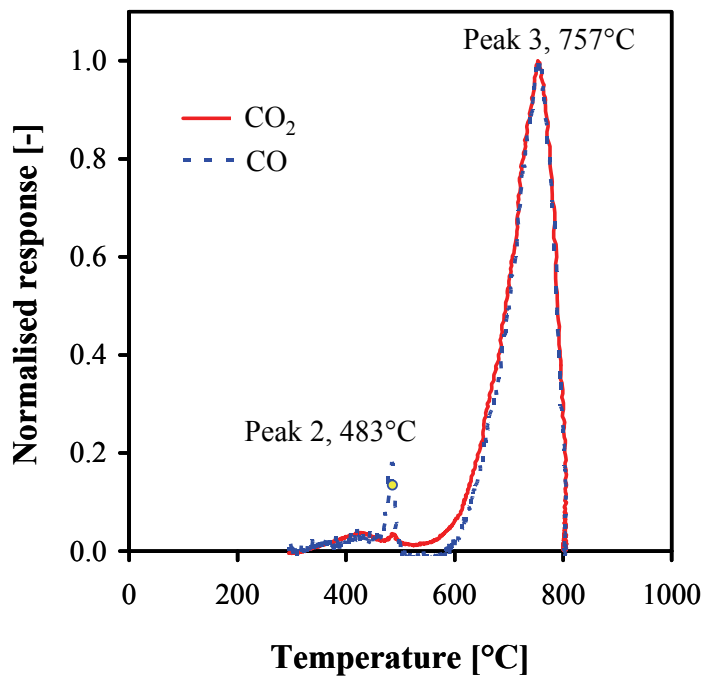


Figure 3.17: CO and CO₂ produced from ex-situ TPH for a spent Fe/K catalyst after FTS at 330°C, 1.2 bar and $H_2/CO = 9$.

amorphous carbon (C_{β}) at 360°C. The iron carbides ($C_{\gamma 1}$ and $C_{\gamma 2}$) occur in the region 435-485°C and also consume C_s which remains active. Finally, we only observed one type of graphitic carbon ($C_{\delta 1}$) which requires temperatures in excess of 750°C to be completely removed.

In summary, we have shown the existence of various carbonaceous surface species on an iron-based catalyst, with the use of transient techniques combined with temperature programmed surface reaction experiments. The combined results are summarised in Table 3.2.

Table 3.2: A summary of the results from the different experiments used to characterise the surface intermediates on a iron-based catalyst during the high temperature Fischer-Tropsch synthesis.

	Surface species (Carbon Pool ^(a))	Peak temperatures (°C)
Fresh Catalyst	$C_2H_{2,s}$, $C_2H_{3,s}$, $C_2H_{2,s}$ ($C_{\alpha 1}$) C_2H_s ($C_{\alpha 2}$)	330 ^(b)
Carbided Catalyst	$CH_{3,s}$, $CH_{2,s}$ ($C_{\alpha 1}$) CH_s , C_2H_s ($C_{\alpha 2}$) Fe-carbides ($C_{\gamma 1}$ & $C_{\gamma 2}$)	205 ^(c) and 260 ^(c) 310 ^(c) 450 and > 450 ^(c)
End of run sample	Fe-carbides ($C_{\gamma 1}$ & $C_{\gamma 2}$) Graphitic carbon ($C_{\delta 1}$)	450 ^(d) and 483 ^(d) 757 ^(e)

^(a) Carbonaceous pools designated similarly to work by Xu and Bartholomew [31].

^(b) Data from *in-situ* isothermal surface reaction measurements (section 3.4).

^(c) Data from *in-situ* temperature programmed hydrogenation measurements (section 3.5).

^(d) Data from *ex-situ* temperature programmed hydrogenation measurements (section 3.6).

^(e) Data from *ex-situ* temperature programmed oxygenation measurements (section 3.6).

We have not specified if any of these surface species contain oxygen as this requires the use of oxygen labelled experiments which will form part of a follow-on study. If the formation of CO₂ occurs on oxygen containing surface intermediates, then this will most probably be part of the C_{α1} pool (see peak at 260°C in Figure 3.15).

3.3. Conclusions

The reactivities of surface carbonaceous intermediates on an iron-based catalyst were characterised during the high temperature Fischer-Tropsch synthesis using isotopic transient kinetic analysis (ITKA), isothermal hydrogenation, and temperature programmed surface reactions. The main conclusions from this work are summarised below:

- (1) The transients observed at the start of the Fischer-Tropsch synthesis were different on a carbided catalyst (a catalyst exposed to synthesis gas) compared to a freshly reduced catalyst. The distinct transient regimes observed at the start of the Fischer-Tropsch reaction are similar to those presented in the work by Schulz *et al.* [28]. On both the fresh and carbided catalysts, carbon deposition still occurs to the same extent but water formation and methane formation are faster on the carbided catalyst. H/D exchanges reactions were used to identify the nature of the surface intermediates. The surface intermediates at the start of the Fischer-Tropsch synthesis were different to those on a carbided catalyst.
- (2) The CH_s and CCH_s surface intermediates were observed on both catalysts for methane formation and C₂ hydrocarbon formation, respectively. The other Fischer-Tropsch surface intermediates, which

were present of the fresh catalyst, either disappeared on the carbided catalyst or were too small in concentration to be detected. This observation is not consistent with the classical carbide mechanism (Chapter 1) in which CH_2 are considered the monomer building blocks and olefins are formed from H-abstraction.

- (3) Surface carbon was deposited via the Boudouard reaction using ^{13}CO on a reduced catalyst. This carbon ($^{13}\text{C}_s$) was active and detected in the C_{2+} hydrocarbon products as a coupling reaction with $^{12}\text{C}_s$ rather than with $^{13}\text{C}_s$.
- (4) Finally, combining the *in-situ* and *ex-situ* temperature programmed surface reaction data with the *in-situ* isothermal reaction data, confirmed the presence of six distinct pools of carbonaceous intermediates. These were assigned to the four main groups of carbon species as proposed by Xu and Bartholomew [31]. Two active pools of carbons ($\text{C}_{\alpha 1}$ and $\text{C}_{\alpha 2}$) can be hydrogenated up to reaction temperature (330°C) with one pool being more active than the other and having a lower coverage. Another carbonaceous intermediate ($\text{C}_{\gamma 1}$) required temperatures in excess of 483°C to be completely hydrogenated. This pool had a larger coverage than the combined C_α pools. Finally, graphitic carbon was detected at 767°C and had the highest coverage of all the surface species.

References

- [1] Steynberg, A. P., Espinoza, R. L., Jager, B., and Vosloo, A. C., *App. Catal. A: Gen.* **186** (1999), pp. 41-54.
- [2] Dry, M.E. and Steynberg, A.P., Chapter 5, in *Stud. Surf. Sci. Catal.* **152** (2004), pp 406-481
- [3] Datye, A. K., Jin, Y., Mansker, L., Motjope, R. T., Dlamini, T. H., and Coville, N. J., *Stud. Surf. Sci. Catal.* **130**, (2000), pp. 1139-1144.
- [4] Sarkar, A., Seth, D., Dozier, A., Neathery, J., Hamdeh, H., and Davis, B., *Catal. Lett.* **117** (2007), pp. 1-17.
- [5] Claeys, M. and Van Steen, E., Chapter 8, in *Stud. Surf. Sci. Catal.* **152**, (2004), pp. 601-680.
- [6] J. Happel, J., *Chem. Eng. Sci.* **33** (1978) 1567.
- [7] Bennett, C.O., Catalysis under transient conditions, ACS Symposium Series (1982) 1.
- [8] Biloen, P., *J. Mol. Catal.* **21** (1983) 17.
- [9] Shannon, S. L. and Goodwin, J., *Chem.Rev.* **95** (1995), pp. 677-695.
- [10] Van Dijk, H. A. J., PhD thesis, (2001), Technische Universiteit Eindhoven, Eindhoven, the Netherlands. <http://alexandria.tue.nl/extra2/200111083.pdf>
- [11] Efstathiou, A. M., *J. Mol. Catal.* **69** (1991), pp.41-60.
- [12] Kieffer, E. P. and van der Baan, H. S., *Appl. Catal.* **3** (1982), pp. 245-254.
- [13] Eliason, S. A. and Bartholomew, C. H., *Stud. Surf. Sci. Catal.* **111**, (1997), pp. 517-526.
- [14] Shroff, M. D. and Datye, A. K., *Catal. Lett.* **37** (1996), pp. 101-106.
- [15] Rabo, J. A., Risch, A. P., and Poutsma, M. L., *J. Catal.* **53** (1978), pp. 295-311.
- [16] Biloen, P., Helle, J. N., and Sachtler, W. M. H., *J. Catal.* **58** (1979), pp. 95-107.
- [17] Blanco, G.L., PhD thesis, (2007), Universiteit Ghent, Ghent, Belgium.
- [18] Mims, C. A. and McCandish, L. E., *J. Am. Chem. Soc.* **107** (1985), pp. 696-697.

- [19] Mims, C. A. and McCandish, L. E., *J. Phys. Chem.* **91** (1987), pp. 929-937.
- [20] Stockwell, D. M., Bianchi, D., and Bennett, C. O., *J. Catal.* **113** (1988), pp. 1324.
- [21] Raupp, G. B. and Delgass, W. N., *J. Catal.* **58** (1979), pp. 337-347.
- [22] Du Plessis, H.E., PhD thesis (2007), University of Johannesburg, South Africa
- [23] Marquez-Alvarez, C., Martin, G. A., and Mirodatos, C., *Stud. Surf. Sci. Catal.* **119** (1998), pp. 155-160.
- [24] Otarod, M., Ozawa, S., Yin, F., Chew, M., Cheh, H. Y., and Happel, J., *J. Catal.* **84** (1983), pp. 156-169.
- [25] Happel, J., Cheh, H. Y., Otarod, M., Ozawa, S., Severdia, A. J., Yoshida, T., and Fthenakis, V., *J. Catal.* **75** (1982), pp. 314-328.
- [26] Happel, J., Suzuki, I., Kokayeff, P., and Fthenakis, V., *J. Catal.* **65** (1980), pp. 59-77.
- [27] Schulz, H., Schaub, G., Claeys, M., and Riedel, T., *App. Catal. A: Gen.* **186** (1999), pp. 215-227.
- [28] Schulz, H., Riedel, T., and Schaub, G., *Top. Catal.* **32** (2005), pp. 117-124.
- [29] Govender, N. S., Botes, F. G., de Croon, M. H. J. M., and Schouten, J. C., *J. Catal.* **260** (2008), pp. 254-261.
- [30] Liu, Z. P. and Hu, P., *J. Am. Chem. Soc.* **124** (2002), pp. 11568-11569.
- [31] Xu, J. and Bartholomew, C. H., *J. Phys. Chem. B* **109** (2005), pp. 2392-2403.

4

Mechanistic pathway for methane formation over an iron-based catalyst

The methanation reaction mechanism under Fischer-Tropsch conditions is investigated with the Steady State Isotopic Transient Kinetic Analysis (SSITKA) technique over a precipitated iron-based catalyst. The $^{13}\text{CH}_4$ transients resulting from a $^{12}\text{CO} \rightarrow ^{13}\text{CO}$ switch (330 °C, 1.2 bar, and $\text{H}_2/\text{CO} = 15$) provided kinetic information for the methanation reaction. Six methanation models were screened and only three of these could describe the methane transient. These models were subsequently extended to account for the Fischer-Tropsch higher hydrocarbon products by considering C-C coupling reactions and the kinetic rate parameters were estimated. The result was two indistinguishable mechanisms which could describe the methane transient as well as the experimental steady-state concentrations. Both mechanisms have two active pools of carbon (C_α and C_β) on the catalyst surface with both leading towards the formation of methane. The C_β pool is 25 to 50 times less active than the C_α pool for methanation and occupies 92% of the total CH_x coverage (0.25 ML). The C-C coupling reaction was shown to involve both the C_α and C_β pools. The concentration of molecularly adsorbed CO on the Fe-based catalyst is shown to be extremely low, with an estimated surface coverage of $9 \cdot 10^{-4}$ ML.

4.1. Introduction

The Fischer-Tropsch synthesis (FTS) is a heterogeneously catalysed process whereby synthesis gas (a mixture of carbon monoxide and hydrogen) is converted to liquid fuels (gasoline and diesel) and chemicals [1]. Dry [2] describes two modes of operation for the Fischer-Tropsch synthesis, each with its specific selectivity targets. The high temperature (300–350°C) Fischer-Tropsch process (HTFT) aims at the production of gasoline and linear low molecular mass olefins, whereas the low temperature (200–240°C) Fischer-Tropsch process (LTFT) is used for the production of diesel and high molecular mass linear waxes. Sasol's commercial HTFT and LTFT processes are described briefly by Steynberg *et al.* [3] and Espinoza *et al.* [4], respectively, whilst details of the entire FTS have recently been published by Steynberg [5]. The HTFT process comprises a complex network of elementary reaction steps. Apart from the usual linear FT products (olefins and paraffins), these steps include the formation of CO₂, carbon, and oxygenates (alcohols, acids, aldehydes and ketones). To date, the product distribution of the HTFT process has not been fully described by the mechanisms in the literature. Kinetic equations proposed for this process have either been developed empirically or based on a mechanism, using a postulated rate determining step. Hence these expressions do not illustrate a uniform picture.

The Steady-State Isotopic Transient Kinetic Analysis (SSITKA) technique was developed by Happel [6], Bennett [7] and Biloen [8], to obtain in-situ kinetic information about reaction mechanisms and reaction intermediates on the catalyst surface. An extensive review of the SSITKA methodology is given by Shannon and Goodwin [9]. In a nutshell, this technique keeps the catalyst under steady-state conditions and introduces an isotopic transient by abruptly replacing one reactant with its isotope. For example, a feed of

$\text{H}_2/^{12}\text{CO}/\text{Ar}$ is switched to $\text{H}_2/^{13}\text{CO}/\text{He}$ with minimum disturbance to the system. The inert gas is also switched to determine the gas hold-up in the reactor. Apart from isothermal and isobaric reactor conditions, the surface composition of the catalyst does not change during SSITKA, making this technique ideal for reaction mechanistic studies. The methanation reaction has proven to be an ideal system for isotopic transient kinetic investigations due to the simple molecules involved, which are easy to trace by mass spectrometry (MS). A study of this reaction under FT conditions would be useful in developing a complete kinetic framework which could also be used to formulate more robust steady-state kinetic models. It is reasonable to assume that methane is formed by the stepwise hydrogenation of C atoms producing CH_x ($x = 1$ to 3) groups. For iron catalysts, there is still uncertainty about the abundance and nature of the surface species and the rate limiting step of the surface reactions. One reason for this is that iron forms several different types of surface carbides [10,11], some of which have been shown to be active for FTS. These key questions regarding iron catalysts have been addressed by several authors also for other FT active metal (Rh, Ru, Co and Ni) catalysts.

High CO coverage, in some cases near a monolayer, has been reported by Efstathiou *et al.* [12-16] and Siddall *et al.* [17] over Rh-based catalysts, Agnelli *et al.* [18] over Ni catalysts, Bajusz and Goodwin [19] for Ru-based catalysts, and Van Dijk *et al.* [20] for Co-based catalysts. In all of these studies, the coverage of CO was reported to be higher than the monomeric building units (CH_x). The authors of this paper are not aware of any reports in the literature for such high CO coverage on Fe-based catalysts. Mims and McCandish [21,22] performed SSITKA experiments on a promoted Fe catalyst at 237°C , $\text{H}_2/\text{CO} = 1$, and 1 bar. There was no measurable delay between the Ar and ^{13}CO transients, implying extremely low CO coverage. Stockwell *et al.* [23] studied the mechanism of methane and hydrocarbon

formation on a 10 wt% Fe/Al₂O₃ catalyst using ¹²CO to ¹³CO SSITKA. The amount of ¹²CO_{ads} measured was very small, only 8 μmol CO_{ads}·g_{cat}⁻¹ equivalent to 0.1 monolayer of CO after 1.5 hr on stream at 285°C, H₂/CO = 9, 1 bar, and 7% conversion to Fischer-Tropsch products.

The rate of CO dissociation was reported to be rate determining by both Efstathiou *et al.* [12-16] and Siddall *et al.* [17] over Rh-based catalysts, whilst for a similar catalyst, Balakos *et al.* [24] reported that hydrogenation of CH_x is the rate determining step. Stockwell *et al.* [25] on the other hand could not distinguish between these two rates on a Ni-based catalyst and concluded that both are kinetically important. More specifically, Van Dijk *et al.* [20] concluded that the C_{ads} → CH_{ads} reaction step was the rate determining step for their Co-based catalyst, whilst Mirodatos *et al.* [18,26] showed that the CH into CH₂ step was rate determining using both ¹³CO and D₂ tracing on a Ni/SiO₂ catalyst. There is uncertainty as to which elementary reaction step is rate determining during methanation. For Fe catalysts, such information obtained from transient studies has not been published.

The most abundant CH_x surface species was identified as CH_{ads} by Happel *et al.* [27] on a Ni-based catalyst. For a Co-based catalyst, Van Dijk *et al.* [20] identified C_{ads} as the most abundant methane intermediate. Krishna and Bell [28] studied chain growth during FTS over Ru/TiO₂ using ¹³CO and D₂ tracing. They concluded that the dominant species are monomeric building units (0.2 to 0.6 ML), whilst growing alkyl chains occupy less than 0.2 ML and CO_{ads} occupied an additional 0.7 ML. There are no transient studies reporting the nature of the surface species on Fe catalysts.

Two parallel pools of surface intermediates, C_αH_x and C_βH_x are proposed by Balakos [24] to react irreversibly to CH₄ on a 3 wt% Rh/SiO₂ catalyst. Happel *et al.* [27,29-31] showed that carbidic carbon consists of two pools, a smaller active C_{ads} pool and a larger methanation inactive C pool which is not

graphitic. More than a decade later [31], they showed that the data in the aforementioned studies could be modeled using a mechanism consisting of two parallel paths, where both paths lead independently to the formation of methane. Bajusz and Goodwin [19] also identified two active pools (C_α and C_β) which can be hydrogenated to methane. Both Van Dijk *et al.* [20] and Soong *et al.* [32] modeled such a pathway for a Co-based and a Raney-nickel catalyst, respectively.

The purpose of this work is to develop a plausible mechanism for the methanation reaction under HTFT conditions for an Fe-based catalysts using SSITKA. Our approach is to model the ^{13}CO and $^{13}\text{CH}_4$ transients obtained from a $^{12}\text{CO} \rightarrow ^{13}\text{CO}$ SSITKA experiment and then to use parameter estimation to discriminate between several rival models. There are no such studies to date reported in the open literature.

4.2. Results and Discussion

4.2.1. Steady State Results

Both the catalyst and the reaction should be at steady state before performing a SSITKA experiment. Steady state was monitored online by calculating the CO conversion. The data for one of our runs in Figure 4.1 shows that there is a sharp decline in the CO conversion in the first 10 hours exposure to synthesis gas. This is attributed to the changes in the catalyst morphology. Dry [33] showed that during this induction period, the iron catalyst changes from iron oxide and iron to mostly iron carbides. Du Plessis [34] observed the same high CO conversion in the first 5 to 10 hours for potassium promoted iron catalyst under HTFT conditions and used *in-situ*

XRD to show that this initial change in activity is due to the formation and stability of the various iron carbides. It is safe to assume, based on the aforementioned study and our data, that minimal changes to the catalyst occur after the first 10 hours of operation. Most of our SSITKA experiments were performed after 20 hours exposure to synthesis gas. To avoid excessive carbon formation, the synthesis was stopped overnight and re-started the following morning. Typically, the catalyst undergoes a quick re-activation (shown in Figure 4.1 at 15 hr) and then reaches the same steady state CO conversion.

4.2.2. SSITKA Results

A delay on the ^{13}CO response is usually observed with $^{12}\text{CO} \rightarrow ^{13}\text{CO}$ SSITKA experiments which results from the time required for the ^{13}CO to replace the reservoir of $^{12}\text{CO}_{\text{ads}}$. This phenomenon is commonly referred to as the chromatographic effect [9,33,34]. The absence of this chromatographic effect in our results, shown in Figure 4.2, suggests an extremely low surface coverage of CO_{ads} . The breakthrough of ^{13}CO is extremely fast and in all cases overlaps the Ne signal. This is consistent with the results by Mims *et al.* [21,22], Saudsakorn *et al.* [35] and Stockwell *et al.* [23] obtained on other Fe-based catalysts using the same transient technique at LTFT conditions. It has also been well documented [36,37] that low temperatures (-80°C) are required to accurately measure CO chemisorbed on iron catalysts because it readily dissociates at room temperature. We could only measure $37 \mu\text{mol CO.g}_{\text{cat}}^{-1}$ at 25°C corresponding to a coverage of 0.1 ML, based on a surface area of $16 \text{ m}^2.\text{g}^{-1}$ obtained by N_2 physisorption.

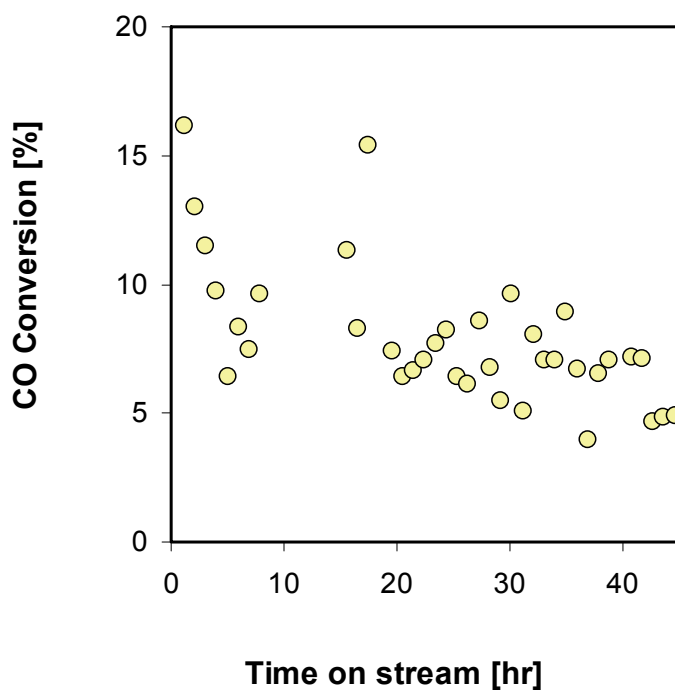


Figure 4.1: CO conversion data obtained at $H_2/CO = 15$, 330°C , 1.2 bar , and $GHSV = 7412\text{ ml}\cdot\text{hr}^{-1}\cdot\text{g}_{\text{cat}}^{-1}$.

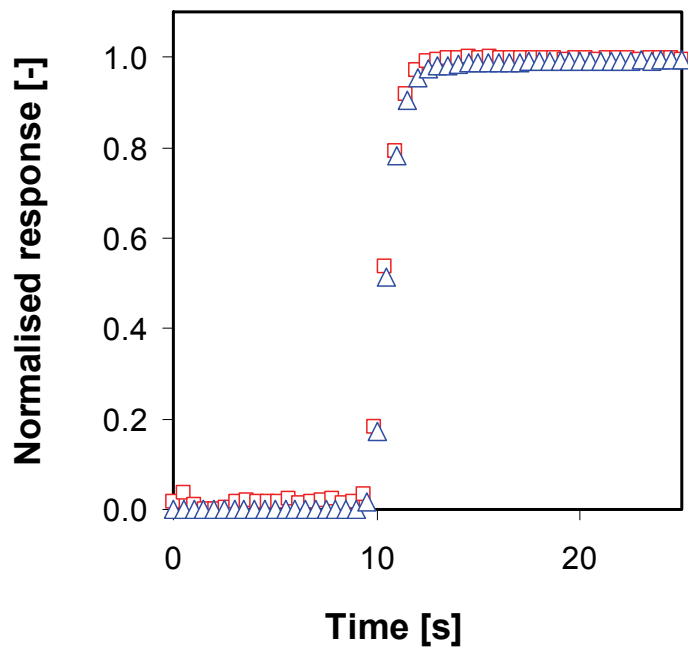


Figure 4.2: Normalised transient responses for ^{13}CO (Δ) and Ne (\square) obtained at $H_2/CO = 15$, 330°C , 1.2 bar , and $GHSV = 7412\text{ ml}\cdot\text{hr}^{-1}\cdot\text{g}_{\text{cat}}^{-1}$. For clarity reasons, data from only one run is shown.

The surface concentration of CO_{ads} can also be calculated according to:

$$L_{CO} = \frac{\tau_{CO} \cdot F_{CO}}{W_{cat}} = \frac{F_{CO}}{W_{cat}} \int_{t=0}^{\infty} [E_{^{12}CO}(t) - E_{Ne}(t)] dt \quad [8]$$

where L_{CO} is the surface concentration of CO_{ads} in mole.kg_{cat}⁻¹; F_{CO} is the molar feed rate of CO in moles.s⁻¹; τ_{CO} is the mean residence time of CO_{ads} in s; W_{cat} is the weight of catalyst in the reactor bed in kg_{cat}; $E_{^{12}CO}$ is the normalised transient of ¹²CO; and E_{Ne} is the normalised transient of Ne. The surface concentration calculated in this way is independent of the reaction mechanism. The mean residence time could not be accurately determined because of the extremely low CO coverage. A maximum value of 0.05 s was used in our study which resulted in a surface concentration of $2.4 \cdot 10^{-4}$ mole.kg_{cat}⁻¹ ($\sim 9 \cdot 10^{-4}$ ML). This amount of CO on our Fe-based catalyst is 32 times lower than that reported by Stockwell *et al.* [23]. This deviation can be best ascribed to the higher temperatures used in this study.

The ¹³CH₄ transients for different runs at the same experimental conditions are presented in Figure 4.3. The ¹³CH₄ transients reached 100% marking after 45 min but 90% of this is observed in the first 15 to 20 min. It seems that there are two distinct processes occurring; a fast route to methanation in the first few minutes and then a slower route which takes at least a further 30 min. The possibility that methane can readsorb and hence causes such a delay was also investigated. This was performed by using the transient switch, Ar → CH₄/Ne after the catalyst reached steady state and the reactor was purged with inert. The results (Figure 4.4) show that there is no delay between the Ne and CH₄ transients confirming that methane does not readsorb onto the catalyst surface under our reaction conditions.

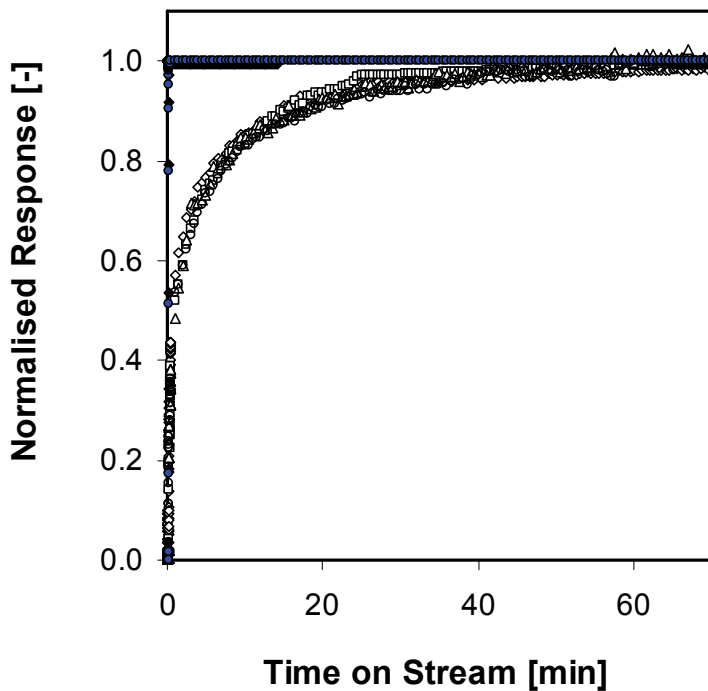


Figure 4.3: Normalised transient responses for ^{13}CO (\blacklozenge), Ne (\bullet) and $^{13}\text{CH}_4$ (\circ , \square , Δ , and \diamond) obtained at $\text{H}_2/\text{CO} = 15$, 330°C , 1.2 bar , and $\text{GHSV} = 7412\text{ ml.hr}^{-1}.\text{g}_{\text{cat}}^{-1}$.

The surface concentration of $\text{C}_{1,\text{ads}}$ can also be calculated from the transient data according to:

$$L_{\text{C}_1} = \frac{\tau_{\text{C}_1} \cdot F_{\text{CO}} \cdot X_{\text{CO}}}{W_{\text{cat}}} = \frac{F_{\text{CO}} \cdot X_{\text{CO}}}{W_{\text{cat}}} \left(\int_{t=0}^{\infty} [E_{^{12}\text{CH}_4}(t) - E_{\text{Ne}}(t)] dt - \frac{1}{2} \int_{t=0}^{\infty} [E_{^{12}\text{CO}}(t) - E_{\text{Ne}}(t)] dt \right) \quad [9]$$

where X_{CO} is the conversion of CO. The mean residence of $\text{C}_{1,\text{ads}}$ was *ca.* 1000 s which resulted in a surface concentration of 0.08 mole.kg^{-1} (or 0.2 ML) for the total $\text{C}_{1,\text{ads}}$ species. This higher surface coverage of $\text{C}_{1,\text{ads}}$ than of CO_{ads} on our Fe catalyst is different to all other FT metals (see introduction). This is consistent with recent kinetic modelling. Botes and Breman [in 38] have shown that at commercially relevant conditions, the reaction order for CO on the iron-based is positive whilst for the cobalt-based catalyst it is

negative. This implies that the CO coverage on the iron-based catalyst is lower than for the cobalt-based catalyst.

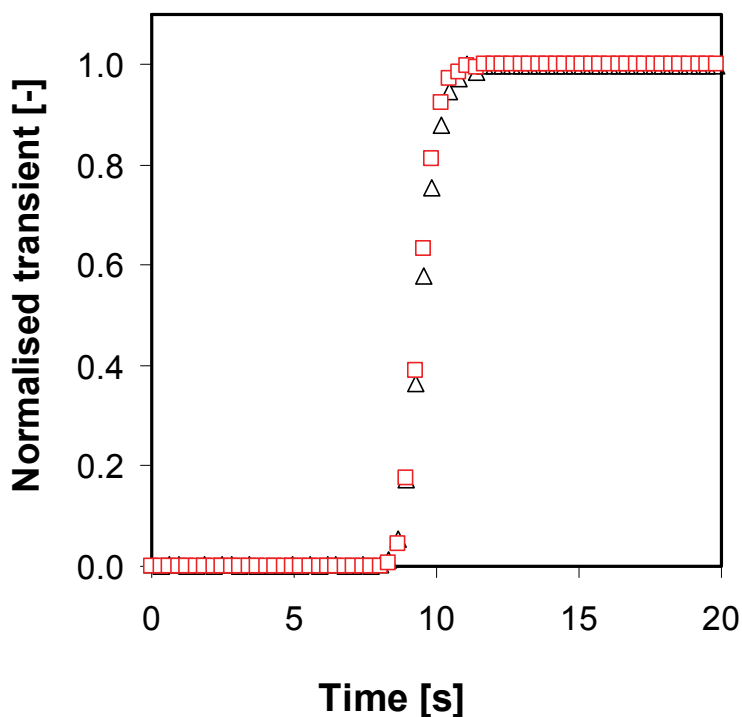


Figure 4.4: . Normalised transient responses for Ne (Δ) and $^{13}\text{CH}_4$ (\square) obtained at 330°C and 1.2 bar after a Ar \rightarrow CH₄/Ne transient switch.

4.2.3. Model Identification and Discrimination

Based on two gas phase components (CO and CH₄) and three surface species components (CO_{ads}, C_{αads}, C_{βads}), Van Dijk *et al.* [20] tested six possible methanation models, shown in Figure 4.5. Some of these models have also been used by Happel [33] and Soong *et al.* [32]. The same set of models was screened in our study using parameter estimation. Apart from model 1, there are six kinetic parameters to be estimated for each model. Our initial efforts showed that some of these parameters are highly correlated. To simplify the parameter estimation process, k_{ads} and k_{des} were fixed. The

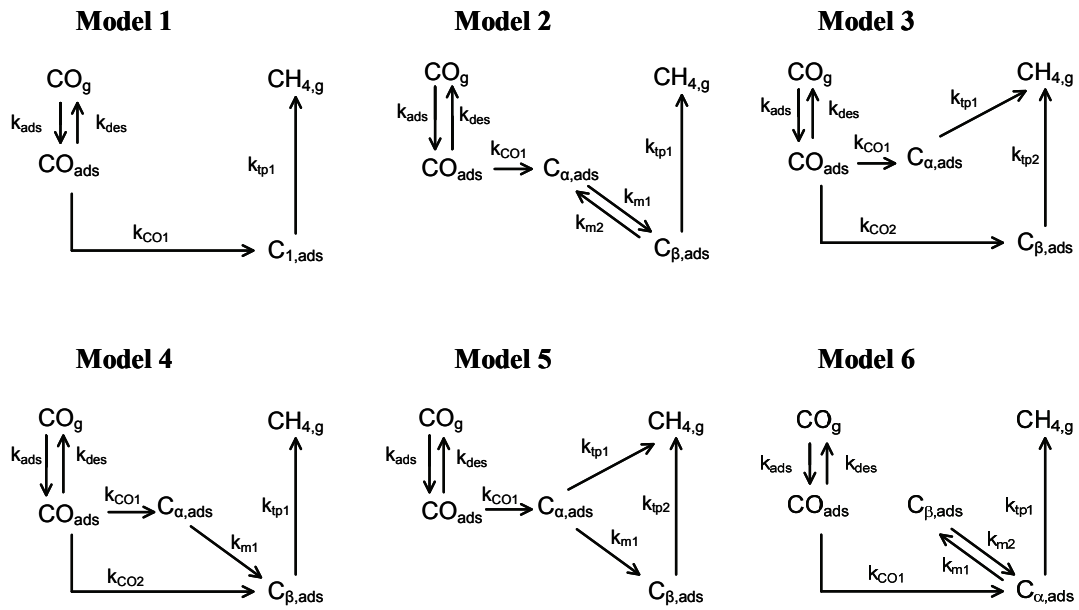


Figure 4.5: Schematic representation of the six methanation models based on CO and CH₄ in the gas phase and CO_{ads}, C_α and C_β as the surface components.

adsorption/desorption of CO was considered to be a fast reaction and in equilibrium. The consumption of CO_{ads} to form FT products relative to desorption into the gas phase was insignificant for k_{ads} values greater than 0.07 moles.kg_{cat}⁻¹.s⁻¹ resulting in a CO equilibrium constant of 2.6 10⁻³ mole.kg_{cat}⁻¹. So, for modeling purposes any arbitrary value of k_{ads} greater than 0.07 moles.kg_{cat}⁻¹.s⁻¹ can be chosen and k_{des} can be calculated from the CO equilibrium constant. In this study, the modeling results for a k_{ads} value of 0.1 moles.kg_{cat}⁻¹.s⁻¹ with a corresponding k_{des} of 38 s⁻¹ are presented.

The model predictions for ¹³CH₄ obtained using the optimised parameters (in Table 4.1) are presented in Figure 4.6. Methanation models 1, 2, and 4 fail to describe the ¹³CH₄ transients, whilst models 3, 5, and 6 give the best fits. A weighted residual value less than the chi-squared value is considered a good fit. In Table 4.1, the weighted residuals for models 3 and 5 are lower than the chi-squared values indicating a good fit, whereas model 6 has a higher weighted residual, and hence is considered a bad fit. However, all three

models predict both the surface concentration of CO_{ads} and the gas phase concentration of CH_4 equally well. So, at this stage of the modeling, we cannot rule out model 6 based only on the weighted residual value. This issue of model identifiability and distinguishability with this type of modeling has been discussed by Happel [33] and was also reported by Van Dijk *et al.* [20]. These authors showed that successful further model discrimination is possible if either more experimental data other than from SSITKA is considered, or the models are extended to incorporate the formation of heavier hydrocarbons. An example of the former approach could be quantification of the surface concentrations of C_α and C_β using a suitable characterization technique. The latter approach is used in this study.

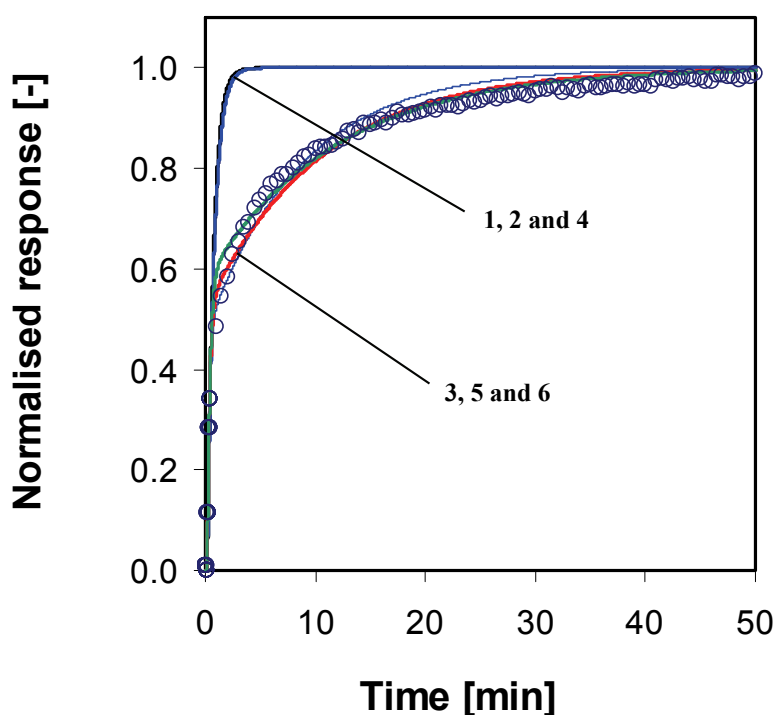


Figure 4.6: Model predictions for the $^{13}\text{CH}_4$ transients for the methanation models shown in Figure 4.5. The symbols (o) are $^{13}\text{CH}_4$ data points obtained at $\text{H}_2/\text{CO} = 15$, 330°C , 1.2 bar , and $\text{GHSV} = 7412 \text{ ml.hr}^{-1}.\text{g}_{\text{cat}}^{-1}$ and the solid lines are the model predictions.

Table 4.1: Optimised parameter estimates for the methanation reaction according to the models in Figure 4.5. The surface concentration of CO_{ads} and the gas phase concentration of CH_4 are the model predictions using the corresponding optimal parameter estimates.

	Model 1	Model 2	Model 3	Model 4	Model 5	Model 6
k_{co1}	$6.24 \cdot 10^{-1} \pm 2.9 \cdot 10^{-2}$	$1.40 \pm 2.4 \cdot 10^{-1}$	$5.26 \cdot 10^{-1} \pm 1.6 \cdot 10^{-2}$	$4.85 \cdot 10^{-1} \pm 12.74$	$6.49 \cdot 10^{-1} \pm 2.9 \cdot 10^{-2}$	$6.26 \cdot 10^{-1} \pm 2.9 \cdot 10^{-2}$
k_{co2}			$1.25 \cdot 10^{-1} \pm 1.6 \cdot 10^{-2}$	$1.51 \cdot 10^{-1} \pm 12.73$		
k_{m1}		$1.62 \cdot 10^{-1} \pm 5.4 \cdot 10^{-2}$		2.29 ± 237	$1.29 \cdot 10^{-2} \pm 2.2 \cdot 10^{-3}$	$2.57 \cdot 10^{-2} \pm 3.6 \cdot 10^{-3}$
k_{m2}		$9.8 \cdot 10^{-2} \pm 6.3 \cdot 10^{-3}$				$2.40 \cdot 10^{-3} \pm 3.0 \cdot 10^{-4}$
k_{fp1}	$9.10 \cdot 10^{-3} \pm 8.0 \cdot 10^{-4}$	$8.40 \cdot 10^{-3} \pm 3.0 \cdot 10^{-3}$	$1.97 \cdot 10^{-2} \pm 2.4 \cdot 10^{-3}$	$9.40 \cdot 10^{-3} \pm 1.0 \cdot 10^{-3}$	$1.49 \cdot 10^{-2} \pm 1.4 \cdot 10^{-3}$	$1.34 \cdot 10^{-2} \pm 1.3 \cdot 10^{-3}$
k_{fp2}			$1.90 \cdot 10^{-3} \pm 2.0 \cdot 10^{-4}$		$1.60 \cdot 10^{-3} \pm 1.0 \cdot 10^{-4}$	
χ^2 ^b	1243	1652	1652	1652	1652	1652
WR ^a	4084	3856	455	2456	436	2070
L_{CO}	$2.80 \cdot 10^{-4} \pm 1 \cdot 10^{-5}$	$2.34 \cdot 10^{-4} \pm 1 \cdot 10^{-5}$	$2.79 \cdot 10^{-4} \pm 1 \cdot 10^{-5}$	$2.80 \cdot 10^{-4} \pm 1 \cdot 10^{-5}$	$2.91 \cdot 10^{-4} \pm 1 \cdot 10^{-5}$	$2.87 \cdot 10^{-4} \pm 1 \cdot 10^{-5}$
$\text{CH}_{4,\text{ss}}$	$1.76 \cdot 10^{-3} \pm 2 \cdot 10^{-4}$	$6.17 \cdot 10^{-4} \pm 2 \cdot 10^{-4}$	$1.96 \cdot 10^{-3} \pm 2 \cdot 10^{-4}$	$1.80 \cdot 10^{-3} \pm 2 \cdot 10^{-4}$	$1.90 \cdot 10^{-3} \pm 2 \cdot 10^{-4}$	$1.70 \cdot 10^{-3} \pm 2 \cdot 10^{-4}$

Units: all k 's in [s^{-1}], L_{CO} in [$\text{mole} \cdot \text{kg}_{\text{cat}}^{-1}$] and $\text{CH}_{4,\text{ss}}$ in [$\text{mole} \cdot \text{m}_g^{-3}$].

^a WR is the weighted residual obtained from the parameter estimation results.

^b χ^2 is the 95% chi-squared value obtained from the parameter estimation results.

4.2.4. Parameter Quantification

The methanation models 3, 5, and 6 (in Figure 4.5) can describe our methanation results better than the other three models. These models are thus suitable to extend towards the formation of the higher hydrocarbon Fischer-Tropsch products, and by doing so, the parameters for the methanation models can be quantified. Both chain-growth and chain-initiation need to be considered when modeling the Fischer-Tropsch synthesis. The latter reaction is not considered in full as this will require modeling the transients of the higher hydrocarbons which is not in the scope of this chapter. However, the formation of the higher hydrocarbons from C_α and C_β is included in our modeling as a net consumption rate [39]. Chain-initiation involves C-C coupling reactions and is included in the models via the combination of: (1) two C_α species, (2) one C_α and one C_β species, and (3) two C_β species, as shown in Figure 4.7 for models 3, 5 and 6. Model 3 is considered symmetrical since the C_α and C_β are interchangeable. In other words, the results for the reaction of two C_α species will be the same as for two C_β species reacting. Hence only two combinations are considered for model 3.

In Table 4.2, the parameter estimation results for all the models in Figure 4.7 are presented and the model descriptions of $^{13}\text{CH}_4$ according to the optimised parameters are shown in Figure 4.8. Model 5.3 is discarded because it could not describe the methane and also failed to predict the steady-state surface and gas phase concentrations. Both combinations of chain-initiation for model 3 can describe the methane transient and both models give good fits according to their weighted residuals. However, model 3.1 predicts a lower $C_{1,\text{tot}}$ coverage (0.07 ML) compared to model 3.2 (0.16 ML). On the basis that our experimental value for $C_{1,\text{tot}}$ is *ca.* 0.2 ML, model 3.1 is discarded. Models 5.1, 6.1 and 6.2 are also discarded for the same reason of predicting a low $C_{1,\text{tot}}$ coverage. For the methanation model 5, the combination of C_α and C_β (model 5.2) can describe the methane transient with a good fit (see Table 4.2).

The predicted surface and gas phase concentrations for this model are similar to model 3.2 and cannot be further distinguished. Lastly, model 6.3 could describe both surface concentrations adequately but the rate of the C-C coupling reaction, k_i , was not statistically significant. In fact, k_i was poorly estimated in all combinations for the methanation model 6 (models 6.1, 6.2 and 6.3).

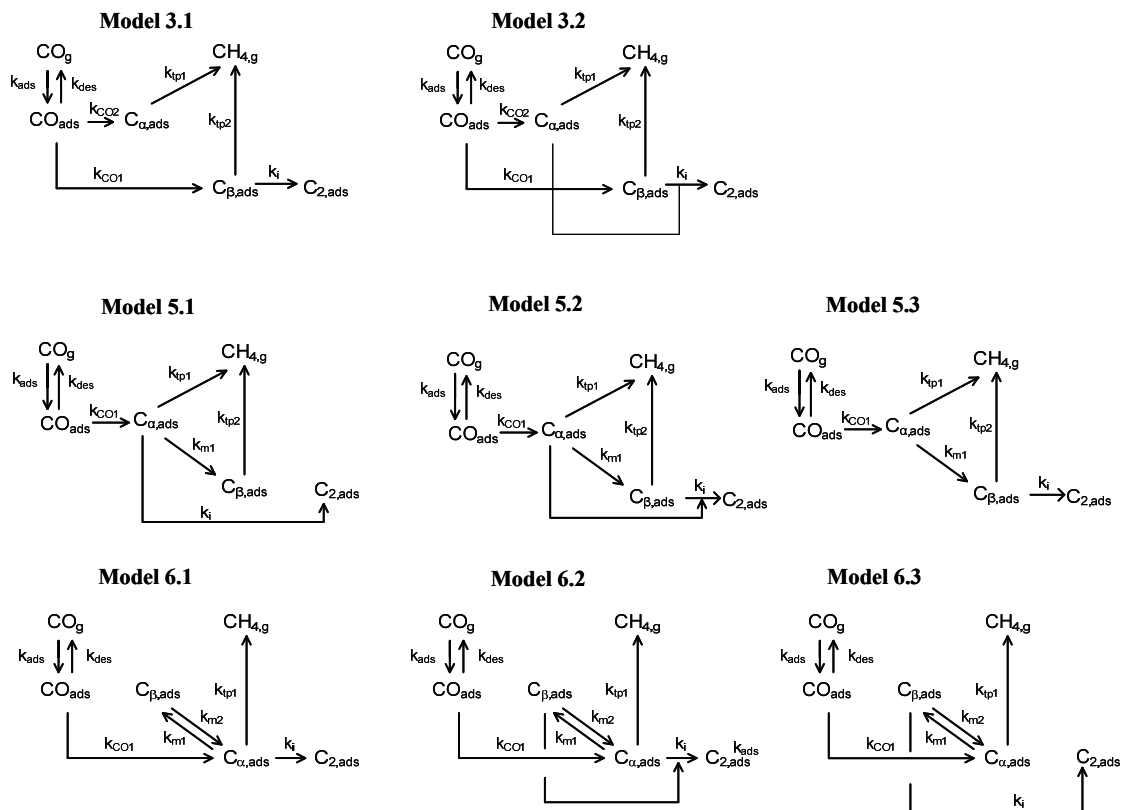


Figure 4.7: Schematic representation of the models for the Fischer-Tropsch reaction taking into account different chain initiation pathways based on the three indistinguishable methanation models in Figure 4.5.

Table 4.2: Optimised parameter estimates for the methanation reaction according to the models in Figure 4.7. The surface concentrations of CO_{ads} , C_{cs} and C_{β} , and the gas phase concentration of CH_4 are the model predictions using the corresponding optimal parameter estimates. *Italic values are insignificant parameter estimates.*

	Model 3.1	Model 3.2	Model 5.1	Model 5.2	Model 5.3	Model 6.1	Model 6.2	Model 6.3
k_{co1}	$3.63 \cdot 10^{-1} \pm 2.3 \cdot 10^{-1}$	$3.38 \cdot 10^{-1} \pm 1.2 \cdot 10^{-1}$	$3.82 \cdot 10^{-1} \pm 2.3 \cdot 10^{-1}$	$6.37 \cdot 10^{-1} \pm 2.4 \cdot 10^{-1}$	$2.60 \cdot 10^{-1} \pm 2.25 \cdot 10^{-1}$	$3.22 \cdot 10^{-1} \pm 2.3 \cdot 10^{-1}$	$3.15 \cdot 10^{-1} \pm 2.3 \cdot 10^{-1}$	$3.29 \cdot 10^{-1} \pm 2.3 \cdot 10^{-1}$
k_{co2}	$1.16 \cdot 10^{-1} \pm 1.3 \cdot 10^{-2}$	$2.39 \cdot 10^{-1} \pm 1.2 \cdot 10^{-1}$	-	-	-	-	-	-
k_{m1}	-	-	$3.10 \cdot 10^{-2} \pm 1.9 \cdot 10^{-2}$	$2.95 \cdot 10^{-2} \pm 3.2 \cdot 10^{-3}$	$2.76 \cdot 10^{-1} \pm 3.63 \cdot 10^{-2}$	$2.40 \cdot 10^{-2} \pm 3.3 \cdot 10^{-3}$	$2.77 \cdot 10^{-1} \pm 1.4 \cdot 10^{-2}$	$4.22 \cdot 10^{-2} \pm 1.9 \cdot 10^{-2}$
k_{m2}	-	-	-	-	-	$2.26 \cdot 10^{-3} \pm 2.7 \cdot 10^{-4}$	$2.59 \cdot 10^{-3} \pm 1.3 \cdot 10^{-3}$	$1.93 \cdot 10^{-3} \pm 9.0 \cdot 10^{-4}$
k_{fp1}	$2.74 \cdot 10^{-2} \pm 1.7 \cdot 10^{-3}$	$2.78 \cdot 10^{-2} \pm 9.9 \cdot 10^{-3}$	$3.11 \cdot 10^{-2} \pm 1.9 \cdot 10^{-2}$	$1.59 \cdot 10^{-2} \pm 5.9 \cdot 10^{-3}$	$1.55 \cdot 10^{-2} \pm 1.6 \cdot 10^{-2}$	$2.76 \cdot 10^{-2} \pm 1.9 \cdot 10^{-2}$	$2.79 \cdot 10^{-2} \pm 2.0 \cdot 10^{-2}$	$2.69 \cdot 10^{-2} \pm 1.9 \cdot 10^{-2}$
k_{fp2}	$1.47 \cdot 10^{-3} \pm 7.3 \cdot 10^{-5}$	$7.69 \cdot 10^{-4} \pm 3.8 \cdot 10^{-4}$	$1.8 \cdot 10^{-3} \pm 8.5 \cdot 10^{-5}$	$6.61 \cdot 10^{-4} \pm 3.0 \cdot 10^{-4}$	$3.02 \cdot 10^{-4} \pm 3.3 \cdot 10^{-4}$	-	-	-
k_f	8.24 ± 5.31	$8.33 \cdot 10^{-1} \pm 1.4 \cdot 10^{-1}$	3.27 ± 21.8	$4.23 \cdot 10^{-1} \pm 5.16 \cdot 10^{-2}$	$2.85 \cdot 10^{-2} \pm 4.9 \cdot 10^{-3}$	$1.60 \cdot 10^{-4} \pm 6.52$	$1.05 \cdot 10^{-3} \pm 6.6 \cdot 10^{-4}$	$2.40 \cdot 10^{-3} \pm 2.4 \cdot 10^{-2}$
χ^2 ^b	1651	1651	1651	1651	1651	1651	1651	1651
WR ^a	1437	1448	1480	1411	2314	2084	2075	2074
L_{CO}	$2.34 \cdot 10^{-4} \pm 1 \cdot 10^{-5}$	$2.31 \cdot 10^{-4} \pm 1 \cdot 10^{-5}$	$2.36 \cdot 10^{-4} \pm 1 \cdot 10^{-5}$	$2.30 \cdot 10^{-4} \pm 1 \cdot 10^{-5}$	$2.40 \cdot 10^{-4} \pm 1 \cdot 10^{-5}$	$2.38 \cdot 10^{-4} \pm 1 \cdot 10^{-5}$	$2.38 \cdot 10^{-4} \pm 1 \cdot 10^{-5}$	$2.38 \cdot 10^{-4} \pm 1 \cdot 10^{-5}$
L_{Ca}	$1.30 \cdot 10^{-3}$	$1.01 \cdot 10^{-3}$	$1.01 \cdot 10^{-3}$	$2.02 \cdot 10^{-3}$	$2.14 \cdot 10^{-4}$	$1.99 \cdot 10^{-3}$	$1.91 \cdot 10^{-3}$	$1.95 \cdot 10^{-3}$
$L_{C\beta}$	$1.82 \cdot 10^{-2}$	$3.40 \cdot 10^{-2}$	$1.72 \cdot 10^{-2}$	$3.89 \cdot 10^{-2}$	$2.32 \cdot 10^{-2}$	$2.06 \cdot 10^{-2}$	$2.04 \cdot 10^{-2}$	$2.96 \cdot 10^{-2}$
$L_{C1,tot}$	$1.90 \cdot 10^{-2}$	$6.94 \cdot 10^{-2}$	$2.52 \cdot 10^{-2}$	$6.11 \cdot 10^{-2}$	$1.21 \cdot 10^{-1}$	$2.86 \cdot 10^{-2}$	$3.06 \cdot 10^{-2}$	$5.84 \cdot 10^{-2}$
θ_{CO}	0.0009	0.0009	0.0009	0.0009	0.0009	0.0009	0.0009	0.0009
$\theta_{C1,tot}$	0.07	0.13	0.07	0.16	0.09	0.09	0.08	0.12
$CH_{4,ss}$	$2.30 \cdot 10^{-3}$	$2.12 \cdot 10^{-3}$	$3.56 \cdot 10^{-3}$	$1.99 \cdot 10^{-3}$	$2.09 \cdot 10^{-3}$	$2.92 \cdot 10^{-3}$	$2.87 \cdot 10^{-3}$	$2.67 \cdot 10^{-3}$

Units: all k 's in [s^{-1}] except k_f in [$kg_{cat} \cdot mole^{-1} \cdot s^{-1}$], L_{CO} in [$mole \cdot kg_{cat}^{-1}$] and $CH_{4,ss}$ in [$mole \cdot m^{-3}$].

^a WR is the weighted residual obtained from the parameter estimation results.; and ^b χ^2 is the 95% chi-squared value obtained from the parameter estimation results.

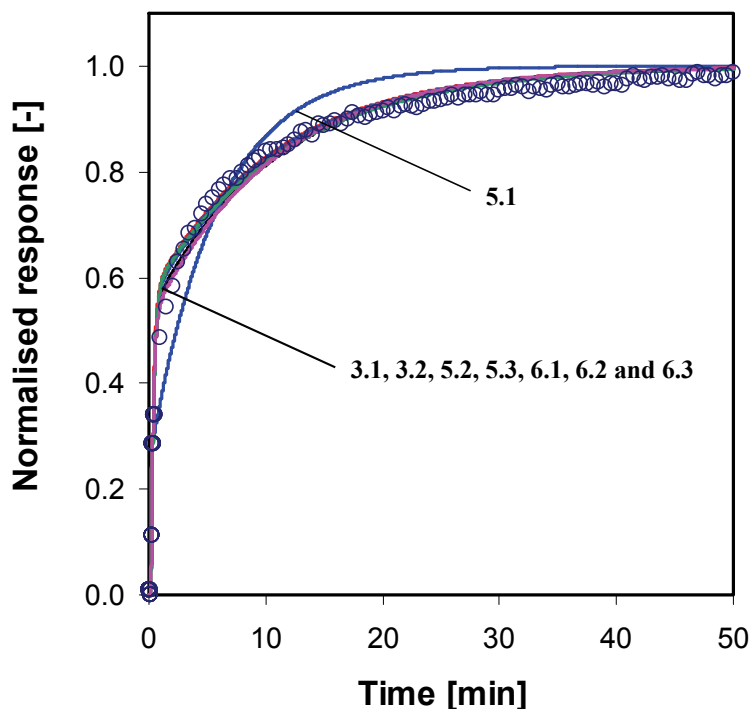


Figure 4.8: Model predictions for the $^{13}\text{CH}_4$ transients for the models in **Figure 4.7**. The symbols (o) are $^{13}\text{CH}_4$ data points obtained at $\text{H}_2/\text{CO} = 15$, 330°C , 1.2 bar , and $\text{GHSV} = 7412 \text{ ml.hr}^{-1}.\text{g}_{\text{cat}}^{-1}$, and the solid lines are the model predictions.

The buffer step in this model seems to play a significant role in the parameter estimation. The rates constants for this buffer step (k_{m1} and k_{m2}) seem to fluctuate to match the desired surface and gas-phase concentrations without adequately accounting for the C-C coupling reactions. Methanation model 6 is a suitable candidate for describing the methanation results alone but it is inconceivable that this model can be extended to account for the Fischer-Tropsch process. Hence these models (6.1, 6.2 and 6.3) are all discarded.

Finally, the rates of the surface reactions for the models 3.2 and 5.2 are compared to obtain more insight. The rate of CO dissociation, $k_{\text{CO}1}$ for model 5.2 and $(k_{\text{CO}1} + k_{\text{CO}2})$ for model 3.2, is $0.8\text{-}0.9 \text{ s}^{-1}$, with $k_{\text{CO}1}$ equivalent to $k_{\text{CO}2}$ in model 3.2. This rate is two times higher than that reported by Van Dijk [39]

for the Co-based catalyst, suggesting that CO dissociates easier on Fe than Co catalysts which is consistent with the study reported by Vannice [40]. Both models have similar termination rate constants with termination from the C_β pool being the rate determining step (25-50 less active for methanation). No further model discrimination between these two models is possible based on the available experimental data.

In summary, models 3.2 and 5.2 both give the best fits for the methanation transients and predict similar steady-state concentrations of CH_4 in the gas-phase and the surface concentrations of CO_{ads} , C_α , and C_β . Both these models have two pathways towards the formation of methane. In model 3.2 these pathways are independent whereas in model 5.2, the C_α and C_β pools are interlinked. Chain-initiation involves the combination of both these carbon pools.

4.3. Conclusions

Experimental observations obtained using a $^{12}\text{CO} \rightarrow ^{13}\text{CO}$ transient switch indicated that molecularly adsorbed CO on the Fe/K catalyst is extremely low, *ca.* $9 \cdot 10^{-4}$ ML, whilst the $C_{1,\text{tot}}$ is much higher, 0.25 ML. For the methanation reactions, the parameter estimation study showed that three models are indistinguishable. All these models have a buffer step or parallel route towards the formation of methane. The chain initiation reaction (C-C coupling) was included which resulted in eight models being tested. The results showed that two models remain indistinguishable. Both these models have two surface intermediates (C_α and C_β) active towards methanation and higher hydrocarbon formation. The quantification of the kinetic rate parameters was performed by accounting for the higher hydrocarbon formation. The results showed that C_β is the larger pool, occupying 92% of the $C_{1,\text{tot}}$ coverage and is 25-50 less active for methanation than C_α . The

chain-initiation reaction (C-C coupling) involves a combination of C_α and C_β to form the C_2 surface intermediate.

References

- [1] M.E. Dry, *Appl. Catal. A* **138** (1996) 319.
- [2] M.E. Dry, *Catal. Today* **71** (2002) 227.
- [3] A.P. Steynberg, R.L. Espinoza, B. Jager, A.C. Vosloo, *Appl. Catal. A* **186** (1999) 41.
- [4] R.L. Espinoza, A.P. Steynberg, B. Jager, A.C. Vosloo, *Appl. Catal. A* **186** (1999) 13.
- [5] A.P. Steynberg, *Studies in Surface Science and Catalysis* **152** (2004) 1.
- [6] J. Happel, *Chem. Eng. Sci.* **33** (1978) 1567.
- [7] C.O. Bennett, *Catalysis under transient conditions*, ACS Symposium Series (1982) **1**.
- [8] P. Biloen, *J. Mol. Catal.* **21** (1983) 17.
- [9] S.L. Shannon, J. Goodwin, *Chem. Rev.* **95** (1995) 677.
- [10] J. Galuszka, T. Sano, J.A. Sawicki, *J. Catal.* **136** (1992) 96.
- [11] J. Xu, C.H. Bartholomew, *J. Phys. Chem. B* **109** (2005) 2392.
- [12] A.M. Efstathiou, C.O. Bennett, *Chem. Eng. Comm.* **83** (1989) 129.
- [13] A.M. Efstathiou, T. Chafik, D. Bianchi, C.O. Bennett, *J. Catal.* **147** (1994) 24.
- [14] A.M. Efstathiou, C.O. Bennett, *J. Catal.* **120** (1989) 118.
- [15] A.M. Efstathiou, C.O. Bennett, *J. Catal.* **120** (1989) 137.
- [16] A.M. Efstathiou, *J. Mol. Catal.* **69** (1991) 41.
- [17] J.H. Siddall, M.L. Miller, W.N. Delgass, *Chem. Eng. Comm.* **83** (1989) 261.
- [18] M. Agnelli, H.M. Swaan, C. Marquez-Alvarez, G.A. Martin, C. Mirodatos, *J. Catal.* **175** (1998) 117.
- [19] I.G. Bajusz, J. Goodwin, *J. Catal.* **169** (1997) 157.
- [20] H.A.J. Van Dijk, J.H.B.J. Hoebink, J.C. Schouten, *Top. Catal.* **26** (2003) 111.
- [21] C.A. Mims, L.E. McCandish, *J. Am. Chem. Soc.* **107** (1985) 696.
- [22] C.A. Mims, L.E. McCandish, *J. Phys. Chem.* **91** (1987) 929.
- [23] D.M. Stockwell, D. Bianchi, C.O. Bennett, *J. Catal.* **113** (1988) 13.
- [24] M.W. Balakos, S.S.C. Chuang, G. Srinivas, M.A. Brundage, *J. Catal.* **157** (1995) 51.
- [25] D.M. Stockwell, J.S. Chung, C.O. Bennett, *J. Catal.* **112** (1988) 135.
- [26] C. Marquez-Alvarez, G.A. Martin, C. Mirodatos, *Studies in Surface Science and Catalysis* **119** (1998) 155.

- [27] J. Happel, H.Y. Cheh, M. Otarod, S. Ozawa, A.J. Severdia, T. Yoshida, V. Fthenakis, *J. Catal.* **75** (1982) 314.
- [28] K.R. Krishna, A.T. Bell, *J. Catal.* **139** (1993) 104.
- [29] J. Happel, I. Suzuki, P. Kokayeff, V. Fthenakis, *J. Catal.* **65** (1980) 59.
- [30] M. Otarod, S. Ozawa, F. Yin, M. Chew, H.Y. Cheh, J. Happel, *J. Catal.* **84** (1983) 156.
- [31] M. Otarod, J. Happel, E. Walter, *Appl. Catal. A* **160** (1997) 3.
- [32] Y. Soong, K. Krishna, P. Biloen, *J. Catal.* **97** (1986) 330.
- [33] J. Happel, *Isotopic Assessment of Heterogeneous Reactors*. Academic Press, Inc., 1986.
- [34] C.O. Bennett, in: A.T. Bell, L.L. Hegedus (Editors), *Catalysis under Transient Conditions*. American Chemical Society, 1982, p. 1.
- [35] gPROMS Advanced User Guide, Process Systems Enterprise, 2004, p. 37.
- [36] M.E. Dry, The Fischer-Tropsch synthesis, in: R.B Anderson, and M. Boudart, (Eds.), *Catalysis Science and Technology*, Vol. 15-255, Springer-Verlag, Berlin (1981). 1
- [37] H.E. du Plessis, *The crystal structures of the iron carbides*, Ph.D thesis, 2007, University of Johannesburg, South Africa.
- [38] P. Biloen, J.N. Helle, F.G.A. van den Berg, W.M.H. Sachtler, *J. Catal.* **81** (1983) 450.
- [39] K. Sudsakorn, J. Goodwin, A.A. Adeyiga, *J. Catal.* **213** (2003) 204.
- [40] D. Bianchi, S. Borcar, F. Teule-Gay, C.O. Bennett, *J. Catal.* **82** (1983) 442.
- [41] M. Boudart, A. Delbouille, J.A. Dumesic, S. Khammouma, H. Topsoe, *J. Catal.* **37** (1975) 486.
- [42] F.G. Botes, *Catal. Rev. Sci. Eng.* (2008), accepted for publication.
- [43] H.A.J. Van Dijk, A mechanistic study using transient isotopic tracing, Ph.D thesis, 2001, Technische Universiteit Eindhoven, Eindhoven, the Netherlands.
<http://alexandria.tue.nl/extra2/200111083.pdf>
- [44] M.A. Vannice, *J. Catal.* **37** (1975) 462.

5

Effects of co-fed ethylene during the high temperature Fischer-Tropsch synthesis

In this chapter, the effect of co-fed ethene on the Fischer-Tropsch synthesis is investigated. The main aim was to identify reaction pathways for readsorbed olefins. Steady state results (at 330°C, 1.2 bar, $H_2/CO = 15$ and $7580 \text{ ml.g}_{\text{cat}}^{-1}.\text{hr}^{-1}$) showed that the hydrogenation of ethene to ethane is the main reaction pathway but chain growth does occur to a lesser extent. Moreover, methane formation was suppressed whilst there was no effect on the water-gas-shift rate. Repeating these co-fed ethene experiments at the same reaction conditions but with ^{13}CO in the feed showed that in terms of chain growth, propene formation was favoured instead of propane. This suggests that the olefins share the same surface intermediate. Mechanisms are proposed to account for the above experimental observations.

5.1. Introduction

The products obtained during the Fischer-Tropsch Synthesis (FTS) were found to follow a polymerization-like distribution, the so-called Anderson-Schulz-Flory (ASF) distribution [1,2]:

$$W_n = n(1 - \alpha)^2 \alpha^{n-1} \quad [1]$$

where W_n is the mass fraction of the products containing n carbon atoms, n is the carbon number and α is the probability of chain growth. Deviations from the ideal (linear) ASF product distribution have been reported in many studies [3,4]. The usual deviations are: (1) a relatively higher selectivity to methane; (2) a relatively lower selectivity to ethane and ethylene (C_2 's); (3) a relatively low olefin:paraffin ratio for C_2 ; (4) an increase in chain growth probability with increasing carbon number; and (5) an exponential decrease of the olefin to paraffin ratio with increasing chain length in comparison to the ideal ASF distribution.

Olefin readsorption studies have received the most attention in terms of describing these deviations from the ASF distribution, which resulted in various hydrocarbon selectivity models. Briefly, Iglesia *et al.* [5] developed their *transport-enhanced α -olefin readsorption model* on a 1.2 wt% Ru/TiO₂ catalyst (at 203°C, H₂/CO = 2.1, 6 bar and 5-60% CO conversion) from residence time and co-feeding studies to explain ASF deviations. They suggested that the diffusion limitation of reactants within the liquid-filled pores slowed down the removal of the α -olefins, causing an increased residence time within the catalyst pores. Kuipers *et al.* [6] attributed the exponentially increasing paraffin/olefin ratio with chain length to a *chain length dependent olefin readsorption mechanism*. They showed, on a Co foil at 220°C, H₂/CO = 2 and 1 bar, that the probability of readsorption depends on the heat of physisorption of the olefins in the catalyst as well as on the heat

of dissolution and diffusivity in the FT wax. Van der Laan and Beenackers [7,8] proposed the *α -olefin readsorption product distribution model* to explain ASF deviations. Their model (developed over a commercial Fe/Cu/K/SiO₂ catalyst at 250°C, 8-32 bar, H₂/CO = 0.5-2.0) combined a mechanistic model of olefin readsorption with kinetics of chain growth and termination on the same catalytic sites. Similar to Kuipers *et al.* [6], they showed that olefin readsorption depends on physisorption strength and solubility inside the catalyst pores. Most recently, Botes [9] developed a chain length dependent desorption model for characterizing the product slate of the Fe-Low Temperature Fischer-Tropsch (Fe-LTFT) synthesis. The model only accounted for primary reactions and could describe the olefin and paraffin selectivities in the C₃ to C₁₀ range very well. However, the model overestimated the ethene/ethane ratio. In a subsequent paper, Botes and Govender [10] showed that the deviation was due to the secondary hydrogenation of ethene to ethane.

In this present study, the effect of co-feeding ethene at High-Temperature Fischer-Tropsch (HTFT) conditions is investigated. At the higher temperatures (330-350°C), certain elementary reactions could be faster with the possibility that olefin incorporation could become significant. Many of the previous studies [10] have focused on LTFT conditions. So, this present work is the first to report co-feeding ethene at HTFT conditions. Furthermore, since the data from normal co-feeding studies are non-trivial to analyse [11], we have also used isotopic labeled ¹³CO to follow the reaction intermediates.

5.2. Experimental

Details about the catalyst preparation and data analysis are described elsewhere [Chapters 2 and 3]. In brief, a Fe/K catalyst is used and prepared by the co-precipitation of the metal nitrates with NH_4OH at ambient temperature and pH of 7. The precipitate is dried in an oven at 120°C for 16 hrs and then heat treated in air at 350°C for 4 hrs. The dried catalyst was crushed and sieved between 150 and 200 μm which was ready to load into the reactor. The conditions used in the above experiments are summarised in Table 5.1.

Table 5.1: List of experiments performed and conditions tested to investigate the effect of co-fed ethene during the Fischer–Tropsch synthesis. The reaction temperature and pressure were kept constant at 330°C and 1.2 bar, respectively.

	Run 1		Run 2		Run 3		Run 4	
H_2/CO in the feed	15	4.5	10	5	15	10	15	9
C_2H_4 in H_2 [$\text{ml}\cdot\text{min}^{-1}$] [#]	45.45	45.45	30.3	25.5	45.45	30.3	45.45	45.45
CO [$\text{ml}\cdot\text{min}^{-1}$]	3	10	3	5	3	3	3	5
Ar/Ne [$\text{ml}\cdot\text{min}^{-1}$]	14.55	7.55	19.7	9.5	14.55	29.7	9.55	7.55
Steady state data	yes	yes	yes	yes	no	no	no	no
SSITKA data	no	no	no	no	yes	yes	yes	yes

[#] 1 mol% C_2H_4 in H_2 mixture (Scott Specialty Gases) was used.

5.3. Results and Discussion

5.3.1. Reactor partial pressures during ethylene addition

At the reaction conditions used here, a period of 20 hr is required to obtain steady state which is attributed to the stabilization of the Fe catalyst

active phases [12], which is generally believed to be the Hägg carbide (χ - Fe_2C_5) [13]. After this period, an abrupt switch was made to the feed as follows: $\text{H}_2/\text{CO} / \text{Ar} \rightarrow 1 \text{ mol } \% \text{ C}_2\text{H}_4$ in $\text{H}_2/\text{Co}/\text{Ar}$. To compensate for additional volume in the second feed due to the added C_2H_4 , an equivalent amount (1 mol %) of Ar was removed from the second feed. The resulting changes to the partial pressures of H_2 and CO are presented in Figure 5.1. There was no observable change to the CO partial pressure but the H_2 partial pressure did initially decrease and thereafter increase to its original value. This is linked to an increase in the H_2 conversion which was also observed. In order to eliminate the effects of the reactant partial pressures on the Fischer-Tropsch selectivity and activity, the data captured during this transition period is not considered when discussing the effect of co-fed ethylene.

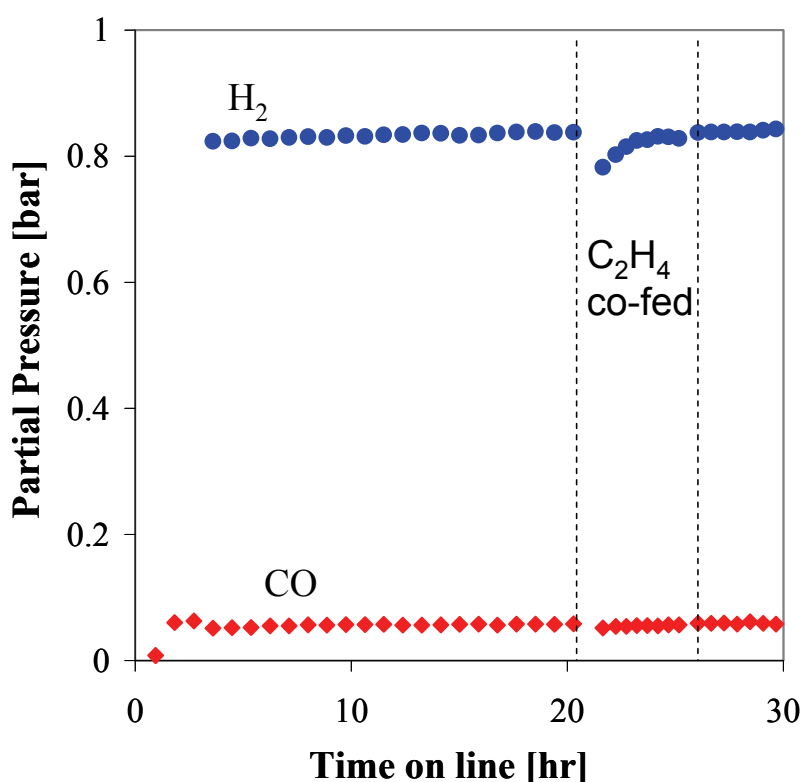


Figure 5.1: H_2 and CO partial pressures before and after 1 mol% C_2H_4 in H_2 was co-fed. Reaction conditions: Fe/K catalyst at 330°C , 1.2 bar, $\text{H}_2/\text{CO} = 15$ and $\text{GHSV} = 7850 \text{ ml.g}_{\text{cat}}^{-1}.\text{hr}^{-1}$.

5.3.2. Fischer-Tropsch activity

The Fischer-Tropsch activity increased by *ca.* 16 % when ethene was co-fed (see Table 5.2) at the same reaction conditions (330°C, 1.2 bar, H₂/CO = 15 and GHSV = 7850 ml.g_{cat}⁻¹.hr⁻¹). Although the partial pressures of H₂ and CO remained the same, the conversions of these reactants also increased by a similar margin as the Fischer-Tropsch activity (15% and 13 %, respectively). This can be attributed to the reactions associated with the added ethene in the fresh feed. For example, ethene could be hydrogenated resulting in increased H₂ conversion or ethene could participate in chain growth consuming C₁ monomers (or CO) resulting in increased CO conversion.

Table 5.2: Fischer-Tropsch steady state results with and without co-feeding ethene. Reaction conditions (330°C, 1.2 bar, H₂/CO = 15 and GHSV = 7850 ml.g_{cat}⁻¹.hr⁻¹) were kept constant.

	Without co-fed olefin	With co-fed olefin
H ₂ partial pressure [bar]	0.80	0.79
CO partial pressure [bar]	0.05	0.05
H ₂ conversion [%]	19	22
CO conversion [%]	20	23
H ₂ /CO-Feed Ratio [-]	15	15
H ₂ /CO-Reactor Ratio [-]	15	15
FT reaction rate [mole CO.g _{cat} ⁻¹ .s ⁻¹]	7.6 10 ⁻⁷	8.8 10 ⁻⁷
Methane formation rate [mole CO.g _{cat} ⁻¹ .s ⁻¹]	1.6 10 ⁻⁷	1.5 10 ⁻⁷
CH ₄ selectivity [C-atom %]	21.3	16.9

Not many researchers have reported changes to the Fischer-Tropsch activity due to the presence of ethylene in the fresh feed. However similar to our study, Hanlon and Satterfield [14] did report an increase in H₂ conversion for a fused Fe catalyst at 248°C and 7.8 – 14.8 bar but unlike our work, there were no observable changes to the CO conversion during the addition of 1-olefins.

5.3.3. Fischer-Tropsch selectivity

5.3.3.1. Methane selectivity

The methane selectivity (see Table 5.2) decreased by *ca.* 21% with the addition of ethene in the feed. Moreover, there was an observed decrease in the methanation rate (*ca.* 8%) which suggests that ethene could be competing for the same adsorption sites as the methane intermediates. The decreased selectivity could also be simply due to fewer adsorbed molecular hydrogen (H_{ads}) on the catalyst surface available for methanation. This could either be due to the ethene competing the H_{ads} sites or H_{ads} reacting preferentially with ethene instead of methane intermediates (CH_x, *x* = 1 to 3). The suppression of methane by the addition of olefins in the fresh feed was claimed by Kim and Hills [15]. They observed a 30% decrease in methane selectivity with 9.6 mol% ethene for a precipitated Fe/K/Cu catalyst at 200°C and H₂/CO = 2 (the total reactor pressure was not reported). Snel and Espinoza [16] reported a 25% decrease in methane selectivity and a 50% reduction in the methanation rate, a factor 2 which is similar to our result.

5.3.3.2. Olefin selectivity

The change in olefinicity, presented in Figure 5.2, shows the differences between the C₂'s and C₃'s. The change in the C₂'s is expected since ethene is added to the fresh feed. The change in the C₃'s is attributed to chain growth. In other words, the co-fed ethene participates in chain growth. Unfortunately, our GC system was setup to separate the C₂'s accurately and as such limited the analysis to mainly the C₁ to C₅ hydrocarbons. Together with the low conversions used here, this resulted in a poor mass balance accounting for the added ethene. At best, we could account for 15% reaction both at H₂/CO = 15 and 10. The CO conversion can influence the extent of the secondary reactions for the added olefin. Hanlon and Satterfield [14] reported that at low CO conversions (*ca.* 30%), the conversion of ethylene in the feed was *ca.* 10%.

The low reactivity of the ethene in our study can be attributed to the low CO conversions used in this study. However, Dwyer and Somorjai [17] reported 80–90% reaction of co-fed ethylene at extremely low conversions (1%) on a Fe (111) crystal at 300°C, 6 bar and H₂/CO = 2. There are two good reasons for this contradiction. Firstly, according to Boelee *et al.* [18] alkali promotion generally has a strong negative influence on the rate of secondary reactions. The Fe crystal used by Dwyer and Somorjai was unpromoted and hence would have been more reactive. Secondly, carbon deposition was a problem for Dwyer and Somorjai and therefore short experiments (approximately 3 hr) were performed. In our study, we allowed for carbon deposition to a certain extent (to allow for phase changes to Fe carbides) and performed our co-feeding experiments at steady-state conditions.

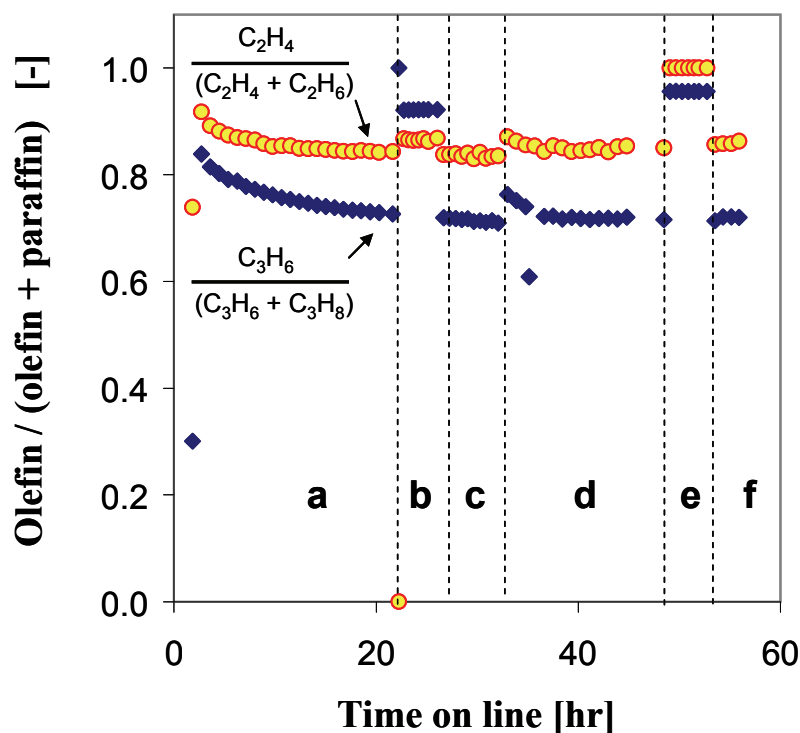


Figure 5.2: Olefinicity [olefin / (olefin + paraffin)] for the C_2 's and C_3 's during the co-fed ethene experiments. Reaction conditions (330°C , 1.2 bar and $\text{GHSV} = 7850 \text{ ml.g}_{\text{cat}}^{-1}.\text{hr}^{-1}$) were kept constant during the various changes to the fresh feed. The fresh feed was changed as follows: (a) $\text{H}_2/\text{CO} = 15$ without C_2H_4 , (b) $\text{H}_2/\text{CO} = 15$ with C_2H_4 , (c) $\text{H}_2/\text{CO} = 15$ without C_2H_4 , (d) $\text{H}_2/\text{CO} = 10$ without C_2H_4 , (e) $\text{H}_2/\text{CO} = 10$ with C_2H_4 , and (f) $\text{H}_2/\text{CO} = 10$ without C_2H_4 .

At these conditions, conversions and selectivities are relatively constant and the activity rates are lower than the initial values due to catalyst deactivation. To summarise, Dwyer and Somorjai worked with an unpromoted (cleaned) Fe catalyst and at the beginning of the reaction where rates of activity are expected to be higher.

5.3.4. Water-gas-shift activity and selectivity

The CO_2 activity and selectivity remained the same when the ethene was added to the fresh feed as shown in Table 5.3. This is in contrast to the

methane activity and selectivity. Although not conclusive, this implies that methanation and water-gas-shift most probably occur on different catalytic sites.

Table 5.3: Water-gas-shift (WGS) steady state results with and without co-feeding ethene. Reaction conditions (330°C, 1.2 bar, $H_2/CO = 15$ and $GHSV = 7850 \text{ ml.g}_{\text{cat}}^{-1}.\text{hr}^{-1}$) were kept constant.

	Without co-fed olefin	With co-fed olefin
WGS reaction rate [mole CO_2 formed. $\text{g}_{\text{cat}}^{-1}.\text{s}^{-1}$]	$1.4 \cdot 10^{-7}$	$1.4 \cdot 10^{-7}$
CO_2 selectivity [C-atom %]	15	14

5.3.5. ^{13}C SSITKA during co-fed ethene experiments

The main aim of performing ^{13}C SSITKA experiments during co-feeding ethene in the fresh feed was to collect transient data for the C_2 - C_4 's and test various C_{2+} mechanistic models. It was later observed that the co-fed C_2H_4 (0.7 mol%) was significantly larger than the *in-situ* formed C_2H_4 (typically 0.1 mol% after 20 hr online). This lead to poor C_2 transients since deconvoluting the unlabeled and labeled species in the presence of the C_2H_4 in the fresh feed was virtually impossible. However, the full transients for the C_3 's could be captured. The first C_3 product will be partially labeled species.

In Figure 5.3, a comparison of this transient is made between with and without the co-fed ethene. Interestingly, there was no change to the partially labeled propane transient but a clear change to the partially labeled propene. This result confirms that ethene does take part in chain growth as mentioned

earlier. Furthermore, it seems that the olefins and paraffins grow on different catalytic sites or do not share the same surface intermediate. Turner *et al.* [19] used ^{13}C NMR spectroscopy to show that $^{13}\text{C}_2\text{H}_4$ reacts with C_1 intermediates to form predominantly 1-alkenes on a Fe/SiO_2 catalyst at 220°C , 1 bar and $\text{H}_2/\text{CO} = 1$.

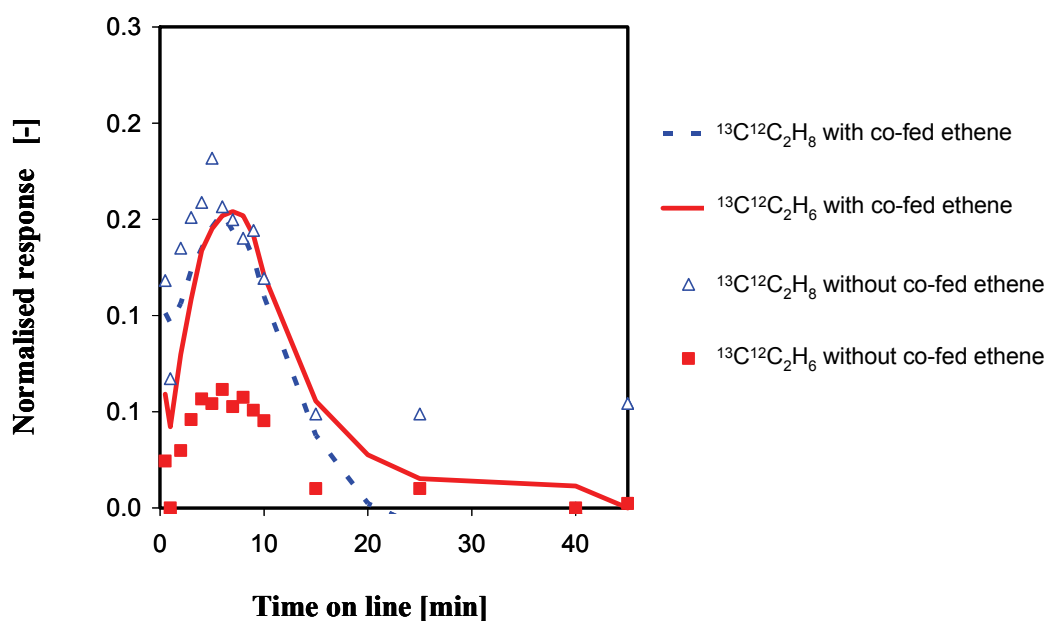


Figure 5.3: Normalised responses for the partially labeled ethene and ethane during a ^{13}CO SSITKA experiment with and without co-fed ethene. Reaction conditions (330°C , 1.2 bar, $\text{H}_2/\text{CO} = 15$ and $\text{GHSV} = 7850 \text{ ml.g}_{\text{cat}}^{-1}.\text{hr}^{-1}$) were the same for both experiments.

5.3.6. Mechanistic implications

The two main experimental observations, viz. (1) ethene is rapidly hydrogenated to ethane, and (2) ethene participates in chain growth with a greater influence on the propene than propane selectivity, need to be accounted for in the Fischer-Tropsch mechanism proposed in this study. Most Fischer-Tropsch mechanisms are described by a typical polymerization

process and as such have three distinct steps, *i.e.* initiation, propagation (chain growth), and termination.

Chain initiation

In our previous work [see Chapter 3], two reactive carbidic surface species, denoted C_α and C_β were identified as the intermediates for methanation and were also shown to be active for the formation of a C_2 intermediate. If ethene readsorbs onto the catalyst surface, one possible C_2 intermediate is $CH_2=CH_{2,ads}$. In terms of initiation, this species could react with either C_α or C_β to form a C_3 intermediate.

Chain propagation

Chain growth can occur by reaction of combinations of C_α or C_β to form reactive C_2 intermediates. These C_2 intermediates (for example, $CH_2=CH_{2,ads}$ or $CH_2=CH_{ads}$) can further react with a monomer (C_α or C_β) to form C_3 's. Another possible reaction is for these C_2 species to react with one another to form C_4 's which is a dimerization reaction.

Chain termination

Surface alkene intermediates can desorb as alkenes, react with another growing chain (to form higher hydrocarbons, including branched products) or react with adsorbed hydrogen to desorb as the corresponding paraffin.

Secondary reactions also need to be taken into account. In this study, it was shown that an olefin, ethene in this case, can readsorb onto the catalyst surface and participate in secondary reactions. Based on the main product observed, ethane, the hydrogenation of ethene was the most predominant reaction. A full product analysis was not performed for reasons stated earlier which makes it difficult to ignore other reactions such as isomerisation. The CO insertion reaction is also plausible, especially if the formation of oxygenates is considered. More work is required in terms of product analysis to fully account for the readsorbed olefin.

5.3.6.1. *Formation of ethane*

Based on the available data and the experimental observation reported here, two alternate mechanisms are proposed here to those reported in the literature [8]. Firstly, in Figure 5.4, olefin readsorption is shown to occur on the same site as the original alkene intermediate ($\text{CH}_2=\text{CH}_{2,\text{ads}}$) and hydrogenation to the corresponding paraffin (ethane in this case) occurs in two steps, firstly reaction with H_{ads} to form a second surface intermediate ($\text{CH}_3-\text{CH}_{2,\text{ads}}$) and then desorption by reaction with another H_{ads} . In this way, the olefin and paraffin surface intermediates are distinguishable and therefore chain growth can occur via the $\text{CH}_2=\text{CH}_{2,\text{ads}}$ species forming propene first which is consistent with the result shown in Figure 5.3.

In the second mechanism, presented in Figure 5.5, the idea of two distinct C_{2+} intermediates is continued. However, here the olefin readsorbs from the gas phase directly to the paraffin intermediate (in this case, $\text{CH}_3-\text{CH}_{2,\text{ads}}$). This accounts to rapid hydrogenation of readsorbed olefins to the corresponding paraffins with the two step process shown in Figure 5.4. Since it was shown that chain growth does occur, the formation of the paraffin intermediate, ($\text{CH}_3-\text{CH}_{2,\text{ads}}$) is also a reversible reaction with the olefin intermediate,

$\text{CH}_2=\text{CH}_{2,\text{ads}}$. The chain propagation to form the C_3 's is still via the $\text{CH}_2=\text{CH}_{2,\text{ads}}$ intermediate as explained above.

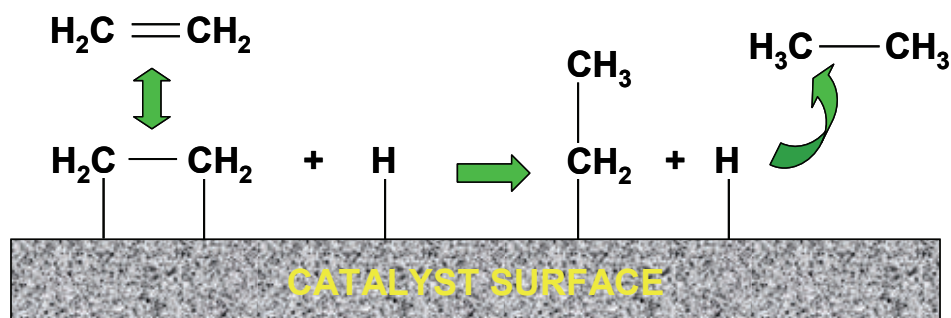


Figure 5.4: Mechanistic scheme showing the surface intermediates for the formation of ethane from ethene.

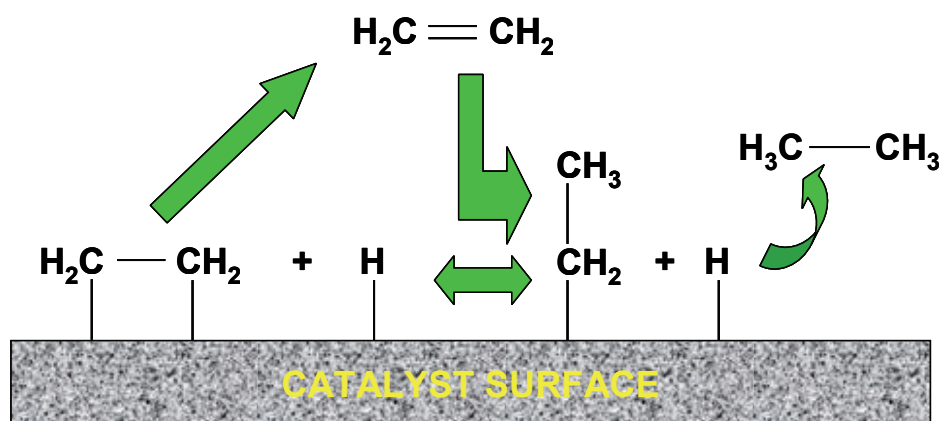


Figure 5.5: Mechanistic scheme showing the direct hydrogenation of ethene in the gas phase to form ethane via the same surface intermediate shown in Figure 5.4.

5.3.6.2. Formation of propene and propane

From the data presented in Figure 5.3, the additional ethene co-fed has a greater influence on the formation of propene compared to the formation of propane. The current mechanisms in the literature [20-29] (also see Chapter 1)

which all claim that olefins are formed via β -H abstraction and paraffins via H-addition, and both from the same species cannot explain the aforementioned result unless H-addition is an extremely slow reaction. Such a scenario is unlikely since deuterium experiments (see Chapter 4) showed that hydrogen-deuterium exchange and hydrogenation reactions are extremely fast compared to C-C coupling reactions. Therefore, two surface intermediates for the C_3 's must also be a possibility, similarly to the C_2 's presented in previous section.

The mechanistic scheme shown in Figure 5.5 can be extended to account for the formation of the C_3 's as shown in Figure 5.6. This scheme can only be valid if either the hydrogenation of the propene intermediate or the readsorption of propene to form propane is extremely slow. Such a case will then explain the result obtained in Figure 5.3 where the formation of propane is slow compare to propene.

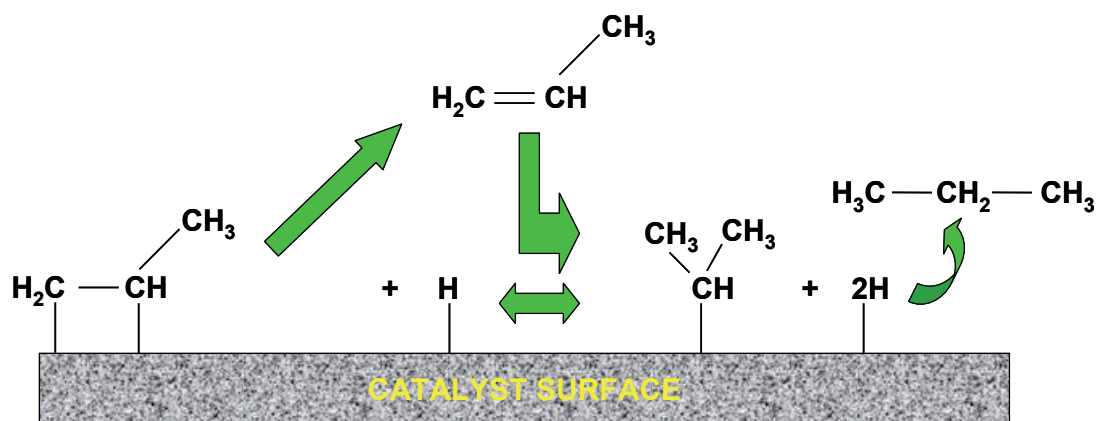


Figure 5.6: Mechanistic scheme showing the formation of propene and propane.

Alternatively, propane can be formed from another surface intermediate independently of the olefins. Egiebor and Cooper [30] proposed a two (or dual) site mechanism in which olefins are mainly synthesised on site 1 and

paraffins (and saturated hydrocarbons) on site 2. In Figure 5.7, the formation of propane is shown which occurs from the same surface intermediate ($\text{CH}_3\text{-CH}_{2,\text{ads}}$) for ethane formation. This mechanistic scheme is still dependent on the co-fed ethene since the $\text{CH}_3\text{-CH}_{2,\text{ads}}$ species also forms from readsorption of the ethene (see Figure 5.5). However, the reaction with the monomeric species, in this case $\text{CH}_{2,\text{ads}}$ is a slow reaction compared to the reaction of ethene to form propene. It was shown in Chapter 3 that the monomeric building units for methanation consist of two distinct carbon pools with different reactivities. So, it is plausible that the $\text{CH}_3\text{-CH}_{2,\text{ads}}$ species reacts with the less reactive C_β pool whilst the olefins are produced from reactions with the C_α pool.

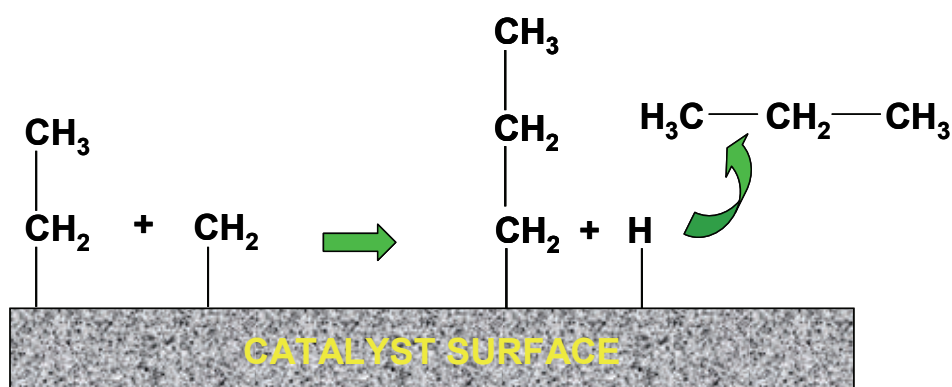


Figure 5.7: Mechanistic scheme showing the formation of propane.

5.4. Conclusions

The main conclusions from this study are as follows:

1. The addition of ethene during Fischer-Tropsch synthesis results in mainly hydrogenation to ethane.

2. Chain growth is also observed but to a lesser extent than hydrogenation (40% ethane formed compared to 1% propene).
3. Based on ^{13}C SSITKA results, propene was the kinetically preferred product when ethene participates in chain growth, implying different sites or intermediates for the olefins and paraffins.
4. Both the methanation rate and the methane selectivity decreased with the addition of ethene in the fresh feed. This could be due to competitive adsorption between the respective surface intermediates, for example between H_{ads} and CH_x ($x = 0$ to 3) surface intermediates sites.
5. Both the water-gas-shift rate and the CO_2 selectivity remained the same during the co-fed ethene experiments. This could imply that methanation and water-gas-shift take place on different surface sites.
6. Lastly, two mechanistic pathways, both with dual sites or intermediates, are proposed to explain the above experimental observations.

References

- (1) R.A.Friedel and R.B.Anderson, *J. Am. Chem. Soc.* **72** (1950) 1211.
- (2) P.J.Flory, *J. Am. Chem. Soc.* **58** (1936) 1877-1885.
- (3) B.Shi and B.H.Davis, *Appl. Catal. A:* **277** (2004) 61-69.
- (4) I.Puskas and R.S.Hurlbut, *Catal. Today* **84** (2003) 99-109.
- (5) E.Iglesia, S.C.Reyes and R.J.Madon, *J. Catal.* **129** (1991) 238-256.
- (6) E.W.Kuipers, I.H.Vinkenburg and H.Oosterbeek, *J. Catal.* **152** (1995) 137-146.

- (7) G.P.Van Der Laan and A.A.C.M.Beenackers, *Stud. Surf. Sci. Catal.*, **119** (1998) 179-184.
- (8) G.P.Van Der Laan and A.A.C.M.Beenackers, *IECR* **38** (1999) 1277-1290.
- (9) F.G.Botes, *Energy & Fuels* **21** (2007) 1379-1389.
- (10) F.G.Botes and N.S.Govender, *Energy & Fuels* **21** (2007) 3095-3101.
- (11) L.M.Tau, H.A.Dabbagh and B.H.Davis, *Energy & Fuels* **4** (1990) 94-99.
- (12) N.S.Govender, F.G.Botes, M.H.J.M.de Croon and J.C.Schouten, *J. Catal.* **260** (2008) 254-261.
- (13) H.E.du Plessis, H.E.du Plessis, University of Johannesburg (2007).
- (14) R.T.Hanlon and C.N.Satterfield, *Energy & Fuels* **2** (1988) 196-204.
- (15) C.J.Kim and N.J.Hills. *Reducing Methane Production in Fischer-Tropsch Reactions*. ed. Exxon Research and Engineering Company, US Patent, US 4,547,525 (1985).
- (16) R.Snel and R.L.Espinoza, *J. Mol. Catal.* **43** (1987) 237-247.
- (17) D.J.Dwyer and G.A.Somorjai, *J. Catal.* **56** (1979) 249-257.
- (18) J.H.Boelee, J.M.G.Custers and K.van der Wiele, *Appl. Catal.* **53** (1989) 1-13.
- (19) M.L.Turner, N.Marsih, B.E.Mann, R.Quyoum, H.C.Long and P.M.Maitlis, *J. Am. Chem. Soc.* **124** (2002) 10456-10472.
- (20) F.Fischer and H.Tropsch, *Brennstoff-Chem.* **7** (1926) 97-104.
- (21) H.H.Storch, N.Golumbic and R.B.Anderson, *The Fischer-Tropsch and Related Syntheses* (1951).
- (22) A.W.Sternberg and I.Wender, *Proc.Intern.Conf.on Coordin.Chem.* (1959) 53.
- (23) H.Pichler, H.Schulz and D.hne, *Brennstoff-Chem.* **49** (1968) 36.
- (24) R.Quyoum, H.C.Long, M.L.Turner and P.M.Maitlis. *A mechanistic study of the chain propagation step in the Fischer-Tropsch synthesis*. ACS meeting, San Francisco, Fuel Preprints **42**, (1997), 62.
- (25) H.C.Long, M.L.Turner, P.Fornasiero, J.par, M.Graziani and P.M.Maitlis, *J. Catal.* **167** (1997) 172-179.
- (26) R.Quyoum, V.Berdini, M.L.Turner, H.C.Long and P.M.Maitlis, *J. Catal.* **173** (1998) 355-365.

- (27) P.M.Maitlis, R.Quyoum, H.C.Long and M.L.Turner, *Appl. Catal. A*: **186** (1999) 363-374.
- (28) P.M.Maitlis and M.L.Turner, *Catal. Today* **65** (2001) 91-97.
- (29) P.M.Maitlis, *J. Organo. Chem.* **689** (2004) 4366-4374.
- (30) N.O.Egiebor and W.C.Cooper, *Appl.Catal.* **14** (1985) 323-332.

6

Mechanistic pathway for C₂₊ hydrocarbons over an iron-based catalyst

Our mechanism for the methanation reaction pathway (presented in Chapter 4) during the Fischer-Tropsch synthesis at high temperature reaction conditions (330°C, H₂/CO = 15 and 1.2 bar) is extended here to account for the formation of C₂₊ hydrocarbons. In addition to the mechanism on cobalt-based catalyst, two additional mechanisms are tested. The latter mechanisms consider two surface intermediates for the C₂₊ hydrocarbons and different pathways for olefin readsorption. It's shown that a mechanism with two surface intermediates for the C₂₊ hydrocarbons and with olefin readsorption directly to the corresponding paraffin surface intermediate describes the data the best. Parameter estimates for the rate constants describing the formation of the C₂'s are reported. The optimal model is also shown to fit the C₃'s.

6.1. Introduction

The elucidation of the Fischer-Tropsch (FT) mechanism still remains one of the major endeavours in heterogeneous catalysis. To date, most researchers favour either the CO-insertion [1] or carbide mechanism [2] (see Chapter 2 for review of the FT mechanisms). Recently, Davis [3] reviewed the reaction mechanisms for iron-based FT catalysts and concluded that their data supports the oxygenate mechanism. Davis had to perform ¹⁴C-label experiments to conclusively eliminate the rival mechanisms. The use of isotopes and isotopic transient methods, such as SSITKA (Steady State Isotopic Transient Kinetic Analysis [4-6]), to provide detailed kinetic analysis and information on the key reaction intermediates is well documented [7].

Mims and co-workers have successfully utilised SSITKA to investigate active carbon intermediates on the catalyst surface. They showed that the chain growth over a Co/SiO₂ (at 201.85°C, 1.2 bar and H₂/CO = 2) and an Fe/K (at 226.85°C, 0.9 bar and H₂/CO = 1) catalyst was rapid in comparison to the rate of displacement of the isotopes [8;9]. The active carbon species was also shown to spend most of its time on the catalyst surface as a C₁ intermediate. Mims [10] also concluded that this intermediate was common to both methanol and hydrocarbon products. This initial work was extended to higher pressures and different H₂/CO ratios [11-14] on a cobalt catalyst and led to the development of their kinetic scheme for carbon reaction pathways in FTS (see Figure B1 in Appendix B). The short-fall of this mechanistic model is its simplicity as it does not take into account olefin readsorption and moreover it does not distinguish between desorption of the olefins and paraffins.

Komaya and Bell [15] improved their previous model [16] by taking into account olefin readsorption over a Ru/TiO₂ catalyst at 250°C and D₂/CO = 3. This was done by varying the bed residence times thus allowing olefins to readsorb. Their model (see Figure B2 in Appendix B) incorporated a physisorbed precursor from which olefins are allowed to reenter. The model also allows for depolymerisation of C₂ species and the conversion of C₁'s species to C_{m,s} species. Similarly to Mims *et al.* [12-17], this model only considers a single C₂ surface intermediate and also does not distinguish between desorption of the olefins and paraffins.

Van Dijk [18] extended the SSITKA technique, by using GC-MS product analysis together with MS, to study the Fischer-Tropsch mechanism and kinetics for a cobalt based catalyst at 210-240°C and 1.2 bar. The main route for the formation of paraffins and olefins was based on the carbide mechanism whereas alcohol formation could be either CO or CH_xO insertion. This mechanism (see Figure B3 in Appendix B) also included the presence of a physisorbed state under dry conditions (no wax formation). Many of the assumptions made by Van Dijk were based on the formation of a wax layer under industrial conditions or higher pressures. This model also only considers a single C₂ intermediate but unlike the aforementioned models, this model does distinguish between desorption of the olefins and paraffins. This is achieved by defining separate physisorbed species for the olefins and paraffins. Apart from the physisorbed species, this model is very similar to the model by Van der Laan and Beenackers [19] (see Figure B4 in Appendix A), which was developed independently using steady state data captured for iron based catalysts at 250°C and 15 bar.

The aim of this study is to develop a plausible mechanism for the Fischer-Tropsch reaction for an Fe-based catalyst under High Temperature Fischer Tropsch (HTFT) conditions (typically at 330°C and 1.2 bar) using isotopic transient methods. The objective is also to develop a mechanism which is consistent with our methanation reaction pathway (see Chapter 4) and our co-feeding experiments with ethene (see Chapter 5). Moreover, the mechanism should be able to describe the formation of oxygenates and other products not captured under the current experimental conditions.

6.2. Fischer-Tropsch mechanistic models

6.2.1. Model selection and description

The transient responses obtained for C₂₊ Fischer-Tropsch products on the Fe-based catalyst in this study differs from those obtained by Van Dijk [18] on the Co-based catalyst. The main difference, illustrated in Figure 6.1, is the transient response for the paraffin in this study is delayed compared to the response for the olefin, which is opposite to Van Dijk's result. Van Dijk used a model with single C_n (n ≥ 2) surface intermediates, with olefin readsorption to describe his data. However, such a model is not capable of describing delays in the ethane formation. Therefore, in this study, three new models A, B and C are proposed and tested against transient data collected for an iron-based catalyst at 330°C and 1.2 bar. In all of the models, the methanation reaction pathway is taken from Chapter 4 and the corresponding rate constants are fixed.

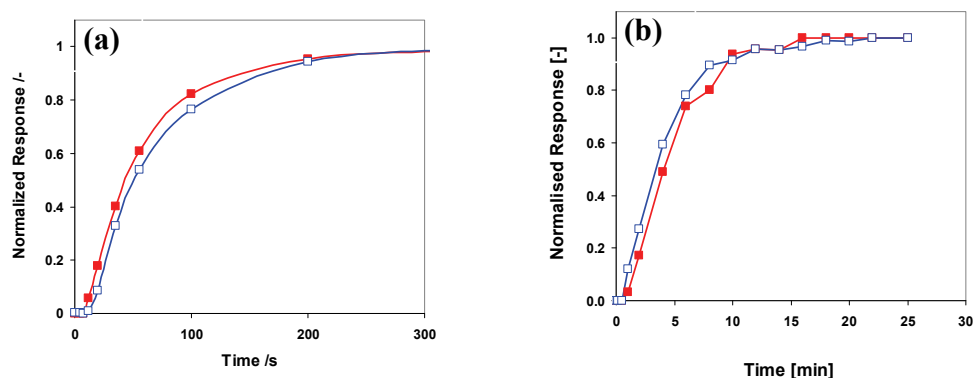


Figure 6.1: Normalised responses of ethane (closed markers) and ethene (open markers) on (a) Cobalt [18] and (b) Iron-based catalyst [this study], during the Fischer Tropsch Synthesis.

MODEL A: A single C_2 surface intermediate with olefin readsorption

This model (see Figure 6.2) is similar to that proposed by Van Dijk [18] and Van der Laan and Beenackers [19]. It has been simplified by removing the physisorbed species in Van Dijk's model but retains the different pathways for the olefins and paraffins directly from the C_2 surface intermediate as proposed in both studies. The formation of the C_{3+} olefins and paraffins is also similar to the C_2 's formation.

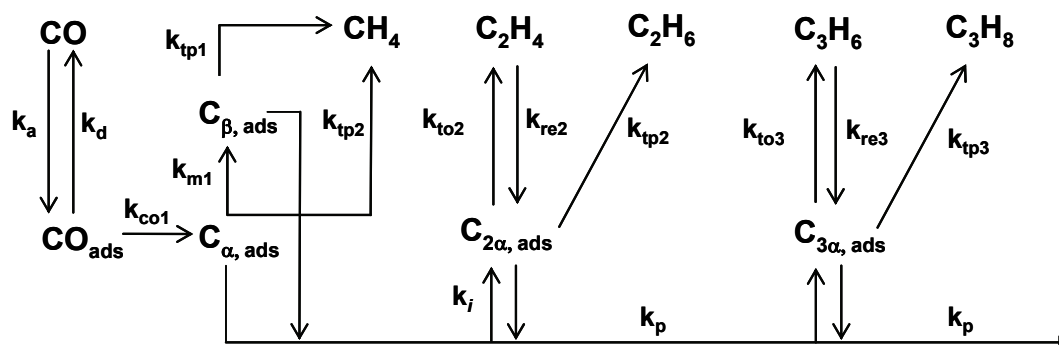


Figure 6.2: Schematic for model A, with a single C_n ($n \geq 2$) surface intermediate

MODEL B: Two C_2 surface intermediates with olefin readsorption

In model B, illustrated in Figure 6.3, an additional C_2 intermediate ($C_{2\beta}$) is introduced in series with the $C_{2\alpha}$ intermediate. The rate of formation of $C_{2\beta}$ (with rate constant, k_h) can be considered as a hydrogenation step. Olefin readsorption and chain growth pathways are similar to model A. It is presumed that the C_{3+} hydrocarbons are also formed from two surface intermediates as illustrated for the $C_{3's}$.

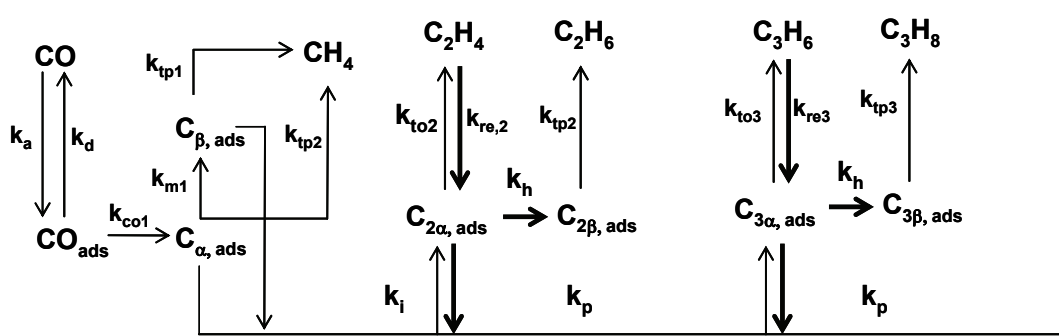


Figure 6.3: Schematic for model B, with two C_n ($n \geq 2$) surface intermediates.

MODEL C: Two C_2 surface intermediates with direct olefin readsorption

In the third model, illustrated in Figure 6.4 an additional C_2 intermediate is introduced in series similar to Model B. However, here the olefin readsorbs directly to the paraffin surface intermediate ($C_{2\beta}$). Moreover, to accommodate for chain growth via olefin readsorption, the hydrogenation step is considered reversible. The pathway for the C_{3+} hydrocarbons is similar to the $C_{2's}$ as shown for propene and propane.

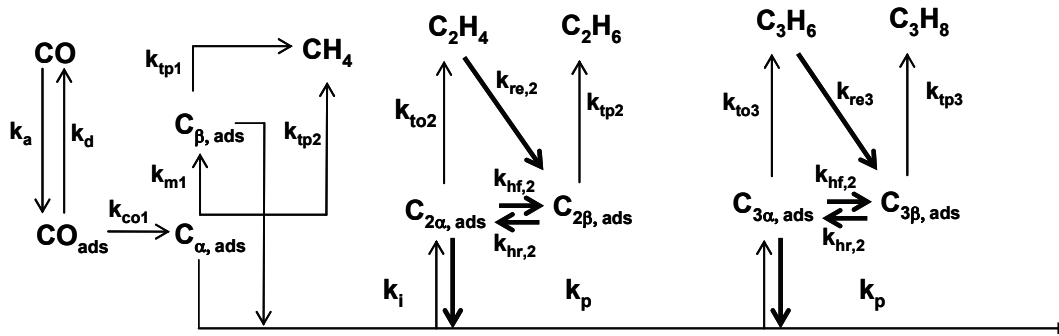


Figure 6.4: Schematic for model C, with two C_n ($n \geq 2$) surface intermediates.

6.2.2. Model assumptions and equations

For each of the mechanistic models, the mole balances for all the components can be derived as explained in Chapter 4 for the case of the methanation reaction. Model assumptions for a plug flow reactor model were also discussed in Chapter 4. As an example for the C_{2+} models equations, the specific mole balances for both the gas phase and surface species for Model A are presented. In the equations, a single ^{13}C -labelled atom is represented as 'C' whilst ^{13}C refers to two ^{13}C -labelled atoms. The subscript 'ss' refers to the sum of the concentrations of the labelled and unlabelled species. The mole balances for the remaining two models are presented in Appendix C.

The mole balances for the fully labelled gas phase components are:

$$\frac{\partial C_{\text{CO}}}{\partial t} + \frac{1}{\tau} \frac{\partial C_{\text{CO}}}{\partial x} = \frac{\rho}{\varepsilon_b} (-k_{\text{ads}} C_{\text{CO}} + k_{\text{des}} L_{\text{CO}}) \quad [1]$$

$$\frac{\partial C_{CH_4}}{\partial t} + \frac{1}{\tau} \frac{\partial C_{CH_4}}{\partial x} = \frac{\rho}{\varepsilon_b} \left(k_{tp1} L_{C\beta} + k_{tp2} L_{C\alpha} \right) \quad [2]$$

$$\frac{\partial C_{C_2H_4}}{\partial t} + \frac{1}{\tau} \frac{\partial C_{C_2H_4}}{\partial x} = \frac{\rho}{\varepsilon_b} \left(k_{to2} L_{C_{2\alpha}} - k_{re2} C_{C_2H_4} \right) \quad [3]$$

$$\frac{\partial C_{C_2H_6}}{\partial t} + \frac{1}{\tau} \frac{\partial C_{C_2H_6}}{\partial x} = \frac{\rho}{\varepsilon_b} \left(k_{tp2} L_{C_{2\alpha}} \right) \quad [4]$$

$$\frac{\partial C_{C_3H_6}}{\partial t} + \frac{1}{\tau} \frac{\partial C_{C_3H_6}}{\partial x} = \frac{\rho}{\varepsilon_b} \left(k_{to3} L_{C_{3\alpha}} - k_{re3} C_{C_3H_6} \right) \quad [5]$$

$$\frac{\partial C_{C_3H_8}}{\partial t} + \frac{1}{\tau} \frac{\partial C_{C_3H_8}}{\partial x} = \frac{\rho}{\varepsilon_b} \left(k_{tp3} L_{C_{3\alpha}} \right) \quad [6]$$

The mole balances for the non-labelled gas phase components are exactly similar to those for the fully labelled species (equations [1] to [6]). Partially labelled gas phase species are also formed from partial labelled surface species, as shown in equations [7] to [12].

$$\frac{\partial C_{C_2H_4}}{\partial t} + \frac{1}{\tau} \frac{\partial C_{C_2H_4}}{\partial x} = \frac{\rho}{\varepsilon_b} \left(k_{to2} L_{C_{2\alpha}} - k_{re2} C_{C_2H_4} \right) \quad [7]$$

$$\frac{\partial C_{C_2H_6}}{\partial t} + \frac{1}{\tau} \frac{\partial C_{C_2H_6}}{\partial x} = \frac{\rho}{\varepsilon_b} \left(k_{tp2} L_{C_{2\alpha}} \right) \quad [8]$$

$$\frac{\partial C_{C_3H_6}}{\partial t} + \frac{1}{\tau} \frac{\partial C_{C_3H_6}}{\partial x} = \frac{\rho}{\varepsilon_b} \left(k_{to3} L_{C_{3\alpha}} - k_{re3} C_{C_3H_6} \right) \quad [9]$$

$$\frac{\partial C_{C_3H_8}}{\partial t} + \frac{1}{\tau} \frac{\partial C_{C_3H_8}}{\partial x} = \frac{\rho}{\varepsilon_b} \left(k_{tp3} L_{C_{3\alpha}} \right) \quad [10]$$

$$\frac{\partial C_{C_3H_6}}{\partial t} + \frac{1}{\tau} \frac{\partial C_{C_3H_6}}{\partial x} = \frac{\rho}{\varepsilon_b} \left(k_{to3} L_{C_{3\alpha}} - k_{re3} C_{C_3H_6} \right) \quad [11]$$

$$\frac{\partial C_{C_3H_8}}{\partial t} + \frac{1}{\tau} \frac{\partial C_{C_3H_8}}{\partial x} = \frac{\rho}{\varepsilon_b} \left(k_{tp3} L_{C_{3\alpha}} \right) \quad [12]$$

The mole balances for the fully labelled surface species are:

$$\frac{\partial L_{CO}}{\partial t} = k_{ads} C_{CO} - k_{des} L_{CO} - k_{co1} L_{CO} \quad [13]$$

$$\begin{aligned} \frac{\partial L_{C_\alpha}}{\partial t} = & k_{co1} L_{CO} - k_{m1} L_{C_\alpha} - k_{tp2} L_{C_\alpha} - k_i L_{C_\alpha} \left(L_{C_\beta} + L_{C_\beta} \right) \\ & - k_p L_{C_\alpha} \left(L_{C_{2\alpha}} + L_{C_{2\alpha}} + L_{C_{2\alpha}} + L_{C_{3\alpha}} + L_{C_{3\alpha}} \right) \\ & \left(+ L_{C_{3\alpha}} + L_{C_{3\alpha}} \right) \\ & - L_{C_\alpha} / L_{C_{\alpha,ss}} * C_{net_consumption} \end{aligned} \quad [14]$$

where $C_{net_consumption}$ represents the net consumption of $C_{\alpha ads}$ into C_{3+} hydrocarbons and is expressed in $\text{mole.kg}_{cat}^{-1}.\text{s}^{-1}$. [see page 109, reference 18 for more details]

$$\frac{\partial L_{C_\beta}}{\partial t} = k_{m1} L_{C_\alpha} - k_{tp1} L_{C_\beta} - k_i L_{C_\beta} \left(L_{C_\alpha} + L_{C_\alpha} \right) \quad [15]$$

$$\begin{aligned} \frac{\partial L_{C_{2\alpha}}}{\partial t} = & k_i L_{C_\alpha} L_{C_\beta} - k_{to2} L_{C_{2\alpha}} - k_{tp2} L_{C_{2\alpha}} + k_{re2} C_{C_2H_4} \\ & - k_p L_{C_{2\alpha}} \left(L_{C_\alpha} + L_{C_\alpha} \right) \end{aligned} \quad [16]$$

$$\begin{aligned} \frac{\partial L'''C_{3\alpha}}{\partial t} = & k_1 L'C_{\alpha} L''C_{2\alpha} - k_{t03} L'''C_{3\alpha} - k_{tp3} L'''C_{3\alpha} + k_{re3} C'''C_{C_3H_6} \\ & - k_p L'''C_{3\alpha} (L'C_{\alpha} + L_{C_{\alpha}}) \end{aligned} \quad [17]$$

Partial labelled surface species are formed by the combination of non-labelled and labelled surface species. These can then desorb to form the partial labelled gas phase components, as presented above in equations [7] to [10]. The following set of equations is obtained for the partial labelled surface species:

$$\begin{aligned} \frac{\partial L'C_{2\alpha}}{\partial t} = & k_i L'C_{\alpha} L_{C_{\beta}} + k_i L_{C_{\alpha}} L'C_{\beta} - k_{t02} L'C_{2\alpha} - k_{tp2} L'C_{2\alpha} \\ & + k_{re2} C'C_{C_2H_4} - k_p L'C_{2\alpha} (L'C_{\alpha} + L_{C_{\alpha}}) \end{aligned} \quad [18]$$

$$\begin{aligned} \frac{\partial L'C_{3\alpha}}{\partial t} = & k_p L'C_{\alpha} L_{C_{2\alpha}} + k_p L_{C_{\alpha}} L'C_{2\alpha} - k_{t03} L'C_{3\alpha} - k_{tp3} L'C_{3\alpha} \\ & + k_{re3} C'C_{C_3H_6} - k_p L'C_{3\alpha} (L'C_{\alpha} + L_{C_{\alpha}}) \end{aligned} \quad [19]$$

$$\begin{aligned} \frac{\partial L''C_{3\alpha}}{\partial t} = & k_p L'C_{\alpha} L'C_{2\alpha} + k_p L_{C_{\alpha}} L''C_{2\alpha} - k_{t03} L''C_{3\alpha} - k_{tp3} L''C_{3\alpha} \\ & + k_{re3} C''C_{C_3H_6} - k_p L''C_{3\alpha} (L'C_{\alpha} + L_{C_{\alpha}}) \end{aligned} \quad [20]$$

6.2.3. Parameter estimation

The rate constants (k_{ads} , k_{des} , k_{co1} , k_{m1} , k_{tp1} and k_{tp2}) estimated in the methanation study (see Chapter 4) were fixed in this part of the modeling

since the carbon mass balance was closed by taking into account the net consumption to C_{2+} species. Moreover, only the rate constants describing the formation of the C_2 's (k_{to2} , k_{re2} , k_{tp2} , k_{ini} , k_p , k_{h2f} and k_{h2r}) were initially estimated. Both these steps reduced the number of parameters that needs to be estimated. The parameter estimation process itself was performed using gPROMS, similarly for the methanation study in [Chapter 4](#).

6.3. Results and Discussion

6.3.1. Fischer Tropsch steady state results

The steady state performance of the catalyst has been discussed in [Chapter 4](#). It was shown that the catalyst activity declines the most during the first 10-15 hrs on line and thereafter reaches steady state. It is at this stage where the SSITKA experiments are performed since there are minimal changes to the catalyst. During this initial period, the olefin/paraffin ratio also changes, as shown in Figure 6.5 for the $C_{2's}$ and $C_{3's}$. For the $C_{2's}$, the olefin/paraffin ratio decreases from *ca.* 9 to a steady state value of *ca.* 3 whilst for the $C_{3's}$, the ratio drops from *ca.* 12 to *ca.* 6. The baseline conditions used in this study were at $H_2/CO = 15$, $330^\circ C$, 1.2 bar, and $GHSV = 7500 \text{ ml.g}_{cat}^{-1}.\text{hr}^{-1}$. The data at these baseline conditions has been used for the parameter estimation. The steady state gas phase concentration of the C_2 's and C_3 's in mole.m_g^{-3} , which are used in the modeling, are presented in Figure 6.6.

However, during the course of the experiments, the syngas flow was stopped to avoid excessive carbon formation (e.g. in Figure 6.5 at TOL = 60-110 hr). When re-commencing the run, the olefin/paraffin ratio returns to the

baseline conditions after 1-2 hrs on line. There were also data points captured where the H_2/CO ratio and GHSV were varied to investigate the effect of process conditions.

6.3.2. SSITKA results

The normalised transients for ethene, ethane, propene and propane captured using a $^{12}CO/ H_2/Ar \rightarrow ^{13}CO/ H_2/Ar/Ne$ switch at feed conditions of $H_2/CO = 15$ and $GHSV = 7500 \text{ ml.g}_{cat}^{-1}.\text{hr}^{-1}$, for three different SSITKA experiments, are presented in Figure 6.7. Many of the data points overlap implying these results are fairly reproducible and could therefore be considered suitable for modelling purposes.

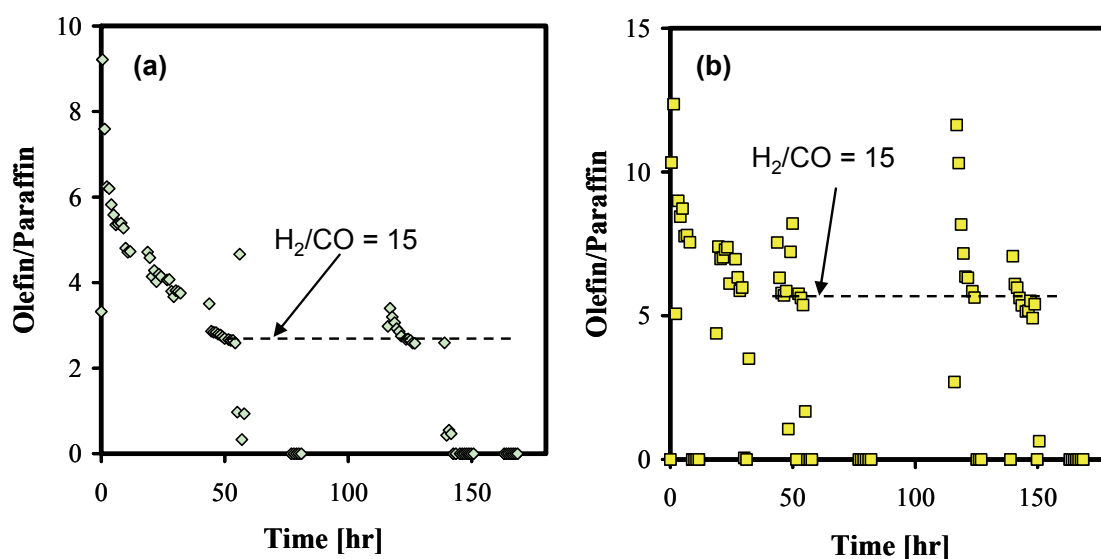


Figure 6.5: The changes to the olefin/paraffin ratio with time on line for (a) $C_{2's}$ and (b) $C_{3's}$. Reactions conditions are $H_2/CO = 15$, 330°C , 1.2 bar , and a $GHSV = 7500 \text{ ml.g}_{cat}^{-1}.\text{hr}^{-1}$

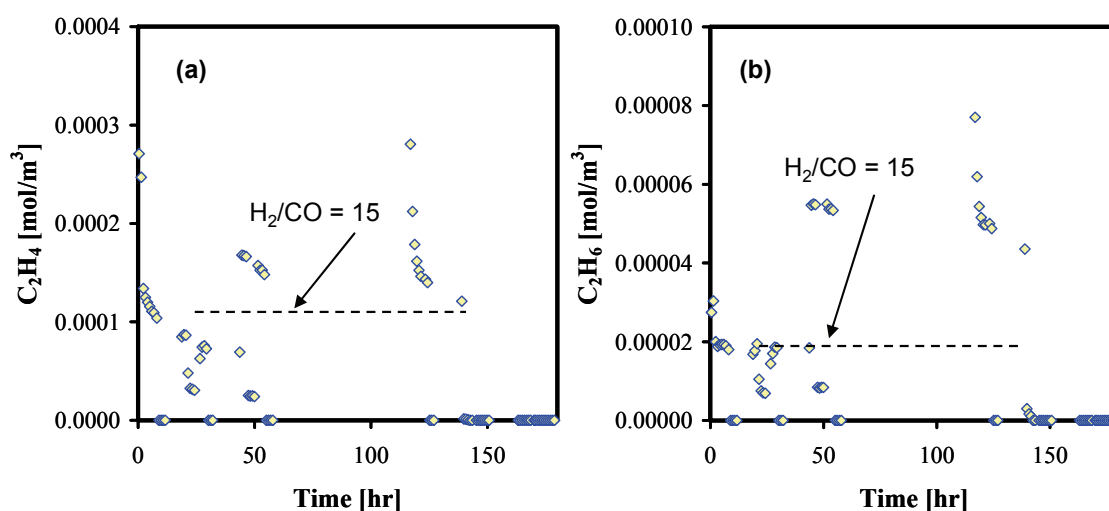


Figure 6.6: The steady state gas phase concentration of (a) C_2H_4 and (b) C_2H_6 with time on line. Changes to process conditions (H_2/CO ratio or space velocity) cause the data to shift away from the baseline condition ($H_2/CO = 15$, $GHSV = 7500 \text{ ml.g}_{cat}^{-1} \cdot \text{hr}^{-1}$)

As discussed by Van Dijk [18], the shapes of the transients of C_1 - C_5 hydrocarbons are dictated by the capacity of the chemisorbed state and contain information about the surface kinetics. Similarly to the methane transient (see Chapter 4), the fully labelled $C_{2's}$ and $C_{3's}$ took more than 40 min to reach steady state. The partially labelled species reached an optimum at *ca.* 5 min but showed a long tailing which also reached steady state (a zero value) at *ca.* 40-45 min. These responses are much longer than those reported on cobalt [18] and ruthenium [15] catalysts. In both of these studies, lower temperatures (210-250°C) were used which resulted in wax formation. Therefore, the long response times for the higher hydrocarbons were attributed to increasing physisorption due to this wax formation.

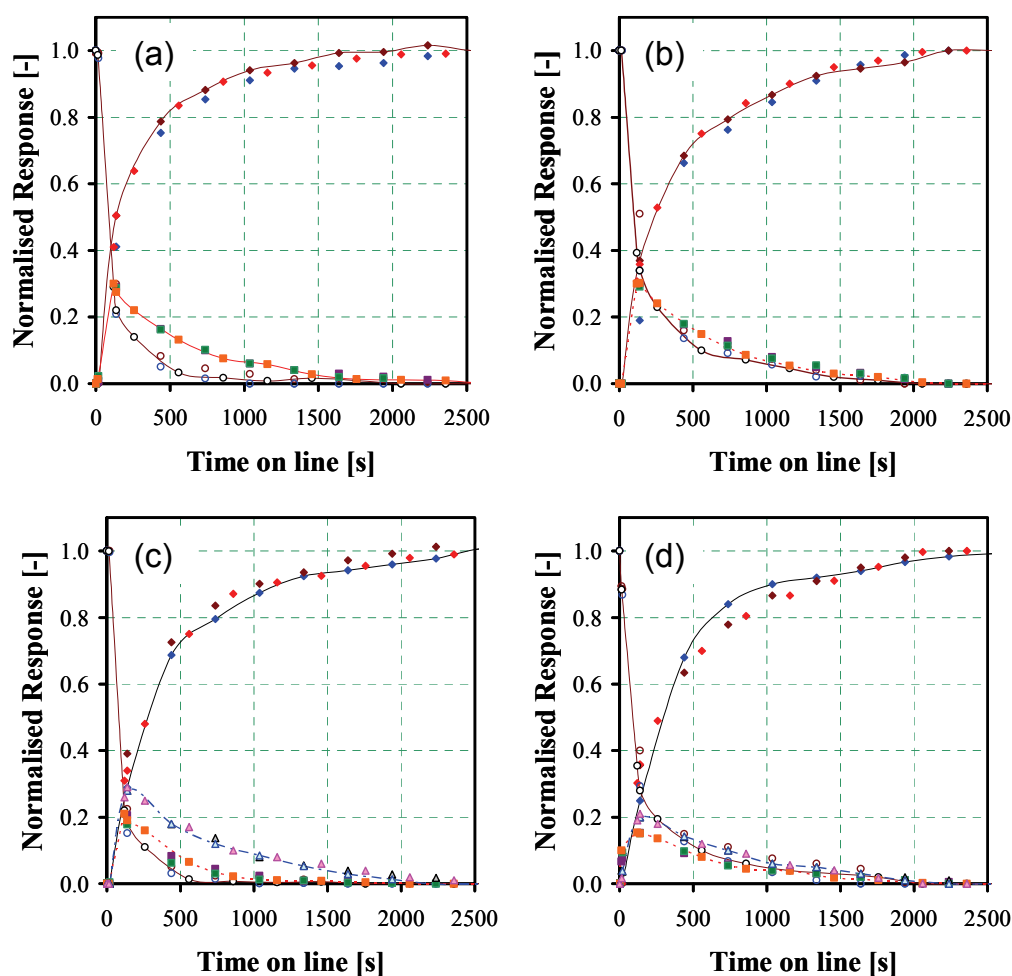


Figure 6.7: Normalised transient responses for (a) C_2H_4 , (b) C_2H_6 , (c) C_3H_6 and (d) C_3H_8 at $H_2/CO = 15$ and $GHSV = 7500 \text{ ml.g}_{cat}^{-1}.hr^{-1}$. The symbols, \diamond , \circ , \blacksquare , and \blacktriangle represent fully labeled, non-labeled, single atom partial labeled and two atoms partial labeled transient, respectively. The solid and dashed lines through the data sets are inserted to better illustrate the shapes of these transients.

However, in this study, there was no significant wax formation at these higher temperatures (330°C) which was mainly due to the low conversions at lower pressures. Therefore, the longer response times observed for the C_1

$C_{3's}$ cannot be attributed to a higher degree of physisorption. It's most likely that these longer responses are due to a carbon reservoir which is difficult to hydrogenate. For the first 5 to 10 min, the transients reached between 75-90% of their final steady state value. Thereafter, there's a slow evolution for the remaining 30 to 40 min. These are two distinct processes. The first seems to be associated with a more reactive carbon pool whilst the second process seems to occur on a less reactive carbon pool. This has been successfully shown to be the case for the methanation reaction (see Chapter 4). Since the less reactive carbon pool (C_{β}) was shown to be active for C-C coupling, the delay in the transient responses for the C_2 - C_3 's can be attributed to the reactivity of this less reactive carbon pool.

6.3.3. C_{2+} model discrimination

Some researchers [16,18,19] have distinguished between the rates of chain initiation ($C_{\alpha} + C_{\alpha} \rightarrow C_{2\alpha}$) and chain growth (e.g. $C_{\alpha} + C_{2\alpha} \rightarrow C_{3\alpha}$) whilst others [20-22] have modeled the Fischer-Tropsch product distribution by presuming these rates are equivalent. Based on this discrepancy, two different cases have been tested in this study. In the first case, the rates of chain initiation and chain growth are fixed whilst in the second case, only the chain initiation rate was fixed and the chain growth rate was estimated. The rate of chain initiation has already been estimated in the methanation study which was accomplished by accounting for the net consumption of C_{α} to form C_{2+} hydrocarbons. This estimated value ($k_i = 0.4798 \text{ s}^{-1} \pm 0.05$) is used in both of these cases.

Case 1: $k_{ini} = k_p$

The model predictions for the ^{13}C -labelled C_2 's ($^{13}C_2H_4$, $^{13}C^{12}CH_4$, $^{13}C_2H_6$ and $^{13}C^{12}CH_6$) are presented in Figure 6.8. Models A and B fail to describe the $^{13}C_2$ transients, especially during the initial 15 min where there is a larger deviation between the model and data points.

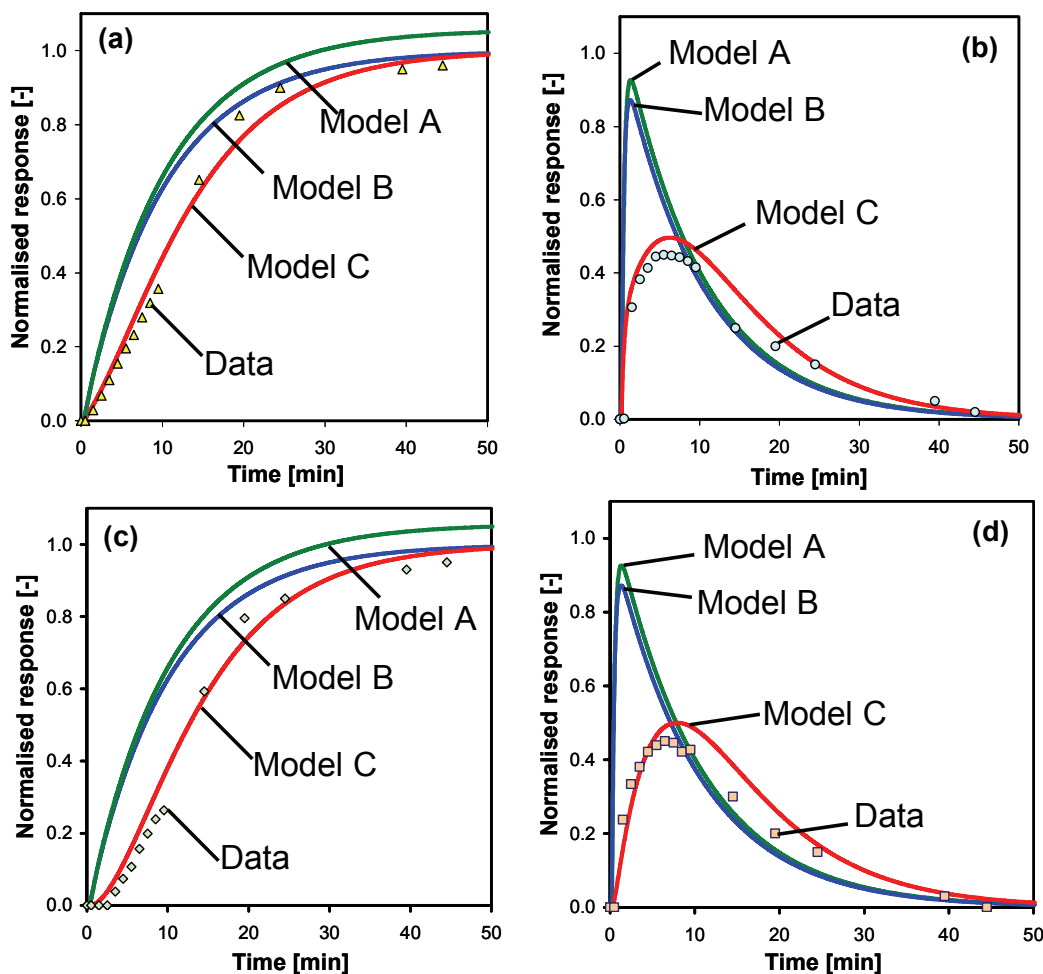


Figure 6.8: Case 1, model predictions (solid lines) for (a) $^{13}C_2H_4$, (b) $^{13}C^{12}CH_4$, (c) $^{13}C_2H_6$ and (d) $^{13}C^{12}CH_6$ transients for the C_{2+} models shown in **Figure 6.2** to **Figure 6.4**. The symbols are the data points obtained at $H_2/CO = 13$, $330^\circ C$, 1.2 bar and $GHSV = 7500$ $ml.g_{cat}^{-1}.hr^{-1}$.

This is also more noticeable for the partially labelled C_2 's (see Figure 6.8b & 6.8d). Model C gives the best fit and is capable of describing both the fully labelled and partially labelled C_2 's. The estimated rate constants used to plot these model predictions are discussed in the next section. In summary, the model with two intermediates and with a direct hydrogenation route for the olefin from the gas phase, gives the best description of the experimental data.

Case 2: $k_{ini} \neq k_p$

For this case, in which k_p was estimated whilst k_{ini} was fixed, both Models A and B overlapped and could not describe the ^{13}C -labelled C_2 's ($^{13}C_2H_4$, $^{13}C^{12}CH_4$, $^{13}C_2H_6$ and $^{13}C^{12}CH_6$), as shown in Figure 6.9. Once again, Model C gave the best fit, describing both the fully labelled and partially labelled C_2 's. The model parameters for this case are similar to Case 1 because certain parameters are highly correlated as discussed in the next section.

6.4. Parameter estimation

The estimated parameter estimates of the rate coefficients for the model predictions in Figure 6.8 and Figure 6.9 are listed in Table 6.1. The rate coefficients for the methanation reaction were fixed from Chapter 4 and are not reported here. Similar to the methanation study [see Chapter 4], a net consumption term (to C_{3+} hydrocarbons) was also used here. In comparison to

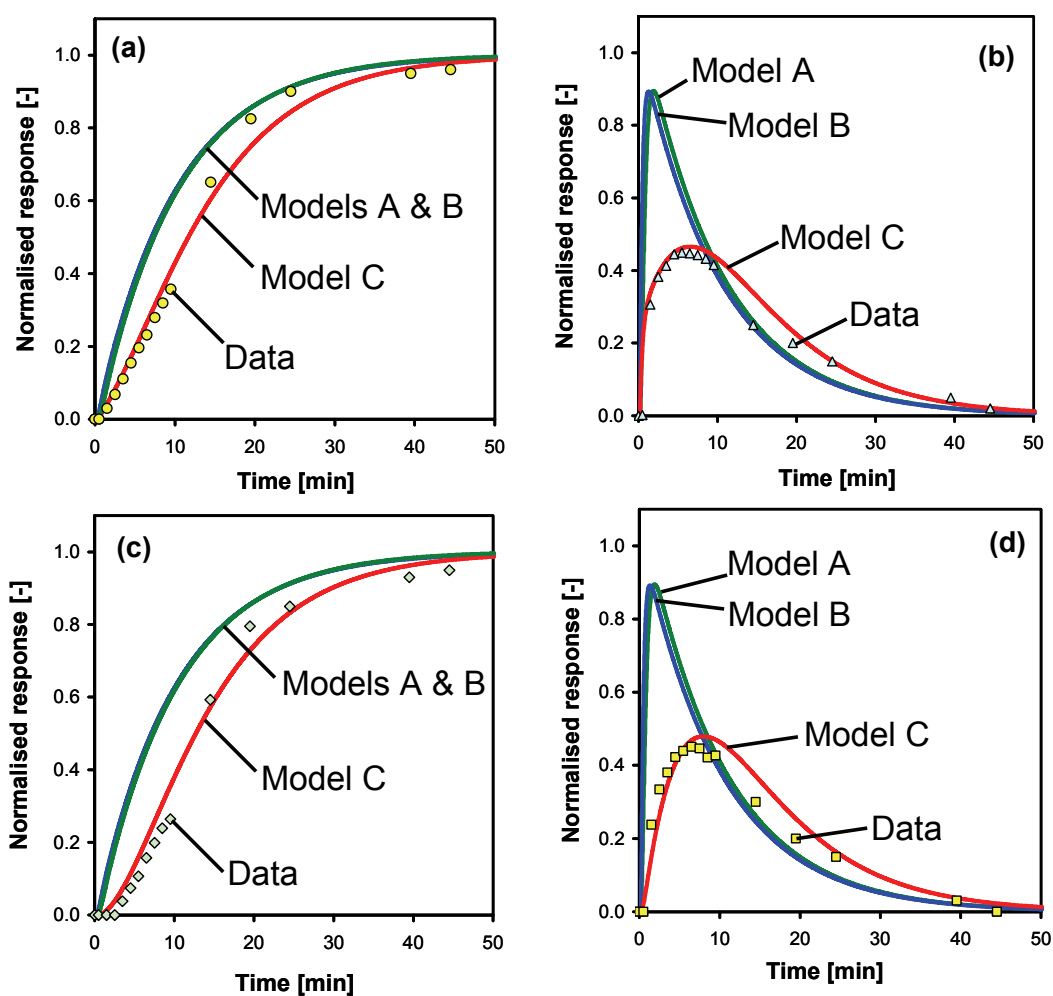


Figure 6.9: Case 2, model predictions (solid lines) for (a) $^{13}C_2H_4$, (b) $^{13}C^{12}CH_4$, (c) $^{13}C_2H_6$ and (d) $^{13}C^{12}CH_6$ transients for the C_{2+} models shown in **Figure 6.2** to **Figure 6.4**. The symbols are the data points obtained at $H_2/CO = 13$, $330^\circ C$, 1.2 bar and $GHSV = 7500$ $ml.g_{cat}^{-1}.hr^{-1}$.

case 1 ($k_{ini} = k_p$), the rate constants for case 2 ($k_{ini} < k_p$ or $k_p = 3.66 \times k_{ini}$) were all different except for the termination constant of the paraffin, $k_{tp,2}$, which remained the same. Both the olefin termination and the olefin readsorption rate constants increased by *ca.* 1.5 and 2 times, respectively. The reverse hydrogenation rate constant, $k_{hr,2}$ decreased by *ca.* 1.2 times but there was a large drop in the forward rate constant, $k_{hf,2}$, being *ca.* 16.6 times lower. These changes did not affect the χ^2 and weighted residual values and therefore both cases give the best fit. Moreover, the predicted steady state gas phase concentrations and surface concentrations are similar for both cases and in the case of the gas phase concentrations, the predicted values closely match the experimental data values.

To test the robustness of this model (sensitivity analysis), each rate constant was individually fixed to zero whilst estimating the remaining parameters. The model fails when both termination rate constants, $k_{to,2}$ and $k_{tp,2}$ are zero. This is expected since a positive value is required to explain the gas phase concentrations. The model also failed when the olefin readsorption rate constant ($k_{re,2}$) was zero. In this case, the paraffin intermediate ($C_{2\beta}$) can only be produced via the hydrogenation of $C_{2\alpha}$ which is not viable according to our data. In contrast, if the forward hydrogenation rate constant ($k_{hf,2}$) is set to zero, the model does not fail. The paraffin can still be produced via olefin readsorption. In the last case, in which the reverse hydrogenation rate constant ($k_{hr,2}$) is zero, the model does not fail but gives a bad fit. This suggests that this rate constant is not essential in the model but if included would give better fits.

One major concern of the current model parameters is the high degree of cross correlation as illustrated in Table 6.2. Any value other than zero implies a correlation with values close to ± 1 implying a high degree of correlation. In

Table 6.1: Estimated parameter estimates of the rate coefficients for the C₂₊ formations at 330°C, 1.2 bar, H₂/CO = 15 and GHSV = 7500 ml.g_{cat}⁻¹.hr⁻¹. Values obtained for Cases 1 and 2 are presented.

	Case 1, k _{ini} = k _p			Case 2, k _{ini} ≠ k _p		
	Model A	Model B	Model C	Model A	Model B	Model C
k_{ini}	0.4798	0.4798	0.4798	0.4798	0.4798	0.4798
k_p	0.4798	0.4798	0.4798	1.0728	0.1657	1.7551
k_{t0,2}	0.3138	13.6890	35.7097	0.0369	6.9148	69.5018
k_{re,2}	0.0032	0.0126	0.0650	0.0002	0.0243	0.1046
k_{tp,2}	0.0038	1.0045	0.0003	0.0082	0.3466	0.0003
k_{hf,2}	-	0.9740	19.2530	-	2.0795	1.1602
k_{hr,2}	-	-	0.0079	-	-	0.0066
χ^{2b}	231	230	229	230	229	228
WR^a	3586	3018	211	2909	2897	213
C₂H_{4,ss}	6.86 10 ⁻⁴	6.04 10 ⁻⁴	5.70 10 ⁻⁴	5.71 10 ⁻⁴	4.45 10 ⁻⁴	5.95 10 ⁻⁴
C₂H_{6,ss}	8.78 10 ⁻⁷	5.26 10 ⁻⁵	5.20 10 ⁻⁵	1.27 10 ⁻⁴	1.93 10 ⁻⁴	5.35 10 ⁻⁵
C_{2α,ss}	6.48 10 ⁻⁵	1.76 10 ⁻⁶	1.45 10 ⁻⁶	4.36 10 ⁻⁴	3.18 10 ⁻⁶	1.11 10 ⁻⁶
C_{2β,ss}	-	1.72 10 ⁻⁶	7.90 10 ⁻³	-	1.91 10 ⁻⁵	9.21 10 ⁻³

Units: all k's in [s⁻¹] except k_i in [kg_{cat}.mole⁻¹.s⁻¹], C_{2α} and C_{2αβ} in [mole.kg_{cat}⁻¹], and C₂H_{4,ss} and C₂H_{6,ss} in [mole.mg⁻³].

^a WR is the weighted residual obtained from the parameter estimation results.

^b χ² is the 95% chi-squared value obtained from the parameter estimation results.

both cases (see Table 6.2 for values in bold), we observed that the olefin termination rate constant is highly correlated with the forward hydrogenation rate constant whilst the olefin readsorption rate constant is highly correlated with the reverse hydrogenation constant. This explains why we currently cannot distinguish between the two cases reported. One idea to resolve this issue was to increase the partial pressure of the olefin (by co-feeding the olefin) and then performing the SSITKA experiment. In this way, the rate of olefin readsorption could be enhanced and perhaps fixed at a suitable value. This was attempted but the experimental data was not suitable for modeling since the olefin concentration in the fresh feed was much higher than that produced during our reaction. This caused difficulties with normalizing the transients due to the constant and much larger value of $^{12}\text{C}_2\text{H}_4$ present in the gas phase.

Table 6.2: Correlation matrix of the estimated parameters for both cases considered.

Parameter	Case 1, $k_{\text{ini}} = k_{\text{p}}$					Case 2, $k_{\text{ini}} \neq k_{\text{p}}$					
	$k_{\text{hf},2}$	$k_{\text{hr},2}$	$k_{\text{re},2}$	$k_{\text{to},2}$	$k_{\text{tp},2}$	$k_{\text{hf},2}$	$k_{\text{hr},2}$	$k_{\text{re},2}$	$k_{\text{to},2}$	$k_{\text{tp},2}$	k_{p}
$k_{\text{hf},2}$	1					1					
$k_{\text{hr},2}$	0.41	1				0.53	1				
$k_{\text{re},2}$	-0.32	-0.97	1			-0.42	-0.97	1			
$k_{\text{to},2}$	1	0.40	-0.31	1		0.99	0.42	-0.31	1		
$k_{\text{tp},2}$	-0.62	-0.28	0.22	-0.62	1	-0.58	-0.27	0.21	-0.58	1	
k_{p}	-	-	-	-	-	0.61	0.31	-0.20	0.60	-0.29	1

6.5. Extension to the model to account for C_{3+} hydrocarbons

The methodology adopted to estimate the rate coefficients for the C_2 's was followed for the C_3 's. A net consumption term was defined which accounted for the formation of C_{4+} hydrocarbons and the rate constants describing the C_1 - C_2 's were fixed from Chapter 4 and Table 2. Unfortunately, a good fit could not be obtained which was mainly due to limited transient data for the partially labeled C_3 's. However, the model did converge and the results for the optimum solution is presented in Figure 6.10 for propene and in Figure 6.11 for propane. From this we can conclude that Model C can be extended to account for the formations of higher hydrocarbons.

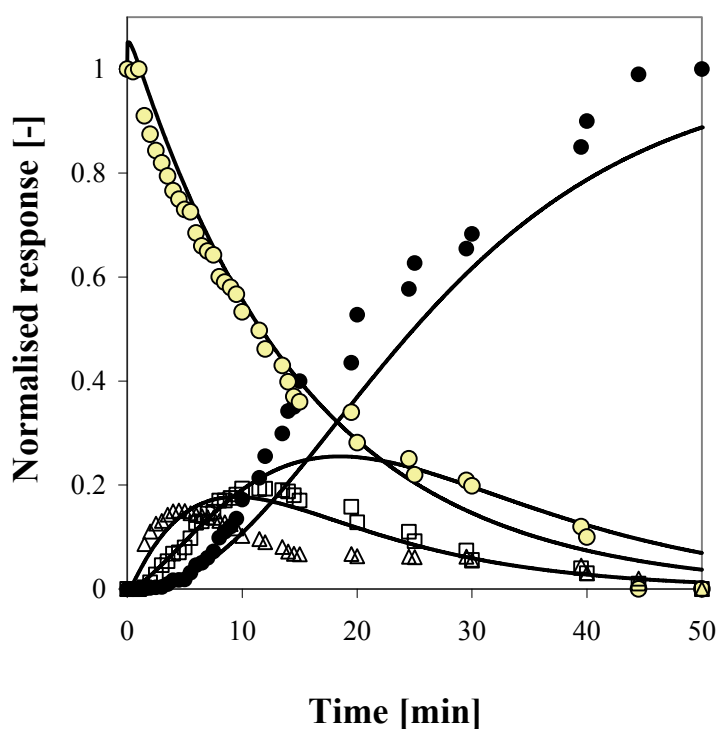


Figure 6.10: Model predictions (represented by solid lines) for propene using Model C (see Figure 6.4) and the optimized parameters from the C_2 study. The symbols: (\bullet) $^{13}C_3H_6$, (\circ) $^{12}C_3H_6$, (\square) $^{13}C^{12}C_2H_6$, and (Δ) $^{13}C_2^{12}CH_6$ are the data points obtained at $H_2/CO = 15$, $330^\circ C$, 1.2 bar and $GHSV = 7500 \text{ ml.g}_{cat}^{-1} \cdot \text{hr}^{-1}$

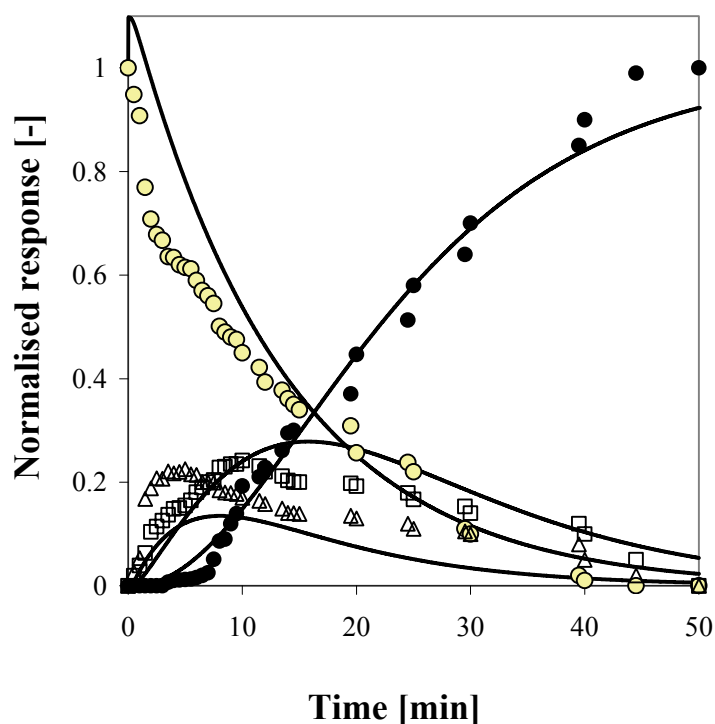


Figure 6.11: Model predictions (represented by solid lines) for propane using Model C (see **Figure 6.4**) and the optimized parameters from the C_2 study. The symbols: (\bullet) $^{13}C_3H_8$, (\circ) $^{12}C_3H_8$, (\square) $^{13}C^{12}C_2H_8$, and (Δ) $^{13}C_2^{12}CH_8$ are the data points obtained at $H_2/CO = 15$, $330^\circ C$, 1.2 bar and $GHSV = 7500$ $ml.g_{cat}^{-1}.hr^{-1}$.

To summarise, we have used our SSITKA results to distinguish between three mechanistic models for higher hydrocarbon formation. We showed that Model C, with two surface intermediates and with a direct pathway for olefins to readsorb and terminate as paraffins, can describe our data the best. The optimized parameters for the C_2 hydrocarbons are highly correlated which made the estimation of the rate constants for the C_3 's more difficult. Fixing the rate constants for case 2 ($k_{ini} = k_p$), Model C could predict the C_3 's but without a high degree of confidence due to lack of sufficient data, especially for the partial labeled species.

6.6. Conclusions

In this chapter, ¹³CO SSITKA experimental data for C₂-C₃ hydrocarbons was used to extend the mechanistic model for the methanation reaction previously reported in Chapter 4. Three different mechanistic models were tested whilst considering two cases, 1. $k_{ini} = k_p$ and 2. $k_{ini} \neq k_p$. Model C, in which there are two surface intermediates for the C_n hydrocarbons ($n \geq 2$) with direct olefin readsorption towards the surface intermediate for paraffin formation, gave the best fit. Both cases gave identical results in terms of goodness of fit and predicted gas phase concentrations. This implies that with the current results, there is no basis for expecting that $k_{ini} \neq k_p$. The results also showed that the rate constants were highly correlated. This coupled with the limited data for the C₃ partially labelled species made it difficult to optimise the rate constants for the C₃'s. However, a simulation of our best case shows that the C₂ model can be extended to account for the formation of C₃'s.

References

- (1) A.W. Sternberg and I. Wender, *Proc.Intern.Conf.on Coordin.Chem.* (1959), p53.
- (2) F. Fischer and H. Tropsch, *Brennstoff-Chem.* **7** (1926), p97.
- (3) B.H. Davis, *Catal. Today* **141** (2009), p25.
- (4) J. Happel, *Chem. Eng. Sci.* **33** (1978), p1567.
- (5) C.O. Bennett, in: *Understanding Heterogeneous Catalysis through the Transient Method*, eds. A.T.Bell and L.L.Hegedus, *Catalysis under Transient Conditions* (American Chemical Society, 1982), p1.
- (6) P. Biloen, *J Mol. Catal.* **21** (1983), p17.

- (7) A. Frennet, B. De, J.M. Bastin and N. Kruse, *J Phys. Chem. B* **109** (2005), p2350.
- (8) C.A. Mims and L.E. McCandish, *J Am. Chem. Soc.* **107** (1985), p696.
- (9) C.A. Mims and L.E. McCandish, *J Phys. Chem.* **91** (1987), p929.
- (10) C.A. Mims, *Catal. Letters* **1** (1988), p293.
- (11) C.J. Bertole, C.A. Mims, G. Kiss and P. Joshi, *Stud.. Surf. Sci. Catal.* **136** (2001), p369.
- (12) C.J. Bertole, C.A. Mims and G. Kiss, *J. Catal.* 210 (2002), p84.
- (13) C.J. Bertole, C.A. Mims and G. Kiss, *J. Catal.* 223 (2004), p309.
- (14) C.J. Bertole, C.A. Mims and G. Kiss, *J. Catal.* 221 (2004), p191.
- (15) T. Komaya and A.T. Bell, *J. Catal.* 146 (1994), 237.
- (16) K.R. Krishna and A.T. Bell, *Journal of Catalysis* 139 (1993), p104.
- (17) C.J. Bertole, C.A. Mims and G. Kiss, *Journal of Catalysis* 221 (2004), p191.
- (18) H.A.J. Van Dijk , A mechanistic study using transient isotopic tracing, Ph.D thesis, 2001, Technische Universiteit Eindhoven, Eindhoven, the Netherlands. <http://alexandria.tue.nl/extra2/200111083.pdf>
- (19) G.P. Van Der Laan and A.A.C.M. Beenackers, *IECR* 38 (1999), p1277.
- (20) H. Schulz and M. Claeys, *Appl. Catal. A* **186** (1999), 91.
- (21) W. Zimmerman, D. Bukur and S. Ledakowicz, *Chem. Eng. Sci.* **47** (1992), 2707.
- (22) L. Nowicki, S. Ledakowicz and D.B. Bukur, *Chem. Eng. Sci.* **56** (2001), 1175.

7

A comparative study of CO and CO₂ hydrogenation on Fe catalysts

In this chapter, the hydrogenation of CO₂ is investigated and compared to CO hydrogenation (normal Fischer-Tropsch synthesis) over an iron based catalyst at high temperature (330°C). At these conditions, the water-gas-shift reaction is closer to equilibrium than at lower temperatures (210-240°C) and so the reverse reaction becomes thermodynamically more favourable making these conditions ideal for CO₂ hydrogenation. In comparison to CO hydrogenation, the catalyst activity, deactivation and olefinicity are the same during CO₂ hydrogenation at similar reactor operating conditions, especially the H₂/CO ratio. However, the transients obtained during ¹³CO and ¹³CO₂ SSITKA experiments differ in both cases. During CO₂ hydrogenation, the reactant and product (CO₂ and CO) become kinetically indistinguishable. From some of the data, a two pool model is proposed based on the shape of the ¹³C decay in ¹³CO₂. In comparison to the work by Botes [1], the model (model B in [1]) in which CHO_s and COOH_s are the surface intermediates during the water-gas-shift reaction is the most plausible for the water-gas-shift mechanism.

7.1. Introduction

The reaction of carbon monoxide and steam to produce carbon dioxide and hydrogen according to Equation 1, is called the water-gas-shift (WGS) reaction. The water-gas-shift reaction is useful for those industrial processes requiring synthesis gas (or syngas) with H₂/CO ratios higher than can be produced by gasification or reforming of hydrocarbons. The WGS reaction is reversible, the reversed reaction often is denoted as reversed WGS, rWGS. It is also sometimes referred to as CO₂ hydrogenation.



A variety of counter measures [2] have been undertaken to mitigate the accumulation of greenhouse gases, especially CO₂ in the atmosphere. Among the methods of chemical fixation, the catalytic hydrogenation of CO₂ into liquid fuels, for example via the Fischer-Tropsch (FT) process [3], has received much interest as a potential CO₂ sink. However, the direct hydrogenation of CO₂ requires a safe and efficient method for the production of required H₂, needed for the reaction. Nevertheless, CO₂ hydrogenation is still being researched for cases of CO₂-rich synthesis gas (for example biomass [4]).

In this chapter, CO₂ hydrogenation at high temperature Fischer-Tropsch (HTFT) conditions is investigated. Specifically, isotopes are used to probe the reaction mechanism.

7.2. Background literature and theory

7.2.1. The water-gas-shift reaction

There are three main processes based on the WGS reaction, *viz.* the high-temperature shift (HTS), operating between 360 and 530 °C, the low-temperature shift (LTS), operating between 210 and 270 °C, and the “sour gas” shift which converts raw gases from gasification of coal or crude oil containing traces of sulphur and which operates at *ca.* 350 °C. Details about the catalysts used in these (non-FT) processes and other background information has been reported in the comprehensive review by Newsome [5].

The WGS reaction is also part of complex reactions, such as steam reforming of methane and the Fischer-Tropsch synthesis. In the case of the latter process, this is mostly significant over an iron-based catalyst.

7.2.2. Thermodynamic considerations

The WGS reaction is an exothermic reaction ($\Delta H = -40.6 \text{ kJ.mol}^{-1}$). The equilibrium constant K_p is defined by Equation 2 and its temperature dependence is expressed by Equation 3 [5] which indicates a decrease with increasing temperature as shown in Figure 7.1. This implies that the WGS reaction becomes thermodynamically less favourable at higher temperatures although the kinetics of the reaction will be much faster. The WGS reaction is normally conducted in multiple stages to overcome the thermodynamic limitation. This can be achieved by a HTS operation in the first stage and thereafter a LTS in the second stage.

$$K_{\text{WGS,exp}} = \frac{[\text{H}_2][\text{CO}_2]}{[\text{H}_2\text{O}][\text{CO}]} \quad [2]$$

$$K_{\text{WGS, equilibrium}} = \exp\left(\frac{4577.8}{T} - 4.33\right) \quad [3]$$

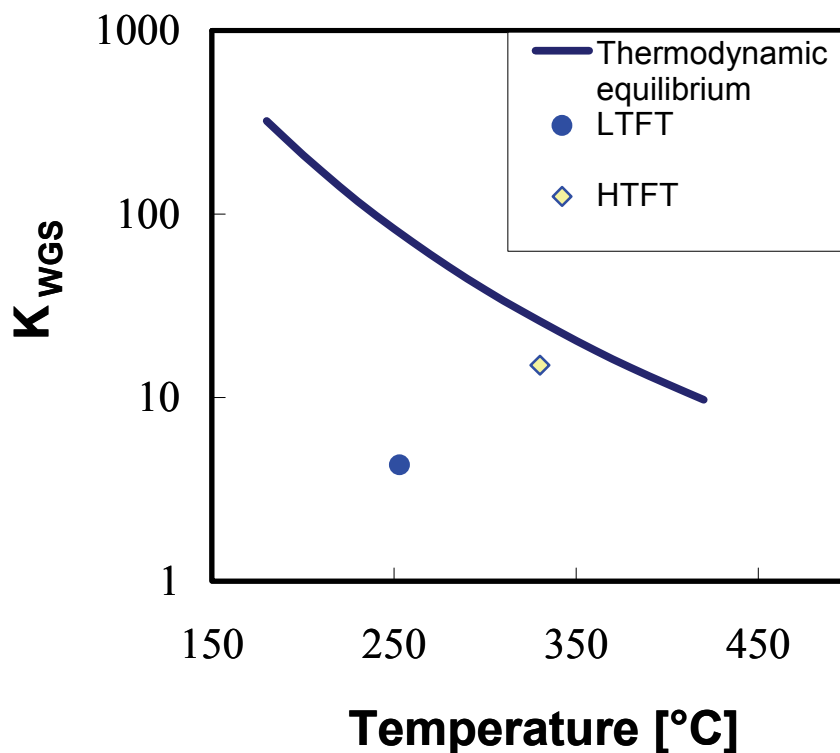


Figure 7.1: A comparison between the thermodynamic equilibrium constant [5] for the water-gas-shift reaction (Equation 3) and experimental constants (Equation 2) for LTFT [6] (H₂/CO = 2, 253°C and 15 bar) and HTFT [this study] (H₂/CO = 15, 330°C and 1.2 bar) conditions.

For the HTFT synthesis the water-gas-shift reaction is sufficiently rapid so that it is nearly at equilibrium [6] ($K_{\text{WGS,exp}} = 15$ at 300 °C) whereas at low temperature Fischer-Tropsch (LTFT) conditions, the reaction is far from equilibrium ($K_{\text{WGS,exp}} = 4.3$ at 253 °C). The removal of water causes the water-gas-shift equilibrium to shift in the case of high temperature Fischer-Tropsch synthesis so that it favours the production of CO. The CO formed, as a result undergoes hydrogenation yielding hydrocarbons.

7.2.3. Iron-based catalysts for the WGS and rWGS reactions

Fe based catalysts, for example Fe-Cr catalysts, used for commercial HTS operations which are not relevant to the Fischer-Tropsch conditions in this study are not discussed here. Background information about these (non-FT) catalysts can be found elsewhere [5]. In this section, the background literature for Fe based catalysts operated at conditions relevant to the Fischer-Tropsch synthesis is discussed.

Riedel *et al.* [3] showed that iron and cobalt catalysts behaved differently in CO₂ hydrogenation. With the iron catalyst, the same hydrocarbon product distribution was obtained with both a H₂/CO and H₂/CO₂ syngas, whereas with a cobalt catalyst, the product composition shifted towards CH₄ at lower CO content in the syngas. A similar conclusion was obtained by Zhang *et al.* [8] for a cobalt based catalyst. For the Fe-based catalysts, Riedel *et al.* [3] also observed *ca.* 43% lower reaction rate for CO₂-rich syngas than the CO-rich syngas (at the same H/C ratio). It was also reported that CO₂ oxidises the silica supported catalysts and therefore the CO₂ hydrogenation is lower. Jun *et al.* [9] also reported lower activity for silica supported Fe-based catalysts than those supported on alumina. In another publication by the same others, Schulz *et al.* [10] concluded that Fischer-Tropsch with H₂/CO₂ gave the same product distribution as with H₂/CO. Interestingly, it was also reported that the transient episodes[†] for a H₂/CO₂ feed were similar but extended compared to the H₂/CO feed. They also reported no significant deactivation with the H₂/CO₂ feed which was attributed to lower carbon formation. In contrast, Hong *et al.* [11] studied the deactivation on precipitated Fe-Cu-K-Al catalysts in CO₂ hydrogenation and reported significant decreases in activity and selectivity after 1500 h at 300°C and 10 atm. This could be due to the higher temperatures used by Hong *et al.* [11] which could have resulted in rWGS activity and hence higher CO partial pressures with the associated increase in carbon deposition.

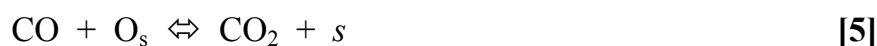
[†] Refers to the time period when the catalyst is undergoing changes, which in the case of Fe-based catalysts means transforming into carbides. During this period, the product slate also changes.

Chemicals, mainly olefins and alcohols, via the FT process have also received attention due to demand of these high value products. Fiato *et al.* [12] claim a process for producing C₂-C₂₀ olefins from a feed stream consisting of H₂ and CO₂ using an iron-carbide catalyst. Both oxygenates and hydrocarbons were produced when CO₂ was added to the syngas feed, as reported by Xu *et al.* [13]. In that study it was also shown that when CO₂ is present at low concentrations (0.2 mol % of CO), it can initiate chain growth but does not contribute to a measurable amount of chain propagation. However, when CO₂ is present in a larger amount relative to CO (CO₂/CO = 3), the water-gas-shift reaction was rapid relative to that of the FT reaction.

7.2.4. Mechanisms and kinetics

Two main types of reaction mechanisms for the WGS reaction have been proposed in the literature [5].

(a) Oxidation-reduction mechanism (Rideal-Eley type, Equations 4 and 5):



where O_s is the surface oxygen and *s* is a vacant surface site.

(b) Multistep mechanism (Langmuir-Hinshelwood type, Equations 6 to 10):



in which one step is rate determining whilst the others are fast and virtually at equilibrium. Here as well, *s* denotes free adsorption sites and the subscript *g* denotes the gas phase.

The WGS reaction on Fe-Cr catalysts has been shown to proceed via an oxidation-reduction mechanism [14]. However, under Fischer-Tropsch conditions, such a mechanism has received little attention. Van der Laan and Beenackers [15] and more recently Botes [1] both considered Langmuir-Hinshelwood type mechanisms for the WGS reaction at low temperature Fischer-Tropsch conditions on an iron precipitated catalyst. Specifically, these mechanisms included the formation of the formate species (COOH_s) either by reacting a hydroxyl species (OH_s) or water (H_2O_s) with carbon monoxide (CO_s). The formation of this formate intermediate can also occur via the CHO_s intermediate. The formate intermediate can then be reduced to either adsorbed or gaseous carbon dioxide. The pathways for the aforementioned reactions are depicted in Figure 7.2.

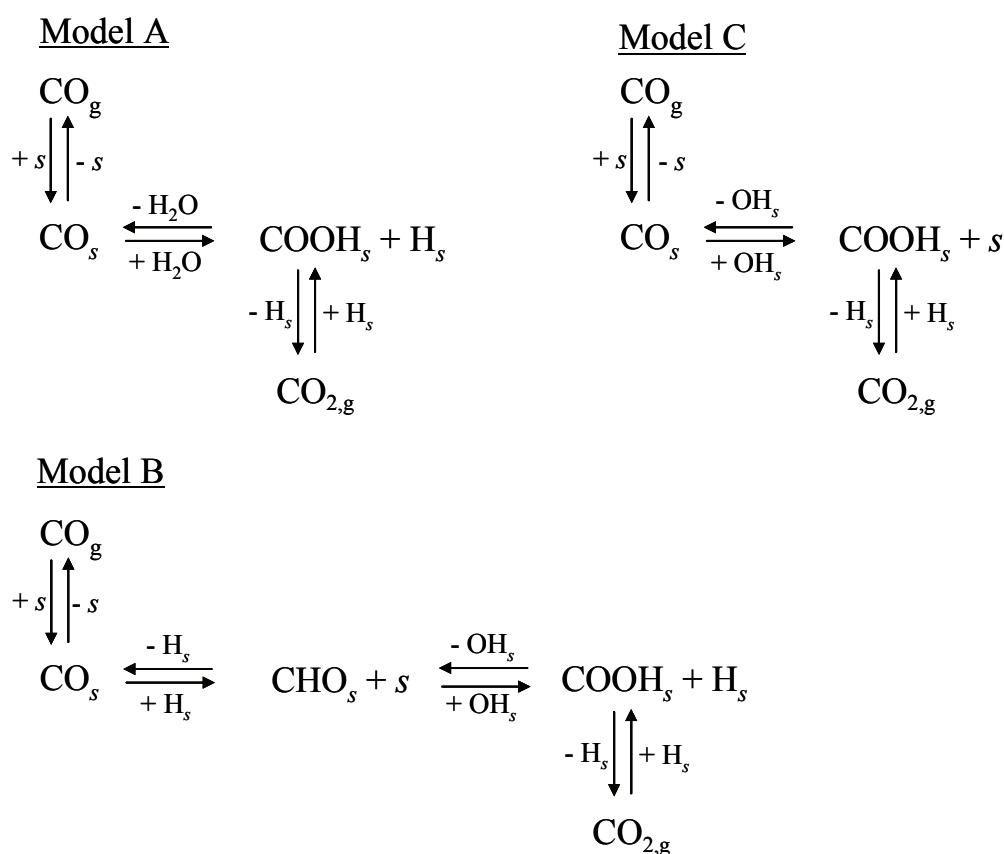


Figure 7.2: Schematic of the formate mechanisms as reported by Botes [1]. The reactions for the H_2 are the same as Equation 10 whilst H_2O can either react as adsorbed H_2O_s or dissociate into OH_s and H_s .

The WGS and FT kinetics cannot be described with the same denominator in the rate equations [1], implying that these reactions occur on separate catalytic sites [16,17]. Assuming the formate mechanism, Equation 11 proposed by Botes [1] can predict the WGS rate within the range of 5 to 20 bar absolute pressure. The terms in the denominator account for the effects of vacant sites and site occupation by adsorbed water and hydroxyl groups.

$$r_{WGS} \propto \frac{P_{CO}P_{H_2O} - \left(\frac{P_{CO_2}P_{H_2}}{K_{WGS}}\right)}{\left(1 + 1.1P_{H_2O} + 6.3\left(\frac{P_{H_2O}}{P_{H_2}^{0.5}}\right)\right)^2} \quad [11]$$

At HTFT conditions, the exact mechanism and kinetics for the WGS are not completely understood. The two main reasons for this are:

- The WGS reaction is closer to equilibrium at HTFT conditions (see Figure 7.1). This makes it experimentally complicated to distinguish between CO and CO₂ at these conditions.
- The CO disproportionation reaction, $2CO \rightarrow CO_2 + C$, becomes more significant at higher temperatures. This causes uncertainty as to the source of CO₂ as it could be the aforementioned reaction or the water-gas-shift reaction.

The aim of this work is to distinguish between CO₂ and CO hydrogenation at HTFT conditions, specifically in terms of activity and selectivity. The use of isotopic methods to elucidate the mechanistic pathways is also presented here.

7.3. Results and Discussion

7.3.1. Fischer-Tropsch activity and selectivity

7.3.1.1. Fischer-Tropsch activity

The Fischer-Tropsch activity over a given catalyst is dependent on the reactant partial pressures and reaction temperature. In the case of CO hydrogenation, normally the FT activity is expressed as the moles of CO converted per unit of time. This implies the conversion of CO to CO₂ via the WGS reaction is also taken into account when reporting the FT activity. However, in the case of CO₂ hydrogenation (without CO in the fresh feed), the FT activity cannot be expressed in the same units since then a negative value is obtained for CO converted. Therefore many researchers report the FT activity during CO₂ hydrogenation in units of moles of CO₂ converted per unit of time.

Another important parameter is the H₂/CO reactor exit ratio, which influences the activity, selectivity and even catalyst deactivation [18]. Davis[18] showed that the CO conversion is lower at H₂/CO = 0.7 compared to H₂/CO = 1.7 at 270°C and 11.6 bar on a Fe-based catalysts. Higher H₂/CO ratios are also often desired to limit carbon formation which can cause catalyst deactivation. In Figure 7.3, the (almost linear) relationship between H₂/CO reactor exit ratio and the H₂/CO₂ fresh feed ratio is illustrated[‡]. Thus, to obtain comparable results as with CO hydrogenation, the correct H₂/CO₂ inlet ratio also needs to be chosen. Most studies have compared CO and CO₂ hydrogenation at the same H₂/CO and H₂/CO₂ inlet ratios [19,20]. Considering the aforementioned discussion and the relationship in Figure 7.3, such a comparison is not realistic, especially at lower temperatures where CO₂ hydrogenation is relatively slower than at the higher temperatures used in this study.

[‡] In the case of H₂/CO experiments, the H₂/CO ratio did not vary across the catalyst bed (differential reaction conditions). For H₂/CO₂, the assumption was the CO₂ hydrogenation is very rapid, and the reactor exit H₂/CO₂ ratio is taken as the average H₂/CO₂ across that catalyst bed.

The baseline conditions used in most of our studies were at $H_2/CO = 15$ which corresponds to *ca.* $H_2/CO_2 = 3$. The FT activity profile, shown in Figure 7.4, is very similar for both cases. The catalyst activation (via carbide formation) is similar for both CO and CO₂ hydrogenations at these conditions. Schulz *et al.* [10] also compared the changes in the catalyst activity of an Fe-based catalyst during the initial stages of the Fischer-Tropsch synthesis. They reported similar kinetic episodes but with longer times for H_2/CO_2 . This is to be expected as they worked at lower temperatures (250°C) where the rWGS reaction is slower as compared to the WGS reaction. Nevertheless, they did not

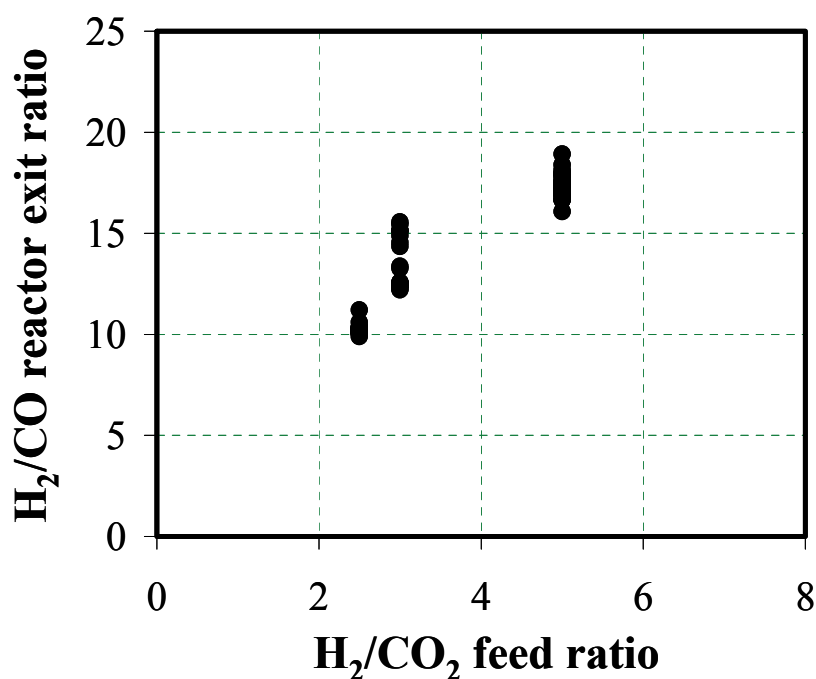


Figure 7.3: Dependence of H_2/CO reactor exit ratio on the H_2/CO_2 fresh feed ratio. Reaction conditions were 330°C and 1.2 bar on a Fe/K catalyst.

report differences in deactivation with CO₂ and so it can be accepted that the hydrogenation of CO₂ to produce FT products proceeds via the rWGS reaction to form the CO intermediate which is subsequently hydrogenated.

7.3.1.2. Methane selectivity

Apart from thermodynamic restrictions, the other major factor against CO₂ hydrogenation is the higher methane selectivity [20,21]. The methane selectivity is not compared here, as negative values were obtained when calculated on a C-atom basis for CO₂ hydrogenation. This is due to the low

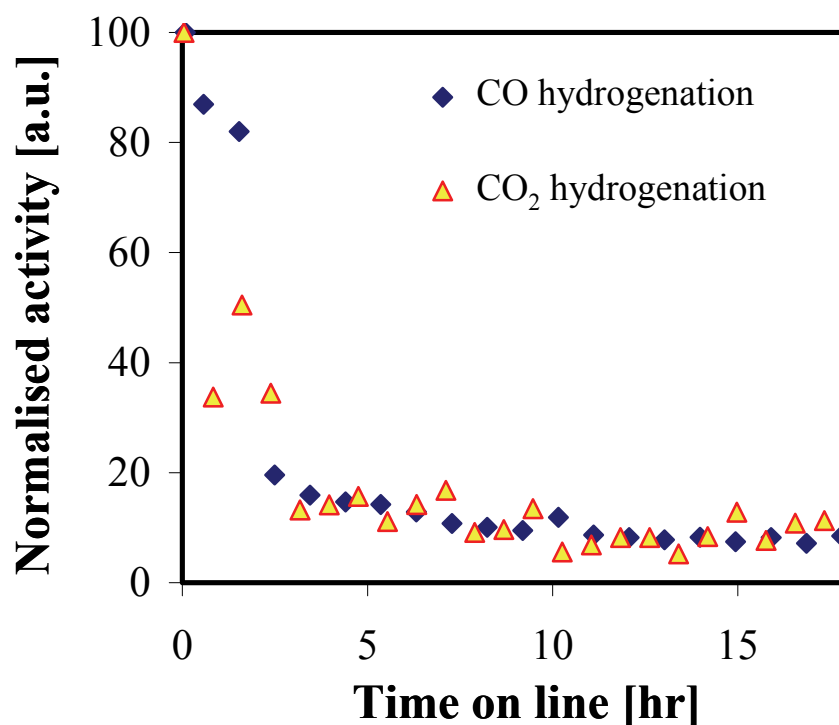


Figure 7.4: Normalised Fischer-Tropsch activity profile comparing CO and CO₂ hydrogenation. Reaction conditions were 330°C, 1.2 bar, H₂/CO = 15 and H₂/CO₂ = 3, respectively.

conversions and also the absence of CO in the fresh feed. At low conversions, the error in the GC analysis is large due to the difference between two almost similar values. Instead, the rate of methane production is reported in Figure 7.5. The rate of methane production for CO₂ hydrogenation is lower than for CO hydrogenation. One possible reason for this could be that more hydrogen is consumed during CO₂ hydrogenation which slows down the methanation rate. Alternatively, it could be that CO₂ hydrogenation produces more surface species than during CO hydrogenation, for example formate intermediates [15] which could block potential methanation sites. It is interesting to note that the

rate of methane production is stable for the first 20 hrs TOL for both CO and CO₂ hydrogenation. This is another indication that severe catalyst deactivation did not occur during the CO₂ hydrogenation experiments in this study since methane selectivity increases during catalyst deactivation [22].

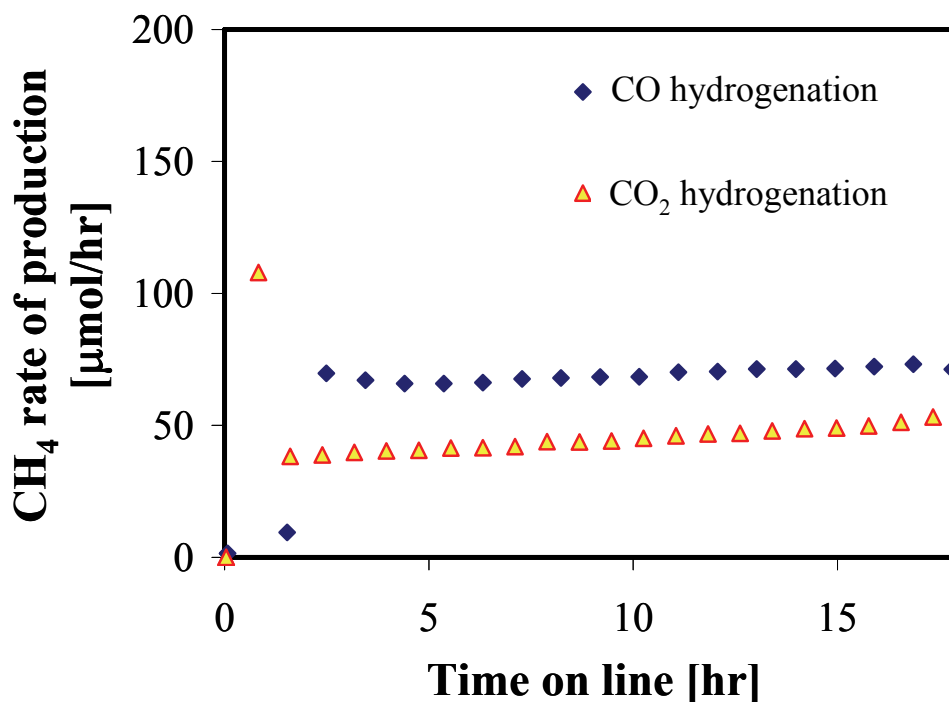


Figure 7.5: Comparison of the methane production for CO and CO₂ hydrogenation at 330°C, 1.2 bar, H₂/CO = 15 and H₂/CO₂ = 3, respectively.

7.3.1.3. Olefinicity (Olefin/Paraffin ratios)

The C₂ and C₃ olefinicities are shown in Figure 7.6 for both CO and CO₂ hydrogenation at similar H₂/CO reactor ratios. The olefinicity for CO₂ hydrogenation is almost the same as for CO hydrogenation. Similar selectivities for CO and CO₂ hydrogenation have also been reported by other researchers [3], once again implying that CO₂ hydrogenation proceeds via the rWGS reaction with CO as an intermediate before the Fischer-Tropsch reaction proceeds.

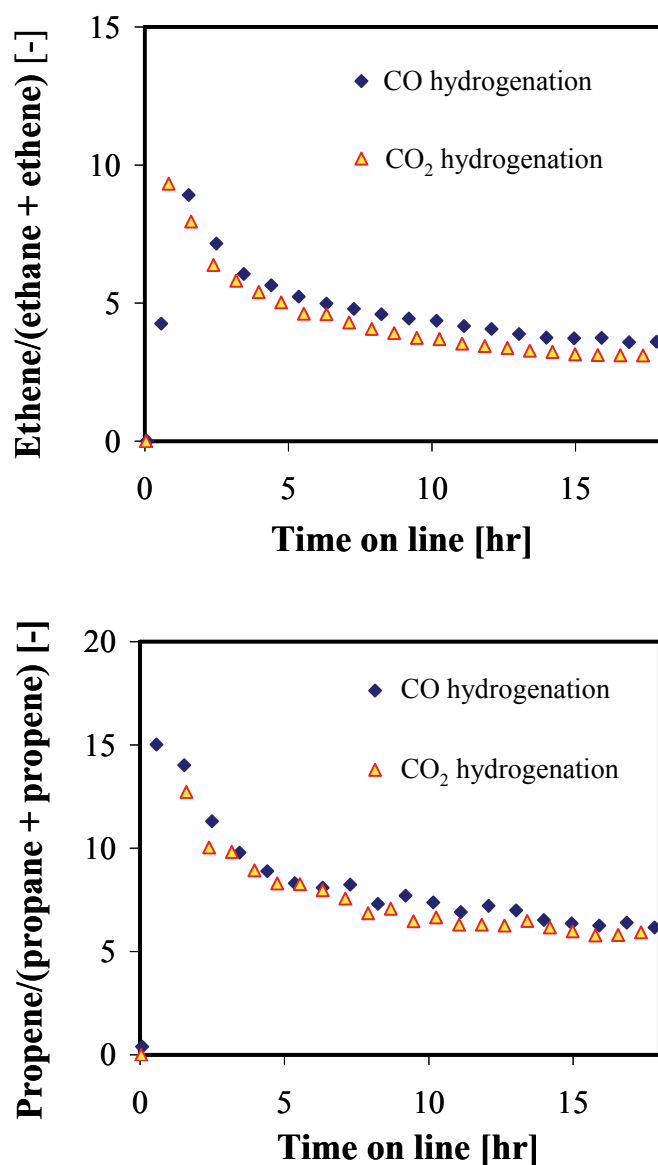


Figure 7.6: Olefinicity (olefin/paraffin ratio) for CO and CO₂ hydrogenation at 330°C, 1.2 bar, $H_2/CO = 15$ and $H_2/CO_2 = 3$. Top is C₂'s and bottom is C₃'s.

7.3.2. A comparison between ¹³CO and ¹³CO₂ SSITKA

The transients for ¹³CH₄ and C₂-C₃ hydrocarbons obtained from ¹³CO SSITKA have been presented earlier (see Chapters 4 and 6). Figure 7.7 shows the normalised transients for ¹³CO₂ obtained from ¹³CO SSITKA experiments. The Ne and ¹³CO signals are also shown for comparison of the relative residence times but these responses were also discussed earlier (see Chapter 4).

During ¹³CO SSITKA, the surface coverage of the reactant CO is shown to be extremely small whilst the product

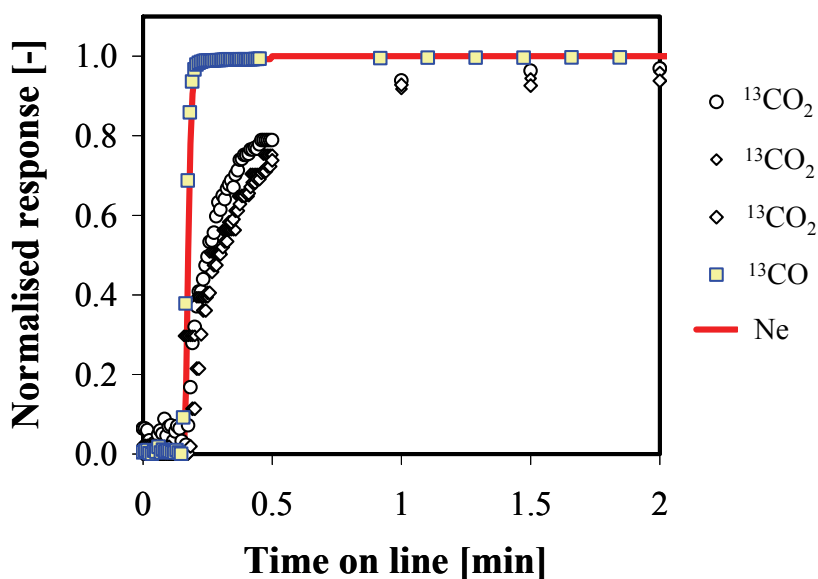


Figure 7.7: Normalised responses for Ne, ¹³CO and ¹³CO₂ from a ¹³CO SSITKA experiment ($H_2/^{12}CO/Ar \rightarrow H_2/^{13}CO/Ar/Ne$), obtained at 330°C, 1.2 bar, $H_2/CO = 15$. The different symbols for ¹³CO₂ are data points from a different time on line or experiment but at the same experimental conditions mentioned above.

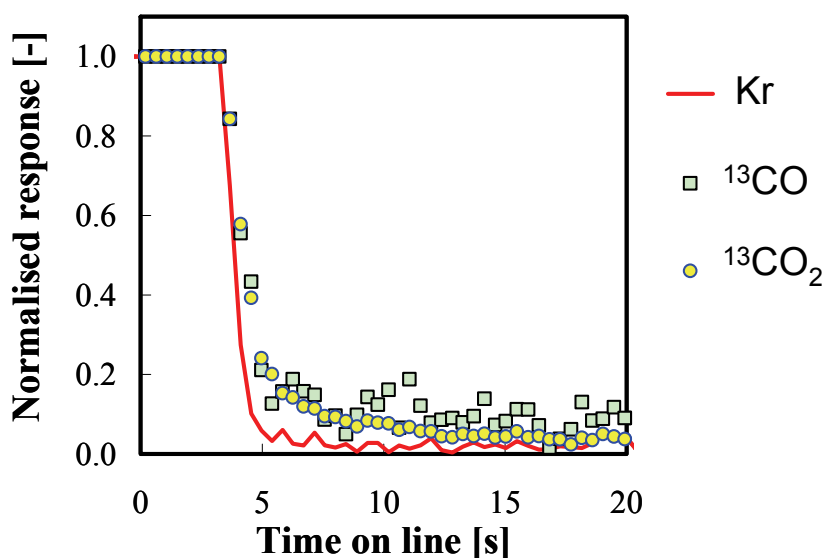


Figure 7.8: Normalised responses for Kr, ¹³CO and ¹³CO₂ from a ¹³CO₂ SSITKA experiment ($H_2/^{12}CO_2/Ar \rightarrow H_2/^{13}CO_2/Ar/Kr$), obtained at 330°C, 1.2 bar, $H_2/CO_2 = 5$.

CO₂ elutes in about 2 min. In contrast, during ¹³CO₂ SSITKA experiments, the reactant CO₂ seems to occupy a measurable coverage and the product CO elutes at the same time as illustrated in Figure 7.8. The latter phenomenon is expected at HTFT conditions (close to the WGS equilibrium) where CO and CO₂ become kinetically indistinguishable from each other.

In the case where CO was present in the fresh feed during CO₂ hydrogenation, the ¹³CO and ¹³CO₂ transients (see Figure 7.9) also eluted at the same time. There also is an effect of H/C ratio on these transients with increasing residence times at the higher H/C ratio. However, this conclusion is based on just these two experiments and therefore more work is required to fully understand the mechanistic reasons for such an observation. There have been contradictory reports in the literature regarding the effect of H₂/CO ratio on the surface concentrations on methane intermediates. Van Dijk [23] reported a decrease for H₂/CO = 1 – 5 on a Co based catalyst, Bajusz *et al.* [24] reported an increase for H₂/CO = 3.9 – 20 on a Ru based catalyst and Chen and Goodwin [25] showed there was no change for H₂/CO = 5 – 15, also on a Ru based catalyst. Therefore, to study the effect on H₂/CO for the more complicated WGS reaction, at close to equilibrium conditions, requires a dedicated experimental plan which was not in the scope of this thesis.

The transients for ¹³CH₄ and ¹²CH₄ from ¹³CO₂ SSITKA experiments during CO₂ hydrogenation are shown in Figure 7.10. These transients cross at a value of 0.5 suggesting that these are the main products and moreover there are no reversible reactions. Such a reaction pathway is consistent with our ¹³CO SSITKA experiments (see Chapter 4). The ¹³CH₄ transient from such an experiment is also included in Figure 7.10 and is shown to have a longer residence time. As discussed, more experiments at varying H₂/(CO + CO₂) ratios are required to fully understand and explain the reason for this observation.

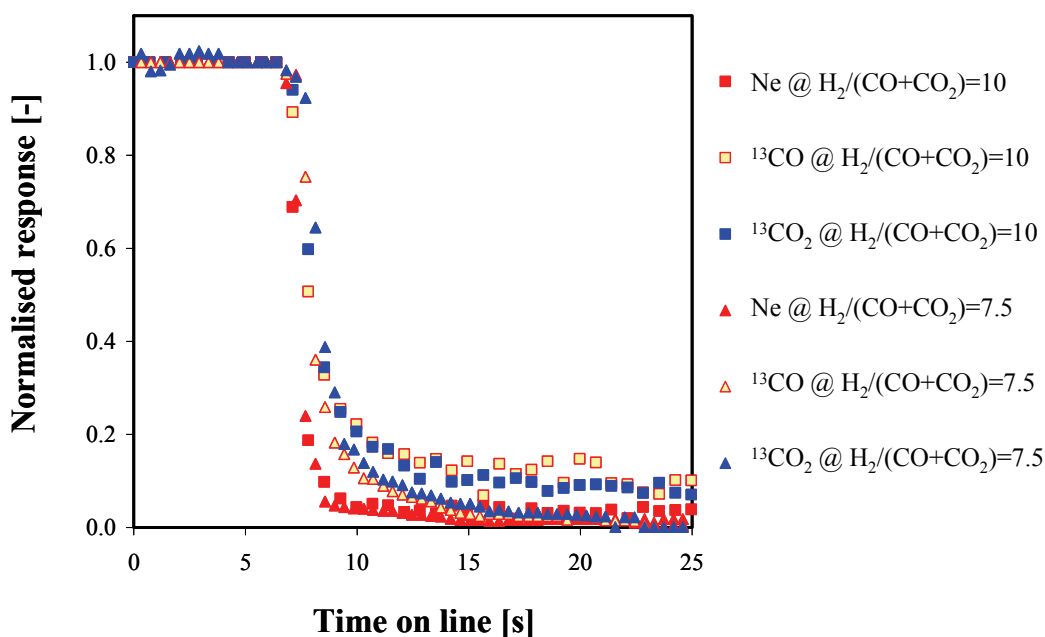


Figure 7.9: Normalised responses for Ne, ¹³CO and ¹³CO₂ from a ¹³CO₂ SSITKA experiment ($H_2/^{12}CO_2/Ar \rightarrow H_2/^{13}CO_2/Ar/Ne$), obtained at 330°C, 1.2 bar and different $H_2/(CO + CO_2)$ ratios.

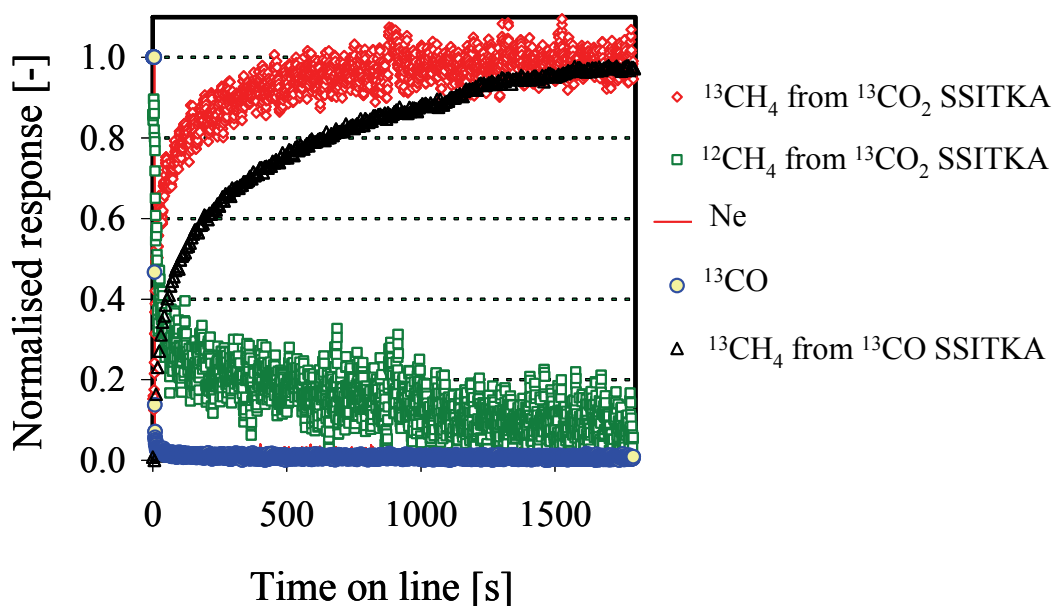


Figure 7.10: Normalised responses for Ne, ¹³CO, ¹²CH₄ and ¹³CH₄ from a ¹³CO₂ SSITKA experiment ($H_2/^{12}CO_2/Ar \rightarrow H_2/^{13}CO_2/Ar/Ne$), obtained at 330°C, 1.2 bar, $H_2/CO_2 = 5$. For comparison, the data for ¹³CH₄ from a ¹³CO SSITKA (presented in Chapter 4) is also included.

Although steady state selectivities for CO and CO₂ hydrogenation are similar, the product transients for the SSTIKA experiments using ¹³CO and ¹³CO₂ are somewhat different, at least for the experiments presented here. This implies that CO₂ hydrogenation to Fischer-Tropsch products most probably proceeds via the formation of CO which is subsequently hydrogenated resulting in similar selectivities. However, from the transients, it can be concluded that the rate of these reactions are different.

7.3.3. Mechanistic implications

The shape of the transients obtained during SSITKA experiments provides information about both the intrinsic kinetics and mechanistic pathways [26]. In Chapters 4 and 6, reactor modeling was utilized to elucidate the mechanistic pathways for methane and C₂-C₃ hydrocarbons, respectively. Such an exercise requires a wealth of experimental data with good reproducibility. Unfortunately in the case of CO₂ hydrogenation, too few data points were collected due to technical problems with the mass spectrometer to allow for completion of a similar study.

However, one simple evaluation of the transient data involves plotting the ¹³C decay versus time. The shape of this graph is known to provide some indication of the type of mechanism, in terms of number of “C” pools [23,26,27]. Details of this approach are given in Appendix D. A concave upwards graph is obtained for the ¹³C decay in ¹³CO₂ for both CO and CO₂ hydrogenation, as presented in Figure 7.12. Such a graph is indicative of a “two pool” model. In other words, this indicates that there are two kinetically distinguishable “C” pools for the WGS reaction mechanism,

7.3.4. Proposed model for WGS reaction

The formate mechanism has recently been accepted as the most plausible pathway for CO₂ formation during Fischer-Tropsch conditions [1,15,28,29]. Botes [1] tested three different formate mechanisms (models A, B and C). In terms of “C-pools”, two of these models were single pool models whilst the other was a two pool model as illustrated in Figure 7.11. In models A and C, the single pool (C₁) is the COOH_s species whilst in model B the two pools (C₁ and C₂) are the CHO_s and COOH_s species, respectively. Based on the ¹³C decay plot (Figure 7.12), our results suggest a two pool model. Although the work by Botes [15] was performed at LTFT conditions, and thus his outcomes may not apply to our system, the most plausible mechanism for CO₂ formation at present is model B in Figure 7.11. Incidentally, Botes [1] concluded that this model was also the best model when tested against steady state experiments.

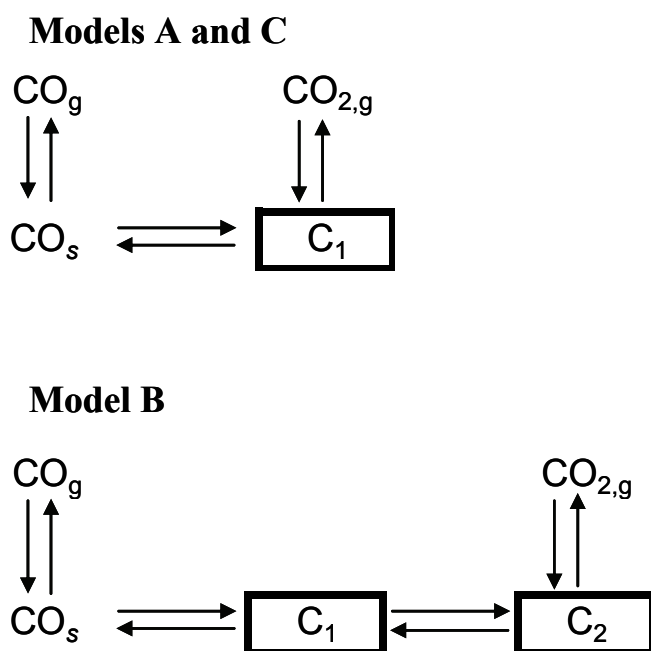


Figure 7.11: Formate mechanisms tested by Botes [1] represented as “C-pools”.

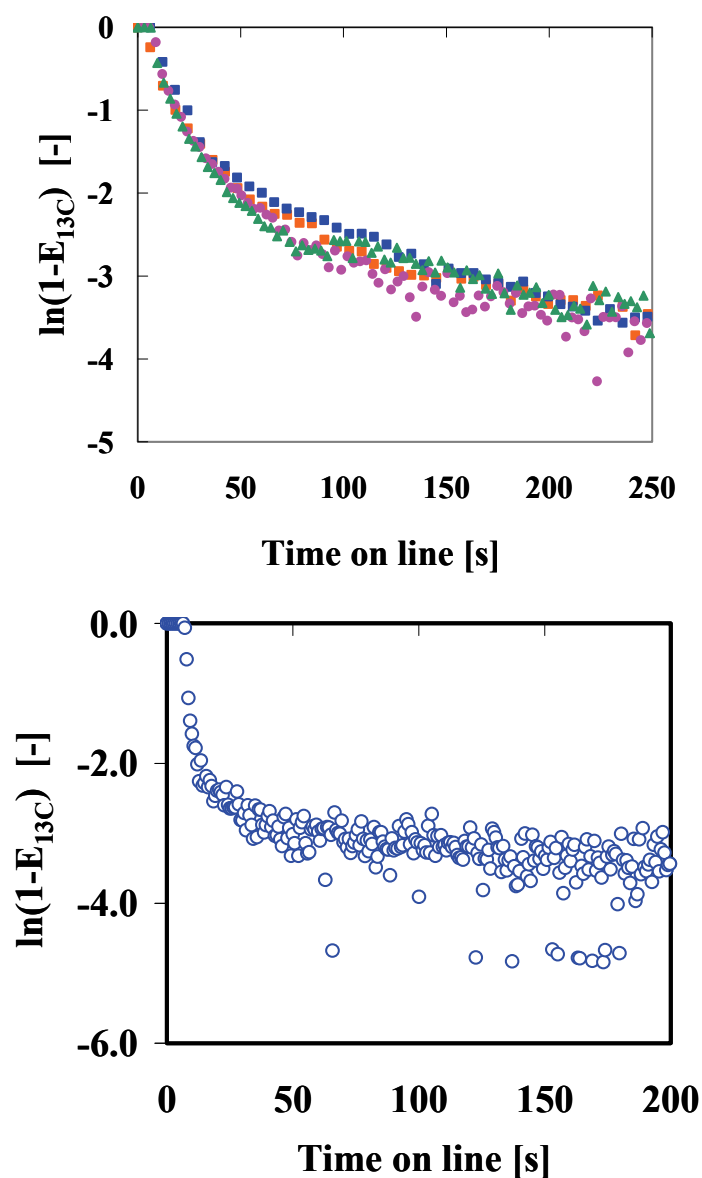


Figure 7.12: Calculated decay of the ^{13}C content in $^{13}\text{CO}_2$ from (top) a ^{13}CO SSITKA experiment ($\text{H}_2/^{12}\text{CO}/\text{Ar} \rightarrow \text{H}_2/^{13}\text{CO}/\text{Ar}/\text{Ne}$), obtained at 330°C , 1.2 bar, $\text{H}_2/\text{CO} = 15$ with symbols representing different data sets, and (bottom) a $^{13}\text{CO}_2$ SSITKA experiment ($\text{H}_2/^{12}\text{CO}_2/\text{Ar} \rightarrow \text{H}_2/^{13}\text{CO}_2/\text{Ar}/\text{Ne}$), obtained at 330°C , 1.2 bar, $\text{H}_2/\text{CO}_2 = 5$.

7.4. Conclusions and recommendations

The H₂/CO₂ feed ratio during the CO₂ hydrogenation influences the H₂/CO reactor ratio and it is therefore important to choose the correct feed ratios (among other reaction conditions) when comparing CO and CO₂ hydrogenation experiments.

At the same reaction conditions during CO and CO₂ hydrogenation, similar steady-state activity and olefinicity were obtained. This is consistent with the study by Schulz *et al.* [10].

In contrast to ¹³C SSITKA experiments during CO hydrogenation, CO and CO₂ become kinetically indistinguishable during ¹³CO₂ SSITKA experiments during CO₂ hydrogenation, indicating that in this case the WGS reaction is near equilibrium.

Based on the ¹³C decay plots, a two pool model for the WGS mechanism is most likely to fit our experimental data. When comparing to the recent formate mechanism reported by Botes [1], model B (see Figure 7.11) is the most plausible mechanism. This mechanism has CHO_s and COOH_s species as the surface intermediates during the WGS reaction.

References

- (1) F.G. Botes, *Appl. Catal. A*: **328** (2007) 237-242.
- (2) United Nations. Kyoto Protocol to the United Nations framework convention on climate change. (1998).
- (3) T. Riedel, M. Claeys, H. Schulz, G. Schaub, S.S. Nam, K.W. Jun, M.J. Choi, G. Kishan and K.W. Lee, *Appl. Catal. A*: **186** (1999) 201-213.
- (4) M. Rohde, D. Unruh, P. Pias, G. Schaub and K.W. Lee, *Stud. Surf. Sci. Catal.* **153** (2004) 97-102.
- (5) D.S. Newsome, *Catal. Rev. Sci. Eng.* **21** (1980) 275-318.

- (6) G. Van Der Laan, Kinetics, selectivity and scale up of the Fischer-Tropsch synthesis, PhD thesis (1999), Rijksuniversiteit Groningen, the Netherlands . <http://dissertations.ub.rug.nl/faculties/science/1999/g.p.van.der.laan/?pLanguage=en&pFullItemRecord=ON>
- (7) M.E. Dry, *ACS Div. Fuel Chem., Preprints* **48** (2003) 211.
- (8) Y. Zhang, G. Jacobs, D.E. Sparks, M.E. Dry and B.H. Davis, *Catal. Today* **71** (2002) 411-418.
- (9) K.W. Jun, H.S. Roh, K.S. Kim, J.S. Ryu and K.W. Lee, *Appl. Catal. A*: **259** (2004) 221-226.
- (10) H. Schulz, G. Schaub, M. Claeys and T. Riedel, *Appl. Catal. A*: **186** (1999) 215-227.
- (11) J.S. Hong, J.S. Hwang, K.W. Jun, J.C. Sur and K.W. Lee, *Appl. Catal. A*: **218** (2001) 53-59.
- (12) R.A. Fiato, S.L. Soled, G.W. Rice and S. Miseo. *Method for producing olefins from H₂ and CO₂ using an iron carbide based catalyst*. ed. Exxon Research and Engineering Company. US Patent 5,140,049, (1992).
- (13) L. Xu, S. Bao, D.J. Houpt, S.H. Lambert and B.H. Davis, *Catal. Today* **36** (1997) 347-355.
- (14) M. Tinkle and J.A. Dumesic, *J. Catal.* **103** (1987) 65-78.
- (15) G.P. Van Der Laan and A.A.C.M. Beenackers, *Appl. Catal. A*: **193** (2000) 39-53.
- (16) E.S. Lox and G.F. Froment, *IECR* **32** (1993) 71-82.
- (17) K.R.P.M. Rao, F.E. Huggins, V. Mahajan, G.P. Huffman, V.U.S. Rao, B.L. Bhatt, D.B. Bukur, B.H. Davis and R.J. O'Brien, *Top. Catal.* **2** (1995) 71-78.
- (18) B.H. Davis, *Catal. Today* **84** (2003) 83-98.
- (19) M.L. Cubeiro, J. González, M.R. Goldwasser, M.J. Pérez-Zurita, E. Pietri and L. García, *Hyperfine Interactions* **134** (2001) 13-25.
- (20) T. Riedel, M. Claeys, H. Schulz, G. Schaub, S.S. Nam, K.W. Jun, M.J. Choi, G. Kishan and K.W. Lee, *Appl. Catal. A* **186** (1999) 201-213.
- (21) G.D. Weatherbee and C.H. Bartholomew, *J. Catal.* **77** (1982) 460-472.
- (22) S.A. Eliason and C.H. Bartholomew, *Appl. Catal. A*: **186** (1999) 229-243.

- (23) H.A.J. Van Dijk , *A mechanistic study using transient isotopic tracing*, Ph.D thesis (2001), Technische Universiteit Eindhoven, Eindhoven, the Netherlands. <http://alexandria.tue.nl/extra2/200111083.pdf>
- (24) I.G. Bajusz and J. Goodwin, *J. Catal.* **169** (1997) 157-165.
- (25) B. Chen and J. Goodwin, *J. Catal.* **158** (1996) 511-520.
- (26) S.L. Shannon and J. Goodwin, *Chem. Rev.* **95** (1995) 677-695.
- (27) Y. Soong, K. Krishna and P. Biloen, *J. Catal.* **97** (1986) 330-343.
- (28) B.T. Teng, J. Chang, J. Yang, G. Wang, C.H. Zhang, Y.Y. Xu, H.W. Xiang and Y.W. Li, *Fuel* **84** (2005) 917-926.
- (29) Y.N. Wang, W.P. Ma, Y.J. Lu, J. Yang, Y.Y. Xu, H.W. Xiang, Y.W. Li, Y.L. Zhao and B.J. Zhang, *Fuel* **82** (2003) 195-213.

8

Conclusions and Outlook

8.1. Conclusions

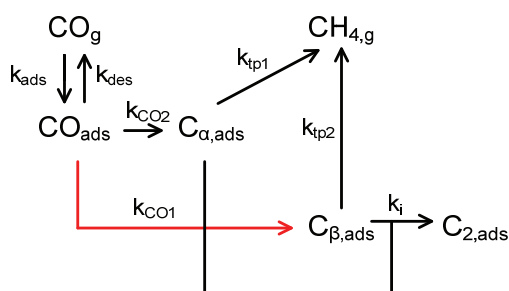
The high temperature (300–350 °C) Fischer-Tropsch (HTFT) process aims at the production of gasoline and linear low molecular mass olefins from a mixture of hydrogen and carbon (synthesis gas) over an Fe-based catalyst. The process comprises a network of complex elementary reaction steps and to date, mechanisms in the literature cannot explain these reaction pathways. For this reason, this thesis has addressed the development of a mechanistic pathway for this process by the use of isotopic methods. The Steady State Isotopic Transient Kinetic Analysis (SSITKA) technique keeps the catalyst at steady state whilst an abrupt switch is made to the feed, changing from a normal feed to an isotopically labelled one. The resulting transient responses provide information about the intrinsic kinetics which in turn can be related to a fundamental reaction pathway. The main outcome of this thesis is presented here.

A mechanism for methanation

In Chapter 4, ^{13}C O SSITKA experimental results showed that molecularly adsorbed CO on the Fe/K catalyst (at 330°C, 1.2 bar and $\text{H}_2/\text{CO} = 15$) is

extremely low, *ca.* $9 \cdot 10^{-4}$ ML, whilst the monomeric carbon pool ($C_{1,tot}$) is much higher at 0.25 ML. A parameter estimation study showed that three (out of six) methanation models are indistinguishable and moreover these models have a buffer step or parallel route towards the formation of methane. In other words, there needs to be **two surface intermediates** in the model to explain the experimental results. In order to distinguish between these models, the chain initiation reaction (C-C coupling) was included which resulted in eight models being tested. The final results showed that two of these eight models (see Figure 4.7, Chapter 4) remain indistinguishable. Both these models have two surface intermediates (C_{α} and C_{β}) which are active towards methanation and higher hydrocarbon formation as shown in Figure 8.1.

Model 3.2



Model 5.2

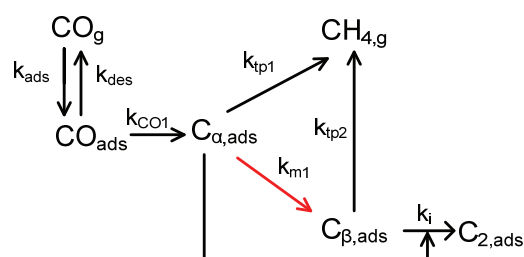


Figure 8.1: Indistinguishable models 3.2 and 5.2 as obtained from the methanation study in Chapter 4.

The quantification of the kinetic rate parameters was performed by accounting for the higher hydrocarbon formation. The results showed that C_{β} is the larger pool, occupying 92% of the $C_{1,tot}$ coverage and is 25-50 times less active for methanation than C_{α} .

Identification of surface species

The aforementioned study of the methanation reaction was completed only with ^{13}CO SSITKA experimental data and hence could not shed any light onto the nature of the carbon pools, specifically C_α and C_β . For this reason, in Chapter 3, the identity and reactivity of surface carbonaceous intermediates were determined by various methods, mostly isotopic tracing using deuterium.

It is well known in literature that the activity and selectivity of an Fe-based Fischer-Tropsch catalyst changes with time on line which is mainly attributed to phase changes (mostly the formation of Fe-carbides). This was also observed in this study (Chapter 4). Therefore, it was decided to perform experiments on a fresh catalyst and a catalyst which was exposed to synthesis gas as well as an end of run sample to investigate the effect of carbiding the Fe-based catalyst. The results showed that the transients at the start of the Fischer-Tropsch synthesis (i.e. when synthesis gas is introduced) were different on a carbided catalyst compared to a freshly reduced catalyst. Moreover, on both the fresh and carbided catalysts, carbon deposition still occurs to the same extent but water formation and methane formation are faster on the carbided catalyst.

H/D exchange reactions were used to identify the nature of the surface intermediates which turned out to be different for the various carbided catalysts. The CH_5 and CCH_5 surface intermediates were observed on both catalysts for methane formation and C_2 hydrocarbon formation, respectively. The other Fischer Tropsch surface intermediates, which were present on the fresh catalyst, either disappeared on the carbided catalyst or were too small in concentration to be detected. These results are summarised in Figure 8.2.

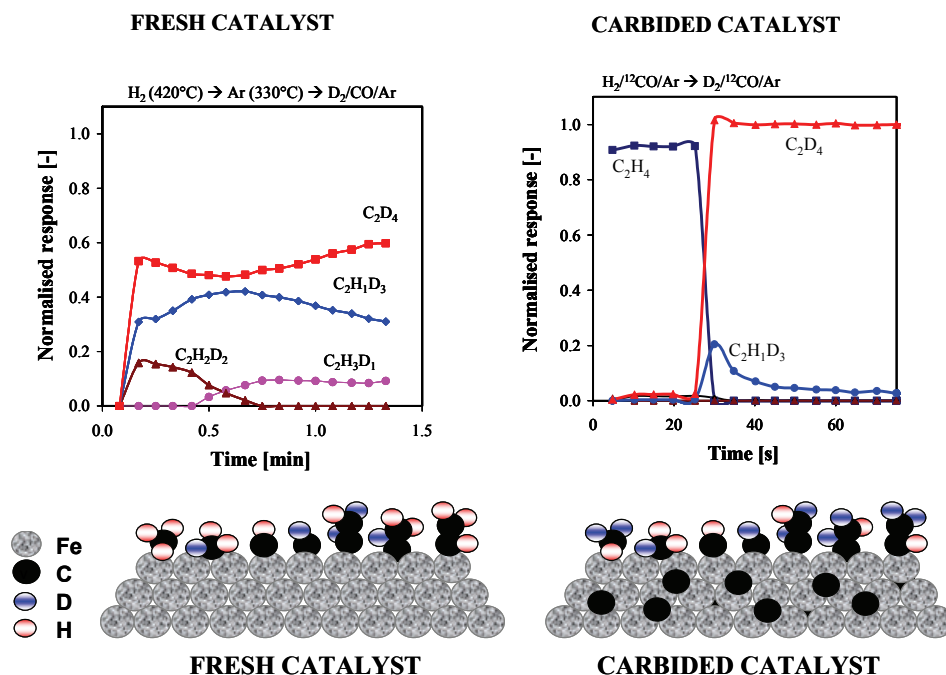


Figure 8.2: Summary of the main results from the H/D exchange experiments on a fresh and carbided catalyst as reported in Chapter 3.

Surface carbon was deposited via the Boudouard reaction using ^{13}CO on a reduced catalyst. This carbon ($^{13}C_s$) was active and detected in the C_{2+} hydrocarbon products as a coupling reaction with $^{12}C_s$ rather than with $^{13}C_s$. Finally, combining the *in-situ* and *ex-situ* temperature programmed surface reaction data with the *in-situ* isothermal reaction data, confirmed the presence of six distinct pools of carbonaceous intermediates. Graphitic carbon, detected at 767°C, had the highest coverage of all the surface species.

Co-feeding ethene during Fe-HTFT

Numerous studies have addressed olefin readsorption either on Fe or Co-based catalysts but mostly at low temperatures (200-270°C). At higher

temperatures, like the experiments in this thesis, these reactions could become more significant. To provide some insight into the mechanistic pathways of olefin readsorption during the HTFT process, ethene was added to the fresh feed (as 1 mol% C₂H₄ in H₂) and ¹³CO SSITKA experiments were performed as presented in Chapter 5.

The main reaction was the hydrogenation of ethene to ethane but chain growth was also observed to a certain extent (40% ethane was formed compared to 1% propene). Based on ¹³CO SSITKA results, propene was the kinetically preferred product when ethene participates in chain growth, implying different sites or different intermediates for olefins and paraffins. It was also observed that both the methanation rate and the methane selectivity decreased with the addition of ethene in the fresh feed. This could be due to competitive adsorption between the respective surface intermediates, for example between H_{ads} and CH_x ($x = 0$ to 3) surface intermediates sites. Both the water-gas-shift rate and the CO₂ selectivity remained the same during the co-fed ethene experiments. This could imply that methanation and water-gas-shift take (WGS) place on different surface sites. These results were used to propose two mechanistic pathways, both with dual sites (or different intermediates) as presented in Figures 5.6 and 5.7.

The Fischer-Tropsch mechanism

In Chapter 6, ¹³CO SSITKA experimental data for C₂-C₃ hydrocarbons were used to extend the mechanistic model for the methanation reaction previously reported in Chapter 4. The results from co-feeding an olefin (presented in Chapter 5) was also considered and used to propose two different mechanistic models. This resulted in testing three different

In Chapter 7, a comparison between the CO and CO₂ hydrogenation was presented. It was shown that the H₂/CO₂ feed ratio during the CO₂ hydrogenation influences the H₂/CO reactor ratio and it is therefore important to choose the correct feed ratios (among other reaction conditions) when comparing CO and CO₂ hydrogenation experiments.

At the same reaction conditions, during CO and CO₂ hydrogenation, similar steady-state activity and olefinicity were obtained. In contrast to ¹³CO SSITKA experiments during CO hydrogenation, CO and CO₂ become kinetically indistinguishable during ¹³CO₂ SSITKA experiments during CO₂ hydrogenation, indicating that in this case the WGS reaction is near equilibrium.

Based on the ¹³C decay plots, a two pool model for the WGS mechanism is the most likely fit to our experimental data. Upon comparison with the open literature, the formate mechanism is the most plausible mechanism. This mechanism has CHO_s and COOH_s species as the surface intermediates during the WGS reaction.

Hypothesis and key questions

The hypothesis and key questions considered in this thesis are presented in Chapter 1 (section 1.5). The hypothesis that C_s is active and should play a role in the mechanism of the HTFT process is indeed true. This was shown in Chapter 3 with the ¹³CO deposition (Boudouard reaction) experiment in which the ¹³C_s was active for Fischer-Tropsch. Moreover, in the deuterium tracing experiment, CCH_s was identified as an active species for C₂ formation. This intermediate most probably forms from the reaction of C_s and CH_s. Responses to the specific key questions are:

The monomer for the HTFT process is most likely the CH_s as identified by the deuterium study in Chapter 3.

In terms of the reactive intermediates, both CH_s and CCH_s were identified as the most abundant whilst graphitic carbon is the most abundant unreactive species (see Chapter 3).

Olefins and paraffins can be described by the same mechanism but do not necessarily share the same surface intermediates (see Chapters 3, 5 and 6). Unfortunately, the experiments to elucidate the oxygenate and water gas shift surface intermediates (using ^{18}O -labelled CO and CO_2) were not performed in this thesis. This will form part of a follow-up study to this thesis.

C_s was shown to be important in the overall mechanism.

The experiments with varying H_2O and CO_2 to study surface carbon (C_s) were not performed here as it posed a few technical challenges and required a modification to the setup. This will also be part of the follow-up study to this thesis.

The readsorption of 1-olefins (ethene) was studied and shown to be relevant in the mechanism of the HTFT process (see Chapter 5). The study of other 1-olefins (especially propene) and alcohols will form part of a follow up study.

The formation of CO_2 seems to be predominantly from the water-gas-shift reaction since H_2O needs to be present before CO_2 is formed (see Figure 3.1). The Boudouard reaction also occurs but the CO_2 formed here is as significant as that from the water-gas-shift reaction.

8.2. Outlook

This thesis presents a basic framework for the HTFT process and successfully describes the formation of methane, ethane and ethene. These results were based on 1.2 bar experiments and so, a first step would be to determine if these reaction pathways hold true at higher pressures (perhaps from 5 to 15 bar). There is also scope to refine the C₃₊ model, specifically to show if it also requires two separate carbon pools as in the case for the CH₄ and the C₂'s.

The formation of oxygenates were not considered in this thesis. These products are important to the overall selectivity of the HTFT process and should therefore be included in the overall mechanism. The key question is whether the oxygenates share the same surface intermediates as the hydrocarbons or maybe with the WGS intermediates. These experiments would probably require a combination of ¹³CO and C¹⁸O SSITKA experiments.

The identification of the surface intermediates for methanation and C₂ formation required numerous experiments with different GCMS sampling programs. Such a study could be extended to the C₃'s and C₄'s to determine if these species share the same surface intermediates. This would provide conclusive proof of the monomer during the Fischer-Tropsch process. Due to the large number of isotopic variants, it would be difficult to perform such experiments for C₅'s, although not impossible. Proper analysis of the C₄'s would also provide some indication as to the mechanism of branched products (e.g. transients for (CH₃)₂-CH-CH₃).

The relationship between the catalyst phase and product selectivity during the HTFT process is still not well understood. SSITKA has the advantage that

the catalyst phase remains the same during the isotopic switch. Bearing this in mind, it would be useful to perform short SSITKA experiments at various times on line. This will provide insight into the changes in surface coverages and selectivity whilst *ex-situ* analysis (for example X-Ray Diffraction) would provide information on the corresponding phase changes. This would allow for a correlation between selectivity and catalyst phases.

Finally, this thesis proposed a mechanistic pathway for the WGS reaction at HTFT conditions. A more detailed study, similar to the methanation study in Chapter 4, is required in order to validate this WGS mechanism. Here as well, the catalyst phase during the experiments should be taken into account. Moreover, apart from the obvious ^{13}C labeled CO and CO_2 reactants, the use of ^{18}O -labelled CO and CO_2 reactants will provide the relevant data to distinguish between the rival formate mechanisms. Another option is to perform coupled DRIFTS-MS and SSITKA experiments to check if the labeled formate intermediate is related to the appearance of the labeled CO_2 .

Nomenclature

Roman symbols

A_k	constants in Equation 2
C_s	surface carbon
C_k^{st}	steady-state concentrations of species in the gas phase.
c	constant
E_{13C}	fractional contribution of ^{13}C -labelled isotopes (eg. ^{13}CO)
ID	internal diameter
I_j	mass spectrometer intensity of component j
k_i	reaction rate coefficient for reaction i
L	length
N	number of exponential functions in constitute the spectrum.
r_i^{st}	rates of steps i
t	time
Z_k^C	relative concentrations of the isotopic label (isotopic fraction) in

the gas phase species.

Z_k^θ relative concentrations of the isotopic label (isotopic fraction) on the catalyst surface

Greek symbols

β dimensionless coefficient that determines the ratio between the active sites on the catalyst surface and the concentrations of reactants in the gas phase.

γ_i number of atoms of the same type capable of carrying a label from one specie to another in a single elementary step.

θ_k^{st} steady-state concentrations of species on the catalyst surface

λ_k the eigenvalues of the corresponding matrix for the right-hand sides of Equations 1.

τ bed residence time

Subscripts and superscripts

a or ads adsorption

b bed

d or des desorption

g	gas phase
h	hydrogenation
i or ini	initiation
p	propagation or chain growth
re	readsorption
tp, <i>i</i>	termination of a paraffin for component <i>i</i>
to, <i>i</i>	termination of an olefin for component <i>i</i>

Abbreviations

ASF	Anderson Schulz Flory
FID	Flame Ionisation Detector
FTS	Fischer-Tropsch Synthesis
GC	Gas Chromatography
GCMS	Gas Chromatography Mass Spectrometer
HTFT	High Temperature Fischer-Tropsch
ISR	Isothermal surface Reaction
LTFT	Low Temperature Fischer-Tropsch
ML	Monolayer
MS	Mass Spectrometer
PFR	Plug Flow Reactor

rWGS	Reverse Water-Gas-Shift
SSITKA	Steady State Isotopic Transient Kinetic Analysis
TPH	Temperature Programmed Hydrogenation
TPO	Temperature Programmed Oxidation
TPR	Temperature Programmed Reduction
TPSR	Temperature Programmed Surface Reaction
WGS	Water-Gas-Shift

Appendix A: The gPROMS modeling language.

In this section, specific information about the gPROMS modelling is described. For more details, the reader is advised to consult the Advanced User Guide¹. A new gPROMS project starts with a tree structure consisting of various folders. Each folder on the project tree represents a group of gPROMS entities. Each entity type represents a fundamental gPROMS concept. In our work, the following entities were used:

1. Variable Type
2. Model
3. Process
4. Parameter Estimation
5. Experiments

Variable and variable types

In gPROMS, all quantities calculated by the Model Equations are Variables which are always real numbers and must always be given a Variable Type. The variable name, default value, and upper and lower limits need to be specified. An example of our Variable Type is shown in Table A1.

¹ Process System Enterprise. *gPROMS Advanced User Guide*. (2005)

Table A1: Details of the Variable Types as specified in the gPROMS model used in this study.

Name	Lower Limit	Default Value	Upper Limit	Units
gas_concentration	0.0	1.0	$1.0 \cdot 10^{30}$	mol/m_g^3
normalized_gas_concentration	0.0	0.0	1.1	-
reaction_rate_constants	0.0	1.0	$1.0 \cdot 10^{30}$	s^{-1}
surface_concentration	0.0	1.0	$1.0 \cdot 10^{30}$	$\text{mol/kg}_{\text{cat}}$

The model entity

Each gPROMS process must contain at least one Model which provides a description of the physical behaviour of a given system in the form of mathematical equations. The gPROMS language tab in a new Model entity comprises of various sections. In our work, the following sections were used:

1. Parameter
2. Distribution_Domain
3. Variable
4. Boundary
5. Equation

The Parameter section is used to declare the parameters of a Model. Parameters are time-invariant quantities that will *not*, under any circumstances, be the result of a calculation. Each parameter is declared a certain type (for example, Real or Integer). An example of the parameters as declared in our model is shown in Figure A1. All distribution domains within our model are specified in the DISTRIBUTION_DOMAIN subsection of the Model entity. In a typical tubular reactor model, Axial and Radial are two such domains defined which are declared as two model parameters, namely reactor length and reactor radius. In our work, the radial domain was ignored and only the axial domain was declared as is shown in Figure A1.

All quantities that are calculated in Model Equations must be declared as model variables in the VARIABLE section. Like Parameters, Variables are always real numbers and must be given a type as shown in Figure A1 for our work.

BOUNDARY conditions are part of the description of the physical system behaviour and are therefore specified within Models in contrast to initial conditions, which may differ from one simulation experiment to another and are therefore specified within Processes. In gPROMS, it is possible to include the Boundary conditions in the Equation section together with all other model equations but for clarity reasons it is often better to have it separated. The Boundary conditions specified in our model are presented in Figure A2.

The EQUATION section is used to declare the equations that determine the time trajectories of the variables already declared in the VARIABLE section.

PARAMETER		
epsg	as	REAL
Fv	as	REAL
V	as	REAL
rocat	as	REAL
SimTime	as	REAL
a1, a2, a3	as	REAL
Cco0	as	REAL
NoComp	as	INTEGER
NoComps	as	INTEGER
NoComp _{pl}	as	INTEGER
NoComps _{pl}	as	INTEGER
ReactorLength	as	REAL

DISTRIBUTION_DOMAIN		
Axial as [0:ReactorLength]		

VARIABLE		
C _l	as	DISTRIBUTION(NoComp _g ,Axial)of gas_concentration
L _l	as	DISTRIBUTION(NoComp _s ,Axial)of surface_concentration
C _{nl}	as	DISTRIBUTION(NoComp _g ,Axial)of gas_concentration
L _{nl}	as	DISTRIBUTION(NoComp _s ,Axial)of surface_concentration
C _{ss}	as	DISTRIBUTION(NoComp _g ,Axial)of gas_concentration
L _{ss}	as	DISTRIBUTION(NoComp _s ,Axial)of surface_concentration
C _{ne}	as	DISTRIBUTION(Axial) of gas_concentration
C _{bound}	as	ARRAY(NoComp _g) of gas_concentration
L _{bound}	as	ARRAY(NoComp _s) of surface_concentration
C _{n_CO_l}	as	ARRAY(Axial) of surface_concentration
C _{n_Product_gases_l}	as	ARRAY(NoComp _g) of normalized_gas_concentration
C _{n_CO_nl}	as	ARRAY(Axial) of normalized_gas_concentration
C _{n_Product_gases_nl}	as	ARRAY(NoComp _g) of normalized_gas_concentration
k _{ads}	as	reaction_rate_constants
k _{des}	as	reaction_rate_constants
k _{1, k2, k3, k4}	as	reaction_rate_constants
k _{5, k6}	as	reaction_rate_constants

Figure A1: An example of a gPROMS model for a transient plug-flow reaction model showing the details of the PARAMETER, DSITRIBUTION_DOMAIN and VARIBALES as specified in this work.

The order in which the equations are declared is of no importance in gPROMS. The model equations for the SSITKA modelling as discussed elsewhere (Chapter 4), are presented in Figure A2. The symbol \$ denotes the partial differentiation operator with respect to time.

The process entity

A Model can be used to study the behaviour of the system under many different circumstances, each one called a *simulation activity*. The coupling of Models with the particulars of a dynamic simulation activity is done in a PROCESS. A PROCESS is partitioned into the following key sections:

1. UNIT
2. SET
3. ASSIGN
4. INTIAL
5. SOLUTION PARAMETERS
6. SCHEDULE

```

BOUNDARY
Cne(0) = (1-(1/(1+exp(-(time-a1)/a2)))^a3);
C_l(1,0) = Cco0*((1/(1+exp(-(time-a1)/a2)))^a3);
C_l(2,0) = Cbound(2);
L_l(1,0) = Lbound(1);
L_l(2,0) = Lbound(2);
L_l(3,0) = Lbound(3);
C_nl(1,0) = Cco0*(1-(1/(1+exp(-(time-a1)/a2)))^a3));
C_nl(2,0) = Cbound(2);
L_nl(1,0) = Lbound(1);
L_nl(2,0) = Lbound(2);
L_nl(3,0) = Lbound(3);
Css(1,0) = Cco0;
Css(2,0) = Cbound(2);
Lss(1,0) = Lbound(1);
Lss(2,0) = Lbound(2);
Lss(3,0) = Lbound(3);

EQUATION
FOR x:=0+ TO ReactorLength DO
$Cne(x)+(Fv/(epsg*V))*PARTIAL(Cne(x),Axial)=0;
$C_l(1,x)+(Fv/(epsg*V))*PARTIAL(C_l(1,x),Axial)=(rocat/epsg)*(-kads*C_l(1,x)
+kdes*L_l(1,x));
$C_l(2,x)+(Fv/(epsg*V))*PARTIAL(C_l(2,x),Axial)=(rocat/epsg)*(ktp1*L_l(3,x));

$L_l(1,x)=kads*C_l(1,x)-kdes*L_l(1,x)-kco2*L_l(1,x)-kco1*L_l(1,x);
$L_l(2,x)=kco2*L_l(1,x)-km1*L_l(2,x);
$L_l(3,x)=km1*L_l(2,x)+kco1*L_l(1,x)-ktp1*L_l(3,x)-L_l(3,x)/Lss(3,x)*C2net;

$C_nl(1,x)+(Fv/(epsg*V))*PARTIAL(C_nl(1,x),Axial)=(rocat/epsg)*(-kads*C_nl(1,x)
+kdes*L_nl(1,x));
$C_nl(2,x)+(Fv/(epsg*V))*PARTIAL(C_nl(2,x),Axial)=(rocat/epsg)*(ktp1*L_nl(3,x));

$L_nl(1,x)=kads*C_nl(1,x)-kdes*L_nl(1,x)-kco1*L_nl(1,x)-kco2*L_nl(1,x);
$L_nl(2,x)=kco2*L_nl(1,x)-km1*L_nl(2,x);
$L_nl(3,x)=km1*L_nl(2,x)+kco1*L_nl(1,x)-ktp1*L_nl(3,x)-L_nl(3,x)/Lss(3,x)*C2net;

(Fv/(epsg*V))*PARTIAL(Css(1,x),Axial)=(rocat/epsg)*(-kads*Css(1,x)+kdes*Lss(1,x));
(Fv/(epsg*V))*PARTIAL(Css(2,x),Axial)=(rocat/epsg)*(ktp1*Lss(3,x));

0=kads*Css(1,x)-kdes*Lss(1,x)-kco1*Lss(1,x)-kco2*Lss(1,x);
0=kco2*Lss(1,x)-km1*Lss(2,x);
0=kco1*Lss(1,x)+km1*Lss(2,x)-ktp1*Lss(3,x)-Lss(3,x)/Lss(3,x)*C2net;

END

```

Figure A2: An example of a gPROMS model for a transient plug-flow reaction model showing the details of the BOUNDARY and EQUATION as specified in this work.

The UNIT section allows for different models to be declared in a single process. This is useful in the simulation of complex plants where each piece of equipment is declared as a UNIT and coupled in the process simulation. In the SET section of a process, all parameters are specified. This must be done

before a model can be used in a simulation. The set of equations resulting from the instantiation of the Models declared in the UNIT section is typically under-determined. This simply means that there are more variables than equations. The number of *degrees of freedom* in the simulation activity is given by:

Number of degrees of freedom (N_{DOF}) = Number of variables - Number of equations.

For the simulation activity to be fully defined, N_{DOF} variables must be specified as either constant values or given functions of time. Variables specified in this way are the input variables of this simulation activity. The remainder of the variables are the *unknown* variables, the time variation of which will be determined by the solution of the system equations. The specification of input variables is provided in the ASSIGN section of the PROCESS. The INITIAL section is used to declare the initial condition information pertaining to a dynamic simulation activity. Solver settings and output specifications can be controlled in the SOLUTION_PARAMETERS section. Information on the external manipulations that are to be simulated is provided in the SCHEDULE section of the PROCESS. These are deliberate actions which cause a disturbance in the simulation. In our case, the simulation was allowed to continue for a specified time period. In Figure A3, the PROCESS entity used in our work is presented.

The parameter estimation and experiment entities

gPROMS can be used to perform *Parameter Estimation* for complex models using both dynamic and steady-state experimental data. A maximum likelihood objective function is used to estimate the parameters¹. This

function allows for several types of variance models to be specified. Parameters to be estimated are declared and given initial guesses, lower and upper bounds. It is also possible to declare parameters to be estimated as fixed values. All performed experiments which are included in the EXPERIMENT entity can be chosen in the experiments and measurement tab under the PARAMETER ESTIMATION entity. At the same time, gPROMS requires the variances of the measurements to be defined. The constant variance model was chosen in order to reduce the number of unknown parameters². Details on the PARAMETER entity used in our work are presented in Figure A4.

² T. Van de Vin, Masters Graduation Report, Technische Universiteit Eindhoven (2007), the Netherlands

```

UNIT
M07 as Model4

SET
M07.epsg:=0.61;
M07.Fv:=1.21e-6;
M07.V:=1.51e-6;
M07.rocat:=856;
M07.NoComp:=2;
M07.NoComps:=3;
M07.ReactorLength:=1;
M07.SimTime:=200;
M07.Axial:=[BFDM,1,100];
M07.a1:=0.46;
M07.a2:=0.37;
M07.a3:=100;
M07.Cco0:=5.84;
M07.C2net:=4.95e-4;

ASSIGN
M07.Cbound(1):=0;
M07.Cbound(2):=0;
M07.Lbound(1):=0;
M07.Lbound(2):=0;
M07.Lbound(3):=0;
M07.kads:=6.2e-2;
M07.kdes:=9.1;
M07.kco1:=1.7e-2;
M07.kco2:=6.6e-3;
M07.ktp1:=5.2e-2;
M07.km1:=3e-2;

INITIAL
FOR x:=0+ TO M07.ReactorLength DO
M07.Cne(x)=0;
M07.C_1(1,x)=0;
M07.C_1(2,x)=0;
M07.L_1(1,x)=0;
M07.L_1(2,x)=0;
M07.L_1(3,x)=0;
M07.C_nl(1,x)=M07.Css(1,x);
M07.C_nl(2,x)=M07.Css(2,x);
M07.L_nl(1,x)=M07.Lss(1,x);
M07.L_nl(2,x)=M07.Lss(2,x);
M07.L_nl(3,x)=M07.Lss(3,x);
END

SOLUTIONPARAMETERS
ReportingInterval:=0.5;

SCHEDULE
CONTINUE FOR M07.SimTime

```

Figure A3: An example of a gPROMS model for a transient plug-flow reaction model showing the details of the Process entity as specified in this work.

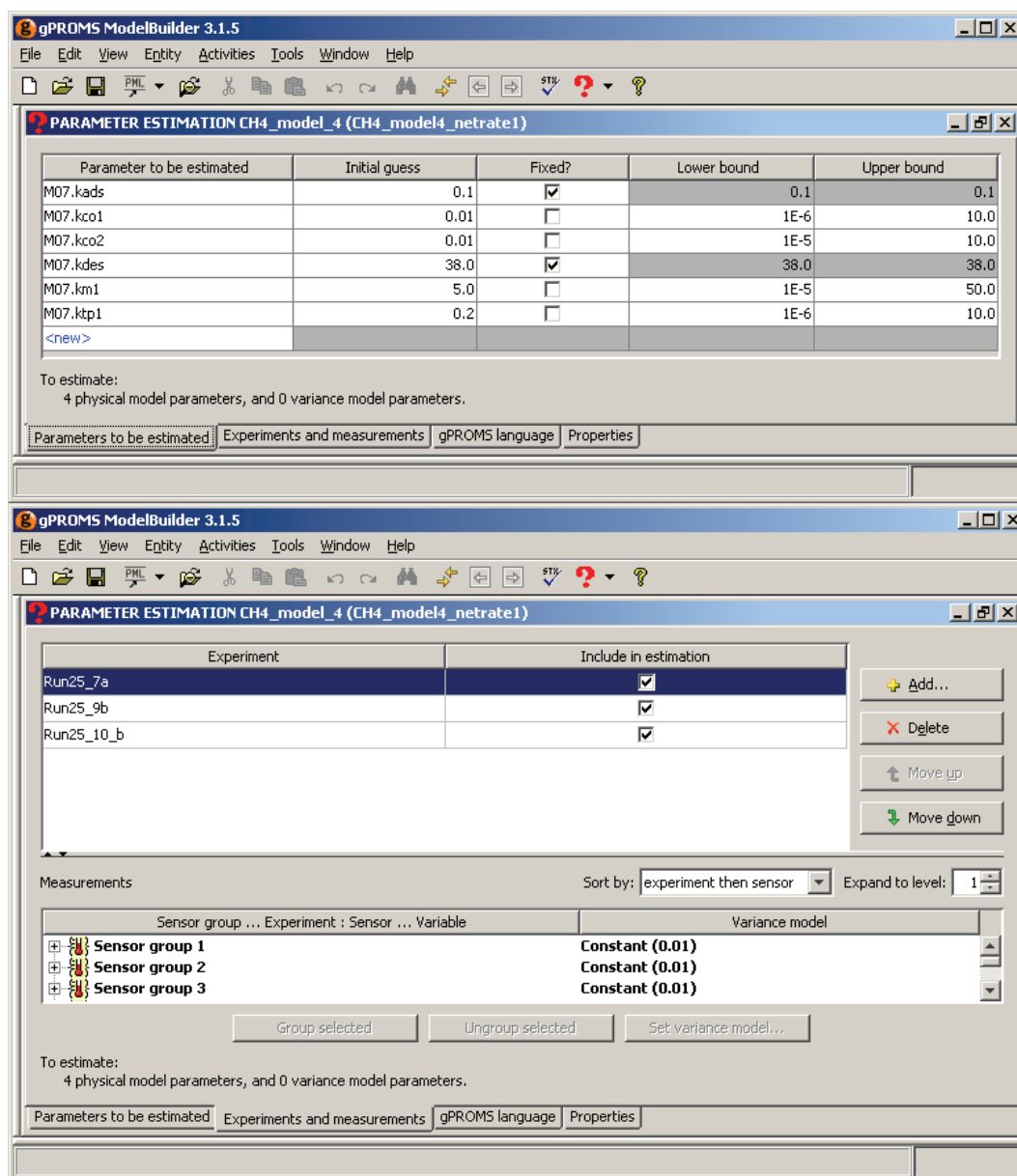


Figure A4: A part of the Parameter Estimation entity from a gPROMS model for a transient plug-flow reaction as specified in this work.

APPENDIX B: Fischer-Tropsch product distribution schemes as published in the open literature

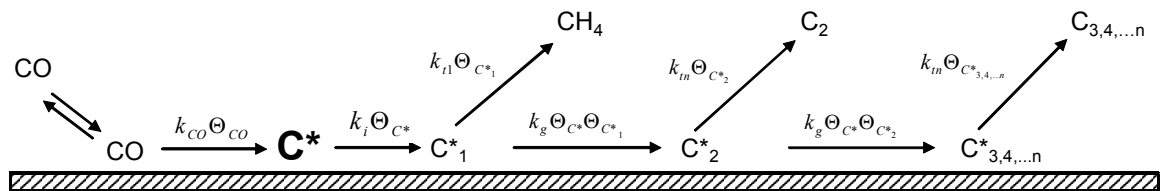


Figure B1. Expanded kinetic scheme depicting pathways to CH_4 and C_{2+} hydrocarbons in the Fischer-Tropsch synthesis (*Adapted from Bertole et al. [1,2]*).

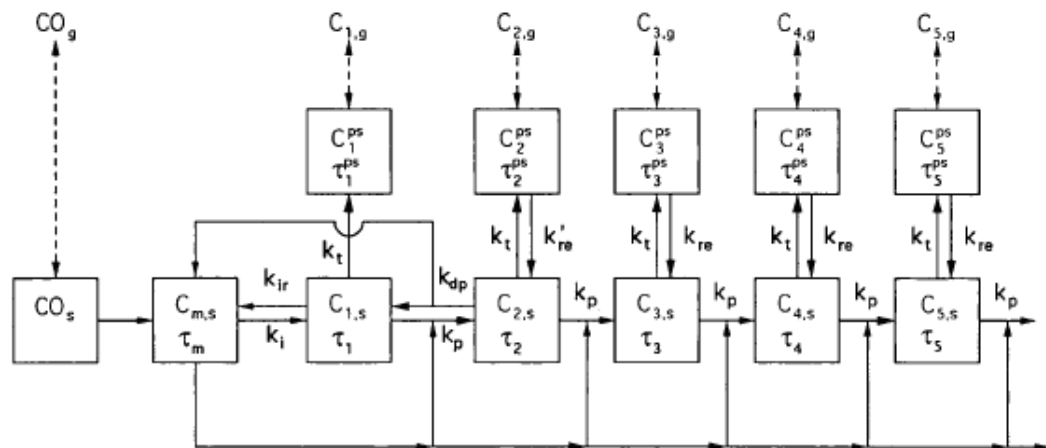


Figure B2. Chain growth model as proposed by Komaya and Bell [3].

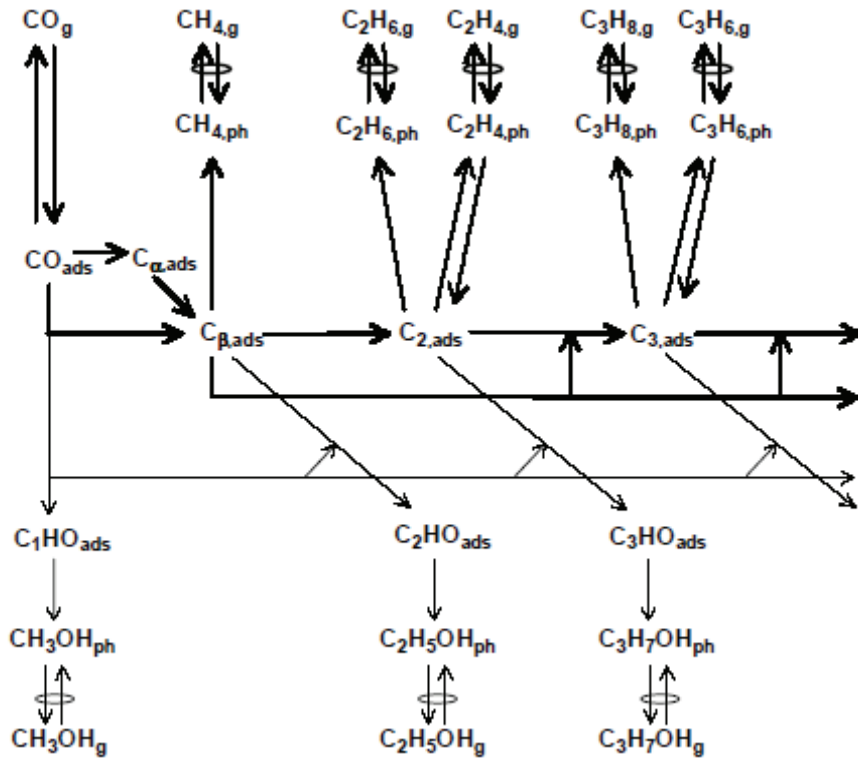


Figure B3.: Chain growth model as proposed by Van Dijk [4].

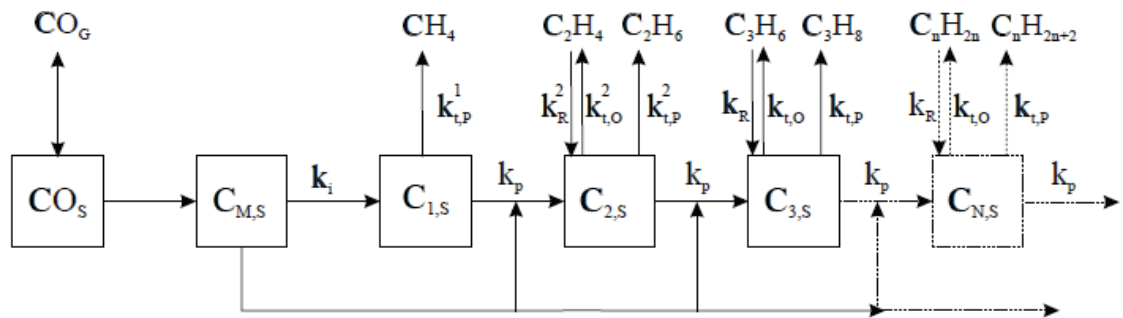


Figure B4.: Alpha-olefin readsorption model as proposed by Van der Laan and Beenackers [5].

APPENDIX C: Model equation for the ^{13}C O-labelling of C_{2+} hydrocarbons for models B & C (see Figures 6.3 and 6.4, Chapter 6).

MODEL B: Two C_2 surface intermediates with olefin readsorption

The mole balances for the CO and CH_4 in the gas phase, and CO_{ads} , C_α and C_β on the catalyst surface remain the same as in Model A. The difference is with the introduction of the second surface intermediate for the C_{2+} hydrocarbons ($\text{C}_{n\beta}$, $n \geq 2$). The equations for olefin termination and readsorption also remain the same as in Model A. The termination rate for the paraffins differs and these with the related expressions for the surface species are presented here.

$$\frac{\partial C''_{\text{C}_2\text{H}_6}}{\partial t} + \frac{1}{\tau} \frac{\partial C''_{\text{C}_2\text{H}_6}}{\partial x} = \frac{\rho}{\varepsilon_b} \left(k_{\text{tp}2} L''_{\text{C}_{2\beta}} \right) \quad [\text{C1}]$$

$$\frac{\partial C'''_{\text{C}_3\text{H}_8}}{\partial t} + \frac{1}{\tau} \frac{\partial C'''_{\text{C}_3\text{H}_8}}{\partial x} = \frac{\rho}{\varepsilon_b} \left(k_{\text{tp}3} L'''_{\text{C}_{3\beta}} \right) \quad [\text{C2}]$$

The mole balances for the non-labelled gas phase are exactly the same as those for the fully labelled species. Partially labelled gas phase species are also formed from partial labelled surface species, as shown in equations [C3] to [C5].

$$\frac{\partial C_{\text{C}_2\text{H}_6}}{\partial t} + \frac{1}{\tau} \frac{\partial C_{\text{C}_2\text{H}_6}}{\partial x} = \frac{\rho}{\varepsilon_b} \left(k_{\text{tp}2} L_{\text{C}_{2\beta}} \right) \quad [\text{C3}]$$

$$\frac{\partial C_{\text{C}_3\text{H}_8}}{\partial t} + \frac{1}{\tau} \frac{\partial C_{\text{C}_3\text{H}_8}}{\partial x} = \frac{\rho}{\varepsilon_b} \left(k_{\text{tp}3} L_{\text{C}_{3\beta}} \right) \quad [\text{C4}]$$

$$\frac{\partial C''_{C_3H_8}}{\partial t} + \frac{1}{\tau} \frac{\partial C''_{C_3H_8}}{\partial x} = \frac{\rho}{\varepsilon_b} \left(k_{tp3} L''_{C_3\beta} \right) \quad [C5]$$

The mole balances for the fully labelled surface species are:

$$\begin{aligned} \frac{\partial L''_{C_{2\alpha}}}{\partial t} = & k_i L'_{C_\alpha} L'_{C_\beta} - k_{to2} L''_{C_{2\alpha}} - k_{h2} L''_{C_{2\alpha}} + k_{re2} C''_{C_2H_4} \\ & - k_p L''_{C_{2\alpha}} (L'_{C_\alpha} + L_{C_\alpha}) \end{aligned} \quad [C6]$$

$$\frac{\partial L''_{C_{2\beta}}}{\partial t} = k_h L''_{C_{2\alpha}} - k_{tp2} L''_{C_{2\beta}} \quad [C7]$$

$$\begin{aligned} \frac{\partial L'''_{C_{3\alpha}}}{\partial t} = & k_p L'_{C_\alpha} L''_{C_{2\alpha}} - k_{to3} L'''_{C_{3\alpha}} - k_{h3} L'''_{C_{3\alpha}} + k_{re3} C'''_{C_3H_6} \\ & - k_p L'''_{C_{3\alpha}} (L'_{C_\alpha} + L_{C_\alpha}) \end{aligned} \quad [C8]$$

$$\frac{\partial L'''_{C_{3\beta}}}{\partial t} = k_h L'''_{C_{3\alpha}} - k_{tp2} L'''_{C_{3\beta}} \quad [C9]$$

The following set of equations is obtained for the partially labelled surface species:

$$\begin{aligned} \frac{\partial L_{C_{2\alpha}}}{\partial t} = & k_i L_{C_\alpha} L_{C_\beta} + k_i L_{C_\alpha} L_{C_\beta} - k_{to2} L_{C_{2\alpha}} - k_{h2} L_{C_{2\alpha}} \\ & + k_{re2} C_{C_{2H_4}} - k_p L_{C_{2\alpha}} (L_{C_\alpha} + L_{C_\alpha}) \end{aligned} \quad [C10]$$

$$\frac{\partial L_{C_{2\beta}}}{\partial t} = k_h L_{C_{2\alpha}} - k_{tp2} L_{C_{2\beta}} \quad [C11]$$

$$\begin{aligned} \frac{\partial L_{C_{3\alpha}}}{\partial t} = & k_p L_{C_\alpha} L_{C_{2\alpha}} + k_p L_{C_\alpha} L_{C_{2\alpha}} + k_i L_{C_\alpha} L_{C_{2\alpha}} - k_{to3} L_{C_{3\alpha}} \\ & - k_{h3} L_{C_{3\alpha}} + k_{re3} C_{C_{3H_6}} - k_p L_{C_{3\alpha}} (L_{C_\alpha} + L_{C_\alpha}) \end{aligned} \quad [C12]$$

$$\frac{\partial L_{C_{3\beta}}}{\partial t} = k_h L_{C_{3\alpha}} - k_{tp2} L_{C_{3\beta}} \quad [C13]$$

$$\begin{aligned} \frac{\partial L''_{C_{3\alpha}}}{\partial t} = & k_p L_{C_\alpha} L_{C_{2\alpha}} + k_p L_{C_\alpha} L_{C_{2\alpha}} - k_{to3} L''_{C_{3\alpha}} - k_{h3} L''_{C_{3\alpha}} \\ & + k_{re3} C''_{C_{3H_6}} - k_p L''_{C_{3\alpha}} (L_{C_\alpha} + L_{C_\alpha}) \end{aligned} \quad [C14]$$

$$\frac{\partial L''_{C_{3\beta}}}{\partial t} = k_h L''_{C_{3\alpha}} - k_{tp2} L''_{C_{3\beta}} \quad [C15]$$

MODEL C: Two C₂ surface intermediates with direct olefin readsorption

The pathway for olefin readsorption and chain growth is different for this model, compared to Model B. The termination pathway for the paraffin is the same (see equations C16 to C20). The mole balances for the CO and CH₄, and C₂₊ hydrocarbons in the gas phase are the same as in Models A and B respectively.

The mole balances for the fully labelled surface species are:

$$\begin{aligned} \frac{\partial L''C_{2\alpha}}{\partial t} = & k_i L'C_\alpha L'C_\beta - k_{to2} L''C_{2\alpha} - k_{h2f} L''C_{2\alpha} + k_{h2r} L''C_{2\beta} \\ & - k_p L''C_{2\alpha} (L'C_\alpha + L_{C_\alpha}) \end{aligned} \quad [C16]$$

$$\frac{\partial L''C_{2\beta}}{\partial t} = k_{h2f} L''C_{2\alpha} + k_{re2} C''C_{2H_4} - k_{h2r} L''C_{2\alpha} - k_{tp2} L''C_{2\beta} \quad [C17]$$

$$\begin{aligned} \frac{\partial L'''C_{3\alpha}}{\partial t} = & k_p L'C_\alpha L''C_{2\alpha} - k_{to3} L'''C_{3\alpha} - k_{h3f} L'''C_{3\alpha} + k_{h3r} L'''C_{3\beta} \\ & - k_p L'''C_{3\alpha} (L'C_\alpha + L_{C_\alpha}) \end{aligned} \quad [C18]$$

$$\frac{\partial L'''C_{3\beta}}{\partial t} = k_{h2f} L'''C_{3\alpha} - k_{tp2} L'''C_{3\beta} - k_{h2r} L'''C_{3\alpha} + k_{re3} C'''C_{3H_6} \quad [C19]$$

The following set of equations is obtained for the partial labelled surface species:

$$\begin{aligned} \frac{\partial L_{C_{2\alpha}}}{\partial t} = & k_i L_{C_\alpha} L_{C_\beta} + k_i L_{C_\alpha} L_{C_\beta} - k_{to2} L_{C_{2\alpha}} - k_{h2f} L_{C_{2\alpha}} \\ & + k_{h2r} L_{C_{2\beta}} - k_p L_{C_{2\alpha}} (L_{C_\alpha} + L_{C_\alpha}) \end{aligned} \quad [\text{C20}]$$

$$\frac{\partial L_{C_{2\beta}}}{\partial t} = k_{h2f} L_{C_{2\alpha}} + k_{re2} C_{C_2H_4} - k_{h2r} L_{C_{2\alpha}} - k_{tp2} L_{C_{2\beta}} \quad [\text{C21}]$$

$$\begin{aligned} \frac{\partial L_{C_{3\alpha}}}{\partial t} = & k_p L_{C_\alpha} L_{C_{2\alpha}} + k_p L_{C_\alpha} L_{C_{2\alpha}} - k_{to3} L_{C_{3\alpha}} - k_{h3f} L_{C_{3\alpha}} \\ & + k_{h3r} L_{C_{3\beta}} - k_p L_{C_{3\alpha}} (L_{C_\alpha} + L_{C_\alpha}) \end{aligned} \quad [\text{C22}]$$

$$\frac{\partial L_{C_{3\beta}}}{\partial t} = k_{h2f} L_{C_{3\alpha}} - k_{tp2} L_{C_{3\beta}} - k_{h2r} L_{C_{3\alpha}} + k_{re3} C_{C_3H_6} \quad [\text{C23}]$$

$$\begin{aligned} \frac{\partial L''_{C_{3\alpha}}}{\partial t} = & k_p L_{C_\alpha} L_{C_{2\alpha}} + k_p L_{C_\alpha} L_{C_{2\alpha}} - k_{to3} L''_{C_{3\alpha}} - k_{h3f} L''_{C_{3\alpha}} \\ & + k_{h3r} L''_{C_{3\beta}} - k_p L''_{C_{3\alpha}} (L_{C_\alpha} + L_{C_\alpha}) \end{aligned} \quad [\text{C24}]$$

$$\frac{\partial L''_{C_{3\beta}}}{\partial t} = k_{h2f} L''_{C_{3\alpha}} - k_{tp2} L''_{C_{3\beta}} - k_{h2r} L''_{C_{3\alpha}} + k_{re3} C_{C_3H_6} \quad [\text{C25}]$$

Appendix D: Relationship between reaction mechanisms and isotopic decay plots from SSITKA data.

During a SSITKA experiment, the isotopic composition of the reactant changes but the chemical composition of the gas phase and adsorbed layer remain the same. Therefore, the isotopic transfer can be viewed as a first-order reaction (assuming mono-labelled species) with respect to the isotopic fraction:

$$C_k^{st} \frac{dZ_k^C}{dt} = \beta \sum_{i=1}^{N_k^C} \gamma_i r_i^{st} Z_j,$$

$$\theta_k^{st} \frac{dZ_k^\theta}{dt} = \sum_{i=1}^{N_k^\theta} \gamma_i r_i^{st} Z_j. \quad \text{[D1]}$$

and with initial conditions, at $t = 0$, $Z_i = Z^0$.

The right-hand sides of Equations D1 are linear and therefore the solution can be described as:

$$Z_i(t) = \sum_{k=1}^N A_k e^{\lambda_k t} + c \quad \text{[D2]}$$

The form of the isotopic response curves depends on the number of exponential functions (N) that constitute the spectrum which is equal to the number of intermediate species in the mechanistic scheme. Furthermore, the rate of a decrease in the exponents λ_k and amplitude A_k influences N , and each mechanistic scheme is characterised by a certain ratio between these parameters.

Mechanistic discrimination can be shown by obtaining corresponding analytical solutions to the sets of equations. For the simplest mechanistic schemes (S_i denotes the intermediate species), the solutions can be found in explicit forms as reported by Shannon and Goodwin³. The solutions to the equations corresponding to mechanistic models 1 to 4 (shown in Figure D1)

³ S.L.Shannon and J.Goodwin, Chem.Rev. 95 (1995) 677-695.

have different values of λ_k and A_k . Thus, these models can be discriminated based on the isotopic response curves (see Figure D2a).

The logarithmic plots of the isotopic fraction versus time demonstrate the specific features of the isotopic response curves for the mechanisms in Figure D1:

If model 1 is true, the logarithmic plot is linear (line 1 in Figure D2b)

If model 2 is true, the corresponding curve has an upward convexity (line 2 in Figure D2b)

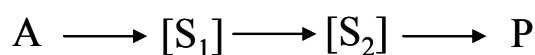
If a scheme has a buffer step (model 3) or parallel steps (model 4), then the curve has a downward convexity (line 3, Figure D2b). Models 3 and 4 can therefore only be discriminated on the basis of solely numerical data.

Therefore, on the basis of the shapes of the isotopic response curves, conclusions can be drawn on the reaction mechanism.

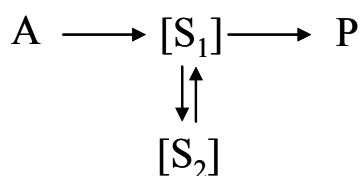
Model 1



Model 2



Model 3



Model 4

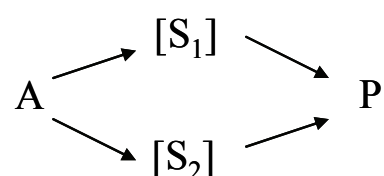


Figure D1: Various mechanistic schemes showing possible pathways from reactant *A* to product *P* via intermediates *S*₁ and *S*₂.

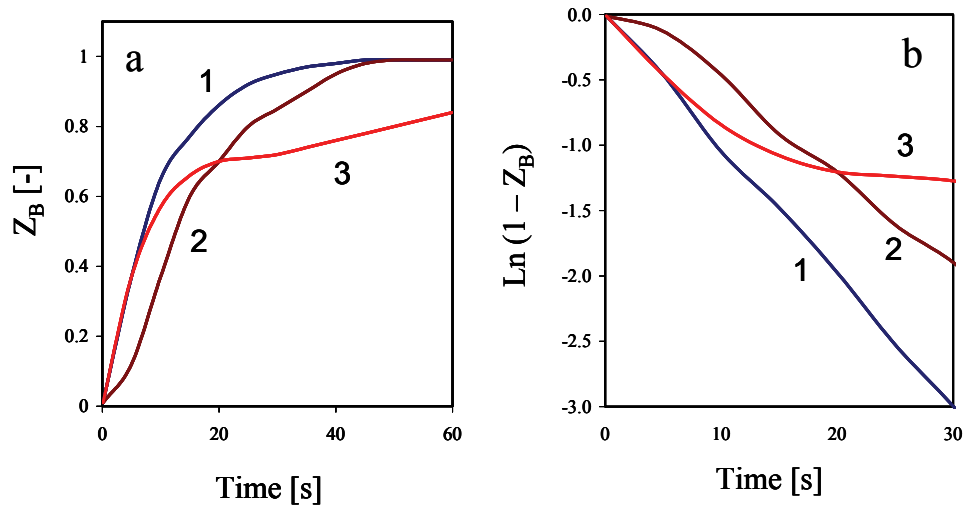


Figure D2: (a) Calculated isotopic response curves for the mechanistic models presented in Figure D1: (1) Model 1, (2) Model 2, and (3) Models 3 and 4; (b) the same curves in logarithmic coordinates showing the decay in the isotopic fraction.

Acknowledgements

This project turned out to a life changing experience and one that I will remember and cherish forever. Such an experience was only made possible with the support of family, friends and colleagues.

I would like to start by thanking the one person who was instrumental in several aspects of my life, **my wife. Ashriti**, this thesis is dedicated to you for all your love and support. Being able to share the experience with our daughter, Suhina, made the experience even more rewarding.

To all our **friends and family** back in South Africa, thanks for keeping us updated and making us feel so welcome during our short visits.

The skill and knowledge of the **SCR technicians**, Peter, Marlies and Frank led by Anton, have proven very valuable in getting my experiments started and then completed with minimum downtime. All of you were friendly from day one and always willing to help and I thank you for this.

To my **students** Tim and Sunil for all their assistance in commissioning the experimental setup and also contributing to the initial development of the mechanistic models.

To my **PhD colleagues**, starting with Vinit who caught me wandering in the hallways on my first day at TU/e and then took me along to the SCR group meeting. I was not impressed when I was put on the spot to tell the group what my project was about (having never met my supervisors!). Of course, all that was soon forgotten when he introduced me to Chaitu and convinced me to play cricket for PSV Tegenbosch. The friendships I've made since then are still standing the test of time (and distance). Vishwa and Vinayak, a special thanks to you for making time for me during my quick visits to Eindhoven, especially in recent times when not many familiar faces were around. To my SCR

roommates, Maurice and Halabi, thanks for the great technical discussions and also the entertainment during lunch. To the rest of the gang (Patrick, Stijn, Niek, Oki, Chattarbir, Jovan, Joost, Charl, Roman, Marco, Bianca, Narendra), thank you for fun conversations either during coffee breaks or Fort. Also, thanks to Michiel and Carlos for all the relaxing conversations about football and also for good laughs in the lab. I would also like to thank Ionel and Sorinela for the wonderful dinners as well as Denzil and Prabashni for sharing in the Dutch experience and also for reminiscing about life back home.

To the other **SCR colleagues**, thanks for all your support. A special thanks to Xander Nijhuis for entertaining us on our trip to New Orleans. Who will ever forget “manager happy hour”? It was also a pleasure working with Elena and yourself on the propene epoxidation project.

I also want to thank **SCR secretary, Denise**. You are simply brilliant and the most efficient secretary I’ve ever known. Thanks for sorting all my documentation.

To Professor Hans Niemantsverdriet and Professor Rutger van Santen for useful technical discussions.

In terms of compiling the final thesis, a few people played a critical role. I would like to start with the promoter of this thesis, **Professor Jaap Schouten** firstly for his patience and support. Thanks for allowing me the extra time to write when I returned to South Africa to work at Sasol. It has been an honour to work with you. I was always impressed by your detailed comments – it still amazes me how you manage to spot the extra spaces between words!

To my daily supervisor, **Dr Mart de Croon** for just being brilliant and challenging me throughout the project. Your competency in mathematics was frightening at times, especially when I took weeks to solve PDE’s in gPROMS and you did a few whilst relaxing in the bath or whilst on the bus. I have to

admit that this has reignited my passion for maths and I thank you for this – though that does not mean you can ask me to solve Laplace equations by hand.

My supervisors from Sasol, **Dr Gideon Botes and Dr Berthold Breman** who initiated this project with TU/e and remained interested in its development all the way. Our telecons always proved to be an eye-opener and your hard but fair and constructive criticism helped my understanding of this work but most of all contributed to my development as an engineering scientist. I have utmost respect for you and hope we can work closely together in the future. A special thank you to my Sasol colleague **Toine Cents** for visiting me at TU/e and participating in our telecons. I also want to thank Dr Gideon Botes for spending hours of his spare time with the **cover design**. I also appreciate all the ingenious ideas and tricks you came up with in Photoshop.

To **Philip Gibson** for offering me the opportunity to do this project, for all his support and guidance and also for his entertaining visits. We always felt like Sasol employees when you were around.

Lastly, together with my fellow colleagues involved in this project, we would like to thank mainly **Sasol** for financial support but also the **NWO** for funding during the first year of the project.

List of Publications

Publications

1. N.S. Govender, M.H.J.M. de Croon, J.C. Schouten, *Reactivity of surface carbonaceous intermediates on an iron-based Fischer-Tropsch catalyst*, Appl. Catal. A, **373**(1-2), 81-89, (2010)
2. T.A. Nijhuis, E. Sacaliuc-Parvulescu, N.S. Govender, J.C. Schouten, B.M. Weckhuysen, *The role of support oxygen in the epoxidation of propene over gold-titania catalysts investigated by isotopic transient kinetics*, J. Catal., **265**(-), 161-169, (2009)
3. N.S. Govender, F.G. Botes, M.H.J.M. de Croon, J.C. Schouten, *Mechanistic pathway for methane formation over an iron-based catalyst*, J. Catal., **260**(-), 254-261, (2008)
4. Botes, F.G.; Govender, N.S. *Secondary reactions of ethylene as studied in a laboratory-scale recycle slurry reactor*, Energy & Fuels, **21**, 3095 (2007).
5. Govender, N.S., Van Vuuren, M.J., Claeys, M., & Van Steen, E., *Importance of the usage ratio in iron-based Fischer-Tropsch synthesis with recycle*, IECR **45**(25), 8629-8633, (2006).
6. Van Vuuren, M.J., Govender, N.S., Kotze, R., Masters, G.J., & Pete, T.P., *The correlation between double bond isomerization, water gas shift and acid production during Fischer-Tropsch synthesis*. Am. Chem. Soc., Div. Petr. Chem., Preprints, **50**(2), 200-202, (2005).

Oral and Poster presentations

Refereed proceedings

1. N.S. Govender, M.H.J.M. de Croon, J.C. Schouten, *Modelling the C₂₊ hydrocarbons during the Fischer-Tropsch Synthesis using transient kinetics*, in Proc. 21st North American Catalysis Society Meeting (NAM); San Francisco, CA, United States, PW23, (2009)
2. N.S. Govender, M.H.J.M. de Croon, J.C. Schouten, *Mechanistic study of the Fischer-Tropsch synthesis using transient kinetics*, in Proc. 235th ACS National Meeting; Editors: -, New Orleans, LA, United States, 231a, (2008)
3. N.S. Govender, M.H.J.M. de Croon, J.C. Schouten, *Mechanistic study of the Fischer-Tropsch synthesis using transient kinetics*, in Proc. 14th Int. Congress on Catalysis; Editors: -, Seoul, Korea, Republic of, OD54, p. 143, (2008)
4. N.S. Govender, M.H.J.M. de Croon, J.C. Schouten, *Mechanistic study of the Fischer-Tropsch synthesis using transient kinetics*, in Proc. 20st Int. Symp. on Chemical Reaction Engineering (ISCRE-20); Kyoto, Japan, pp. 268-269, (2008)

Non-refereed proceedings

1. N.S. Govender, M.H.J.M. de Croon, J.C. Schouten, *Mechanistic study of the High Temperature Fischer-Tropsch (HTFT) process on an Fe-based catalyst using Steady-State Isotopic Kinetic Analysis (SSITKA)*, in Book of Abstracts Netherlands' Catalysis & Chemistry Conference; Editors: -, Noordwijkerhout, Netherlands, P50, page 202, (2007)

About the author



Nilenindran Sundra Govender (Gregory) was born in Durban, South Africa on 18 July 1975. In 1993, he matriculated from Umzinto Secondary School in the lower south coast of Kwazulu Natal. He initially registered for Chemical Engineering at University of Kwazulu-Natal in 1994 but later graduated with a Bachelors degree (B.Sc.) in Chemistry and Applied mathematics in 1999. In 2000, he obtained his National Diploma (Chemical Engineering) from ML Sultan Technikon in Durban. Gregory was employed by Sasol in March 2001 and started work on the preparation of iron precipitated catalysts. He continued his studies via correspondence and in 2004 obtained in B.Sc. Honors Degree in Chemistry from the University of South Africa. In the same year, he registered for the Taught Masters in Catalysis at the University of Cape Town and a year later graduated with Professor Eric van Steen with a thesis entitled “Recycling the tail-gas during the Low Temperature Fischer-Tropsch Process”. In June 2005, Sasol seconded him to the Eindhoven University of Technology (TU/e) to start his PhD project in the group of Professor Jaap Schouten. The results of this project are presented in this dissertation.